



Zambelloni, Riccardo (2017) *Generation of anti-virulence compounds against the type three secretion system of Escherichia coli O157:H7*. PhD thesis.

<http://theses.gla.ac.uk/7924/>

Copyright and moral rights for this work are retained by the author

A copy can be downloaded for personal non-commercial research or study, without prior permission or charge

This work cannot be reproduced or quoted extensively from without first obtaining permission in writing from the author

The content must not be changed in any way or sold commercially in any format or medium without the formal permission of the author

When referring to this work, full bibliographic details including the author, title, awarding institution and date of the thesis must be given

Glasgow Theses Service

<http://theses.gla.ac.uk/>

theses@ gla.ac.uk



**Generation of anti-virulence compounds against the  
type three secretion system of *Escherichia coli*  
O157:H7**

A thesis submitted to the University of Glasgow for the degree of  
Doctor of Philosophy

Riccardo Zambelloni MSci

Submitted September 2016

Institute of Infection, Immunity and Inflammation  
College of Medical, Veterinary and Life Sciences  
University of Glasgow

## **Author's declaration**

I declare that, except where explicit reference is made to the contribution of others, this dissertation is the result of my own work and has not been submitted for any other degree at the University of Glasgow or at any other institution.

Riccardo Zambelloni

September 2016

## Acknowledgements

First of all, I owe a huge thank you to Dr. Andrew Roe for his endless support throughout these years. His help has been priceless and I will be always grateful for that. Thank you also to Dr. Rudi Marquez for his advice on the chemical syntheses.

A big thank you to all past and present members of the Roe and Marquez group. Alan Sewell, Alejandro Huerta Uribe, Ezequiel Silva Nigenda, Mhairi Matheson, Tom Cogswell, Liyana Azmi, James Connolly, Kate Beckham, Tom Parker, Anna Hansen, Hugh Scarlin, Sean O' Byrnes, Liam Adair, Colin Pearson, Faustine Dubar, Zoe Marjenberg, Ricardo Gonzalez Lopez. You are all wonderful people and I feel very lucky to have worked with all of you.

Another big thank you to my family, my girlfriend and friends in Italy for their constant support. Thanks to Prof. Robert Liskamp for his critical read of this thesis and to Dr. Karl Burgess and Dr. Margaret Mullin for their help with specific techniques.

Thank you all for putting up with me. I will always remember these 4 years in Glasgow.



## Abstract

*Escherichia coli* is normally found in the intestinal microbiota of most mammals and is regarded as a commensal bacterium. However, several strains have evolved as pathogens through the acquisition of pathogenicity islands. *E. coli* O157:H7 is a commensal bacterium for cattle, but can be transmitted to humans where it acts as a pathogen. In humans, *E. coli* O157:H7 infections cause bloody diarrhoea, haemorrhagic colitis and in some cases haemolytic uremic syndrome (HUS), which can lead to death. Treatment of this bacterial infection is rather complicated as traditional antibiotics have demonstrated to worsen the clinical symptoms and the outcome of the infection. Therefore, the discovery of new treatments for this infection is of great relevance.

Anti-virulence (AV) compounds are one of the most promising classes of drugs for the treatment of *E. coli* O157:H7 infections, as they selectively target key virulence factors. This approach selectively decreases the ability of the pathogen to cause disease rather than its ability to survive, thus reducing the chances for the development of resistance. The type three secretion system (T3SS) is a key virulence factor for *E. coli* O157:H7 as it enables the tight attachment of the bacterium to the host cell and the secretion of effector proteins to initiate the colonisation process. The T3SS is a very attractive target for the development of selective AV compounds for *E. coli* O157:H7.

Salicylidene acylhydrazides (SA) are the most well-studied class of AV compounds targeting the T3SS in several Gram-negative bacteria. ME0055 was found to be one of the best SA compounds against the T3SS in *E. coli* O157:H7, but it is considered as a promiscuous binder since its effects derived from a modulation of several metabolic pathways rather than a direct interaction with the T3SS. However, ME0055 provides an excellent starting point for chemical optimisation and the generation of more stable and potent T3SS inhibitors.

The aim of this work was to chemically modify the ME0055 scaffold in order to create a small focused library of new anti-virulence compounds. Three new active scaffolds based on the SA compound's core were found to be active against *E. coli* O157:H7 T3SS. Further biological studies also revealed the main protein target of this new class of anti-virulence compounds, enabling future investigations in the pursuit of new and more potent molecules against the T3SS.

# Table of Contents

|  |    |
|--|----|
| Author's declaration.....  | 2  |
| Acknowledgements .....   | 3  |
| Abstract .....   | 4  |
| List of Figures .....  | 11 |
| List of Tables .....   | 13 |
| Abbreviations.....   | 15 |
| Introduction .....   | 20 |
| 1 <i>Escherichia coli</i> O157:H7 .....  | 21 |
| 2 <i>E. coli</i> O157:H7 virulence factors.....                                      | 22 |
| 2.1 Type three secretion system (T3SS) .....   | 22 |
| 2.2 Locus of enterocyte effacement (LEE).....  | 25 |
| 2.3 Effector proteins .....  | 28 |
| 2.4 Shiga toxin .....  | 28 |
| 3 Therapies for EHEC infection.....  | 29 |
| 4 Anti-virulence compounds .....   | 30 |
| 4.1 Quorum sensing inhibitors .....  | 30 |
| 4.2 Adhesin inhibitors .....   | 32 |
| 4.3 T3SS inhibitors .....  | 34 |
| 4.3.1 Natural products.....  | 35 |
| 4.3.2 Other synthetic T3SS inhibitors .....  | 37 |
| 4.3.3 Salicylidene acylhydrazide (SA).....   | 38 |
| 4.3.4 Mode of action of SA compounds .....   | 42 |
| 5 Aims of the project .....  | 43 |
| Results and Discussion .....   | 45 |
| 6 Introduction .....   | 46 |
| 7 1,4,5,6-Tetrahydropyridazine (THP) and 1,2-Dihydrophthalazine (DHP) Derivatives... | 48 |
| 7.1 Design and rationale of the THP and DHP cores.....                               | 48 |
| 7.2 Synthesis of the THP and DHP derivatives .....                                   | 49 |
| 7.3 Biological evaluation of the THP and DHP derivatives.....                        | 51 |
| 7.3.1 Bacterial growth .....   | 51 |
| 7.3.2 THP and DHP screening .....  | 53 |

|  |           |
|--|-----------|
| 7.3.4 Western blot analyses for RCZ12 and RCZ20 .....              | 54        |
| 7.3.5 T3SS genes transcription.....                                | 58        |
| 7.3.6 Additional transcriptional evaluation .....                  | 61        |
| 7.3.7 Transmission electron microscopy (TEM) experiment .....      | 63        |
| <b>7.4 Conclusions .....</b>                                       | <b>64</b> |
| <b>8 Understanding RCZ12 and RCZ20 Mode of Action .....</b>        | <b>67</b> |
| 8.1 Introduction .....   | 67        |
| 8.2 Design of RCZ12 and RCZ20 labelled version.....                | 67        |
| 8.3 Alternative route for RCZ12 and RCZ20 synthesis .....          | 68        |
| 8.4 Pull-down assay .....  | 70        |
| 8.4.1 Synthesis of biotinylated RCZ12 and RCZ20 .....              | 71        |
| 8.4.2 Pull-down assay results.....                                 | 73        |
| 8.4.3 Conclusions .....  | 75        |
| 8.5 Metabolomics analysis .....                                    | 76        |
| 8.6 Surface plasmon resonance (SPR).....                           | 77        |
| 8.6.1 SPR analysis with biotinylated RCZ12 and RCZ20 .....         | 78        |
| 8.6.2 Synthesis of amino-labelled RCZ12 and RCZ20.....             | 78        |
| 8.6.3 SPR analysis with amino-labelled RCZ12 and RCZ20 .....       | 79        |
| 8.7 Micro-scale thermophoresis (MST).....                          | 79        |
| 8.7.1 Synthesis of BODIPY-labelled RCZ12 and RCZ20.....            | 80        |
| 8.7.2 MST analysis with BODIPY-labelled RCZ12 and RCZ20 .....      | 81        |
| 8.7.3 Generation of <i>ΔespD</i> pRZ001 strain.....                | 81        |
| 8.7.4 MST analysis with EspD-GFP .....                             | 82        |
| 8.7.5 Pull-down assay with EspD-GFP.....                           | 84        |
| 8.8 Generation of truncated-EspD-HA strains.....                   | 85        |
| 8.8.1 Creation of TUV 93-0 EspD-HA .....                           | 86        |
| 8.8.2 Creation of truncated-EspD-HA strains.....                   | 87        |
| 8.8.3 Western blot analysis with RCZ12 .....                       | 88        |
| 8.9 Conclusions and future work.....                               | 90        |
| <b>9 RCZ12 and RCZ20 Derivatives.....</b>                          | <b>93</b> |
| 9.1 Structural analysis on RCZ12 and RCZ20 .....                   | 93        |
| 9.2 Synthesis of RCZ12 and RCZ20 derivatives .....                 | 95        |
| 9.3 Conclusions and future work.....                               | 96        |
| <b>10 [1,2,4]-Triazolo[4,3-b]pyridazine (TZP) Derivatives.....</b> | <b>98</b> |
| 10.1 Design and rationale of the TZP core .....                    | 98        |
| 10.2 Synthesis of the TZP derivative.....                          | 99        |
| 10.3 Biological evaluation of RCZ57.....                           | 100       |
| 10.3.1 Bacterial growth .....                                      | 100       |
| 10.3.2 RCZ57 vs. ME0055 .....                                      | 101       |
| 10.3.3 RCZ57 vs. RCZ12.....  | 102       |

|  |            |
|--|------------|
| 10.3.4 Transcriptional effects of RCZ57 .....  | 103        |
| 10.3.5 Secreted protein profile.....   | 104        |
| 10.3.6 Transmission electron microscopy (TEM) analysis .....                                       | 106        |
| 10.3.7 Metabolomics analysis for RCZ57 .....   | 107        |
| <b>10.4 Synthesis of RCZ57 modular derivatives .....</b>   | <b>108</b> |
| <b>10.5 Biological evaluation of RCZ57 modular derivatives.....</b>                                | <b>110</b> |
| 10.5.1 Bacterial growth .....  | 110        |
| 10.5.2 Virulence protein secretion .....   | 111        |
| 10.5.3 Structure-activity relationship (SAR) .....   | 112        |
| <b>10.6 Conclusions and future work .....</b>  | <b>113</b> |
| <b>11 Final Discussion .....</b>   | <b>115</b> |
| 11.1 RCZ12 and RCZ20.....  | 115        |
| 11.2 The future of RCZ12 and RCZ20 .....   | 117        |
| 11.3 RCZ57 .....   | 118        |
| 11.4 The future of RCZ57 .....   | 119        |
| 11.5 Conclusion.....   | 120        |
| <b>References .....</b>  | <b>121</b> |
| <b>Appendix.....</b>   | <b>141</b> |
| <b>Experimental Part .....</b>   | <b>147</b> |
| <b>12 Chemistry experimental part .....</b>  | <b>148</b> |
| <b>12.1 Procedure for Friedel-Crafts acylation: .....</b>  | <b>148</b> |
| 4-(2,4-Dimethoxy-phenyl)-4-oxo-butyric acid (18):.....   | 148        |
| 2-(2,4-Dimethoxy-benzoyl)-benzoic acid (19): .....   | 149        |
| <b>12.2 Procedure for hydrazine coupling:.....</b>   | <b>149</b> |
| 6-(2,4-Dimethoxy-phenyl)-4,5-dihydro-2H-pyridazin-3-one (20): .....                                | 149        |
| 4-(2,4-Dimethoxy-phenyl)-2H-phthalazin-1-one (21):.....  | 150        |
| <b>12.3 Procedure for LiAlH<sub>4</sub> reduction (Combs et al., 1995): .....</b>                  | <b>150</b> |
| 3-(2,4-Dimethoxy-phenyl)-1,4,5,6-tetrahydro-pyridazine (22): .....                                 | 150        |
| 4-(2,4-Dimethoxy-phenyl)-1,2-dihydro-phthalazine (23): .....                                       | 151        |
| <b>12.4 Procedure for acylation/sulphonylation: .....</b>  | <b>151</b> |
| [3-(2,4-Dimethoxy-phenyl)-5,6-dihydro-4H-pyridazin-1-yl]-(4-nitro-phenyl)-methanone (RCZ09): ..... | 151        |
| 3-(2,4-Dimethoxy-phenyl)-1-(4-nitro-benzenesulphonyl)-1,4,5,6-tetrahydro-pyridazine (RCZ11): ..... | 152        |
| [4-(2,4-Dimethoxy-phenyl)-1H-phthalazin-2-yl]-(4-nitro-phenyl)-methanone (RCZ17): .....            | 152        |
| 4-(2,4-Dimethoxy-phenyl)-2-(4-nitro-benzenesulphonyl)-1,2-dihydro-phthalazine (RCZ19):.....        | 153        |
| <b>12.5 Procedure for de-methylation: .....</b>  | <b>153</b> |
| [3-(2,4-Dihydroxy-phenyl)-5,6-dihydro-4H-pyridazin-1-yl]-(4-nitro-phenyl)-methanone (RCZ10):.....  | 154        |
| 4-[1-(4-Nitro-benzenesulphonyl)-1,4,5,6-tetrahydro-pyridazin-3-yl]-benzene-1,3-diol (RCZ12): ..... | 154        |
| [4-(2,4-Dihydroxy-phenyl)-1H-phthalazin-2-yl]-(4-nitro-phenyl)-methanone (RCZ18): .....            | 155        |
| 4-[3-(4-Nitro-benzenesulphonyl)-3,4-dihydro-phthalazin-1-yl]-benzene-1,3-diol (RCZ20): .....       | 155        |

|  |            |
|--|------------|
| <b>12.6 Alternative synthesis of RCZ12 and RCZ20 .....</b>   | <b>156</b> |
| 4-(6-Chloro-pyridazin-3-yl)-benzene-1,3-diol (Pal, Batchu, & Parasuraman, 2003) (25): .....  | 156        |
| 3-Chloro-6-(2,4-diisopropoxy-phenyl)-pyridazine (26): .....  | 156        |
| 6-(2,4-Diisopropoxy-phenyl)-2H-pyridazin-3-one (Pal, Batchu, & Parasuraman, 2003) (27): .....  | 157        |
| 3-(2,4-Diisopropoxy-phenyl)-1,4,5,6-tetrahydro-pyridazine (Combs et al., 1995) (28): .....   | 157        |
| 3-(2,4-Diisopropoxy-phenyl)-1-(4-nitro-benzenesulphonyl)-1,4,5,6-tetrahydro-pyridazine (29): .....   | 158        |
| 4-[1-(4-Nitro-benzenesulphonyl)-1,4,5,6-tetrahydro-pyridazin-3-yl]-benzene-1,3-diol (RCZ12): .....   | 158        |
| 1,4-Dichloro-phthalazine (31): .....   | 159        |
| 4-(4-Chloro-phthalazin-1-yl)-benzene-1,3-diol (Pal, Batchu, & Parasuraman, 2003) (32): .....   | 159        |
| 1-Chloro-4-(2,4-diisopropoxy-phenyl)-phthalazine (33): .....   | 160        |
| 4-(2,4-Diisopropoxy-phenyl)-2H-phthalazin-1-one (Pal, Batchu, & Parasuraman, 2003) (34): .....   | 160        |
| 4-(2,4-Diisopropoxy-phenyl)-1,2-dihydro-phthalazine (Combs et al., 1995) (35): .....   | 161        |
| 4-(2,4-Diisopropoxy-phenyl)-2-(4-nitro-benzenesulphonyl)-1,2-dihydro-phthalazine (36): .....   | 161        |
| 4-[3-(4-Nitro-benzenesulphonyl)-3,4-dihydro-phthalazin-1-yl]-benzene-1,3-diol (RCZ20): .....   | 162        |
| <b>12.7 Procedure for allylation: .....</b>  | <b>163</b> |
| 3-(2,4-Bis-allyloxy-phenyl)-1-(4-nitro-benzenesulphonyl)-1,4,5,6-tetrahydro-pyridazine (37): .....   | 163        |
| 4-(2,4-Bis-allyloxy-phenyl)-2-(4-nitro-benzenesulphonyl)-1,2-dihydro-phthalazine (38): .....   | 163        |
| <b>12.8 Procedure for nitro reduction: .....</b>   | <b>164</b> |
| 4-[3-(2,4-Bis-allyloxy-phenyl)-5,6-dihydro-4H-pyridazine-1-sulphonyl]-phenylamine (39): .....  | 164        |
| 4-[4-(2,4-Bis-allyloxy-phenyl)-1H-phthalazine-2-sulphonyl]-phenylamine (40): .....   | 165        |
| <b>12.9 Procedure for hex-5-ynoyl chloride coupling: .....</b>   | <b>166</b> |
| Hex-5-ynoyl Chloride: .....  | 166        |
| Hex-5-ynoic acid {4-[3-(2,4-bis-allyloxy-phenyl)-5,6-dihydro-4H-pyridazine-1-sulphonyl]-phenyl}-amide (RCZ12 Synthon): .....   | 166        |
| Hex-5-ynoic acid {4-[4-(2,4-bis-allyloxy-phenyl)-1H-phthalazine-2-sulphonyl]-phenyl}-amide (RCZ20 Synthon): .....  | 167        |
| (+)-Biotin N-succinimidyl ester (W. L. Yu et al., 2010) (41): .....  | 168        |
| 3-Azidopropylamine (Zabrodski, Baskin, Kaniraj, & Maayan, 2014) (43): .....  | 168        |
| 5-(2-Oxo-hexahydro-thieno[3,4-d]imidazol-4-yl)-pentanoic acid (3-azido-propyl)-amide (Biotin Synthon): .....   | 168        |
| <b>12.10 Procedure for click reaction (Biotin Labelling): .....</b>  | <b>169</b> |
| 5-(2-Oxo-hexahydro-thieno[3,4-d]imidazol-4-yl)-pentanoic acid {3-[4-(3-[4-(3-(2,4-bis-allyloxy-phenyl)-5,6-dihydro-4H-pyridazine-1-sulphonyl]-phenylcarbamoyl)-propyl)-[1,2,3]triazol-1-yl]-propyl}-amide (44): .....        | 169        |
| 5-(2-Oxo-hexahydro-thieno[3,4-d]imidazol-4-yl)-pentanoic acid {3-[4-(3-[4-(2,4-bis-allyloxy-phenyl)-1H-phthalazine-2-sulphonyl]-phenylcarbamoyl)-propyl)-[1,2,3]triazol-1-yl]-propyl}-amide (45): .....                      | 170        |
| <b>12.11 Procedure for click reaction (BODIPY Labelling): .....</b>  | <b>171</b> |
| BODIPY-Allyl-RCZ12 (48): .....   | 172        |
| BODIPY-Allyl-RCZ20 (49): .....   | 172        |
| <b>12.12 Procedure for de-allylation: .....</b>  | <b>173</b> |
| 5-(2-Oxo-hexahydro-thieno[3,4-d]imidazol-4-yl)-pentanoic acid {3-[4-(3-[4-(3-(2,4-dihydroxy-phenyl)-5,6-dihydro-4H-pyridazine-1-sulphonyl]-phenylcarbamoyl)-propyl)-[1,2,3]triazol-1-yl]-propyl}-amide (Biotin-RCZ12): ..... | 174        |
| 5-(2-Oxo-hexahydro-thieno[3,4-d]imidazol-4-yl)-pentanoic acid {3-[4-(3-[4-(2,4-dihydroxy-phenyl)-1H-phthalazine-2-sulphonyl]-phenylcarbamoyl)-propyl)-[1,2,3]triazol-1-yl]-propyl}-amide (Biotin-RCZ20): .....               | 174        |
| BODIPY-RCZ12: .....  | 175        |
| BODIPY-RCZ20: .....  | 176        |
| <b>12.13 Procedure for 6-azido-hexanoyl chloride coupling: .....</b>   | <b>177</b> |

|   |            |
|---|------------|
| 6-Azido-hexanoic acid (Beld et al., 2014): .....  | 177        |
| 6-Azido-hexanoyl chloride: .....  | 177        |
| 6-Azido-hexanoic acid {4-[3-(2,4-bis-allyloxy-phenyl)-5,6-dihydro-4H-pyridazine-1-sulphonyl]-phenyl}-amide (46): .....                  | 177        |
| 6-Azido-hexanoic acid {4-[4-(2,4-bis-allyloxy-phenyl)-1H-phthalazine-2-sulphonyl]-phenyl}-amide (47): .....                             | 178        |
| 6-Azido-hexanoic acid {4-[3-(2,4-dihydroxy-phenyl)-5,6-dihydro-4H-pyridazine-1-sulphonyl]-phenyl}-amide: ...                            | 179        |
| 6-Azido-hexanoic acid {4-[4-(2,4-dihydroxy-phenyl)-1H-phthalazine-2-sulphonyl]-phenyl}-amide: .....                                     | 180        |
| <b>12.14 Procedure for Staudinger reaction: .....</b>   | <b>180</b> |
| 6-Amino-hexanoic acid {4-[3-(2,4-dihydroxy-phenyl)-5,6-dihydro-4H-pyridazine-1-sulphonyl]-phenyl}-amide (NH <sub>2</sub> -RCZ12): ..... | 180        |
| 6-Amino-hexanoic acid {4-[4-(2,4-dihydroxy-phenyl)-1H-phthalazine-2-sulphonyl]-phenyl}-amide (NH <sub>2</sub> -RCZ20): .....            | 181        |
| <b>12.15 General Procedure for sulphonylation/de-protection: .....</b>  | <b>182</b> |
| 4-(1-Benzenesulphonyl)-1,4,5,6-tetrahydro-pyridazin-3-yl)-benzene-1,3-diol (RCZ30): .....   | 182        |
| 4-[1-(Toluene-4-sulphonyl)-1,4,5,6-tetrahydro-pyridazin-3-yl]-benzene-1,3-diol (RCZ32): .....   | 183        |
| 4-(1-Methanesulphonyl)-1,4,5,6-tetrahydro-pyridazin-3-yl)-benzene-1,3-diol (RCZ31): .....   | 183        |
| 4-[1-(Octane-1-sulphonyl)-1,4,5,6-tetrahydro-pyridazin-3-yl]-benzene-1,3-diol (RCZ35): .....  | 183        |
| 4-[1-(4-Trifluoromethyl-benzenesulphonyl)-1,4,5,6-tetrahydro-pyridazin-3-yl]-benzene-1,3-diol (RCZ34): .....                            | 184        |
| 4-[1-(4-Isopropyl-benzenesulfonyl)-1,4,5,6-tetrahydro-pyridazin-3-yl]-benzene-1,3-diol (RCZ33): .....                                   | 184        |
| 4-[1-(3-Nitro-benzenesulphonyl)-1,4,5,6-tetrahydro-pyridazin-3-yl]-benzene-1,3-diol (RCZ36): .....                                      | 185        |
| <b>12.16 General Procedure for sulphonylation/de-protection: .....</b>  | <b>185</b> |
| 4-(3-Benzenesulphonyl)-3,4-dihydro-phthalazin-1-yl)-benzene-1,3-diol (RCZ40): .....   | 186        |
| 4-[3-(Toluene-4-sulphonyl)-3,4-dihydro-phthalazin-1-yl]-benzene-1,3-diol (RCZ42): .....   | 186        |
| 4-(3-Methanesulphonyl)-3,4-dihydro-phthalazin-1-yl)-benzene-1,3-diol (RCZ41): .....   | 187        |
| 4-[3-(Octane-1-sulphonyl)-3,4-dihydro-phthalazin-1-yl]-benzene-1,3-diol (RCZ45): .....  | 187        |
| 4-[3-(4-Trifluoromethyl-benzenesulphonyl)-3,4-dihydro-phthalazin-1-yl]-benzene-1,3-diol (RCZ44): .....                                  | 188        |
| 4-[3-(4-Isopropyl-benzenesulphonyl)-3,4-dihydro-phthalazin-1-yl]-benzene-1,3-diol (RCZ43): .....  | 188        |
| 4-[3-(3-Nitro-benzenesulphonyl)-3,4-dihydro-phthalazin-1-yl]-benzene-1,3-diol (RCZ46): .....  | 189        |
| <b>12.17 Procedure for triazole formation (Albright et al., 1981): .....</b>  | <b>189</b> |
| 6-(2,4-Diisopropoxy-phenyl)-3-(4-nitro-phenyl)-[1,2,4]triazolo[4,3-b]pyridazine (50) and (RCZ60): .....                                 | 190        |
| 6-(2,4-Diisopropoxy-phenyl)-3-(4-nitro-phenyl)-[1,2,4]triazolo[3,4-a]phthalazine (52): .....  | 190        |
| 6-(2,4-Diisopropoxy-phenyl)-3-(phenyl)-[1,2,4]triazolo[4,3-b]pyridazine (51): .....   | 191        |
| <b>12.18 Procedure for isopropyl de-protection: .....</b>   | <b>191</b> |
| 4-[3-(4-Nitro-phenyl)-[1,2,4]triazolo[4,3-b]pyridazin-6-yl]-benzene-1,3-diol (RCZ57): .....   | 191        |
| 4-[3-(4-Nitro-phenyl)-[1,2,4]triazolo[3,4-a]phthalazin-6-yl]-benzene-1,3-diol (RCZ59): .....  | 192        |
| 4-[3-(Phenyl)-[1,2,4]triazolo[4,3-b]pyridazin-6-yl]-benzene-1,3-diol (RCZ58): .....   | 192        |
| <b>13 Biology experimental part .....</b>   | <b>193</b> |
| <b>13.1 Strains, plasmids, growth media and storage .....</b>   | <b>193</b> |
| 13.1.1 Growth media .....   | 193        |
| 13.1.2 Strains .....  | 194        |
| 13.1.3 Plasmids .....   | 195        |
| 13.1.4 Storage of bacteria .....  | 196        |
| 13.1.5 Growth of bacteria .....   | 196        |

|   |            |
|---|------------|
| <b>13.2 Molecular techniques.....</b>                                       | <b>196</b> |
| 13.2.1 Preparation of genomic DNA .....                                     | 196        |
| 13.2.2 Oligonucleotide primers .....  | 196        |
| 13.2.3 Polymerase chain reaction (PCR) .....                                | 197        |
| 13.2.4 High-fidelity polymerase chain reaction (HF-PCR) .....               | 198        |
| 13.2.5 Agarose gel electrophoresis .....                                    | 198        |
| 13.2.6 Restriction enzyme digestion.....                                    | 199        |
| 13.2.7 DNA gel purification.....  | 199        |
| 13.2.8 Ligation reaction .....  | 199        |
| 13.2.9 Plasmid assembly reaction .....                                      | 200        |
| 13.2.10 Heat shock transformation .....                                     | 200        |
| 13.2.11 Production of electrocompetent <i>E. coli</i> .....                 | 200        |
| 13.2.12 Electroporation transformation.....                                 | 201        |
| 13.2.13 Extraction of plasmid DNA.....                                      | 201        |
| 13.2.14 Creation of TUV 93-0 EspD-HA strain by allelic exchange .....       | 201        |
| 13.2.15 Creation of plasmids for TUV 93-0 EspD-HA allelic exchange.....     | 202        |
| 13.2.16 Creation of truncated-EspD-HA strains by allelic exchange.....      | 203        |
| 13.2.17 Creation of plasmids for truncated-EspD-HA allelic exchange .....   | 204        |
| <b>13.3 Biochemical techniques.....</b>                                     | <b>210</b> |
| 13.3.1 SDS-PAGE .....   | 210        |
| 13.3.2 Western blot .....   | 210        |
| 13.3.3 Pull-down assay with biotinylated RCZ12 and RCZ20 .....              | 211        |
| 13.3.4 Sample preparation for metabolomics analysis .....                   | 212        |
| <b>13.4 Transcriptome analysis.....</b>                                     | <b>213</b> |
| 13.4.1 Total RNA extraction and mRNA enrichment .....                       | 213        |
| 13.4.2 RNA-sequencing and transcriptome analysis .....                      | 213        |
| <b>13.5 Phenotypic characterisation techniques .....</b>                    | <b>214</b> |
| 13.5.1 <i>E. coli</i> O157 secreted protein profiling .....                 | 214        |
| 13.5.2 GFP reporter fusion assay.....                                       | 214        |
| <b>13.6 Microscopy techniques.....</b>                                      | <b>215</b> |
| 13.6.1 Transmission electron microscopy (TEM).....                          | 215        |
| 13.6.2 Transmission electron microscopy (TEM) for membrane morphology ..... | 215        |
| <b>13.7 Bioinformatics and statistical analysis .....</b>                   | <b>216</b> |
| 13.7.1 Bioinformatic and database tools.....                                | 216        |
| 13.7.2 Statistical analysis .....   | 216        |

## List of Figures

|  |    |
|--|----|
| Fig. 1: EHEC T3SS: .....   | 23 |
| Fig. 2: Genetic organisation of the LEE pathogenicity island in EHEC: .....  | 26 |
| Fig. 3: Regulation of the LEE pathogenicity island: .....  | 27 |
| Fig. 4: QseC signalling pathway (left) and the chemical structure of LED209 (right):.....  | 30 |
| Fig. 5: Pilus biogenesis (left) and the chemical structure of the tyrosine derivative 1 and pyridinone 2 (right):.....   | 32 |
| Fig. 6: SAR studies on the pyridinone 2:.....  | 33 |
| Fig. 7: Chemical structure of known non-natural T3SS inhibitors: .....   | 37 |
| Fig. 8: Scaffold hopping based on the SA compounds core: .....   | 41 |
| Fig. 9: Chemical structures of relevant hydrazine-containing heterocycle drugs.....  | 46 |
| Fig. 10: Rational design of the THP and DHP cores:.....  | 48 |
| Fig. 11: Synthetic route for THP and DHP derivatives: .....  | 50 |
| Fig. 12: Synthesis of sulphonyl THP and DHP derivatives: .....   | 50 |
| Fig. 13: $\alpha$ -EspD Western blot for THP and DHP derivatives at 50 $\mu$ M (top) and plotted relative EspD secretion percentage graph (bottom): .....  | 53 |
| Fig. 14: $\alpha$ -Tir (S/N), $\alpha$ -EspD (S/N and W/C) and $\alpha$ -GroEL (W/C) Western blots for RCZ12 and RCZ20 at 50 $\mu$ M: .....  | 54 |
| Fig. 15: $\alpha$ -EspD Western blot for RCZ12 and RCZ20 (200 $\mu$ M - 10 $\mu$ M) (left) and $\alpha$ -EspD, $\alpha$ -Tir and $\alpha$ -GroEL Western blot for RCZ12 and RCZ20 at 200 $\mu$ M (right):..... | 57 |
| Fig. 16: RNAseq data summary and LEE-related genes heatmap: .....  | 58 |
| Fig. 17: <i>rpsM:gfp</i> , <i>LEE1:gfp</i> and <i>tir:gfp</i> promoter activity at OD <sub>600</sub> = 0.6 with ME0055, RCZ12 and RCZ20 at 50 and 200 $\mu$ M: .....   | 59 |
| Fig. 18: $\Delta espD$ <i>LEE1:gfp</i> and $\Delta espD$ <i>tir:gfp</i> promoter activity at OD <sub>600</sub> = 0.7 compared with their TUV 93-0 counterpart and with RCZ12 and RCZ20 at 200 $\mu$ M:.....    | 62 |
| Fig. 19: TEM images of EspA filaments with RCZ12 and RCZ20: .....  | 64 |
| Fig. 20: Design of RCZ12 and RCZ20 labelled version:.....  | 68 |
| Fig. 21: New synthetic route for RCZ12: .....  | 68 |
| Fig. 22: New synthetic route for RCZ20: .....  | 69 |
| Fig. 23: Retrosynthetic scheme of Biotin-RCZ12 and Biotin-RCZ20: .....   | 71 |
| Fig. 24: Synthetic route for RCZ12 and RCZ20 synthons: .....   | 72 |
| Fig. 25: Synthetic route for Biotin Synthons: .....  | 72 |
| Fig. 26: Huisgen 1,3-dipolar cycloaddition and synthesis of biotin-RCZ12 and 20: .....   | 73 |



|  |     |
|--|-----|
| Fig. 27: SDS-PAGE gel for the pull-down assay: .....   | 75  |
| Fig. 28: Synthetic route for amino-labelled RCZ12 and RCZ20:.....  | 78  |
| Fig. 29: Synthetic route for BODIPY-labelled RCZ12 and RCZ20:.....   | 80  |
| Fig. 30: Western blot results for $\alpha$ -EspD and $\alpha$ -GFP antibodies (left) and GFP intensity of the $\Delta$ espD pRZ001 strain (right):.....  | 82  |
| Fig. 31: SDS-PAGE gel for the pull-down assay with $\Delta$ espD pRZ001 strain: .....  | 84  |
| Fig. 32: TUV 93-0 EspD-HA Western blot analysis: .....   | 86  |
| Fig. 33: Western blots of the truncated-EspD-HA producing strains (left) and cartoon showing the 4 deleted functional regions of EspD (right):.....  | 88  |
| Fig. 34: Western blot analyses of truncated-EspD-HA strains with and without RCZ12 treatment at 200 $\mu$ M:.....  | 89  |
| Fig. 35: Rational design of RCZ12 and RCZ20 derivatives: .....   | 93  |
| Fig. 36: Synthetic route for RCZ12 and RCZ20 derivatives: .....  | 95  |
| Fig. 37: Design of the TZP core:.....  | 98  |
| Fig. 38: Synthetic route for the TZP derivative: .....   | 99  |
| Fig. 39: Bacterial growth evaluation: .....  | 100 |
| Fig. 40: $\alpha$ -EspD, $\alpha$ -Tir and $\alpha$ -GroEL Western blot for ME0055 and RCZ57 at 200 $\mu$ M (left) and $\alpha$ -EspD Western blot with decreasing concentrations of RCZ57 (right):..... | 101 |
| Fig. 41: $\alpha$ -EspD, $\alpha$ -Tir and $\alpha$ -GroEL Western blot for RCZ12 and RCZ57 at 200 $\mu$ M (left): ..  | 103 |
| Fig. 42: <i>rpsM:gfp</i> and <i>LEE1:gfp</i> promoter activity at OD <sub>600</sub> = 0.6 with ME0055 and RCZ57 at 200 $\mu$ M: .....  | 104 |
| Fig. 43: SDS-PAGE electrophoresis of secreted proteins (left) and the list of identified proteins by tandem mass spectrometry (right):.....  | 105 |
| Fig. 44: TEM images of EspA filaments with RCZ57:.....   | 107 |
| Fig. 45: Structural design of RCZ57 modular derivatives:.....  | 108 |
| Fig. 46: RCZ58 synthesis: .....  | 109 |
| Fig. 47: RCZ59 synthesis: .....  | 109 |
| Fig. 48: Bacterial growth evaluation: .....  | 110 |
| Fig. 49: $\alpha$ -EspD $\alpha$ -Tir and $\alpha$ -GroEL Western blot for RCZ57 modular derivatives RCZ58, RCZ59 and RCZ60 at 200 $\mu$ M:.....   | 112 |
| Fig. 50: TEM images of sectioned bacteria treated with RCZ57:.....   | 146 |
| Fig. 51: Alignment of EspD amino acid sequence from EHEC, EPEC, <i>C. rodentium</i> , <i>Y. pseudotuberculosis</i> and <i>S. typhimurium</i> and calculated percentage of homology: ...                  | 146 |

|  |     |
|--|-----|
| Fig. 52: Creation of temperature sensitive plasmids for allelic exchange:.....         | 204 |
| Fig. 53: Creation of TUV 93-0 $\Delta espD$ - <i>sacBkan</i> intermediate strain:..... | 206 |
| Fig. 54: Creation of TUV 93-0 EspD-HA strain:.....                                     | 207 |
| Fig. 55: Creation of truncated EspD-HA strains: .....                                  | 209 |

## List of Tables

|   |     |
|---|-----|
| Table 1: Nomenclature of homologous T3SS proteins in <i>E. coli</i> , <i>C. rodentium</i> , <i>Yersinia</i> sp. and <i>Salmonella</i> sp.:..... | 25  |
| Table 2: List of active natural products against T3SS:.....   | 35  |
| Table 3: List of the SA compounds active against T3SS: .....  | 40  |
| Table 4: Bacterial growth after 5 hours of incubation:.....   | 52  |
| Table 5: Colony count for RCZ12 and RCZ20 at 200 $\mu$ M: .....   | 55  |
| Table 6: Summary of the effects of RCZ20 on LEE-related genes expression as identified by RNAseq experiment:.....                               | 60  |
| Table 7: Determination of the number of EspA filaments (>500 nm) for bacteria treated with RCZ12 and RCZ20: .....                               | 63  |
| Table 8: Metabolomics data for RCZ12 and RCZ20 cellular uptake: .....   | 77  |
| Table 9: RCZ12 and RCZ20 derivatives yields:.....   | 96  |
| Table 10: Metabolomics data for RCZ12 and RCZ20 cellular uptake: .....  | 108 |
| Table 11: List of protein identified by the first pull-down assay with biotin-RCZ12 and biotin-RCZ20: .....                                     | 142 |
| Table 12: List of protein identified by the second pull-down assay with biotin-RCZ12 and biotin-RCZ20: .....                                    | 142 |
| Table 13: List of additional genes influenced by RCZ20 at 50 $\mu$ M: .....   | 144 |
| Table 14: Functioning EspA filaments (>500 nm) for the TEM experiment with RCZ57: ...   | 146 |
| Table 15: Media recipes. ....   | 193 |
| Table 16: List of strains used and generated in this study. ....  | 194 |
| Table 17: List of plasmids used and generated in this study. ....   | 195 |
| Table 18: List of oligonucleotides used in this study. ....   | 197 |
| Table 19: Standard PCR cycle conditions (30 cycles) .....   | 198 |
| Table 20: Coomassie Brilliant Blue stain recipe. ....   | 210 |
| Table 21: Destain solution recipe .....   | 210 |

|   |     |
|---|-----|
| Table 22: Antibodies and relevant concentrations used in this study ..... | 211 |
|---|-----|

## Abbreviations

|        |   |
|--------|---|
| °C     | Degrees Celsius                                 |
| Δ      | Deletion  |
| AdhE   | Bifunctional acetaldehyde/alcohol dehydrogenase |
| A/E    | Attaching and effacing                          |
| Amp    | Ampicillin                                      |
| Arg    | Arginine  |
| AV     | Anti-virulence                                  |
| AI     | Autoinducer                                     |
| BODIPY | Boron-dipyrromethene                            |
| bp     | Base pair                                       |
| CFU    | Colony forming unit                             |
| Chl    | Chloramphenicol                                 |
| COX-2  | Cyclooxygenase-2                                |
| DCE    | Dichloroethane                                  |
| DCM    | Dichloromethane                                 |
| DIPEA  | Diisopropylethylamine                           |
| DMAP   | 4-Dimethylaminopyridine                         |
| DMF    | Dimethylformamide                               |
| DMSO   | Dimethylsulphoxide                              |
| DNA    | Deoxyribonucleic acid                           |
| DHP    | 1,2-Dihydrophthalazine                          |
| EAEC   | Enteraggregative <i>Escherichia coli</i>        |
| ECL    | Enhanced chemi-luminescence                     |
| EDC    | 1-Ethyl-3-(3-dimethylaminopropyl)carbodiimide   |
| EHEC   | Enterohaemorrhagic <i>Escherichia coli</i>      |
| EIEC   | Enteroinvasive <i>Escherichia coli</i>          |
| EPEC   | Enteropathogenic <i>Escherichia coli</i>        |
| ESI    | Electrospray ionisation                         |
| ETEC   | Enterotoxigenic <i>Escherichia coli</i>         |
| FolX   | 7,8-dihydroneopterin-triphosphate-epimerase     |
| g      | Gram  |
| gDNA   | Genomic DNA                                     |
| GFP    | Green fluorescent protein                       |

|                  |  |
|------------------|--|
| GI tract         | Gastrointestinal tract                             |
| GrIA/R           | Global regulator of LEE-activator/repressor        |
| h                | Hour   |
| HA               | Haemagglutinin                                     |
| HEPES            | 4-(2-hydroxyethyl)-1-piperazineethanesulfonic acid |
| HGT              | Horizontal gene transfer                           |
| HRP              | Horseradish peroxidase                             |
| IC <sub>50</sub> | Half maximal inhibitory concentration              |
| ITC              | Isothermal titration calorimetry                   |
| Kan              | Kanamycin  |
| Kb               | Kilobase pair                                      |
| KDa              | Kilodalton   |
| L                | Litre  |
| LB               | Luria-Bertani broth                                |
| LEE              | Locus of enterocyte effacement                     |
| Ler              | LEE-encoded regulator                              |
| LogP             | Partition coefficient                              |
| Lys              | Lysine   |
| MEM              | Minimum essential media                            |
| mg               | Milligram(s)                                       |
| MHz              | Megahertz  |
| min              | Minute(s)  |
| mL               | Millilitre(s)                                      |
| mM               | Millimolar   |
| MNEC             | Meningitis associated <i>Escherichia coli</i>      |
| m.p.             | Melting point                                      |
| mRNA             | Messenger ribonucleic acid                         |
| MST              | Microscale thermophoresis                          |
| MW               | Molecular weight                                   |
| NADH             | Nicotinamide adenine dinucleotide                  |
| NHS              | N-Hydroxysuccinimide                               |
| Nle              | Non-LEE encoded effector(s)                        |
| nm               | Nanometer  |

|                   |  |
|-------------------|--|
| nM                | Nanomolar  |
| NSAID             | Non-steroidal anti-inflammatory drug                       |
| NMR               | Nuclear magnetic resonance                                 |
| OD <sub>600</sub> | Optical density at 600 nm                                  |
| ORF               | Open reading frame   |
| PAI               | Pathogenicity island                                       |
| PARP              | Poly ADP ribose polymerase                                 |
| PBS               | Phosphate buffered saline                                  |
| PCR               | Polymerase chain reaction                                  |
| RAJ               | Rectal-anal junction                                       |
| rpm               | Revolutions per minute                                     |
| rt                | Room temperature   |
| SA                | Salicylidene acylhydrazide                                 |
| SAR               | Structure-activity relationship                            |
| SDS-PAGE          | Sodium dodecyl sulphate-polyacrilamide gel electrophoresis |
| S/N               | Supernatant  |
| SPR               | Surface plasmon resonance                                  |
| Stx               | Shiga toxin  |
| T3SS              | Type three secretion system                                |
| TAE               | Tris-acetate EDTA  |
| TEA               | Triethylamine  |
| TEM               | Transmission electron microscopy                           |
| THF               | Tetrahydrofuran  |
| THP               | 1,4,5,6-Tetrahydro pyridazine                              |
| Tir               | Translocated intimin receptor                              |
| TLC               | Thin layer chromatography                                  |
| Tpx               | Thiol peroxidase   |
| TZP               | [1,2,4]-Triazolo[4,3-b]pyridazine                          |
| UK                | United Kingdom   |
| UPEC              | Uropathogenic <i>Escherichia coli</i>                      |
| USA               | United States of America                                   |
| UTI               | Urinary tract infection                                    |
| v/v               | Volume per volume  |

|               |                                      |
|---------------|--------------------------------------|
| W/C           | Whole cell lysate                    |
| WrbA          | Tryptophan repressor binding protein |
| WT            | Wild type                            |
| $\mu\text{L}$ | Microlitre(s)                        |
| $\mu\text{M}$ | Micromolar                           |
| $\mu\text{m}$ | Micron(s)                            |



## Introduction

## 1 *Escherichia coli* O157:H7

*Escherichia coli* (*E. coli*) is a rod-shaped Gram-negative bacterium belonging to the genus of the Enterobacteriaceae. This bacterium is one the best-studied prokaryotic organisms in research laboratories due to its fast growth and easy genetic manipulation. *E. coli* is considered a commensal bacterium and is found in the gastro-intestinal tract (GI tract) of warm-blooded animals, especially ruminants. In humans, *E. coli* can be found as part of the commensal microbiota in the mucosal surface of the colon. Under normal circumstances, this bacterium lives in a beneficial symbiotic relationship with its host. However, the acquisition of virulence factors generated pathogenic strains of *E. coli*, which mainly cause diarrhoeal disease, urinary tract infections (UTIs) and meningitis. Virulence factors are transferred between strains by horizontal gene transfer (HGT) or mobile gene elements; therefore, several pathogenic serotypes of *E. coli* employ homologous virulence systems <sup>1-3</sup>. A total of 5 diarrhoeagenic groups of *E. coli* has been identified: enteroaggregative *E. coli* (EAEC), enterohaemorrhagic *E. coli* (EHEC), enteropathogenic *E. coli* (EPEC), enteroinvasive *E. coli* (EIEC) and enterotoxigenic *E. coli* (ETEC) <sup>4</sup>. Urinary tract infections are mainly caused by strains belonging to the uropathogenic *E. coli* (UPEC) family <sup>5,6</sup>, while meningitis associated *E. coli* (MNEC) pathotypes are responsible for meningitis <sup>7</sup>.

*E. coli* O157:H7 belongs to the enterohaemorrhagic *E. coli* (EHEC) group and, according to the World Health Organisation, is considered the most dangerous serotype of this family (Organisation, 2011). The first outbreak of this bacterium was reported in 1982 and traced to the contamination of hamburger meat <sup>10</sup>. It is known that *E. coli* O157:H7 colonises cattle asymptotically in the rectal-anal junction (RAJ), facilitating the bacterium's shedding in the faeces <sup>11-13</sup>. Thus, infection in humans typically arise via the faecal-oral route from the consumption of contaminated meat and vegetables. Once the food is contaminated, the infective dose required to colonise a healthy individual is very low (estimated to be 50-100 colony-forming unit (CFUs)) <sup>14</sup>. Symptoms associated with *E. coli* O157:H7 infections are typically haemorrhagic colitis leading to bloody diarrhoea, severe abdominal cramps and haemolytic uremic syndrome (HUS), which is characterised by a combination of acute renal failure, thrombocytopenia and microangiopathic haemolytic anemia <sup>10,15</sup>. HUS onset is associated with the production of Shiga toxin (Stx), a cytotoxin capable of damaging both intestinal and renal tissue <sup>16</sup>. It is thought that the ability to produce Stx has been acquired by the enteropathogenic *E. coli* (EPEC) strain O55 through a Stx-encoding lambdoid-like bacteriophage, which lead to the generation of the EHEC strain

*E. coli* O157:H7<sup>3</sup>. It has also been demonstrated that traditional antibiotic treatments of *E. coli* O157:H7 infections resulted in an increase of diseases severity, promoting an enhanced release of Stx, which leads to HUS<sup>17</sup>. Selective treatments, such as anti-virulence (AV) compounds, might be the ideal solution for eradicating the infection without the release of the toxin, thus avoiding its harsh symptoms.

## 2 *E. coli* O157:H7 virulence factors

### 2.1 Type three secretion system (T3SS)

One of the main *E. coli* O157:H7 virulence factors is the type three secretion system (T3SS). The T3SS is a needle-like multi-protein complex that spans outside the bacterium and hijacks the host cell membrane. This injection system translocates effector proteins into the host cytoplasm to create a niche to allow bacterial colonisation<sup>18</sup>. The T3SS is also required for the intimate attachment of the bacterium to epithelial cells, which causes attaching and effacing (A/E) lesions, a characteristic trait of EHEC and EPEC infections<sup>19,20</sup>. The formation of these lesions is a complex process and it is initiated by specific translocated effector proteins which trigger actin and cytoskeleton rearrangements, resulting in the formation of “pedestal” structure and intimate bacterial attachment to the host cell<sup>19,21,22</sup>.

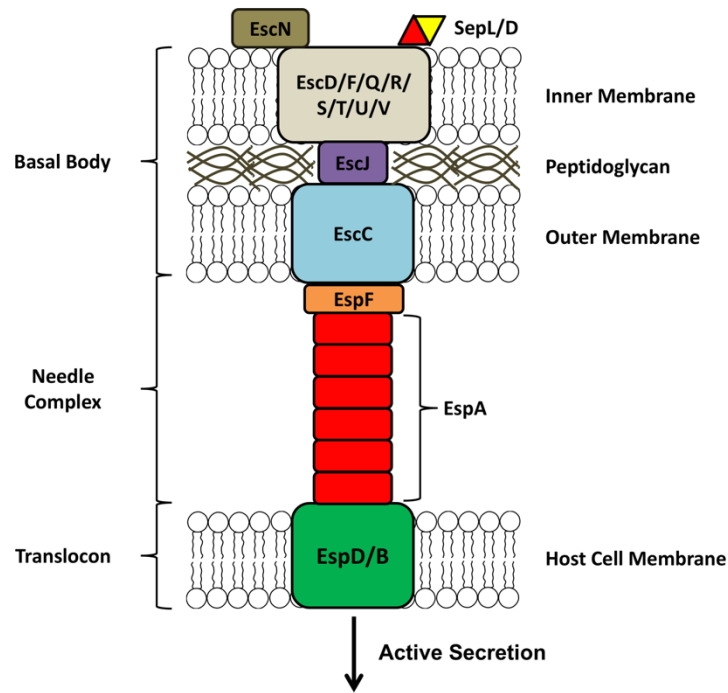


**Fig. 1: EHEC T3SS:** Schematic representation of the EHEC T3SS. The basal body spans between the inner and outer membrane, while the needle filament and the translocon function as a conduit to the host cell. Figure adapted from <sup>199</sup>.

The T3SS apparatus comprises three main structural components: the basal body, the needle filament and the translocon (Fig. 1). The basal body stretches between the bacterial inner and outer membrane and functions as an export apparatus for other T3SS proteins. EscJ is a “neck-like” protein that protrudes into the periplasmic space and consequently oligomerises in a 24-mer ring. It is thought that the correct assembly of this key protein initiates the recruitment of other basal body proteins, namely EscT, R, S and V, to form the inner membrane complex <sup>23</sup>. EscU is another component of this complex and is supposed to partially regulate the export of virulence proteins <sup>24</sup>. EscN is an ATPase and energises the whole export mechanism of T3SS components and effector proteins. EscN sits onto the cytosolic side of the basal body anchoring itself to EscL and EscQ <sup>25</sup>. SepL and SepD are other proteins that sit outside the export apparatus and function as “gatekeepers”, enabling the injection of effector proteins only when the needle-like structure is complete <sup>26,27</sup>. EscC is an oligomeric protein formed by 20 subunits that lies on the outer membrane and closely interacts with EscJ. EscC N-terminal domain is positioned into the periplasmic space and bound to EscJ, while the C-terminal domain is protruding into the outer membrane <sup>28</sup>.

The initial portion of the needle filament is formed by EspF, an outer membrane protein which interacts with both EscC and EscJ. EspF acts as a platform for the assembly of the needle-like structure by EspA. EspA is secreted through the export apparatus and polymerises in a helical arrangement with 5 to 6 subunits per turn<sup>29</sup>. EspA interacts with a selective chaperone CseA to prevent premature polymerisation within the cytoplasm<sup>23</sup>. Once the needle structure has reached the desired length (normally up to 600 nm), 2 pore-forming proteins, EspD and EspB, are secreted to generate the translocon pore into the host cell membrane with a 4:1 EspD:EspB ratio<sup>30</sup>. EspD, a 39 kDa protein, is another key protein of the T3SS, which is secreted through the needle and inserted into the host cell membrane<sup>31,32</sup>. Once the translocon pore is formed, EspA can anchor to EspD to complete the correct assembly of the T3SS and to initiate the translocation of effector proteins into the host cytoplasm<sup>32-34</sup>. It has been demonstrated that an absence or malfunctioning of this pore-forming protein blocks the correct assembly of the T3SS and, therefore, *E. coli* O157:H7 colonisation<sup>31,32,34</sup>. Despite the well-known role, EspD structure is still unclear due to its complex biological properties. It has been predicted that this virulence protein contains 2 coiled-coil domains for host cell membrane anchoring and homooligomerisation, 2 transmembrane domains for host cell membrane insertion and two amphipathic regions thought to be involved in the secretion process of the protein and in chaperone recognition<sup>31,32,34</sup>. To date, no crystallographic data are available for this membrane protein.

The overall structure of the T3SS is also well-conserved in more than 25 species of Gram-negative bacteria such as *Salmonella* sp., *Yersinia* sp., *S. flexneri*, *C. rodentium*, *Chlamydia* sp. and *P. Aeruginosa*<sup>35</sup>. The protein nomenclature differs between species, as listed in Table 1. The T3SS in the mouse pathogen *Citrobacter rodentium* is especially important for *in vivo* model of EHEC infection, since EHEC cannot infect mice<sup>36,37</sup>. Bioluminescence imaging (BLI) was utilised by Wiles *et al.* to generate a bioluminescent *C. rodentium* strain for colonisation imaging in live animals as a reproducible *in vivo* model to evaluate potential T3SS inhibitors<sup>36</sup>. This homology between different pathogens makes the T3SS a very attractive target for the development of potential broad spectrum compounds focused on the inhibition of this virulence weapon. A detailed list of T3SS inhibitors is discussed in Paragraph 4.3.

| <i>E. coli</i> | <i>C. rodentium</i> | <i>Yersinia</i> | <i>Salmonella</i> |
|----------------|---------------------|-----------------|-------------------|
| EscC           | EscC                | YscC            | InvG              |
| EscD           | EscD                | YscD            | PrgH              |
| EscJ           | EscJ                | YscJ            | PrgK              |
| EscN           | EscN                | YscN            | InvC              |
| EscR           | EscR                | YscR            | SpaP              |
| EscS           | EscS                | YscS            | SpaQ              |
| EscT           | EscT                | YscT            | SpaR              |
| EscU           | EscU                | YscU            | SpaS              |
| EscV           | EscV                | YscV            | InvA              |
| EspA           | EspA                | LcrV            | SipD              |
| EspB           | EspB                | YopV            | SipC              |
| EspD           | EspD                | YopB            | SipB              |
| EspF           | EspF                | YscF            | PrgI              |

**Table 1: Nomenclature of homologous T3SS proteins in *E. coli*, *C. rodentium*, *Yersinia* sp. and *Salmonella* sp.:** The T3SS proteins nomenclature for different Gram-negative bacteria is listed in the table above.

## 2.2 Locus of enterocyte effacement (LEE)

The T3SS is encoded in the locus of enterocyte effacement (LEE), a pathogenicity island (PAI) containing 41 genes arranged in 5 polycistronic operons, namely *LEE1*, *LEE2*, *LEE3*, *LEE4* and *LEE5* <sup>38,39</sup>. *LEE1*, *LEE2* and *LEE3* primarily encode genes for the production of the T3SS basal body proteins, esc and sep proteins <sup>40</sup>, while *LEE4* is responsible for the proteins of the needle structure (EspF and EspA) and the translocon (EspD and EspB) <sup>31,33,41,42</sup> (Fig. 2). *LEE5*, instead, contains genes for adhesion proteins such as Tir and intimin <sup>43</sup>.

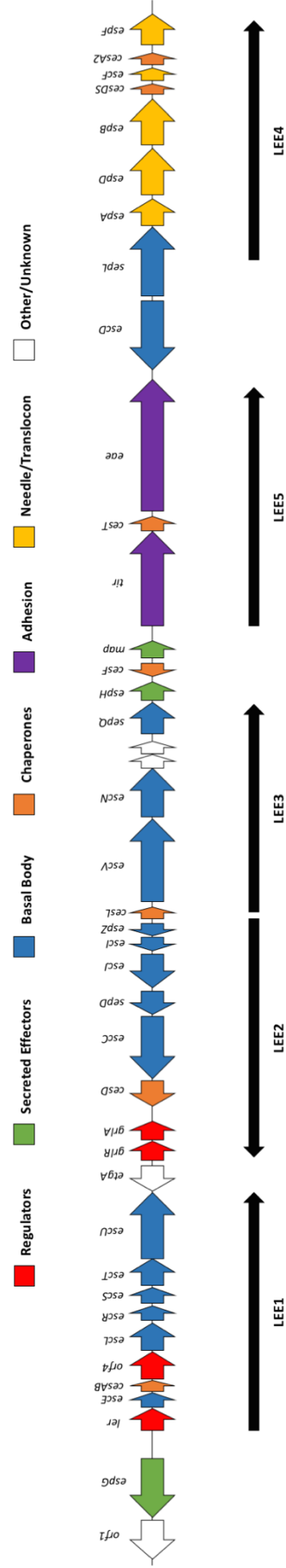


**Fig. 2: Genetic organisation of the LEE pathogenicity island in EHEC:** Schematic representation of the whole locus of enterocyte effacement (LEE) from EHEC. The 41 ORFs are labelled above the corresponding gene. Each gene is colour coded as indicated by the legend. The LEE is further divided into 5 main operons, namely LEE1-5, represented by black arrows below the LEE island. Figure is adapted from <sup>200</sup>

Expression of this pathogenicity island is mainly regulated by the master regulator (Ler), encoded in the first operon (*LEE1*)<sup>44</sup> (Fig. 3). Ler is a transcriptional activator and its function is to release the H-NS repressor to allow *LEE2-5* transcription<sup>45,46</sup>. The expression of Ler is also regulated by several factors within the bacterium.

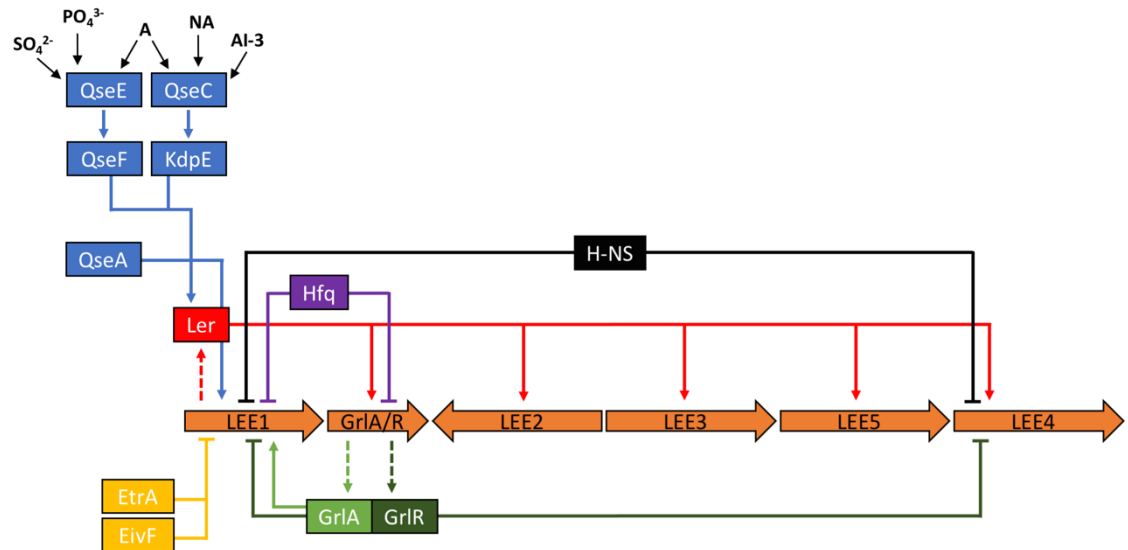


**Fig. 3: Regulation of the LEE pathogenicity island:** Schematic representation of the LEE regulation. Regulators are shown by colour coded rectangle and arrows. Normal arrows represent positive regulation and blunt arrows specify negative regulation. Dashed arrows indicate expression of a regulatory protein from the LEE. The LEE operons (LEE1-5) are shown by the orange arrows. Figure adapted from<sup>201</sup>

The Global Regulator of the LEE Activator (GrlA) and its opposing Repressor (GrlR) are other regulatory elements encoded in the LEE which interact with Ler. While GrlA activates Ler and consequently the expression of the T3SS, GrlR functions as a repressor for the LEE transcription<sup>37,47</sup>. QseA, instead, is a direct activator of Ler encoded outside the LEE<sup>48</sup>. QseE and QseC are 2 sensor kinase receptors sensitive to the outer and endogenous stimuli (i.e. sulphates, phosphates, adrenaline and EHEC Autoinducer (AI)), which indirectly regulate Ler through phosphorylation of QseF and KdpE respectively<sup>48,49</sup>. Other external regulators of the whole LEE pathogenicity island are EtrA and EivF, which repress the LEE transcription, and the RNA chaperone Hfq, known to bind to *ler* mRNA in order to block its transcription through the ribosome<sup>50,51</sup>. Environmental factors, such as media nutrients, are also key regulators of the LEE and Ler. For example, it has been observed that 0.4% of glucose in EHEC growth media reduced *ler* expression, whereas 0.1% of glucose activated the *ler* transcription due to the gluconeogenesis-like conditions<sup>49</sup>. MEM-HEPES media is also known to greatly increase the LEE expression during growth and it is, therefore, used



as a T3SS-inducing media for *in vitro* experiments<sup>20,35</sup>. However, the mechanism of this up-regulation is still unclear. Furthermore, the LEE expression is also regulated by the expression of other EHEC virulence factors such as the flagella<sup>47</sup>.

The complex and multi-layered regulation of this pathogenicity island highlights the relevant role of the T3SS for EHEC colonisation. T3SS is an essential and energetically “expensive” virulence weapon for the bacterium’s infection and, therefore, it must be expressed only in favourable environmental and endogenous conditions.

### 2.3 Effector proteins

The LEE pathogenicity island also encodes 7 effector proteins (Tir, Map, EspF, EspZ, EspG, EspB and EspH) that are translocated into the host cell as well as intimin, which is expressed on the bacterium’s outer membrane. Tir is one of the first effectors to be transported into the host after the T3SS assembly. Once translocated, Tir is inserted into the outer membrane and binds to the bacterial intimin with its extracellular domain, providing an intimate attachment between the bacterium and the host cell<sup>52</sup>. Tir intracellular domain phosphorylates the host cell protein N-WASP, which then recruits actin related proteins 2 and 3 (Arp2/3), causing nucleation of actin filaments. This process promotes the pedestal-like rearrangements of the host, forming the characteristic A/E lesions<sup>53</sup>. Other effector proteins act on the host cell cytoskeleton (i.e. EspB and EspF) and on the disruption of mitochondrial functions (i.e. Map and EspF)<sup>54–56</sup>. More than 60 non-LEE encoded effectors (NLEs) have been identified and studied, but they will not be discussed further here (for a recent and detailed review refer to<sup>57</sup>).

### 2.4 Shiga toxin

Shiga toxin (Stx) is another relevant *E. coli* O157:H7 virulence factor and belongs to the AB<sub>5</sub> toxin family, where the catalytic subunit A is non-covalently bound to a pentamer formed by subunit B<sup>58</sup>. The subunit A possesses N-glycosidase activity that cleaves an adenosine residue from the 28S ribosomal RNA of the 60S ribosomal subunit, leading to protein synthesis inhibition and then to apoptosis<sup>59</sup>. It has been demonstrated that the subunit B has specific affinity for the globotriaosylceramide receptor (Gb3) on the surface of eukaryotic cells such as intestinal and renal epithelial cells. Once the subunit B is bound to the receptor, Stx is endocytosed by the cell and can inhibit the protein synthesis<sup>60</sup>. As

mentioned before (Paragraph 1), *E. coli* O157:H7 has the ability of producing Shiga toxin <sup>3</sup>. The manifestation of its release is the selective apoptosis of the intestinal and renal epithelial cells, which leads to bloody diarrhoea and HUS <sup>4</sup>. Stx is a relevant EHEC virulence weapon and has been extensively studied, but it will not be discussed any further here (for detailed reviews refer to <sup>4,61,62</sup>).

### 3 Therapies for EHEC infection

Treatment of EHEC infections, especially *E. coli* O157:H7, with antibiotics is not recommended due to the increase of Stx release and, therefore, enhanced disease severity from cell lysis <sup>63–65</sup>. In addition, antibiotics induce the bacterial general stress responses, which lead to up-regulation of Shiga toxin expression and to the development of resistance <sup>48</sup>. Currently, EHEC infection therapies are only supportive and a rehydration therapy is the most relevant treatment for children and elderly with diarrhoea. There are many areas of ongoing research targeting the reduction of EHEC infections and, thus, limiting the effects of the Stx release. For example, SYNSORB Pk (SYNSORB, Canada) is a competitive antagonist of Stx for the Gb3 receptor. The higher affinity of this drug displaces the toxin from the receptor, thus, reducing tissue damage. Unfortunately, SYNSORB Pk was found to be almost inactive during human clinical trials due to the poor uptake in the bloodstream <sup>66,67</sup>. Another alternative is the development of a vaccine to reduce EHEC infection. Investigation for the use of an inactive form of the Stx antigen have been performed and showed promising results of protection in mouse models <sup>68</sup>. Other studies, instead, are focused to reduce the carriage of EHEC in cattle, therefore decreasing the possibility of food contamination <sup>69</sup>. Aiming to other EHEC virulence weapons, such as the bacterial adhesion, biofilm formation, intercellular signalling or the T3SS, is another alternative treatment. The use of anti-virulence (AV) compounds that selectively target virulence without inducing any stress or SOS responses is a promising area of research. This is discussed in Paragraph 4.

## 4 Anti-virulence compounds

As mentioned previously (Paragraph 3), *E. coli* O157:H7 infections are difficult to treat with traditional antibiotics therapies due to the Shiga toxin release. Anti-virulence compounds (AV) are one of the most promising class of drugs for an alternative EHEC infection treatment. The selectivity of AV results in less evolutionary pressure and SOS responses, which consequently lead to reduced possibilities for bacteria to develop resistance and to release Shiga toxin. Due to the limited options in EHEC treatments, the investigation on specific AV compounds for EHEC virulence weapons is essential for fighting this bacterial infection.

### 4.1 Quorum sensing inhibitors

The quorum sensing system is the essential cell-to-cell communication apparatus that controls various biological processes in both Gram-positive and Gram-negative bacteria. This system recognises specific signalling molecules secreted by growing bacteria and then regulates relevant cell pathways, including bioluminescence, toxin release, biofilm formation and virulence gene expression. Therefore, blocking the quorum sensing can result in the inhibition of bacterial virulence weapons, making it a plausible target for anti-virulence compounds.

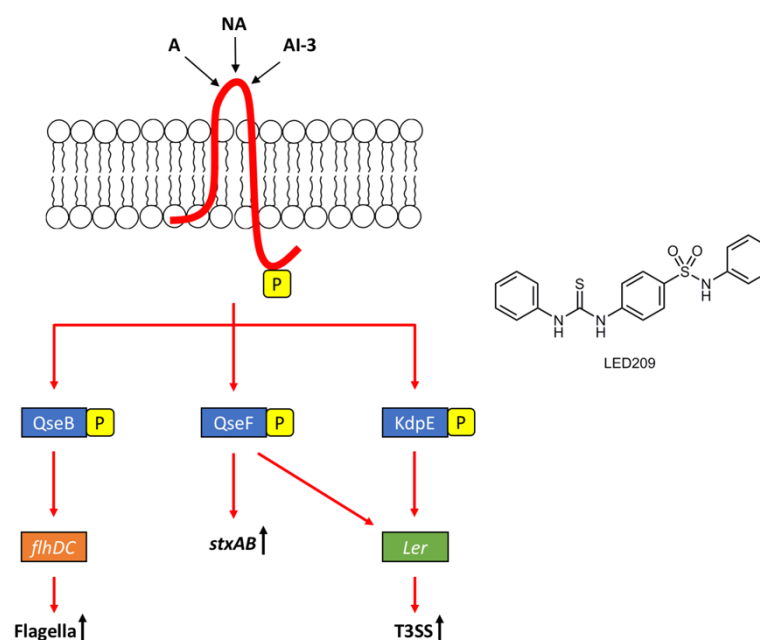


**Fig. 4: QseC signalling pathway (left) and the chemical structure of LED209 (right):** Schematic representation of the QseC signalling pathway is shown on the left. Phosphorylation is represented by the P in the yellow rectangles. Red arrows indicate positive regulation. Figure adapted from <sup>74</sup>. The chemical structure of LED209 is depicted on the right.

The main quorum sensing receptor in *E. coli* O157:H7 is the histidine kinase QseC<sup>70</sup> (Fig. 4). QseC is a highly conserved membrane protein which auto-phosphorylates in the presence of epinephrine, norepinephrine and the endogenous aromatic autoinducer (AI-3)<sup>70–72</sup>. Once phosphorylated, QseC activates 3 transcription factors through phosphorylation, namely QseB, QseF and KdpE. QseB is involved in the activation of the flagellar and motility systems, binding to the master regulator *flhDC*<sup>48,73</sup>. QseF and KdpE are directly involved in the up-regulation of the T3SS expression, interacting with the master regulator Ler. In addition, QseF is also responsible for the initiation of the Shiga toxin production<sup>48,74,75</sup>. It has already been demonstrated that generation of a *qseC* null mutant ( $\Delta qseC$ ) leads to attenuated expression of the T3SS system in EHEC, *Salmonella* sp. and *Francisella* sp.<sup>70,76</sup>. Therefore, inhibitors of the QseC receptor can selectively block virulence genes transcription without affecting essential cell pathways.

In 2008, Rasko *et al.* identified through a high-throughput screening the promising molecule LED209 as QseC inhibitor for its potency and low toxicity. LED209, a phenyl-thiourea derivative, demonstrated to have a selective affinity for the bacterial receptor and to antagonise epinephrine, norepinephrine and AI-3 at 5 pM, acting as a competitive antagonist for the active substrates. Consequently, the inhibition of the QseC signalling resulted in down-regulation of the expression of both T3SS proteins EspA and EspB and the attenuation of A/E lesions. Furthermore, LED209 did not affect bacterial growth nor induced SOS responses. The compound also displayed activity against QseC in other Gram-negative bacteria such as *S. typhimurium* and *Francisella* sp., due to the well-conserved homology of the receptor in various Gram-negative bacteria<sup>74</sup>. Positive results were obtained in EHEC infection mouse models, while rabbit models did not show any prevention of intestinal colonisation due to rapid GI tract absorption. Despite LED209 encouraging effects in reducing bacterial virulence weapons, its mode of action falls at the edge of what can be considered an anti-virulence compound since QseC indirectly controls the expression of the T3SS and Shiga toxin. Nonetheless, LED209 is a promising lead compound which can be chemically optimised and used in combination with other anti-virulence compounds to block virulence weapons.

## 4.2 Adhesin inhibitors

The preliminary binding of the bacteria to the host cell is mediated by hair-like organelles called pili or fimbriae, which initiate the bacterial adhesion. The biogenesis of these fibers is characterised by a complex and well-studied chaperone-usher pathway and, therefore, inhibition of the pili's biosynthesis can lead specifically to a less effective bacterial colonisation<sup>77,78</sup>.

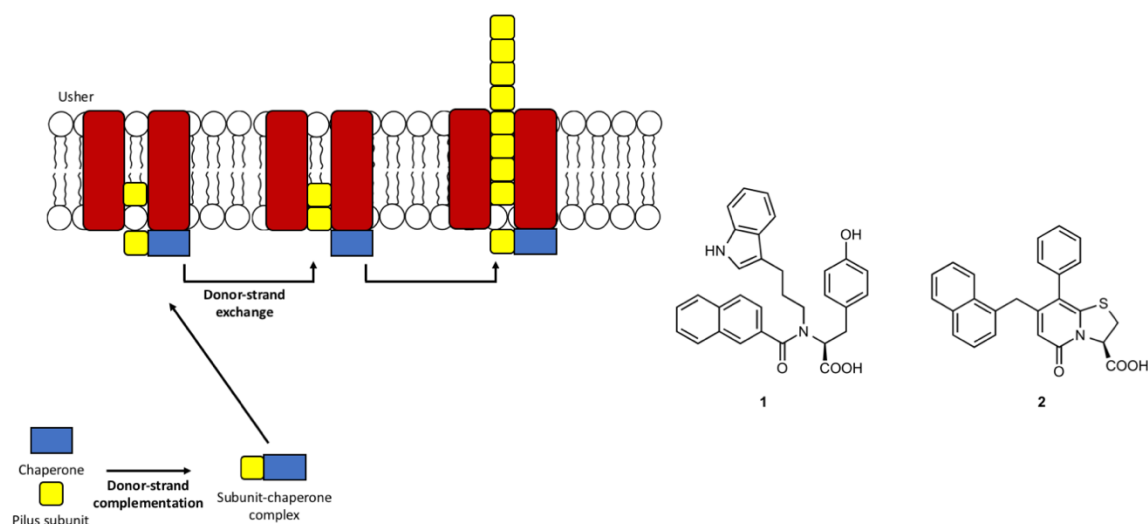


**Fig. 5: Pilus biogenesis (left) and the chemical structure of the tyrosine derivative 1 and pyridinone 2 (right):** Schematic representation of the pilus biogenesis through the chaperone-usher pathway is shown on the left. The usher and the chaperone are indicated in red and blue respectively, while the pilus subunit is coloured in yellow. Both donor-strand complementation and exchange are highlighted by black arrows. Figure adapted from<sup>184</sup>. The chemical structure of the first discovered pilus biogenesis inhibitors **1** and **2** are represented on the right.

P pili and type I pili are the most well-characterised types of fibers produced by Uropathogenic *E. coli* (UPEC), responsible for urinary tract infections. P pili contain the adhesin PapG selective for renal epithelial cells, while type I pili contain FimH adhesin, responsible for *E. coli* invasion into the bladder epithelium<sup>79–82</sup>. As just mentioned above, the biosynthesis of the pili involves a chaperone-usher pathway, where mechanistically cognate periplasmic chaperones are essential for the correct assembly, stabilisation and elongation of the fibers<sup>77</sup> (Fig. 5). PapD and FimC are specific chaperones for P pili and type I pili respectively and they catalyse the folding of every pilus subunit in the periplasm<sup>83,84</sup>. The binding between the pilus subunit and the chaperone is characterised by a process called donor-strand complementation, where the subunit anchors to the chaperone G1- $\beta$ -strand through an ion pair formation in a cleft containing two residues: Arg8 and Lys112<sup>85–88</sup>. Once the pilus subunit-chaperone complex is formed is selectively recognised by the outer membrane usher, responsible for the pilus assembly<sup>89,90</sup>. The

subunit-chaperone complex binds to a hydrophobic patch on the N-terminal portion of the usher and releases the pilus subunit inside its cavity<sup>91,92</sup>.

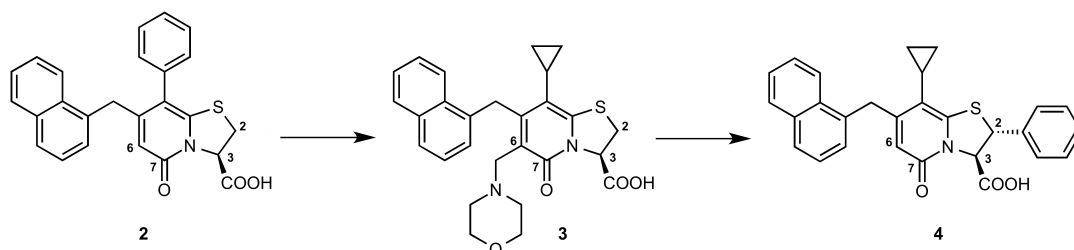


**Fig. 6: SAR studies on the pyridinone 2:** Scheme of the structural changes on the lead compound **2**. Installation of a morpholine moiety in C6 produced a more hydrophilic analogue **3**, which yielded the crystal structure of the pyridinone bound to the pilus subunit-chaperone-usher complex. From the crystal structure, it was possible to design and synthesise a very potent derivative **4**.

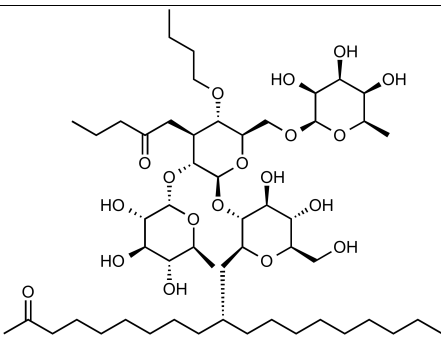
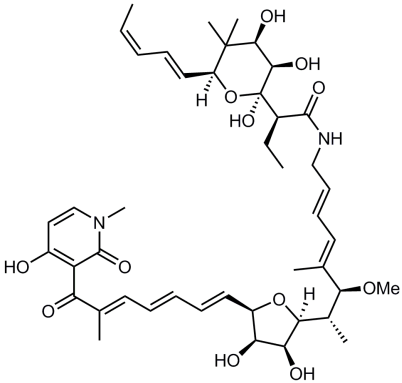
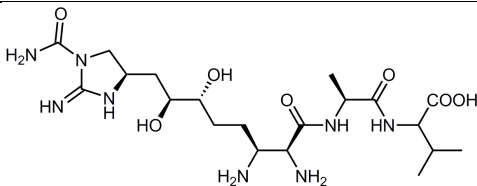
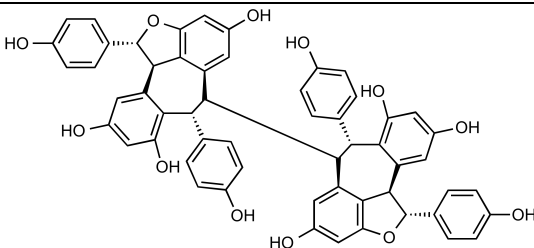
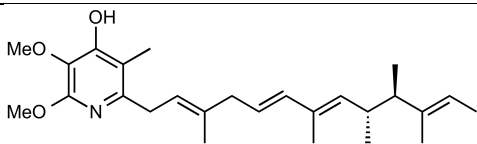
Through a process called donor-strand exchange, the pilus subunit unravels from the chaperone G1- $\beta$ -strand and binds to the N-terminal portion of a second pilus subunit within the usher's cavity<sup>88,93–95</sup>. This process is then reiterated several times to elongate the pilus outside the bacterial membrane.

In 2001, Kilhberg *et al.* designed and synthesised two classes of molecules to inhibit the pilus subunit-chaperone complex based on the anchoring of the pilus subunit into the Arg-Lys cleft<sup>96,97</sup> (Fig. 5). A tyrosine derivative **1** and a pyridinone **2** were found to be strong binders of both chaperones PapD and FimC and, after further biological evaluation, pyridinone **2** was subjected to chemical modifications to improve its solubility (Fig. 6). Morpholine installation onto position C6 yielded a potent compound (**3**) against the P pili and type I pili formation with enhanced solubility properties. In addition, Almqvist *et al.* also crystallised the new pyridinone **3** with the pilus subunit-chaperone-usher complex, revealing that the molecule binds between the usher and the chaperone instead of the Arg-Lys cleft, thus blocking the correct pilus subunit release<sup>98</sup>. The crystal structure obtained also disclosed the relevance of the carbonyl group in C7 and the carboxylic acid in C3, both interacting with the usher through hydrogen bonding. Further chemical modifications in C2 provided a very potent derivative (**4**) against the pili biogenesis *in vitro* and in UPEC mouse model infections, thanks to the position and stereochemistry of the new phenyl ring<sup>99,100</sup>. All the compounds demonstrated to be highly efficient against *E. coli* infections only when the bacteria were treated before the infection. However, this does not represent a real-life scenario, where the infection is established and then treated.

### 4.3 T3SS inhibitors

As discussed before in Paragraph 2.1, the T3SS is a needle-like complex that protrudes from the prokaryotic cells and allows the bacterium to hijack the host cell, facilitating colonisation. It has been previously demonstrated that the T3SS is essential for the virulence of many pathogens<sup>101</sup>, indeed deletion of EspA prevent EHEC colonisation of the bovine host<sup>12</sup>. The fact that this system is well-conserved amongst Gram-negative bacteria makes it a very promising target to selectively block virulence in different bacteria, leading to a potential broad-spectrum anti-virulence compounds concept. For these reasons, the T3SS has been widely studied and many research groups have focused their efforts on the discovery and understanding of selective T3SS inhibitors.

### 4.3.1 Natural products

| Name          | Chemical Structure   | Effective against                                 | Reference |
|---------------|--|---|-----------|
| Camioside B   |    | EPEC T3SS   | 102       |
| Aurodox       |     | EPEC/ <i>C. rodentium</i> T3SS                    | 103,104   |
| Guadinomine A |   | EPEC T3SS   | 105       |
| Hopeaphenol   |  | <i>Yersinia/P. aeruginosa/C. trachomatis</i> T3SS | 106       |
| Piericidin A1 |  | <i>Yersinia</i> T3SS                              | 107       |

**Table 2: List of active natural products against T3SS:** The chemical structure of bioactive natural product against T3SS is listed above. The species and the T3SS targeted by the different molecules is also listed.

The first T3SS inhibitor was reported by Linington *et al.* in 2002 after screening various extracts from the marine sponge *Caminus sphaeroconia* against the virulence protein EspB. Camioside B, a carbohydrate derivative formed by a 6-deoxytalose ring, a quinovose ring and two glucose subunits, was found to be active against EPEC at 5.1  $\mu$ M without affecting



bacterial growth. Unfortunately, due to the complex synthesis, its mode of action is still unknown<sup>102,108</sup> (Table 2).

Another natural product of interest is Aurodox, a complex compound produced by *Streptomyces goldiniensis*. Initially, Aurodox was described as an anti-bacterial compound against Gram-positive bacteria due to its affinity to the elongation factor Tu<sup>109</sup>. It has been recently shown by Kimura *et al.* that Aurodox inhibited EPEC T3SS-mediated haemolysis at 1.5  $\mu$ M by down-regulating T3SS proteins such as EspB, EspF and Map, with no anti-bacterial effect. Mouse models of *C. rodentium* infections demonstrated that Aurodox had the ability to protect the mice from an otherwise lethal dose of bacteria<sup>104</sup>. Despite its known anti-bacterial target, the mode of action of the Aurodox anti-virulence effect is still unclear. However, the selective decrease in production of T3SS proteins might indicate a potential interaction with LEE-related transcriptional regulators.

Guadinomines are unusual natural products produced by *Streptomyces* K01-509 and were found to be active against the T3SS in EPEC by Iwatsuki *et al.*. Guadinomines A and B displayed a high activity in inhibiting EPEC-induced haemolysis in a dose-dependent manner, with an IC<sub>50</sub> of 0.01  $\mu$ M. Further SAR studies revealed that the diamine moiety and the valine subunit on the right-hand of the molecule are essential for the anti-virulence effect of these compounds<sup>105</sup>. Guadinomines are very promising lead scaffolds against the T3SS due to their high potency; however, their mode of action and their efficacy *in vivo* have yet to be confirmed.

Recently, Elofsson *et al.* isolated the natural product (-)-hopeaphenol, a resveratrol tetramer which was found to be active against *Y. pseudotuberculosis* T3SS protein YopD. It has been demonstrated that this complex molecule inhibited secretion of Yops proteins without affecting their transcription and it has been postulated that hopeaphenol might bind irreversibly to its still unknown protein target. Furthermore, this molecule was found to have a similar activity against *P. aeruginosa* and *C. trachomatis* blocking the secrete effector ExoS in the first pathogen and interfering with the cell entry and intracellular growth with the second one<sup>106</sup>. Even in this case, the cellular target of hopeaphenol is unknown. However, it has been speculated that the compound, considering its size and the amount of polar groups, might act on the outer membrane of the bacterial cell.

The marine natural products piericidin A1 and its derivative Mer-A 2026B were also found to be active against *Y. pseudotuberculosis* T3SS, inhibiting Yops proteins secretion and YopM translocation in CHO cells in the low micromolar range. No anti-bacterial activity was

detected for these new compounds that selectively blocked the T3SS<sup>107</sup>. Interestingly, both molecules contain a  $\gamma$ -pyridone ring, an extremely rare feature in nature that also belongs to Aurodox. It is easy to speculate a potential common protein target between these two classes of natural products, but direct evidences are yet to be confirmed.

#### 4.3.2 Other synthetic T3SS inhibitors

High-throughput screenings of synthetic libraries have also been employed as a fast method to identify new non-natural compounds against the T3SS (Fig. 7). In 2008, Goguen *et al.* screened a library of more than 70'000 compounds against *Y. pestis* by means of a monitored growth assay where the expression of the T3SS resulted in growth inhibition. From this method, 4 putative T3SS inhibitors of different chemical nature were identified and selected for further evaluation. Biological tests revealed that the candidates also had different effects on the virulence effectors YopM and YopH and the structural protein YopD, which forms the terminal pore of the T3SS in *Y. pestis*. The best potency was displayed by compound **5**, a 4,4'-thiobis-(3-methylphenol), which proved to be active against all 3 virulence proteins in low micromolar range and to protect HeLa cells from the pathogen infection. However, the compound demonstrated to be toxic for mammalian cells, suggesting that further chemical modifications may be required<sup>110</sup>.

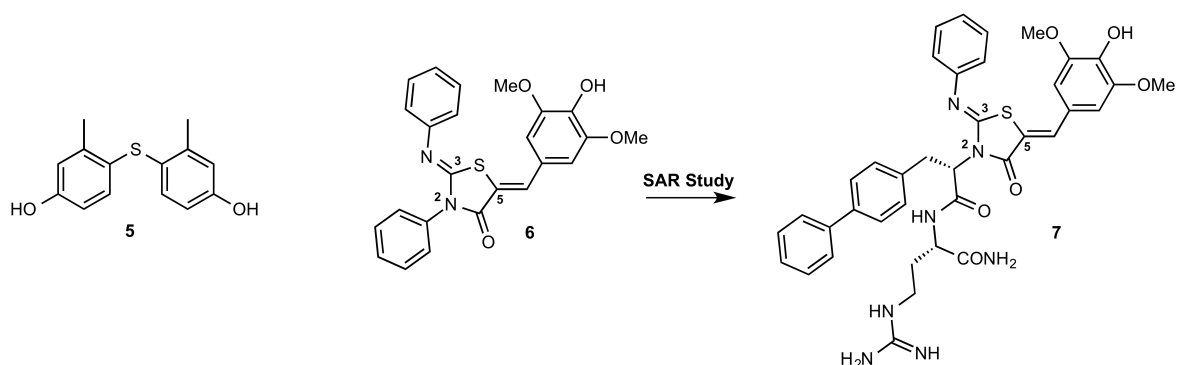


**Fig. 7: Chemical structure of known non-natural T3SS inhibitors:** The structure of the 4,4'-thiobis-(3-methylphenol) derivative (**5**) identified by Goguen *et al* is shown on the left. The structure of the lead compound 2-imino-5-arylidene thiazolidinone **6** is depicted on the right. SAR studies allowed to yield the amino acid derivative **7**, which demonstrated to possess an improved solubility profile and to be a more potent inhibitor than **6**.

An important class of synthetic compounds active against the T3SS is the 2-imino-5-arylidene thiazolidinones. The lead compound (**6**) of this class was identified through a high-throughput screening against *S. typhimurium* using a reporter fusion assay of the

secreted effector SipA expression. Thiazolidinone **6** was found to be active against SipA without affecting bacterial growth or motility. In addition, the candidate exhibited activity against the T3SS of *P. syringae*, *F. novicida* and *F. tularensis*, demonstrating a broad spectrum activity. *In vivo* studies proved that compound **6** protected eukaryotic cells from *S. typhimurium* and *P. syringae* respectively in a macrophage tissue experiment and in tobacco plant model, while showing no toxic effect on macrophages. These findings drove the authors to conclude that thiazolidinone **6** might be targeting a common and well-preserved structural component of the T3SS, but no evidence of this has yet been demonstrated <sup>111</sup>. To investigate the structure-activity relationship (SAR) of this scaffold, Kline *et al.* designed and synthesised different structural derivatives in order to evaluate the thiazolidinone core. Both 3-phenylimido and 5-phenylidene features were found to be essential for activity against SipA expression, while the N2 position showed to be almost irrelevant for the activity. Especially the position C5 (5-phenylidene) demonstrated to be the interactive site of the molecule, since even small modifications on this substituent caused drastic reductions in activity. Position N2 was then targeted for further chemical changes in order to achieve a better solubility profile. For these reason, a polar chain that vaguely recall an arginine motif was installed in N2 to yield compound **7**. This derivative was directly compared with **6** and resulted to be a better T3SS inhibitor than the lead compound <sup>112</sup>. Given the ease of synthesis and the broad spectrum activity, the thiazolidinone class are a promising group of T3SS inhibitors.

#### 4.3.3 Salicylidene acylhydrazide (SA)

Salicylidene acylhydrazides (SA) are the most studied T3SS inhibitors due to their activity on different pathogens and their ease of synthesis (Table 3). The first SA compound was discovered in 2003 by Kauppi *et al.* by means of a high-throughput screening with a *yopE*:luciferase reporter assay against *Y. pseudotuberculosis*. In this screening method, the luciferase intensity was proportional to the *yopE* expression; therefore, a reduction of luciferase intensity represented activity against *yopE* transcription. A total of 4 candidates were selected from the screening and the SA compound INP0007 demonstrated to be the best compound, inhibiting the secretion of other T3SS proteins, such as YopD and YopH, in a dose-dependent manner and with an IC<sub>50</sub> of less than 50 µM. Due to the similarity between the *Yersinia* T3SS and the flagellar system, the 4 candidates were also tested

against motility and INP0007 resulted to be the only molecule to inhibit the pathogen's motility as well <sup>113</sup>. This indicates that the SA compound may bind to a common regulator or structural components of these two systems.

After these findings, several research groups also tested similar SA compounds against various T3SS-harboring Gram-negative bacteria. Wolf *et al.* employed INP0007 and other SA compounds identified by Kauppi *et al.* against the obligate intracellular bacterium *C. trachomatis*. The biological evaluation showed that the compounds significantly affected the pathogen's infective cycle, disrupting differentiation and multiplication in mammalian cells <sup>114,115</sup>. At the time of the study little was known about the role of the T3SS in *C. trachomatis* and, therefore, the use of these compounds revealed relevant insights of the regulation of the T3SS in *Chlamydia*.

SA compounds were also found active against *S. enterica* serovar *typhimurium*, where INP0007 and INP0403 displayed inhibition of the SPI-1 T3SS at 10 and 100  $\mu$ M without affecting the bacterial growth. Furthermore, both SA compounds demonstrated to protect HeLa cells from infection at up to 60% and to reduce inflammation levels in a bovine intestinal ligated loop model, highlighting the ability of these compounds to reduce virulence *in vivo* <sup>116</sup>. In the same year, Negrea *et al.* used other SA compounds (INP0400-0406) to confirm their activity against SPI-1 and also SPI-2 in *S. typhimurium*. The compounds inhibited intracellular replication and two of them reduced the motility by affecting the flagellar system <sup>117</sup>.

| Name    | Structure | Effective against  | Reference |
|---------|-----------|--|-----------|
| INP0007 |           | <i>Yersinia</i> T3SS, <i>C. trachomatis</i> T3SS, <i>Salmonella</i> T3SS | 113–117   |
| INP0010 |           | <i>Salmonella</i> T3SS, EHEC T3SS  | 117,118   |
| INP0400 |           | <i>Salmonella</i> T3SS, <i>S. flexneri</i> T3SS                          | 117,119   |
| INP0401 |           | <i>Salmonella</i> T3SS   | 117       |
| INP0402 |           | <i>Salmonella</i> T3SS, <i>S. flexneri</i> T3SS                          | 117,119   |
| INP0403 |           | <i>Salmonella</i> T3SS, EHEC T3SS  | 117,118   |
| INP0404 |           | <i>Salmonella</i> T3SS   | 117       |
| INP0405 |           | <i>Salmonella</i> T3SS   | 117       |
| INP0406 |           | <i>Salmonella</i> T3SS   | 117       |
| ME0055  |           | EHEC T3SS  | 118       |

**Table 3: List of the SA compounds active against T3SS:** The chemical structure of active SA compounds against T3SS is listed above. The species and the T3SS targeted by the different molecules is also listed, highlighting the broad spectrum activity of these synthetic molecules.

The same group of SA compounds was also evaluated against the invasive intracellular pathogen *S. flexneri* by Veenendaal *et al.*. All SA compounds resulted to be active against Ipa T3SS and INP0400 showed the best activity profile of the group. In addition, the compounds demonstrated to reduce cell invasion in HeLa cells and induced macrophage apoptosis as well <sup>119</sup>.

In 2009, Tree *et al.* tested 4 SA compounds against EHEC (*E. coli* O157:H7 TUV 93-0 strain) and ME0055 was found to be the best T3SS inhibitor, blocking transcription and secretion of the virulence proteins EspD and Tir at 20  $\mu$ M. This SA compound also showed protection of HeLa cells from the characteristic A/E lesions, typically associated with EHEC infections. However, ME0055 was found to also have anti-bacterial effects with concentrations higher than 20  $\mu$ M <sup>118</sup>.

Despite the promising activity, the SA compounds chemical structure includes an imine bond prone to hydrolysis in acidic media. However, this limitation makes these molecules a more than optimal lead compound to build more stable and more potent inhibitors based on the SA scaffold. In 2010, Elofsson *et al.* conducted a scaffold hopping study for the modification of the acylhydrazone core. A 2-(2-aminopyrimidine)-2,2-difluoroethanol (**8**) and a [4-(2-hydroxyphenyl)thiazol-2-yl]methanone (**9**) core were identified from the structural study and used to replace the weak imine bond of the SA compounds (Fig. 8). These new heterocycles were designed in order to retain the intracellular hydrogen bond between the *ortho*-positioned hydroxyl group and the nitrogen of the hydrazone moiety. Two new series of molecules based on these heterocycles were synthesised and tested against the T3SS in *Yersinia*. Unfortunately, the new derivatives did not show any significant activity against the T3SS to pursue further biological investigations <sup>120,121</sup>. The promiscuity of the SA compounds makes their structural optimisation and biological evaluation very challenging, since only whole-cell based assays are available and, therefore, many factors can influence the derivatives' activity.

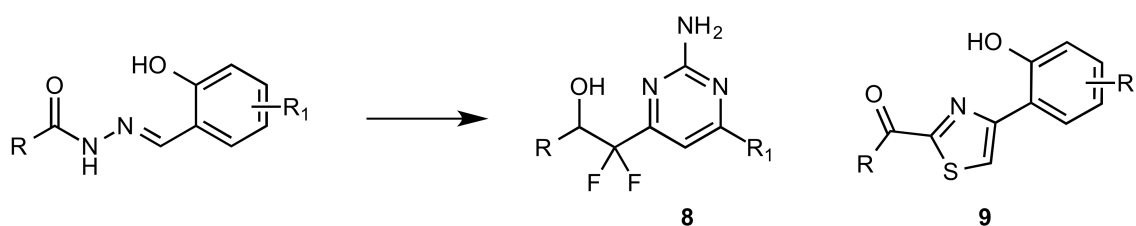


**Fig. 8: Scaffold hopping based on the SA compounds core:** Scheme representing the two heterocycle cores **8** and **9** resulted from the scaffold hopping study based on the SA compound structure.

To conclude, SA compounds are a well-studied class of T3SS inhibitors with a broad spectrum activity. In different cases, the compounds also showed to affect the flagellar system together with the T3SS<sup>113,117</sup>; however, this effect between species resulted to be inconsistent. Although SA compounds have been described as T3SS inhibitors, their mode of action is still unclear and is yet to be elucidated. Nonetheless, this class of T3SS inhibitors is ideal for further chemical optimisation that could lead to more stable and more potent derivatives and to clarify their mechanism of action.

#### 4.3.4 Mode of action of SA compounds

Three different hypotheses have been suggested regarding the mode of action of the SA compound. Slepkin *et al.* have proposed and studied the possibility that the SA molecules could chelate iron and thus disrupt the cellular iron stores. The study showed how addition of iron salts to HeLa cells infected with *C. trachomatis* reversed the effect of the SA compound. In addition, this effect was only observed with iron and not with other divalent metal ions, suggesting a selective affinity of the acylhydrazone moiety with the Fe<sup>2+</sup> ions. However, this study has to be considered inconclusive since the inactive SA compound against *C. trachomatis* T3SS chelated iron as well as the active ones<sup>122</sup>. An analogous study on *Salmonella* by Layton *et al.* demonstrated that the addition of iron salts only partially reversed the SA compound's effect. Transcriptomic analysis revealed an up-regulation of the genes involved in the iron regulation; however, the addition of iron did not fully reverse the inhibitory effect of the SA compounds<sup>123</sup>. Another transcriptomic analysis performed on EHEC treated with the SA compounds and additional iron salts displayed a significant down-regulation of T3SS-related genes; thus, suggesting that iron did not reverse the SA compound's activity<sup>118</sup>. To sum up, it is still unclear how iron can influence the SA compound's effects on the T3SS in certain bacteria. Further studies have to be performed in order to elucidate this peculiar interaction.

Veenendaal *et al.*, instead, have proposed that the SA compound might bind to a structural component of the T3SS. Since the compounds were found to also affect motility in *Shigella* and *Yersinia*, the target may be a homologous component between the T3SS and the flagellar system. In the study, it was also observed that the needle of the T3SS of *S. flexneri* was significantly shorter upon treatment with SA compounds, indicating an interference

with the T3SS assembly<sup>119</sup>. A recent study aimed to clarify this mode of action hypothesis by using strains lacking different flagellar component in *Salmonella*. Unfortunately, the study was unable to detect the interaction between the SA compound and the potential flagellar component, excluding the possibility of a direct binding to the T3SS apparatus. It is likely that, in this case, the SA compound interact with other intracellular targets and then indirectly inhibit the T3SS assembly<sup>124</sup>.

The last mode of action hypothesis is that the SA compound may somehow affect the regulation of the T3SS. To identify the target proteins, Wang *et al.* designed and synthesised an Affi-Gel and biotin labelled version of the SA compounds ME0052 and ME0055 for an affinity pull-down experiment against EHEC cell lysate. Once the immobilised labelled molecule was incubated with the whole cell lysate solution, unspecific bound proteins were washed off and high concentrations of the SA compound were employed to displace the specific bound proteins. These proteins were then analysed by SDS-PAGE electrophoresis and tandem mass spectrometry for identification. From this study, 19 putative target proteins were identified<sup>125</sup>. The research group mainly focused on 4 of them, namely FolX, Tpx, WrbA and AdhE<sup>125-131</sup>. Subsequent work validated the binding of ME0055 with Tpx and WrbA through chemical shift NMR and co-crystallisation techniques, but the most significant target regarding the control of EHEC virulence weapons was AdhE. Beckham *et al.* found that deletion of the AdhE gene (*adhE*) yielded a stark pleiotropic phenotype with strong T3SS down-regulation and over-expression of non-functional flagella. It was showed that the suppression of the T3SS was post-transcriptional and triggered by the *Ler* mRNA regulator Hfq, resulting in a less virulent phenotype. However, this studies highlighted the complexity and promiscuity of the SA compounds and their mechanism of action. It was concluded that their effects on the T3SS is a result of the modulation of several metabolic pathways rather than a direct control of the virulence factors themselves<sup>132</sup>.

## 5 Aims of the project

The aim of this project was to build a library of EHEC T3SS inhibitors based on the the most promising SA compound, ME0055. Despite the promising activity against the T3SS of multiple pathogens, this SA compound possessed a poor solubility in biological media and



was prone to hydrolysis in acidic media due to the weak imine bond. In addition, ME0055 mode of action is still partially unclear and derivatives of this molecule could better elucidate its mechanism of action. Therefore, ME0055 represents an attractive lead compound for chemical optimisation. Once designed and synthesised new potential chemical scaffolds, the aim was to screen and biologically evaluate the series against EHEC T3SS using phenotypic characterisation assays. Three active scaffolds were identified and tested against EHEC T3SS. By means of biotin labelling, it was possible to identify the main protein target of the new inhibitors, enabling future investigations on the determined protein and encouraging the pursuit of new and more potent molecules against the T3SS.

## Results and Discussion

## 6 Introduction

Hydrazine-containing heterocycles are valuable building blocks for drugs. It has been estimated that 50% of all drug molecules contain a phenyl ring, which can be consequently substituted with different nitrogen-containing rings. The replacement with hydrazine-containing heterocycles opens a variety of potential diaza analogues (i.e. pyrazole, pyridazine, phthalazine, cinnoline, etc), presenting more interaction possibilities thanks to the two nitrogens (hydrogen bond acceptors), lower LogP values and improved crystalline properties<sup>133</sup>.

Many commercially available drugs include hydrazine-containing heterocycles such as the selective COX-2 inhibitor Celecoxib (**10**) by Pfizer, which is used for acute pain, osteoarthritis and rheumatoid arthritis (Fig. 9). Other inhibitors of the same NSAID family bear a 3- or 5-pyrazolone ring as pharmacophore. Ampyrone (**11**), metamizole (**12**) and phenazone (**13**) are all used as pain reliever, antispasmodic and fever reducer with effects similar to paracetamol. A historic example of a pyridazine is the commercially available sulphonamide antibiotic sulphamethoxypyridazine (**14**), which was introduced on the market around 1950s as one of the first hydrazine-containing heterocycle drugs<sup>133</sup>.

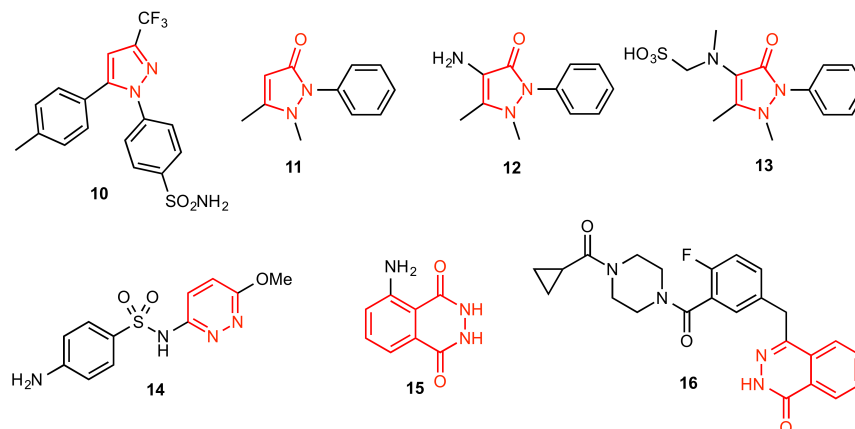


**Fig. 9: Chemical structures of relevant hydrazine-containing heterocycle drugs.** From left to right: Celecoxib (**10**) from Pfizer, ampyrone (**11**), metamizole (**12**), phenazone (**13**), sulphamethoxypyridazine (**14**), Luminol (**15**) and Olaparib (**16**).

Another hydrazine-containing heterocycle of interest is the phthalazinone ring, which is usually used as a chromophore scaffold (i.e Luminol (**15**)), but recently has gained interest as a drug building block. Olaparib (**16**) is an experimental drug by AstraZeneca for treating prostate cancer, which binds to poly ADP ribose polymerase (PARP). The phthalazinone

ring is one of the key elements for the inhibitory effect and replaces the original nicotinamide pharmacophore<sup>134</sup>.

## 7 1,4,5,6-Tetrahydropyridazine (THP) and 1,2-Dihydrophthalazine (DHP) Derivatives

### 7.1 Design and rationale of the THP and DHP cores

Previous studies in our group were focused on the characterisation of potential type three secretion system (T3SS) inhibitors such as salicylidene acylhydrazide (SA) <sup>118</sup>. A number of SA compounds tested against *E. coli* T3SS produced positive results and experiments were performed to understand their mode of action <sup>125</sup>. Amongst the compounds tested, ME0055 showed the most promising effects as a potential selective inhibitor of the T3SS. However, the mode of action of this acylhydrazone is still unclear due to its promiscuity in binding several off-target proteins, which makes it difficult to establish a clear and specific target <sup>125</sup>. The poor solubility of ME0055 in biological media has also hampered many binding studies such as isothermal calorimetric experiments (ITC), enzyme kinetics assays and NMR, which could clarify its mode of action (unpublished data). The imine bond of ME0055 was found to be prone to hydrolysis in aqueous acidic media through electronic ionisation mass spectrometry and NMR analysis (data not shown). Due to these limitations, ME0055 was chosen as the lead compound to build a small focused library of new potential anti-virulence compounds, in order to improve the stability and selectivity of the SA compound. Furthermore, a new series of more stable compounds could provide essential data to elucidate the mode of action and the structure-activity relationship around the SA compounds core.

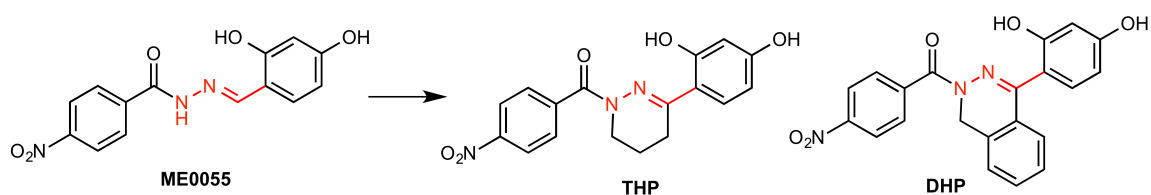


**Fig. 10: Rational design of the THP and DHP cores:** It was decided to include the imine motif in two hydrazine-containing heterocycles (THP and DHP), in order to stabilise the chemical structure of the SA compound ME0055. The THP core provided a stable derivative, allowing to also explore the chemical space around the central core of the molecule, since its half chair conformation. The DHP analogue, instead, offered a planar central core to facilitate possible pi-stacking with the target.

It was decided to modify the molecule by including the imine bond of the SA scaffold in hydrazine-containing heterocycles (Fig. 10). A pyridazine and a phthalazine core were

chosen to be introduced in the central part of the molecule. In addition, retention of the intra-molecular hydrogen bond between the *ortho*-hydroxyl group and the nitrogen was also planned to mimic ME0055 chemical features. Two different hydrazine-containing rings were selected: the 1,4,5,6-tetrahydro pyridazine (THP) and the 1,2-dihydrophthalazine (DHP). The THP core includes the two nitrogen in a six-membered ring with a half-chair conformation, allowing the investigation of the chemical space around the hydrazine core with a minimum of steric hindrance. The DHP core, on the other hand, has a completely planar conformation and the *ortho*-fused phenyl ring gives a much greater hindrance in the central core of the molecule than the THP scaffold, also increasing the lipophilicity of the compound. At the same time, this fused heterocycle can take part in hypothetical hydrophobic interactions as pi stacking overlaps. All the substituents of ME0055 were retained to have a direct comparison of the impact of the two cores on the activity of the compounds.

## 7.2 Synthesis of the THP and DHP derivatives

The synthesis of both THP and DHP derivatives started from resorcindimethylether (**17**), which underwent Friedel-Crafts acylation with both succinic (**A**) and phthalic anhydride (**B**) to afford carboxylic acids intermediates **18** and **19** (Fig. 11). Pyridazinone **20** and phthalazinone **21** were obtained in excellent yield by treating **18** and **19** with hydrazine hydrate in refluxing ethanol. Lithium aluminiumhydride reduction afforded the corresponding amines **22** and **23**<sup>135</sup>. Acylation with 4-nitrobenzoyl chloride subsequently achieved the di-methoxyl analogues **RCZ09** (THP) and **RCZ17** (DHP) in moderate yield. After trying different de-methylation conditions, the di-hydroxyl derivatives **RCZ10** (THP) and **RCZ18** (DHP) were obtained with boron tribromide at 40 °C.

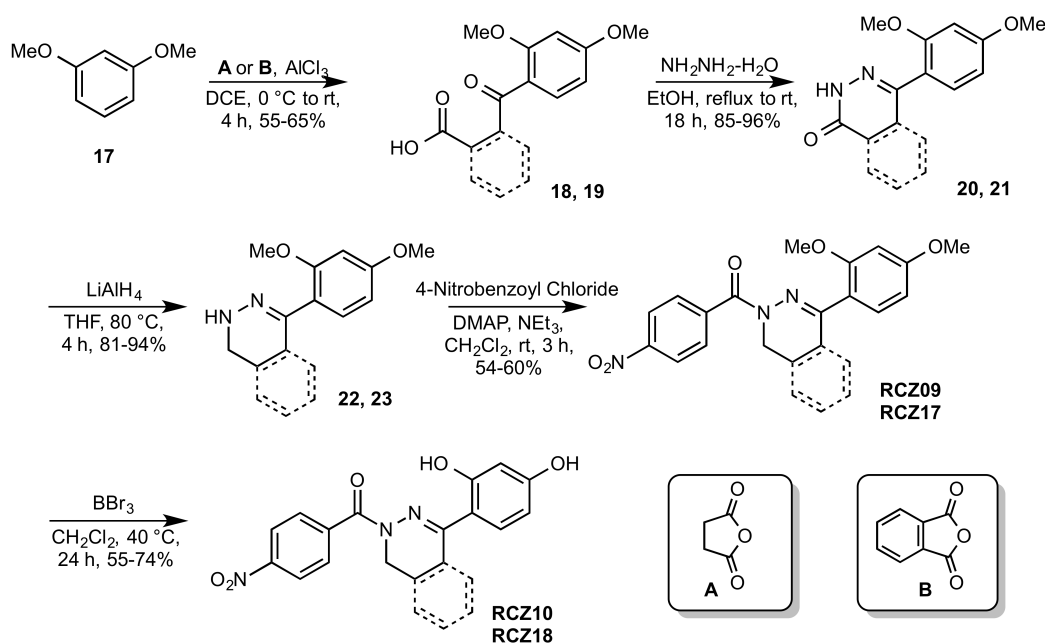


**Fig. 11: Synthetic route for THP and DHP derivatives:** The synthesis started from resorcindimethylether (**17**) which reacted with both succinic (**A**) or phthalic (**B**) anhydride in presence of  $\text{AlCl}_3$ . Intermediates **18** and **19** were converted in the corresponding amides **20** and **21** in very good yield upon hydrazine treatment in refluxing ethanol.  $\text{LiAlH}_4$  reduction yielded amines **22** and **23**, which were consequently acylated with 4-nitrobenzoyl chloride to obtain the di-methoxyl THP and DHP derivatives **RCZ09** and **RCZ17**. Demethylation was carried out with  $\text{BBr}_3$  in DCM at 40 °C to finally afford the two di-hydroxyl analogues **RCZ10** and **RCZ18**.

In order to expand the series, it was decided to replace the carbonyl function with a sulphone group (Fig. 12). Consequently, the two amines, **22** and **23**, were sulphonylated with nosyl chloride and then de-methylated with the previous conditions, to afford **RCZ12** (THP) and **RCZ20** (DHP). Although in this case the de-methylation step was found to be problematic and provided very poor yield, we obtained enough final material to carry on with biological tests.

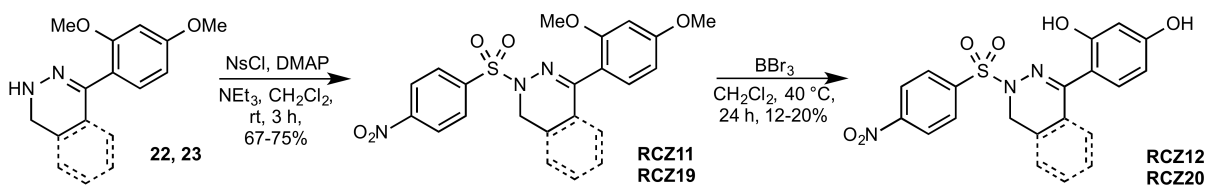


**Fig. 12: Synthesis of sulphonyl THP and DHP derivatives:** To expand our series, amines **22** and **23** were sulphonylated with nosyl chloride to afford di-methoxyl analogues **RCZ11** and **RCZ19**. Demethylation was carried out with the same protocol used previously to yield **RCZ12** and **RCZ20** in poor yields. Despite the inefficient de-protection, the amount obtained of the di-hydroxyl sulphonyl compounds was found to be enough to perform various biological tests.

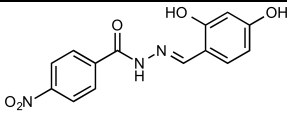
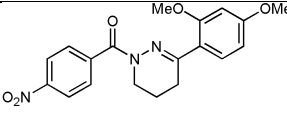
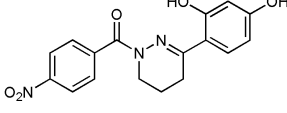
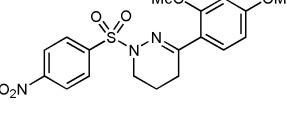
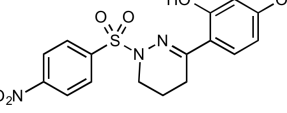
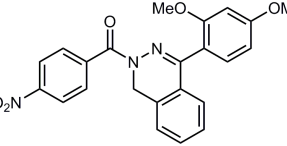
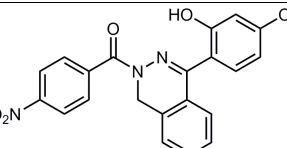
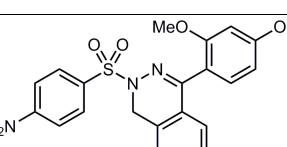
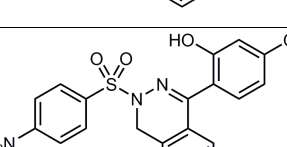
### 7.3 Biological evaluation of the THP and DHP derivatives

A total of 8 compounds (**RCZ09-20**) were selected to be tested for activity against the expression of the T3SS in *E. coli* O157:H7. The strain TUV 93-0 was used as this lacks the potent Shiga toxin making it suitable for work in category II containment facilities. Together with the di-hydroxyl carbonyl and sulphonyl derivatives (**RCZ10**, **RCZ18**, **RCZ12** and **20**), we also included all 4 di-methoxyl compounds (**RCZ09**, **11**, **17** and **19**) derived from our synthetic route. This allowed us to investigate the relevance of the carbonyl (hydrogen bond acceptor) on the left hand side of the molecule and, at the same time, the role played by the two hydroxyl groups (hydrogen bond acceptor/donor) on the right side. All compounds were firstly evaluated for their ability to affect bacterial growth and then screened on the ability to block secretion of the T3SS associated virulence protein EspD.

#### 7.3.1 Bacterial growth

Anti-virulence compounds are specifically designed to disarm the bacterial virulence weapons without affecting essential pathways such as bacterial growth or protein synthesis. This particular feature is essential to reduce the evolutionary pressure and SOS responses associated with treatment using traditional antibiotic treatments. Thus, our new molecules were firstly tested against the bacterial growth of *E. coli* O157 TUV 93-0.



| Entry (50 $\mu$ M) | Structure  | OD <sub>600</sub> after 5 h |
|--------------------|--|-----------------------------|
| WT                 | -  | 0.680 $\pm$ 0.008           |
| ME0055**           |    | 0.507 $\pm$ 0.021           |
| RCZ09              |    | 0.690 $\pm$ 0.018           |
| RCZ10              |    | 0.745 $\pm$ 0.026           |
| RCZ11              |    | 0.724 $\pm$ 0.029           |
| RCZ12              |    | 0.705 $\pm$ 0.024           |
| RCZ17              |   | 0.693 $\pm$ 0.014           |
| RCZ18              |  | 0.708 $\pm$ 0.011           |
| RCZ19*             |  | 0.760 $\pm$ 0.066           |
| RCZ20              |  | 0.706 $\pm$ 0.010           |

**Table 4: Bacterial growth after 5 hours of incubation:** The mean OD<sub>600</sub> values and their standard deviation for each sample are represented in the table on the left. Mean OD<sub>600</sub> values were obtained through linear regression analysis of the growth curve interpolated at desired time value (5 h). Mean OD<sub>600</sub> values of treated samples were compared to the control sample (WT) by Student's t-test for statistical significance ( $P$  value < 0.05). Significant samples are indicated by an asterisk. ME0055 growth inhibition resulted to be very statistically significant ( $P$  = 0.0056), while **RCZ19** showed a small significant increase in the growth rate ( $P$  = 0.0143).

The 8 compounds were incubated at 50  $\mu$ M with TUV 93-0 strain in a T3SS-inducing media and the bacterial concentration ( $OD_{600}$ ) was calculated hourly by means of a refractometer (Table 4). As previously observed in our group, ME0055 showed a significant effect (1.4-fold reduction) on the rate of bacterial growth at this concentration<sup>118</sup>. In comparison, all the derivatives did not show any substantial effect on the growth of the pathogen, which was deemed a desirable trait for a potential anti-virulence compound.

### 7.3.2 THP and DHP screening

The amount of secreted virulence proteins by *E. coli* O157 TUV 93-0 strain was investigated by western blot analysis as a screening experiment for our small series of ME0055 analogues (Fig. 13). The derivatives were evaluated by measuring the quantity of the secreted virulence protein EspD, essential part of the translocon pore<sup>136</sup>, at 50  $\mu$ M as a preliminary assessment. ME0055 showed a 5-fold reduction of the secretion of EspD as previously demonstrated<sup>118</sup>.

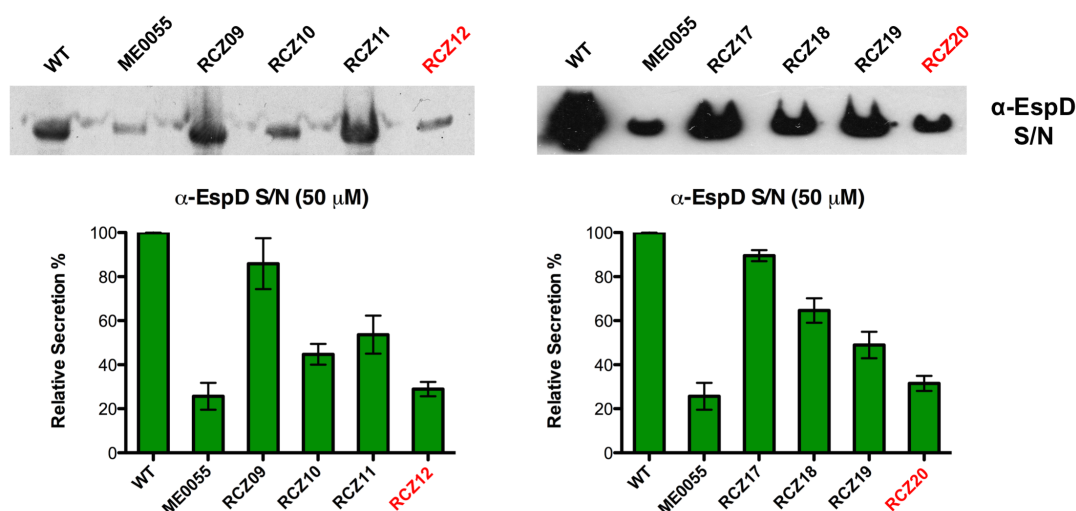


**Fig. 13:  $\alpha$ -EspD Western blot for THP and DHP derivatives at 50  $\mu$ M (top) and plotted relative EspD secretion percentage graph (bottom):** Western blot analysis were carried out according to standard procedure (see Experimental Part for methods and Ab dilutions). Blots were performed in triplicates coming from three independent experiments. The plotted relative secretion was obtained evaluating X-rays film pixel density by means of ImageJ program from three independent experiments. Untreated samples (WT) were considered as total secretion (100%) and treated samples were normalised accordingly. Mean relative secretion values are represented in the graph. Standard deviation from the mean is shown by error bars. **RCZ12** and **RCZ20** demonstrated to be the best compounds of the series, decreasing by four-fold EspD secretion. The di-hydroxyl sulphonyl activity was found to be comparable to ME0055 and, since they share common structural features, further biological tests were performed focusing on **RCZ12** and **RCZ20**.

The effects of the new compounds on EspD secretion were also assessed. Carbonyl di-methoxyl analogues (**RCZ09** and **RCZ17**) did not significantly reduce EspD secretion, while the sulphonyl di-methoxyl molecules (**RCZ11** and **RCZ19**) decreased the secretion of the protein by 2-fold compared to the uninhibited control. The same activity pattern was detected for the 4 di-hydroxyl compounds (**RCZ10**, **12**, **18** and **20**) with the sulphonyl derivatives having a better inhibition profile than the carbonyl. **RCZ18** showed a poor activity (1.3-fold reduction), while **RCZ10** lowered the virulence protein secretion by 2.5-fold. **RCZ12** and **RCZ20** displayed a significant activity against EspD decreasing its relative secretion by 4-fold and resulting the most active compounds of the entire series. It was interesting to notice that the inhibition by the 4 di-hydroxyl derivatives was generally more marked than that observed for the 4 di-methoxyl molecules, suggesting that the hydroxyl groups may be contributing to activity. The inhibition observed for **RCZ12** and **RCZ20** was found to be slightly weaker than the inhibition by ME0055: however, it was planned to pursue further biological assays with the two sulphonyl di-hydroxyl candidates.

#### 7.3.4 Western blot analyses for RCZ12 and RCZ20

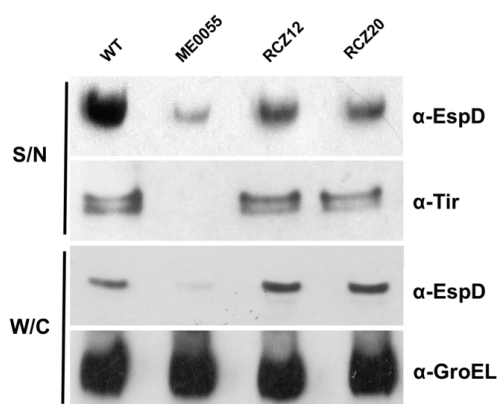


**Fig. 14: α-Tir (S/N), α-EspD (S/N and W/C) and α-GroEL (W/C) Western blots for RCZ12 and RCZ20 at 50 μM:** Western blot analyses were carried out according to standard procedure (see Experimental Part for methods and Ab dilutions). Both supernatant proteins (S/N) and whole cell lysate solution (W/C) were analysed. The relative secretion values were obtained evaluating X-rays film pixel density by means of ImageJ from three independent experiments. Untreated samples (WT) were considered as total secretion/expression (100%) and treated samples were normalised accordingly. Both **RCZ12** and **RCZ20** displayed a different effect on T3SS proteins than ME0055 at 50 μM. Reduction of EspD secretion seems to be a selective post-transcriptional effect, since equal amount of the virulence protein were found inside the cell when TUV 93-0 was treated with our new derivatives. A very weak effect was also detected for another T3SS protein (Tir) for **RCZ20**, but it couldn't be considered comparable to ME0055 effects.

To complete the profile of the T3SS proteins secretion in presence of **RCZ12** and **RCZ20** at 50  $\mu$ M, the amount of secreted Tir (translocated intimin receptor) was measured through western blot analysis (Fig. 14). As previously observed, ME0055 completely inhibited the secretion of this virulence protein<sup>118</sup>. **RCZ12** and **RCZ20** resulted in a very weak effect on Tir secretion (1.2-fold reduction). Both candidates demonstrated a more marked effect on EspD secretion than Tir. To further understand the basis of this selectivity, the intracellular quantity of EspD was also analysed by western blot. A total reduction of the protein into the cytosol was detected for the SA compound<sup>118</sup>, indicating a strong effect at transcriptional level for this virulence protein. Interestingly, both **RCZ12** and **RCZ20** resulted in a very different phenotype to the SA compound. Intracellular EspD did not decrease, instead resulting in the retention of the protein inside the cell. Unlike ME0055, which reduced both EspD transcription and secretion, the two derivatives only appeared to interfere with protein secretion. As previously demonstrated, ME0055 activity seemed to be mediated by down-regulating the expression of the entire locus that encodes for the T3SS apparatus, inhibiting both EspD and Tir secretion<sup>118</sup>. Interestingly, **RCZ12** and **RCZ20** mode of action appeared to be focused selectively on EspD secretion at a post-transcriptional level, without significantly affecting the protein's intracellular concentration and Tir secretion. GroEL concentration was also evaluated as an experimental control and to exclude any other possible effect on bacterial housekeeping activity by our new molecules. As previously demonstrated, ME0055 did not affect GroEL production<sup>118</sup>, a trait that was mirrored by the candidate compounds.

| Entry | CFU/mL               | Standard deviation       |
|-------|----------------------|--------------------------|
| WT    | $2.00 \cdot 10^{11}$ | $\pm 3.46 \cdot 10^{10}$ |
| RCZ12 | $1.97 \cdot 10^{11}$ | $\pm 2.78 \cdot 10^{10}$ |
| RCZ20 | $1.96 \cdot 10^{11}$ | $\pm 2.91 \cdot 10^{10}$ |

**Table 5: Colony count for RCZ12 and RCZ20 at 200  $\mu$ M:** Colony count analysis was carried out through a modified version of the Miles and Misra protocol (see Experimental Part). A total of 9 independent experiments were performed for each entry, plating a dilution range between  $10^{-3}$  to  $10^{-10}$ . CFU/mL mean values are represented in the table above with the corresponding standard deviation values. No effects on bacterial growth were observed for either **RCZ12** and **RCZ20** at 200  $\mu$ M.

The results obtained by these analyses drove us to propose that the THP and DHP derivatives might selectively block EspD secretion at the post-transcriptional level. To examine this further, a range of concentrations of these compounds was tested. *E. coli*

O157 TUV 93-0 was treated with decreasing concentrations of **RCZ12** and **RCZ20**, from a maximum concentration of 200  $\mu$ M and a minimum concentration of 10  $\mu$ M (Fig. 15). Bacterial growth was assessed to evaluate any effects on growth rates and colony counts was performed to determine any detrimental effects on bacterial viability (Table 5). TUV 93-0 was incubated with 200  $\mu$ M of the two candidates for 6 hours, the cultures diluted and then plated at the desired dilution ranges. Colonies were counted and processed to obtain the CFU/mL unit values. Neither **RCZ12** or **RCZ20** affected the bacterial growth or survival at 200  $\mu$ M, the highest concentration of the compound used in any assays. EspD secretion was then measured with decreasing concentrations of the two candidates by western blotting. Both **RCZ12** and **RCZ20** interfered with the protein secretion in a concentration-dependent manner. A strong inhibition of EspD secretion (25-fold reduction) was detected at 200  $\mu$ M and a significant 5-fold reduction was also observed at 100  $\mu$ M. Both candidates showed an absent or weak 1.5-fold reduction of the T3SS protein secretion at 25  $\mu$ M and 10  $\mu$ M. Intracellular amounts of EspD were also measured at 200  $\mu$ M to verify the correct transcription of the virulence protein even at higher concentrations. Retention of the T3SS protein was also observed in this case for both our candidates. Slightly increased amounts of EspD were detected inside the cells treated with **RCZ12** and **RCZ20**, which confirmed the retention of the virulence protein in absence of secretion. At this concentration, also Tir secretion was inhibited and a  $\alpha$ -Tir analysis on the whole cell lysate showed reduction of Tir expression. GroEL immunoblotting was performed as an experimental control and to assess any effects of the compounds on non-T3SS associated pathways at high concentrations. The two sulphonyl derivatives did not affect GroEL expression. The western blot results demonstrated that 200  $\mu$ M is the optimal concentration to obtain a total inhibition of EspD secretion. At this high concentration, our new compounds also showed to block Tir secretion and expression as resulted from the  $\alpha$ -Tir analyses inside and outside the cell. It can be postulated that **RCZ12** and **RCZ20** share the same mechanism of action, which primarily interfere with EspD secretion in a concentration-dependent manner and also affects other T3SS proteins transcription (i.e. Tir).

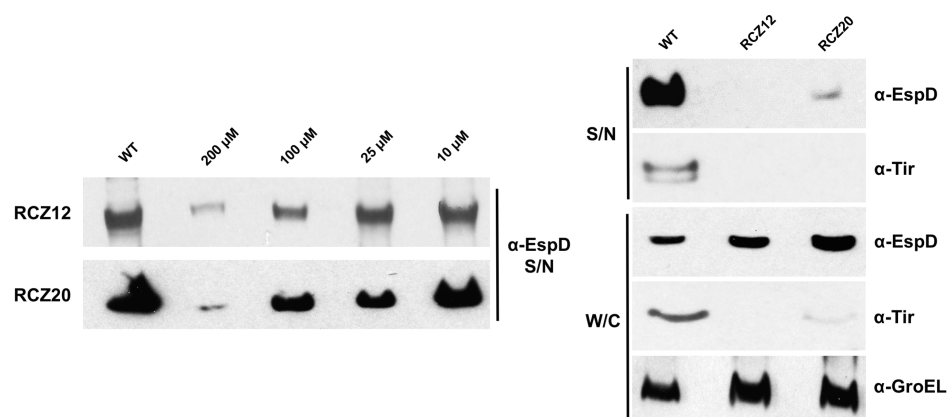


**Fig. 15: α-EspD Western blot for RCZ12 and RCZ20 (200 μM - 10 μM) (left) and α-EspD, α-Tir and α-GroEL Western blot for RCZ12 and RCZ20 at 200 μM (right):** Western blot analyses were carried out according to standard procedure (see Experimental Part for methods and Ab dilutions). Both supernatant proteins (S/N) and whole cell lysate solution (W/C) were analysed. The relative secretion values were obtained evaluating X-rays film pixel density by means of ImageJ from three independent experiments. Untreated samples (WT) were considered as total secretion (100%) and treated samples were normalised accordingly. **RCZ12** and **RCZ20** demonstrated to have a concentration-dependant effect on EspD secretion. 200 μM was considered as the ideal concentration to have an almost total inhibition of the secretion without affecting the bacterial growth. To complete the activity profile of **RCZ12** and **RCZ20** at 200 μM, α-EspD, α-Tir and α-GroEL Western blot were performed. Both candidates showed to inhibit EspD secretion, while retaining the virulence protein inside the cell, as suggested by the α-EspD W/C Western blot result. Also Tir secretion and expression resulted decreased at this high concentration. Secretion of this T3SS protein was totally inhibited, while Tir expression was found to be 10-fold reduced.

### 7.3.5 T3SS genes transcription

The western blot analyses showed that EspD secretion is affected by the THP and DHP derivatives, but also that Tir secretion and expression were influenced. To further investigate these transcriptional effects, transcriptomic analyses were carried out for **RCZ20** at 50  $\mu$ M (Fig. 16). This concentration was selected as it provided a direct comparison with our previous study into the effects of the SA compounds<sup>118</sup>. mRNA reads of samples of untreated TUV 93-0 and TUV 93-0 treated with **RCZ20** grown in T3SS-inducing media were compared and analysed to visualise any changes in transcription in the whole *E. coli* genome.

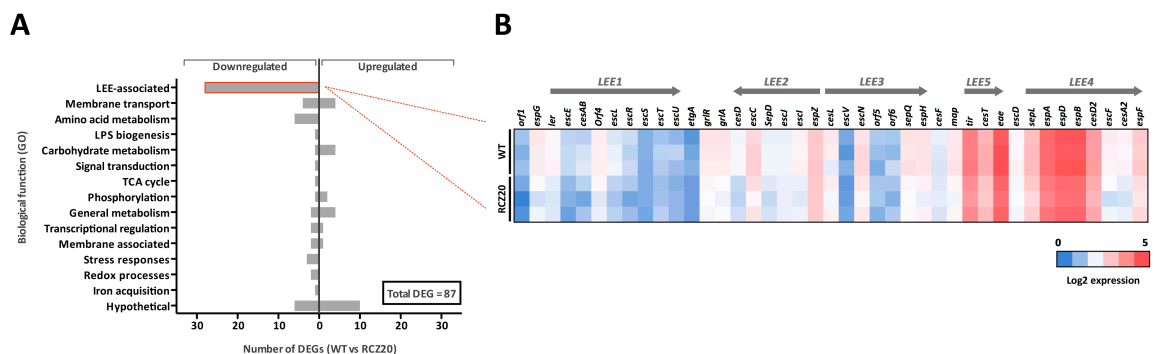


**Fig. 16: RNAseq data summary and LEE-related genes heatmap: A)** Summary of differentially expressed genes (DEGs) identified by RNA-seq. EHEC TUV 93-0 was cultured under T3SS-inducing conditions (MEM-HEPES; 37 °C, 200 rpm) with and without **RCZ20** supplemented at 50  $\mu$ M. The total number of DEGs is indicated with the proportion of up- or down-regulated genes illustrated by the appropriate bars. A gene was considered differentially expressed if it exhibited a fold change greater than 1.5 from the wild type (FDR  $P$ -value < 0.05). DEGs were clustered into biological functional groups according to gene ontology (GO). LEE-associated genes are highlighted in red. **B)** Heatmap of normalised genes expression values within the LEE island specifically as identified by RNA-seq. Wild type EHEC and the **RCZ20** treated replicates are indicated on the left and the structure of the LEE operons and associated ORFs are labelled above. The corresponding gene expression values for each LEE ORF are illustrated according to the colour scale below the graph.

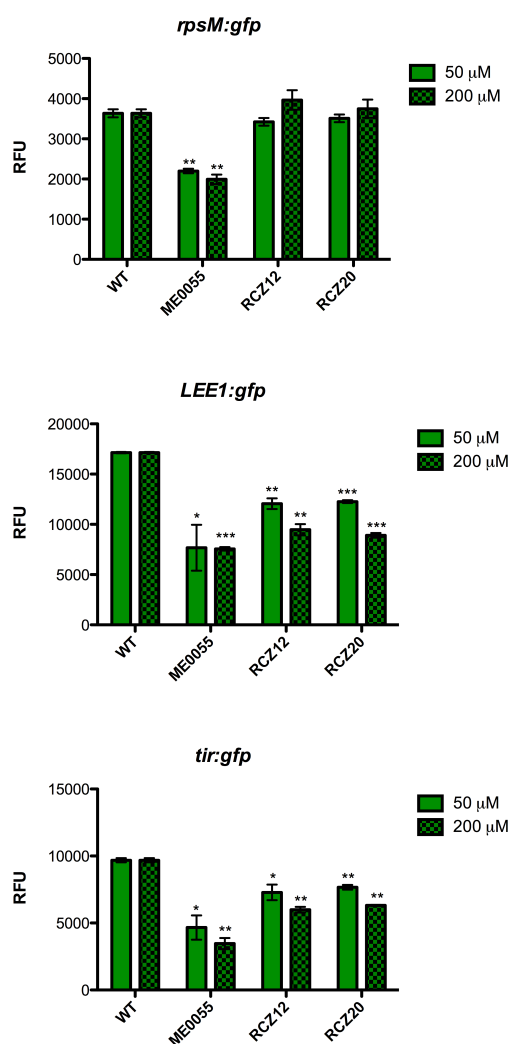


**Fig. 17: *rpsM:gfp*, *LEE1:gfp* and *tir:gfp* promoter activity at  $OD_{600} = 0.6$  with ME0055, RCZ12 and RCZ20 at 50 and 200  $\mu$ M:** GFP-reporter fusion assays were carried out according to standard procedure (see Experimental Part for methods). The promoter activity was measured for every sample plotting fluorescence (RFU) against  $OD_{600}$ . The curves thus obtained were analysed through linear regression and interpolated with a determined  $OD_{600}$  value (0.6). Interpolated RFU mean values are represented in the graphs on the left. Standard deviation from the mean is shown by error bars. RFU values of treated samples were compared to the control sample (WT) by Student's t-test for statistical significance ( $P$  value < 0.05). Significant samples are indicated by an asterisk, very significant samples by two asterisks and extremely significant samples by three asterisks. **RCZ12** and **RCZ20** demonstrated to have an effect at transcriptional level. Promoter activities of both *LEE1* and *tir* were found to be down-regulated at 50 and 200  $\mu$ M. The effect detected by our compounds was weaker and more selective than ME0055, which resulted in a greater down-regulation of the two T3SS-related genes, but also influenced house-keeping genes (*rpsM*) as shown in previous studies<sup>118</sup>. These results are in accordance with the RNAseq findings.

A specific but mild down-regulation effect (between 1.5- and 2-fold decrement) on T3SS genes was detected especially in *LEE1*, *LEE4* and *LEE5* operon regions, which contain genes such as *ler*, *tir*, *espD*, *espB*, *eae* and *espA*, while no particular effects were observed in other areas of the genome<sup>44</sup> (Table 6). These findings proved that our new derivatives act also at a transcriptional level, selectively down-regulating T3SS genes. Although the influence on the LEE-based genes is mild, it is an indication that both **RCZ12** and **RCZ20** display also activity against the T3SS genes transcription. In addition, the down-regulation provided by our compounds is specific to the LEE region, while ME0055 previously demonstrated to have more widespread transcriptional effects, affecting many non T3SS-related genes<sup>118</sup>.

To validate the RNAseq data, **RCZ12** and **RCZ20** transcriptional effects were evaluated through a GFP reporter fusion assay at both 50 and 200  $\mu$ M, where the activity of the promoter of the desired gene is proportional to GFP expression (Fig. 17). *rpsM* promoter



activity (30S ribosomal subunit) was firstly assessed as a control, in order to analyse any unwanted effect by the candidates on an essential housekeeping gene not related to T3SS. *rpsM* transcription was found to be significantly down-regulated in the presence of ME0055 at 50 and 200  $\mu\text{M}$ <sup>118</sup>. In addition, the SA compound displayed a very strong effect on bacterial growth at 200  $\mu\text{M}$ , reducing by more than 2-fold the growth rate.

| Gene        | Log <sup>2</sup> fold change | P value  | Function                           |
|-------------|------------------------------|----------|------------------------------------|
| <i>escN</i> | -1.5                         | 6.09E-05 | ATPase                             |
| <i>map</i>  | -1.54                        | 9.35E-05 | Secreted effector protein          |
| <i>espD</i> | -1.55                        | 1.78E-04 | Translocon                         |
| <i>espA</i> | -1.57                        | 1.05E-04 | Needle filament                    |
| <i>espH</i> | -1.59                        | 7.15E-05 | Secreted effector protein          |
| <i>eae</i>  | -1.61                        | 2.37E-07 | Intimin                            |
| <i>tir</i>  | -1.62                        | 6.91E-06 | Translocated intimin receptor      |
| <i>espF</i> | -1.63                        | 3.10E-05 | Secreted effector protein          |
| <i>espB</i> | -1.64                        | 3.53E-05 | Translocon                         |
| <i>escC</i> | -1.64                        | 7.83E-06 | Secretin (T3SS basal body protein) |
| <i>espJ</i> | -1.66                        | 2.51E-05 | Secreted effector protein          |
| <i>escF</i> | -1.66                        | 3.09E-04 | T3SS basal body protein            |
| <i>sepL</i> | -1.66                        | 3.12E-07 | Gatekeeper protein                 |
| <i>ler</i>  | -1.69                        | 1.55E-05 | LEE master regulator               |
| <i>sepQ</i> | -1.75                        | 5.05E-06 | T3SS basal body protein            |
| <i>espG</i> | -1.9                         | 8.39E-06 | Secreted effector protein          |
| <i>escR</i> | -1.95                        | 4.94E-05 | Unknown                            |

**Table 6: Summary of the effects of RCZ20 on LEE-related genes expression as identified by RNAseq experiment:** The name of the LEE-related genes expression affected from the treatment of **RCZ20** at 50  $\mu\text{M}$ . The Log<sup>2</sup> fold change and the P values are also listed. The function of the corresponding proteins is specified on the right-hand side of the table.

Our derivatives did not show a statistically significant activity against *rpsM* transcription at both concentrations. *LEE1* transcription was then measured as this encodes the master regulator of the entire T3SS and is key to activation. As previously shown, ME0055 significantly down-regulated by 2.2 and 2.5-fold *LEE1* transcription at 50  $\mu\text{M}$  and 200  $\mu\text{M}$  respectively<sup>118</sup>. A noteworthy down-regulation (1.8 and 1.9-fold reduction at 200  $\mu\text{M}$ ) of the promoter activity was also detected for **RCZ12** and **RCZ20** in a concentration-dependent way. However, the transcriptional effects of our compounds were weaker than those observed for the SA compound. The activity of the *tir* promoter was also measured to further examine the RNAseq and western blot data and to understand the basis of the

down-regulation. ME0055 resulted in a very strong down-regulation of the promoter (2.7-fold reduction at 200  $\mu$ M), as previously reported<sup>118</sup>. Also **RCZ12** and **RCZ20** influenced the promoter activity of this gene, but exhibited a significantly weaker activity than the SA compound, down-regulating *tir* transcription by 1.5-fold. The results obtained from the GFP-reporter fusion assays were in accordance with the transcriptomic and western blot data. **RCZ12** and **RCZ20** showed to have a selective transcriptional effect on T3SS-related genes, as shown by the *rpsM:gfp* results, where no influence was detected for our compounds while a significant activity was registered for ME0055. Down-regulation of the promoters of both T3SS-related genes *LEE1* and *tir* was also observed. However, the magnitude of the effect of the THP and DHP derivatives was weaker than the SA compound activity. This confirms that **RCZ12** and **RCZ20** have a transcriptional effect beside a direct activity on EspD secretion. RNAseq and GFP-reporter fusion assays results highlighted the specific transcriptional effect, even though it resulted to be weaker than ME0055 activity. In summary, these data demonstrated that the transcriptional effects of **RCZ12** and **RCZ20** are largely focused on the T3SS-related genes, while the SA compound has a broader influence across the whole *E. coli* genome.

### 7.3.6 Additional transcriptional evaluation

The transcriptional results obtained from the RNAseq and GFP reporter fusion assays drew us to hypothesise a potential inhibitory feedback circuit due to the reduced EspD secretion. It is possible that the intracellular retention of EspD caused by **RCZ12** and **RCZ20** could trigger inhibitory signals towards the expression of other T3SS proteins, leading to the down-regulation of the LEE. It has previously been demonstrated in *C. rodentium* that *espD* null mutants express and secrete Tir and other T3SS proteins normally, indicating a lack of LEE-encoded feedback circuits. However, the same study highlighted that the LEE regulation is extremely species-dependent, as differences in T3SS proteins were observed in EPEC, EHEC and *C. rodentium*<sup>37</sup>. On the other hand, the THP and DHP derivatives may also act directly on LEE transcription. The down-regulation of both *LEE1* and *tir* is especially marked when the compounds are employed in high concentrations (200  $\mu$ M), thus it might be the result of secondary interactions within the cell.

To investigate the transcriptional effect caused by **RCZ12** and **RCZ20**, it was planned to create two GFP reporter strains in an *E. coli* O157 TUV 93-0  $\Delta$ *espD* strain. The strains were

generated by transforming the GFP reporter plasmids for *LEE1* and *tir* in EHEC  $\Delta espD$  strain, thus creating  $\Delta espD$  *LEE1:gfp* and  $\Delta espD$  *tir:gfp*. The new  $\Delta espD$  GFP reporter strains were first compared with the corresponding TUV 93-0 GFP reporter strains in order to highlight a potential down-regulation caused by the lack of the virulence protein EspD (Fig. 18). While the promoter activity of *LEE1* was found to be comparable in both strains, *tir* transcription proved to be slightly down-regulated by 1.3-fold in the  $\Delta espD$  mutant, suggesting a mild effect on *tir* expression due to the lack of EspD. The 2 new strains were then treated with **RCZ12** and **RCZ20** at 200  $\mu$ M to evaluate their transcriptional effect on the LEE in absence of the virulence protein EspD. In both cases, **RCZ12** and **RCZ20** negatively influenced the promoters' activity in the  $\Delta espD$  GFP strains. *LEE1* transcription was reduced by 1.5-fold, while *tir* expression was inhibited by 2-fold, highlighting **RCZ12** and **RCZ20** effect on transcription at 200  $\mu$ M.

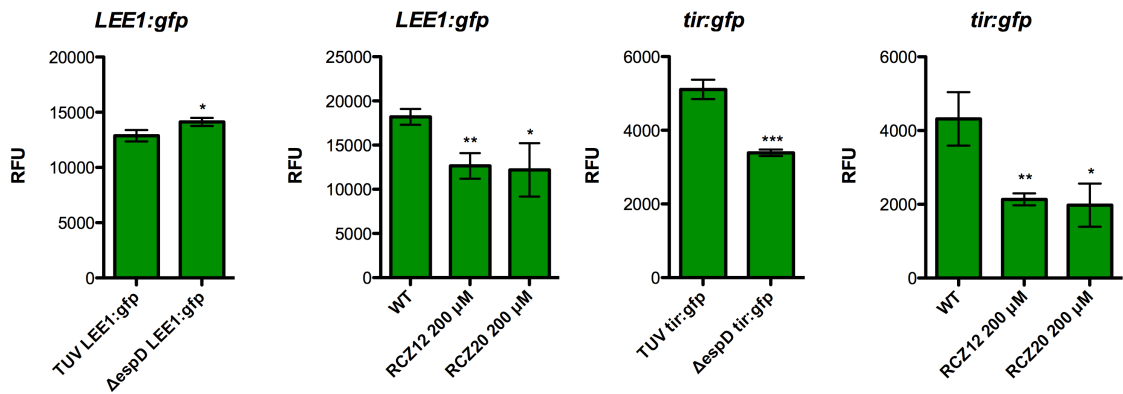


**Fig. 18:  $\Delta espD$  *LEE1:gfp* and  $\Delta espD$  *tir:gfp* promoter activity at  $OD_{600} = 0.7$  compared with their TUV 93-0 counterpart and with RCZ12 and RCZ20 at 200  $\mu$ M:** GFP-reporter fusion assays analyses were carried out according to standard procedure (see Experimental Part for methods). The promoter's activity was calculated at  $OD_{600} = 0.7$  and RFU mean values are represented in the graphs above. Standard deviation from the mean is shown by error bars. RFU values of treated samples were compared to the control sample (WT) by Student's t-test for statistical significance. Significant samples are indicated by an asterisk ( $P$  value  $< 0.05$ ), very significant samples by two asterisks ( $P$  value  $< 0.01$ ) and extremely significant samples by three asterisks ( $P$  value  $< 0.005$ ).  $\Delta espD$  *LEE1:gfp* was firstly compared with TUV *LEE1:gfp* (first graph from the left) and then treated with **RCZ12** and **RCZ20** at 200  $\mu$ M (second graph from the left).  $\Delta espD$  *tir:gfp* was firstly compared with TUV *tir:gfp* (third graph from the left) and then treated with **RCZ12** and **RCZ20** at 200  $\mu$ M (fourth graph from the left). Both the THP and DHP compounds displayed a direct influence on *LEE1* and *tir* transcription. In addition, the lack of *espD* in  $\Delta espD$  *tir:gfp* also down-regulated *tir* expression compared to the TUV 93-0 expression.

The results obtained by this additional GFP reporter fusion assay revealed that EspD has a mild negative feedback on *tir* transcription, as  $\Delta espD$  *tir:gfp* showed a reduced activity of the *tir* promoter than the TUV 93-0 *tir:gfp*. Treatment of the 2 new  $\Delta espD$  GFP strains with

**RCZ12** and **RCZ20** at 200  $\mu$ M also demonstrated that both compounds have a direct effect on *LEE1* and *tir* transcription. In conclusion, it is clear that our THP and DHP candidates act primarily on EspD secretion and also directly influence the transcription of LEE-related genes. However, it cannot be excluded that the lack or the incorrect secretion of the virulence protein EspD might also down-regulate *tir* expression.

### 7.3.7 Transmission electron microscopy (TEM) experiment

**RCZ12** and **RCZ20** demonstrated to primarily affect the secretion of the virulence protein EspD, causing its intracellular accumulation. It has been previously reported that the lack or malfunctioning of EspD result in the production of aborted T3SS filaments. Kresse *et al.* demonstrated that *espD* null mutant strains displayed an impaired attachment to HeLa cells. Microscopy studies revealed only a focal accumulation of the protein EspA on the bacterium's surface instead of the correct assembly of the T3SS, showing significantly smaller needle formation than the wild type<sup>33</sup>. It was then decided to evaluate through microscopy studies the formation of EspA filaments in the presence of our compound, as both **RCZ12** and **RCZ20** affected EspD secretion (Fig. 19). Untreated *E. coli* O157 TUV 93-0 and the  $\Delta espD$  strain were employed as positive and negative controls respectively.

| Sample        | n° EspA filaments (>500 nm) | SD          | N  |
|---------------|-----------------------------|-------------|----|
| WT            | 4.960                       | $\pm 2.791$ | 25 |
| RCZ12         | 1.040                       | $\pm 1.020$ | 25 |
| RCZ20         | 1.720                       | $\pm 1.646$ | 25 |
| $\Delta espD$ | 0.785                       | $\pm 1.475$ | 25 |

**Table 7: Determination of the number of EspA filaments (>500 nm) for bacteria treated with RCZ12 and RCZ20:** The average number of EspA filaments (>500 nm) for the TEM samples is shown in the table above. The values have been calculated from 25 different images taken from 5 independent experiments. Standard deviation from the mean value is also shown in the table.

Bacteria were grown in a T3SS-inducing media and then immobilised in paraformaldehyde. Before exposure to the microscope, the samples were incubated with a  $\alpha$ -EspA antibody and then with the corresponding secondary antibody conjugate with gold nanoparticle for visualisation. Untreated *E. coli* O157 TUV 93-0 produced an average of five long needle formations (>500 nm) per bacterium, while  $\Delta espD$  did not show any EspA filament formations as expected (an average of 0.78 functioning needles). **RCZ12**- and **RCZ20**-treated bacteria demonstrated to inhibit the formation of EspA filaments (an average of 1

functioning needle per bacterium), as the bacteria revealed only short needle structures (<500 nm) and accumulation of EspA on the surface, indicating an aborted T3SS apparatus. The count of EspA filaments longer than 500 nm revealed that the samples treated with **RCZ12** and **RCZ20** produced an average of 1 functioning T3SS needle apparatus, a reduction of 5-fold compared to the wild type (Table 7).

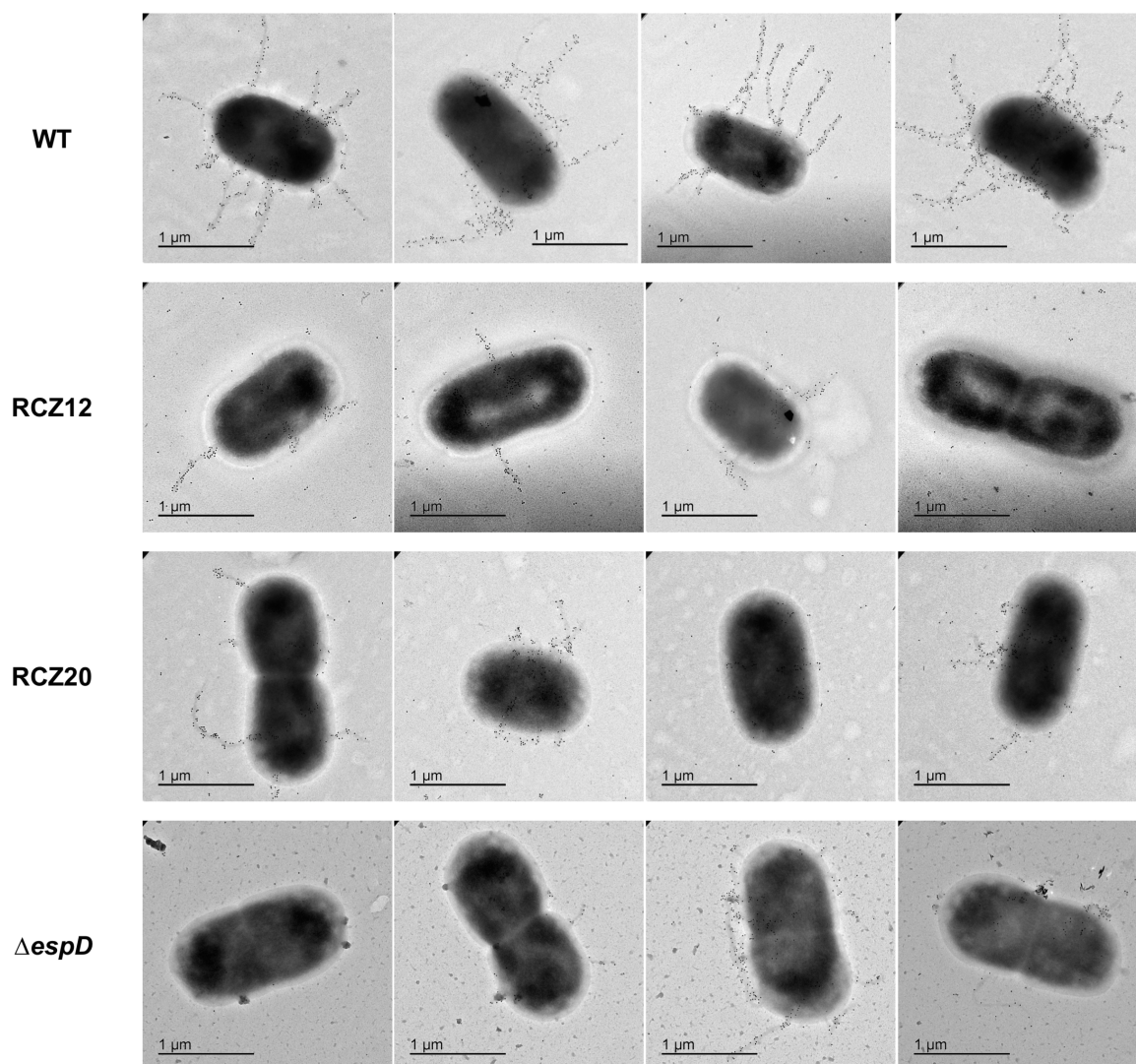


**Fig. 19: TEM images of EspA filaments with RCZ12 and RCZ20:** Bacteria were grown in T3SS-inducing media and immobilised in paraformaldehyde. Before exposure on the microscope, the samples were incubated with an  $\alpha$ -EspA primary antibody and then with the corresponding secondary antibody conjugated with gold nanoparticle. The black dots on the images represents the gold particles, which specifically identify EspA. **RCZ12** and **RCZ20** demonstrated to reduce the correct EspA filament formation by 5-fold, causing a focal accumulation of the protein on the bacterium's surface.

## 7.4 Conclusions

The SA compound ME0055 was used as a starting point to create a small series of potentially more selective and stable T3SS inhibitors of *E. coli* O157:H7. Two different

cores (THP and DHP) were designed and synthesised, incorporating the imine feature in heterocycles and retaining all ME0055 substituents. Synthesis started with a common commercially available starting material, resorcindimethylether (**17**), and was completed in only 5 steps. A total of 8 derivatives was synthesised and evaluated against the T3SS of *E. coli* TUV 93-0 strain. In addition to the two carbonyl di-hydroxyl inhibitors (**RCZ10** and **18**), we synthesised two sulphonyl di-hydroxyl analogues (**RCZ12** and **20**) to explore the left hand side of the molecule and we also included all 4 di-methoxyl compounds (**RCZ09**, **11**, **17** and **19**), derived from our synthetic route. These inclusions allowed examination of the relevance of the carbonyl and the hydroxyl groups. A preliminary biological evaluation showed that all our molecules did not affect bacterial growth, making them suitable anti-virulence candidates. The secretion of T3SS protein EspD by western blot was used as a screening assay to evaluate the activity of the series. The two sulphonyl di-hydroxyl molecules (**RCZ12** and **20**) demonstrated to be the most active compounds of the series and the only two candidates to have a comparable effect to the lead compound ME0055, with a 4-fold reduction of EspD secretion at 50  $\mu$ M. Further western blot analyses showed that **RCZ12** and **RCZ20** acted in a mechanism somewhat distinct from ME0055, since their activity was focused more on EspD secretion and not on the whole T3SS apparatus. Analysis on the secreted T3SS proteins revealed the inhibition of EspD and a weaker effect on Tir. Interestingly, the virulence protein was retained inside the cell as shown by western blot of the whole cell lysate solution. This EspD retention into the cytosol indicated a post-transcriptional effect on the T3SS protein by our compounds, which differs from ME0055 activity. Therefore, the inclusion of the imine feature into a heterocycles provided more stable compounds with a different activity against *E. coli* O157:H7. When employed in decreasing concentrations, **RCZ12** and **RCZ20** also displayed a concentration-dependent effect on EspD secretion. The experiment also highlighted a total inhibition of the secretion at 200  $\mu$ M and retention of such virulence protein inside the bacterial cytosol.  $\alpha$ -Tir at this high concentration showed also inhibition of Tir secretion and expression, suggesting a potential effect on transcription at 200  $\mu$ M. RNAseq analysis proved a mild and selective transcriptional effect on T3SS-related genes. GFP-reporter fusion assays on *rpsM*, *LEE1* and *tir* promoter activity confirmed the transcriptional activity of **RCZ12** and **RCZ20** at both 50 and 200  $\mu$ M. However, the effect exhibited by our compounds was weaker than ME0055 activity. In addition, the down-regulation was limited to LEE-based genes, while the SA compound previously demonstrated to also interfere with many non T3SS-related genes

<sup>118</sup>. We postulated that the primary activity of both **RCZ12** and **RCZ20** is the post-transcriptional inhibition of EspD secretion, while the selective transcriptional down-regulation of T3SS genes was considered as a secondary activity. The milder effect on LEE-based genes drew us to think that the down-regulation might be a consequence of the EspD secretion inhibition. It has been demonstrated that *espD* null mutant strain produces the virulence effector Tir normally, indicating a lack of LEE-encoded feedback inhibitory mechanism in *C. rodentium*. However, the study also reveals that the T3SS proteins regulation is highly species-dependent, as discrepancies in the LEE transcription were shown in EPEC, EHEC and *C. rodentium* <sup>37</sup>. Generation of  $\Delta espD$  *LEE1:gfp* and  $\Delta espD$  *tir:gfp* strains revealed that the THP and DHP derivatives acted directly on *LEE1* and *tir* transcription as a secondary interaction within the cell. It is easy to also speculate a possible negative feedback pathway derived from the incorrect secretion of EspD to suppress the T3SS proteins production, but, unfortunately, we did not explore these effects any further. The major focus was to try and examine the mode of action of **RCZ12** and **RCZ20**. Transmission electron microscopy experiment also showed that our compounds blocked the correct formation of EspA filaments; a consequence of the inhibition of the secretion of EspD.

## 8 Understanding RCZ12 and RCZ20 Mode of Action

### 8.1 Introduction

**RCZ12** and **RCZ20** proved to be active against T3SS protein expression and secretion in a relatively selective manner, compared to the lead compound. EspD secretion was inhibited by increasing concentrations of the two candidates and retention of this protein was observed into the pathogen cytosol. Tir was found to be inhibited at a transcriptional and post-transcriptional level by our derivatives at 200  $\mu$ M. Despite both molecules being derived from ME0055, they seemed to act on bacterial virulence weapons in a different and more selective way than the SA compound.

Previous studies within our group were focused to discover ME0055 mode of action through different affinity assays. A biotinylated derivative of the salicylidene acylhydrazide was employed for a pull-down experiment, revealing more than 16 putative proteins as targets<sup>125</sup>. Investigation of these possible targets confirmed that ME0055 was a very promiscuous binder and its efficiency could have been the result of multiple metabolic effects within the pathogen<sup>125</sup>. Since both our candidates displayed a more selective activity than the lead compound, it was decided to investigate the mode of action of **RCZ12** and **RCZ20** by labelling the two compounds with a variety of affinity tags, in order to investigate the molecular mechanism of action.

### 8.2 Design of RCZ12 and RCZ20 labelled version

To further investigate the mechanism of action of the new derivatives, it was chosen to label both molecules with specific probes to perform affinity experiments. Due to the candidates' small dimensions, we selected just two potential sites to place the tag; on the left-hand side (Fig.20 in blue) or on the right-hand side (Fig.20 in red) phenyl rings. From our previous biological assays, results showed how the di-hydroxyl derivatives displayed a better activity profile than the di-methoxyl ones, underlining the relevance of the free hydroxyl groups for activity against EspD secretion. In addition, in earlier studies<sup>125</sup>, ME0055 tag was placed on the left-hand side phenyl ring to perform pull-down experiments. Due to these findings, it was opted to position the tag on the left-hand side and to reduce the nitro group to an amino group to place a small linker between the molecule and the probe (Fig.20).



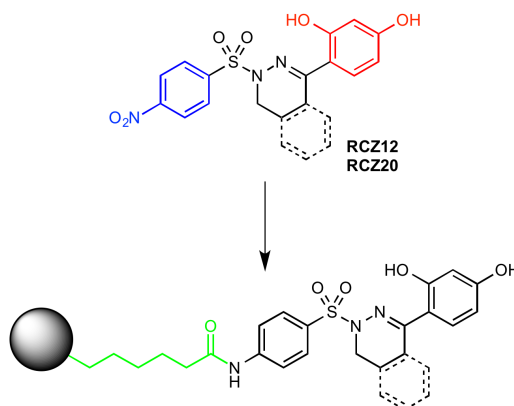


**Fig. 20: Design of RCZ12 and RCZ20 labelled version:** Due to RCZ12 and RCZ20 small dimensions, only the left-hand side (blue) and right-hand side (red) phenyl rings were chosen as plausible labelling sites. Since our findings suggested that the two hydroxyl groups might be relevant to the activity of the molecules, it was opted to place the affinity tag (sphere) on the left-hand side of the molecule and to reduce the nitro group to amino group to install a linker (green) between the molecule and the specific probe.

### 8.3 Alternative route for RCZ12 and RCZ20 synthesis

Our initial synthesis of THP and DHP cores proved to be problematic in the final step especially for the two sulphonyl derivatives **RCZ12** and **RCZ20**.  $\text{BBr}_3$ -mediated demethylation at 40 °C provided very poor yields and difficult separation of the desired product. Thus, we designed a new synthetic route to afford our two analogues of interest in a more efficient way for our labelling synthesis.

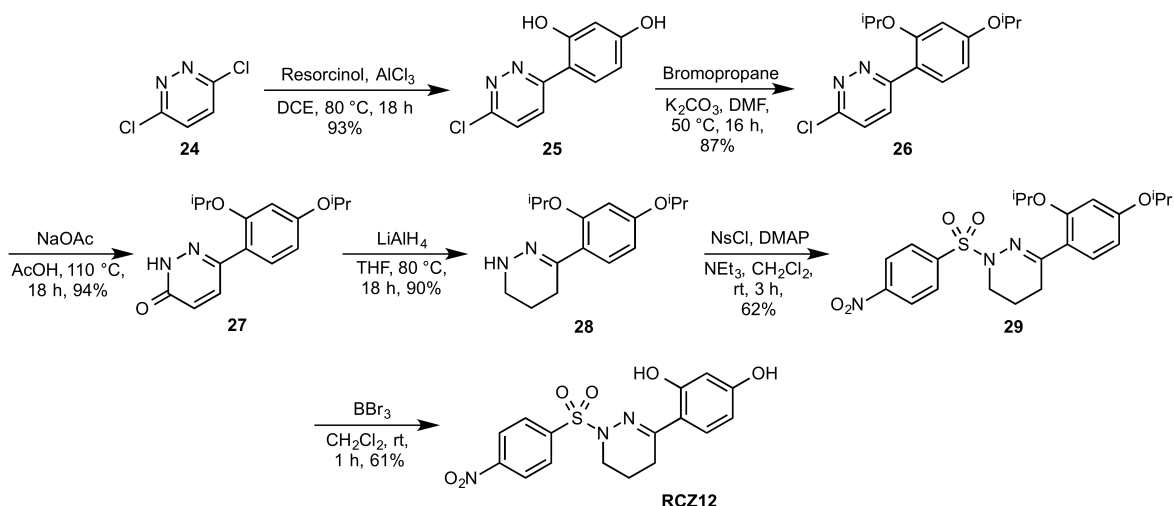


**Fig. 21: New synthetic route for RCZ12:** The alternative route for **RCZ12** started from 3,6-dichloropyridazine (**24**) which underwent Friedel-Crafts acylation with resorcinol to afford intermediate **25**. The two hydroxyl groups were protected with 2-bromo propane and intermediate **26** was then converted to the corresponding amide **27** in presence of sodium acetate in refluxing acetic acid.  $\text{LiAlH}_4$  reduction was performed following the previous protocol to obtain amine **28**. Sulphonylation with nosyl chloride afforded the protected intermediate **29**, which was consequently de-protected by  $\text{BBr}_3$  in DCM in very good yield. **RCZ12** was synthesised in 6 steps from **24**.

It was firstly planned to retain the  $\text{LiAlH}_4$  amide reduction of the previous route and to avoid any protecting groups. Unfortunately, this approach resulted in an unstable substrate for the reduction step that decomposed quickly and forced us to change immediately our strategy. Placement of other non-ether-like protecting groups was attempted, but they all demonstrated to be too sensitive to  $\text{LiAlH}_4$  (data not shown). It was then decided to place a branched ether (*iso*-propyl) as protection of the hydroxyl groups, which proved to be sufficiently stable for the harsh conditions of the reduction step and was found to be easier to remove than the methyl groups.

Our alternative synthesis of **RCZ12** started with 3,6-dichloropyridazine (**24**), which underwent Friedel-Crafts acylation with resorcinol to afford the desired adduct **25**<sup>137</sup> (Fig. 21). The two hydroxyl groups were protected with 2-bromo propane and intermediate **26** was subsequently converted into the corresponding amide **27**<sup>137</sup>. **28** was afforded in excellent yield by means of the same  $\text{LiAlH}_4$  reduction protocol of our initial synthesis<sup>135</sup>. The corresponding amine (**28**) was sulphonylated according to our previous conditions and adduct **29** was de-protected with  $\text{BBr}_3$  at room temperature in good yield.

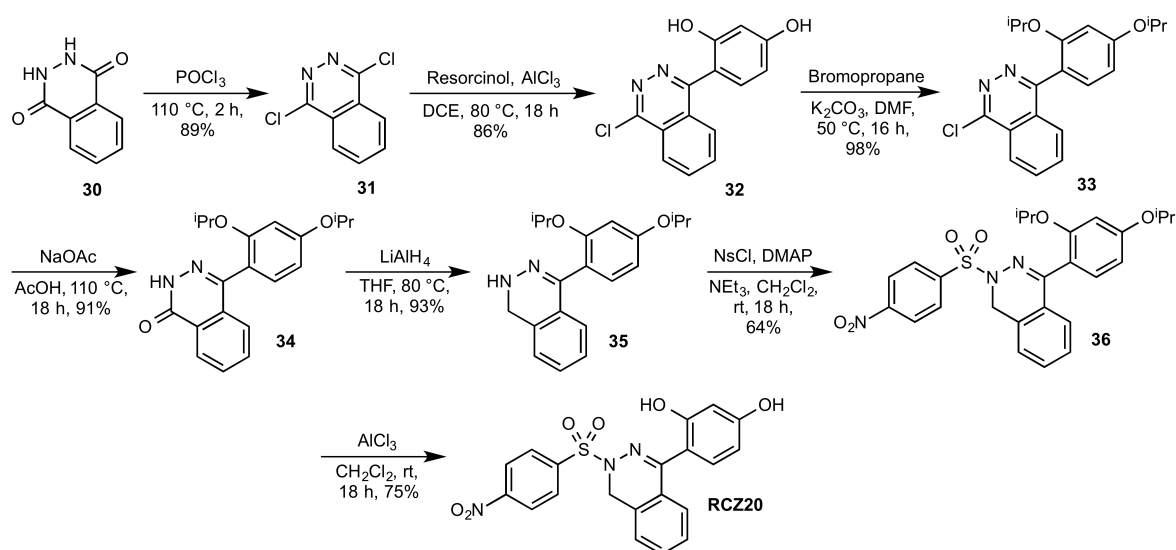


**Fig. 22: New synthetic route for RCZ20:** The alternative route for **RCZ20** started from phthalhydrazide (**30**) which was converted in 1,4-dichlorophthalazine (**31**) upon treatment with refluxing  $\text{POCl}_3$ . **31** was reacted with resorcinol in presence of  $\text{AlCl}_3$  to obtain intermediate **32** in very good yield. The two hydroxyl groups were protected with 2-bromo propane and intermediate **33** was converted in the corresponding amide **34** with sodium acetate. Amine **35** was achieved by the previous  $\text{LiAlH}_4$  reduction protocol and then sulphonylated with nosyl chloride to yield the protected intermediate **36**. De-protection was performed with  $\text{AlCl}_3$  to remove the two *iso*-propyl groups in very good yield. **RCZ20** was obtained in 7 steps from **30**.

**RCZ20** new synthesis was carried out similarly to **RCZ12** route (Fig. 22). Phthalhydrazide (**30**) was stirred in refluxing POCl<sub>3</sub> to obtain 1,4-dichloro phthalazine (**31**) in very good yield<sup>138</sup>. **31** reacted with resorcinol to afford intermediate **32**<sup>137</sup>, which was consequently protected with 2-bromo propane. Adduct **33** was converted into the corresponding amide (**34**) with sodium acetate in refluxing acetic acid overnight<sup>137</sup> and LiAlH<sub>4</sub> reduction afforded the desired amine **35** in excellent yield<sup>135</sup>. Sulfonylated product **36** was generated with standard conditions and the de-protecting step was completed by a milder reagent (AlCl<sub>3</sub>) overnight to obtain **RCZ20** in very good yield.

Although these two new synthetic routes employed respectively 6 and 7 steps against 5 steps of our initial synthesis, they provided high yielding reactions with easy and fast purification procedures. Furthermore, the last de-protecting step, which resulted problematic in the previous synthesis (yield 12% and 25%), afforded our final products, **RCZ12** and **RCZ20**, in good yield (61% and 75%) and with an easier chromatographic purification. We were also able to replace the use of BBr<sub>3</sub> with AlCl<sub>3</sub> in the case of **RCZ20** synthesis as the substrate was protected with weaker protecting groups. *Iso*-propyl groups demonstrated to be more sensitive to strong Lewis acid than methyl groups thanks to their ability to stabilise carbocation and consequently to lower the activation free energies involved in the BBr<sub>3</sub>-assisted de-protection mechanism<sup>139</sup>.

#### 8.4 Pull-down assay

Following previous works in our research group on the identification of ME0055 putative targets<sup>125</sup>, biotin was chosen as the first tag for labelling **RCZ12** and **RCZ20** thereby creating the compounds to perform a pull-down assay. Since biotin has a high specific affinity for the protein streptavidin, the biotinylated compounds were attached to streptavidin-coated magnetic beads and incubated with a whole cell lysate to determine the possible protein targets.

#### 8.4.1 Synthesis of biotinylated RCZ12 and RCZ20

Two major synthons were created to generate the two desired biotin labelled adducts by means of a Huisgen 1,3-dipolar copper-catalysed cycloaddition (Fig.23). It was planned to install the azide group on the biotin synthon, while the alkyne feature was thought to be inserted in the RCZ synthon through acylation with an acid chloride after the nitro group reduction. In order to avoid the drastic conditions of the de-protection of the two *iso*-propyl groups in the last step, it was decided to start from **RCZ12** and **RCZ20** and to re-protect the hydroxyl groups with an allyl ether, which resulted to be easy to remove in mild conditions.

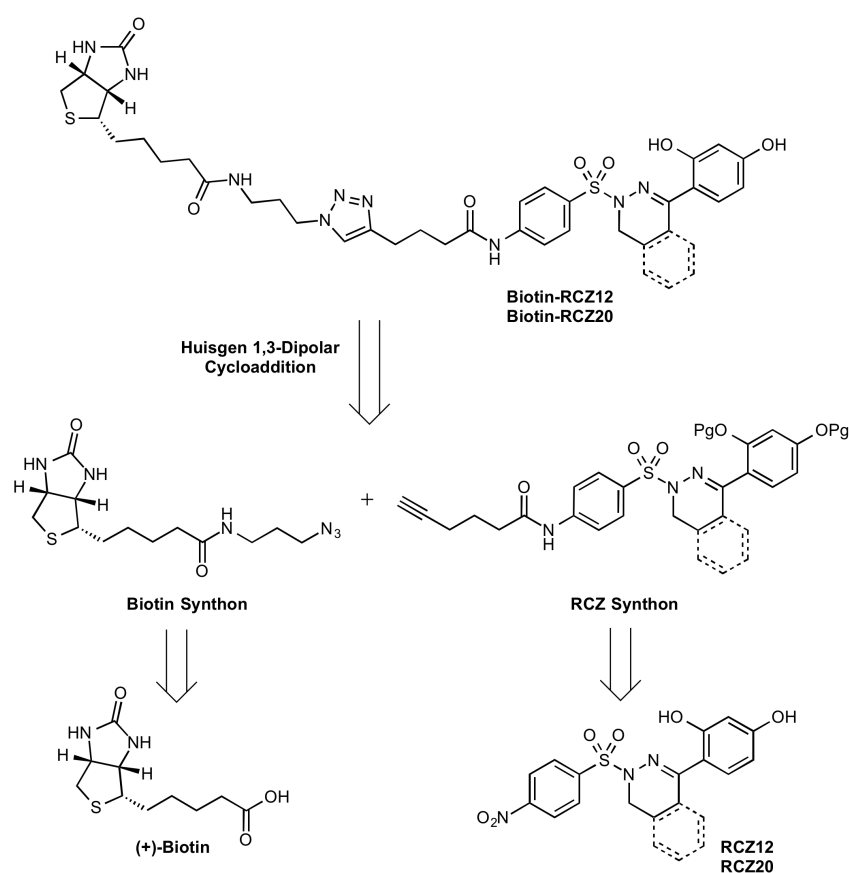


**Fig. 23: Retrosynthetic scheme of Biotin-RCZ12 and Biotin-RCZ20:** A Huisgen copper-catalysed 1,3-dipolar cycloaddition was chosen to generate the two biotinylated version of our candidates. The azide group was planned to be installed onto the biotin synthon and the alkyne group onto the RCZ synthon. Reduction of the nitro group on the **RCZ12** and **RCZ20** scaffold could then lead to acylation with the appropriate acid chloride. The biotin synthon could instead be prepared from commercially available (+)-biotin.

To create the RCZ synthons, **RCZ12** and **RCZ20** were firstly treated with allyl bromide to afford intermediates **37** and **38** in excellent yields (Fig. 24). Nitro reduction was carried out in mild conditions in the presence of iron and an aqueous solution of  $\text{NH}_4\text{Cl}$  in refluxing ethanol. Intermediates **39** and **40**, thus obtained, underwent acylation with freshly made hex-5-ynoyl chloride in very good yields to obtain both RCZ synthons in just 3 steps.

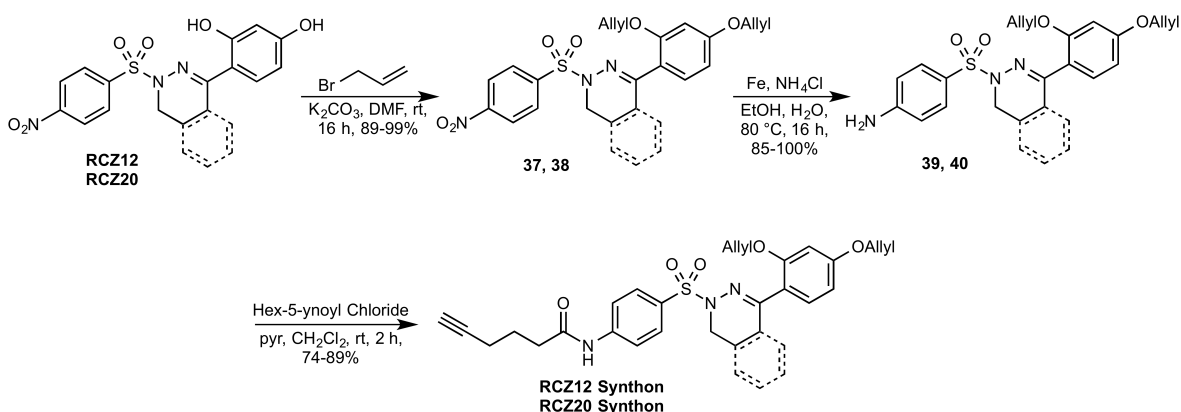


**Fig. 24: Synthetic route for RCZ12 and RCZ20 synthons:** The two desired synthons were obtained starting from **RCZ12** and **RCZ20** in only 3 steps. After the allyl protection, intermediate **37** and **38** were reduced to the corresponding aniline in order to be acylated with hex-5-ynoyl chloride. Hex-5-ynoyl chloride was prepared from hex-5-ynoic acid the same day of the acylation and used immediately (see Experimental Part).

The biotin synthon synthesis started with an EDC/NHS amide coupling reaction to create the reactive biotin-succinimide ester **41**<sup>140</sup> (Fig. 25). The ester was then replaced to generate the desired biotin synthon by 3-azidopropylamine **43**, which was prepared from 3-chloropropylamine hydrochloride **42**.

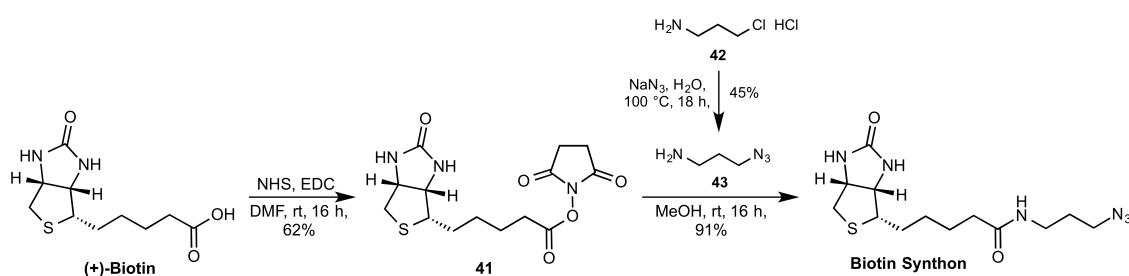


**Fig. 25: Synthetic route for Biotin Synthons:** Commercially available (+)-biotin was treated with standard EDC/NHS succinimide ester coupling conditions<sup>140</sup> to afford the reactive NHS ester **41**. The biotin synthon was obtained by amide formation with freshly prepared 3-azidopropylamine.

Huisgen copper catalysed 1,3-dipolar cycloaddition was performed in presence of copper(II)sulphate and sodium ascorbate in a 3:1 mixture of THF and water at  $50^\circ\text{C}$ <sup>141</sup> (Fig. 26). The protected biotin-RCZ12 and biotin-RCZ20 **44** and **45**, thus obtained, were de-

protected with tetrakis(triphenylphosphine) palladium in refluxing methanol in good yields<sup>142</sup>. Biotin-RCZ12 and biotin-RCZ20 were synthesised in just 5 steps starting from **RCZ12** and **RCZ20**.

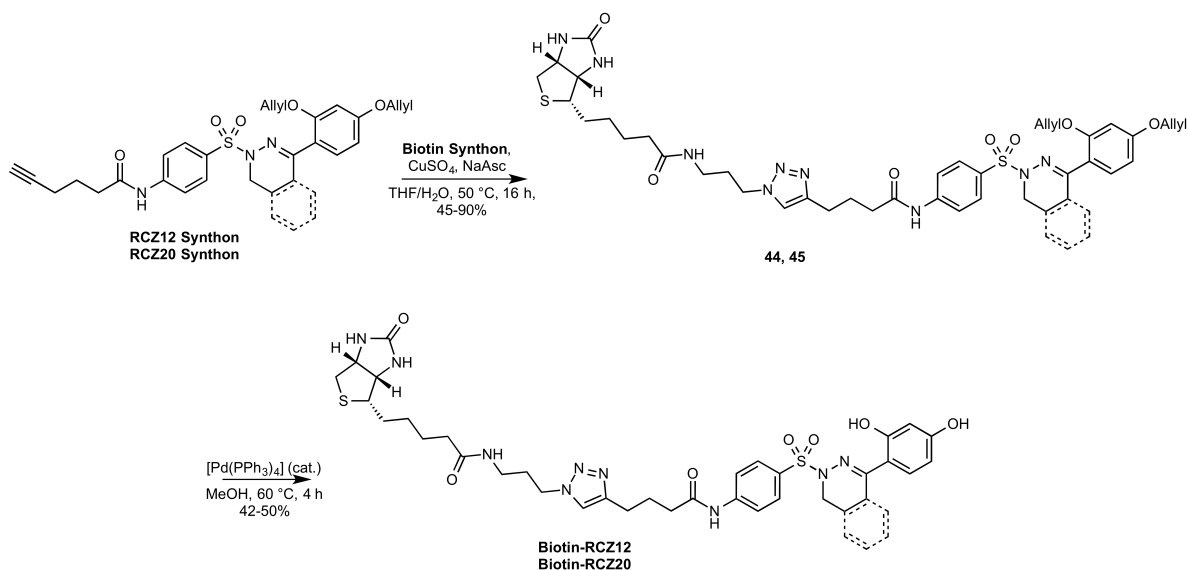


**Fig. 26: Huisgen 1,3-dipolar cycloaddition and synthesis of biotin-RCZ12 and 20:** Copper(II)sulphate and ascorbic acid were used to catalyse the cycloaddition to afford intermediate **44** and **45**. De-protection of the two allyl groups was performed in presence of catalytic amount of tetrakis(triphenylphosphine)palladium in refluxing methanol<sup>142</sup>.

#### 8.4.2 Pull-down assay results

Streptavidin-coated magnetic beads were employed to perform the pull-down assay with our two biotinylated compounds. The beads were first incubated with the biotin derivatives and then with an *E. coli* O157 TUV 93-0 whole cell lysate. Following extensive washing to reduce low affinity or non specifically bound proteins, the beads were boiled in SDS for proteins denaturation and run on a SDS-PAGE gel for separation. Visible bands were removed and then analysed by tandem mass spectrometry for identification.

Biotin-RCZ12 and biotin-RCZ20 showed to have affinity for similar targets as the same 3 protein bands appeared in both final samples (Fig. 27). Interestingly, the most visible bands in the assay (band 3 and 3') resulted to be the virulence protein EspD (MOWSE score/# peptides matched: 1266/45 for **RCZ12** and 1174/40 for **RCZ20**), while the other bands were found to be unrelated to the T3SS. EspD (39 kDa) is the main component of the T3SS translocon and is secreted through the needle-like complex to generate the terminal tip of the virulence apparatus into the host cell membrane<sup>31,33,143</sup>. Once EspD has formed the pore, all the virulence effectors can be injected into the host cell to start the colonisation

process. It is also involved in the control of the secretion of other T3SS proteins (EspA and EspB) and the consequent attaching/effacing lesions (A/E lesions) typical of *E. coli* O157:H7 infections <sup>143,144</sup>. This result, thus obtained, is in accordance with the effects observed on EspD secretion in the western blot experiment.

Bands number 1 and 1' were identified as 2-oxoglutarate dehydrogenase (MOWSE score/# peptides matched: 1716/106 for **RCZ12**), which is an enzyme complex involved in the decarboxylation of 2-oxoglutarate to succinyl coenzyme A, CO<sub>2</sub> and NADH <sup>145</sup>, but not involved in EspD secretion or T3SS assembly. Band 2 was identified as the elongation factor Tu (Ef-Tu) (MOWSE score/# peptide matched: 745/75 for **RCZ12**), a guanine nucleotide-binding protein (GBP) which functions as a carrier of amino acyl-tRNA to the ribosome <sup>146,147</sup>. This protein has also never been linked to the regulation of the T3SS. Bands number 4 and 4' resulted as the 30S ribosomal subunit protein S10 (MOWSE score/# peptide matched: 235/10 for **RCZ12**) and it demonstrated to be an unspecific interacting protein bound to streptavidin rather than our biotinylated compounds, as shown by our negative control. These additional results were all treated as unlikely to be associated with the mechanism of action, since **RCZ12** and **RCZ20** might just have a slight effect on the succinyl coenzyme A metabolism and bind Ef-Tu, but neither of them is linked to the T3SS apparatus synthesis and especially to EspD secretion.

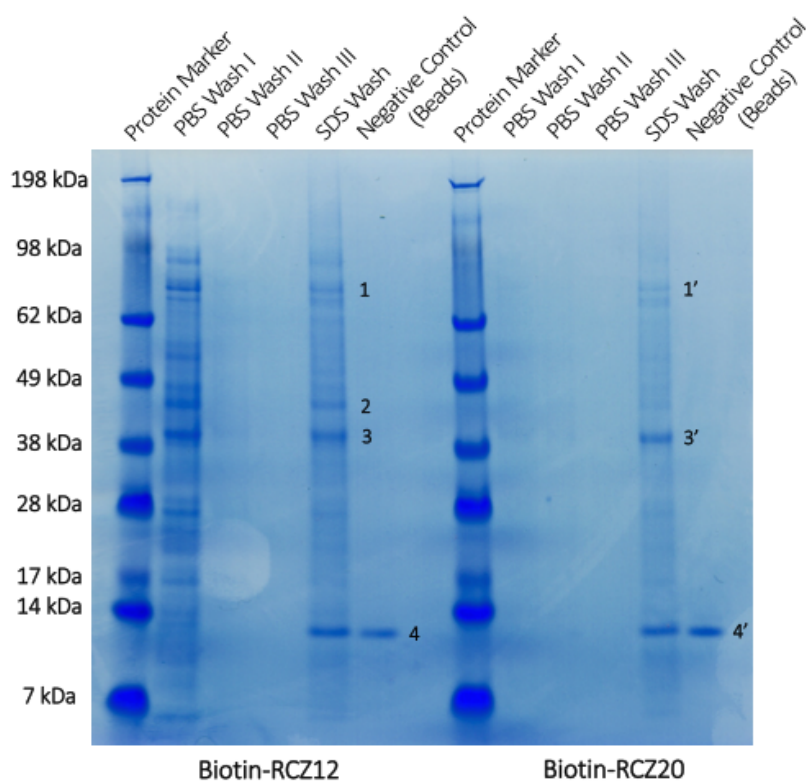


**Fig. 27: SDS-PAGE gel for the pull-down assay:** Biotin-RCZ12 and biotin-RCZ20 pull-down assay is shown in the gel above (see Experimental Part). PBS washes were carried out three times after incubation of the whole cell lysate to remove the unspecific bound proteins (PBS Wash lanes I, II and III). The beads were then boiled in SDS and run through an SDS-PAGE gel with constant voltage to separate the proteins (SDS wash lanes). Negative control was performed in order to visualise unspecific proteins interacting with streptavidin (Negative control lanes). Relevant protein bands (1, 2, 3, 3' and 4) were excised, trypsin digested and analysed through tandem mass spectrometry. Both bands 3 and 3' resulted to be the virulence protein EspD, while the other bands (1 and 2) proved to be proteins unrelated to the T3SS apparatus and assembly, hence considered off-targets. Bands 4 resulted as 30S ribosomal subunit S10 and regarded as unspecific due to the binding in the negative control lanes. From this result, we hypothesised that EspD is the only genuine T3SS-related protein bound to our compounds and that **RCZ12** and **RCZ20** bind directly to EspD to block its secretion.

From the two SDS wash lanes, **RCZ20** proved to be marginally more selective for EspD than **RCZ12**. The concentration of the off-target band 1' was less evident for the DHP derivative and the off-target band 2 was absent from its SDS wash lane. These results suggested that **RCZ20** might have fewer interactions with other unrelated T3SS proteins than **RCZ12**. Nonetheless, both molecules appeared to bind the virulence protein EspD and this result was consistent with the phenotype observed in previous assays.

### 8.4.3 Conclusions

A selective affinity for the virulence protein EspD was observed for both our biotinylated compounds from the pull-down assay results. Other bands were detected and proved to



be proteins bound to streptavidin or unrelated to the T3SS, which were considered as off-targets and unlikely to be responsible for the phenotype. These results, together with the western blot data, drew us to propose that **RCZ12** and **RCZ20** might bind to EspD in the cytosol inducing conformational changes, that dramatically affect its proper secretion and cause a retention of the protein inside the bacterial cell. This is consistent with the western blot analyses of EspD expression and secretion in presence of these candidates. This assumes that the compounds have to be taken up by the bacterial cell or freely cross the bacterial membrane in order to interact with the protein in its intracellular conformations. It is thought that native EspD adopts a chaotic configuration to then be recognised by selective chaperones, CesD and CesD2, for the correct secretion through the T3SS apparatus<sup>32,148,149</sup>. **RCZ12** and **RCZ20** could then interact either with the protein in its “native” configuration or to the chaperone-EspD complex to enable their inhibitory effect. This protein target and all the consequent hypotheses have to be validated by means of other binding techniques and assays.

Attempts in the over-expression and purification of EspD have been carried out without any success. The protein proved to be extremely difficult to handle and purify through several standard and non-standard protocols (data not shown). Chatterjee *et al.* successfully produced the first recombinant purified EspD (rEspD) in 2015<sup>34</sup>. Several batches of the purified protein were kindly donated from this research group, but rEspD was found to be problematic to solubilise and to fold in its correct intracellular conformation. High concentration of urea (8 M) and detergents had to be used to dissolve the protein in a “semi-native” configuration, which resulted to be incompatible with our compounds and/or instruments. Pull-down experiments with rEspD failed to replicate the previous results as the recombinant protein showed no binding to our biotinylated derivatives (See Paragraph 8.7.5, Fig. 31). This finding proved that EspD is a very insoluble and sensitive membrane protein that probably has to be folded in its original intracellular conformation to bind to the two candidates.

## 8.5 Metabolomics analysis

From the pull-down results, it was postulated a putative interaction between our derivatives and EspD into the bacterial cytosol. **RCZ12** and **RCZ20** are then likely to cross the bacterial membrane to perform this hypothetical binding. Metabolomics analyses were performed to confirm the cellular uptake of our compounds by *E. coli* O157 TUV 93-0

(Table 8). Bacteria were grown in M9 minimal medium and then incubated with **RCZ12** or **RCZ20**. Once centrifuged, both bacterial pellets and supernatant solutions were treated with a 1:1:3 (CHCl<sub>3</sub>:H<sub>2</sub>O:CH<sub>3</sub>OH) solution and analysed by hydrophilic interaction liquid chromatography (HILIC) to highlight the differences in concentration of the two samples. A noteworthy cellular uptake was detected for both our derivatives as the concentrations found inside the bacterial pellets were higher than the supernatant, indicating a strong *E. coli* uptake. Both molecules crossed the membrane and the final concentrations inside the cells were found to be three fold higher than the supernatant. These results assessed the cellular uptake of **RCZ12** and **RCZ20** inside the bacterial cells and then confirmed that the interaction with EspD occurs inside the bacterial cytosol.

| Entry | Experimental Blank | Supernatant                           | Bacterial pellets                     |
|-------|--------------------|---------------------------------------|---------------------------------------|
| RCZ12 | $6.7 \cdot 10^5$   | $10.3 \cdot 10^6 \pm 1.7 \cdot 10^6$  | $5.93 \cdot 10^9 \pm 4.48 \cdot 10^8$ |
| RCZ20 | $6.6 \cdot 10^6$   | $12.2 \cdot 10^6 \pm 6.16 \cdot 10^5$ | $9.06 \cdot 10^9 \pm 7.54 \cdot 10^8$ |

**Table 8: Metabolomics data for RCZ12 and RCZ20 cellular uptake:** Average intensities of **RCZ12** and **RCZ20** and corresponding standard deviation in Supernatant and Bacterial pellets samples are represented in the table above. Experimental triplicates were prepared and analysed through hydrophilic interaction liquid chromatography (HILIC). A three magnitude increase of the compounds' concentration was registered for the Bacterial pellets samples, indicating a cellular uptake of both drugs inside the bacteria. This confirms that the compound-EspD interaction can occur inside the bacterial cytosol.

## 8.6 Surface plasmon resonance (SPR)

Both biotinylated version of **RCZ12** and **RCZ20** proved to bind EspD through a pull-down assay using a whole cell lysate solution from *E. coli* O157 TUV 93-0. A plausible interaction between our compounds and EspD inside the bacterial cell could occur, inhibiting the secretion of this virulence protein. The mode of action hypothesised is supported by western blot and metabolomics analyses previously carried out.

In order to validate this hypothesis, we chose to prove the binding of our candidates with EspD by means of a surface plasmon resonance experiment (SPR). SPR is a common and sensitive technique widely used for detecting protein-protein, DNA-protein or ligand-protein interactions through the measurement of the refractive index variations induced by an analyte adsorption onto an appropriate gold or silver stationary phase<sup>150–152</sup>. The most commonly used stationary phases are commercially available gold chip which could be employed in different SPR assay and then treated with the analyte solution to calculate the affinity of the interaction. This method has also been used for calculation of drug-

target affinity ( $IC_{50}$ ) and it is considered one of the key tools for proving biochemical interactions<sup>153</sup>.

### 8.6.1 SPR analysis with biotinylated RCZ12 and RCZ20

A carboxymethylated dextran-coated gold chip (BiaCore® chip CM5) was used to validate the binding between our candidates and EspD through SPR. The coating is extremely versatile and can be modified by attaching different functional groups on the gold surface. Neutravidin, a derivative of streptavidin, was covalently bound to the dextran coating and the chip was then incubated with one of the two biotinylated compounds. The reaction wasn't successful as expected since only a small amount of the labelled molecules was bound to the dextran surface. The chips were incubated with a whole cell lysate solution as planned, but, unfortunately, the data were too inaccurate due to the instrument background noise and the poor amount of biotin-RCZ12 and biotin-RCZ20 on the gold surface. The outcome of the experiment was considered inconclusive.

### 8.6.2 Synthesis of amino-labelled RCZ12 and RCZ20

Following the initial unsuccessful strategy, the biotin tag was replaced with a primary amino group in order to immobilise our compounds directly onto the gold chip.

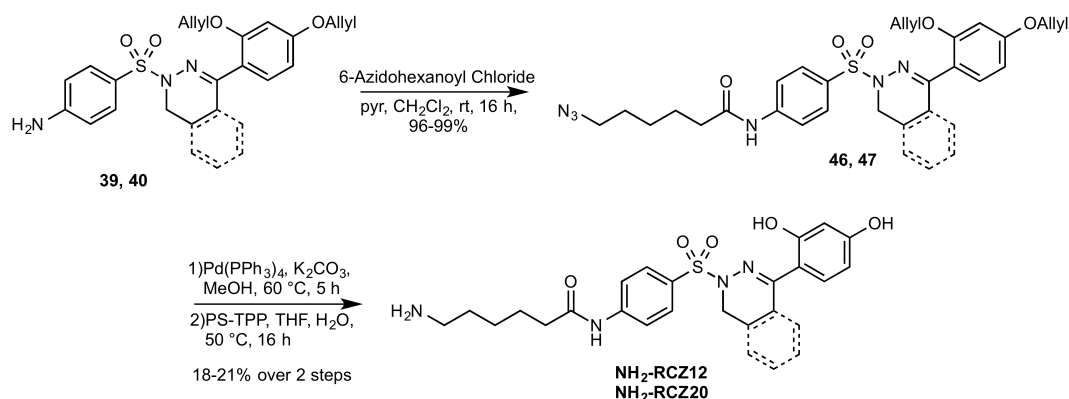


**Fig. 28: Synthetic route for amino-labelled RCZ12 and RCZ20:** 6-Bromohexanoic acid was reacted with sodium azide in DMF<sup>154</sup> and the corresponding carboxylic acid was then converted into the desired 6-azidohexanoyl chloride, which was used to acylate intermediate **39** and **40**. The azido derivatives **46** and **47**, thus obtained, were de-allylated with tetrakis(triphenylphosphine)palladium following our previous conditions<sup>142</sup>. The azido group was then reduced with a Staudinger reaction by means of polymer supported-triphenylphosphine to afford the two desired amino-labelled **RCZ12** and **RCZ20**.

The carboxymethylated dextran could be treated with EDC/NHS conditions to create a reactive succinimide ester and then coupled with the two amino-labelled RCZ molecules. Previously obtained intermediates **39** and **40** were reacted with 6-azidohexanoyl chloride<sup>154</sup> to afford the acylated adduct **46** and **47** (Fig. 28). Tetrakis(triphenylphosphine)palladium-mediated de-allylation<sup>142</sup> followed by Staudinger reaction with polymer supported-triphenylphosphine and water were performed to yield the two desired amino-labelled **RCZ12** and **RCZ20** in 3 steps.

### 8.6.3 SPR analysis with amino-labelled **RCZ12** and **RCZ20**

An identical carboxymethylated dextran-coated gold chip was used for this second SPR experiment. EDC/NHS conditions were employed to generate a reactive succinimide ester on the gold chip. The two amino-labelled compounds reacted with the esters and bound successfully onto the dextran surface. Incubation of a whole cell lysate solution from *E. coli* O157 TUV 93-0 was let to flow through the chip. Unfortunately, no refractive index variations were detected by the instrument, meaning that no interaction occurred between our derivatives and any protein of the whole cell lysate. The outcome of this experiment was probably influenced by the different dilution of the whole cell solution used for the pull-down assay and the SPR analysis. In the pull-down assay, the whole cell lysate had a dense and viscous form due to the high concentration of proteins, membrane remnants and DNA. Since the SPR instrument is very sensitive, the same concentrated whole cell lysate solution had to be diluted by 1/1'000 in order to be flowed through the chip channel. This might have compromised the compound-EspD interaction, since our amino-labelled compounds were exposed to smaller concentration of EspD in the whole cell lysate solution. The outcome of the experiment was deemed inconclusive.

### 8.7 Micro-scale thermophoresis (MST)

Biotinylated version of **RCZ12** and **RCZ20** proved to bind to the virulence protein EspD in the pull-down assay, but failed in validating this target through SPR experiment. Amino-labelled derivatives were synthesised to overcome binding issue to the SPR chip, but, even in this case, the binding between our candidates and EspD was not detected. However, concentrated whole cell lysate solution had to be diluted due to the instrument safety protocols and this could have played a key role in the outcome of the assay, as our

compounds were exposed to a much smaller concentration of EspD than the pull-down experiment. Therefore, to validate the binding previously observed, it was planned to try micro-scale thermophoresis (MST).

MST analysis are based on thermophoresis, which describes the movement of molecules in a temperature gradient <sup>155</sup>. The molecules motion depends on a plethora of properties such as size, charge, hydration shell and conformation <sup>155,156</sup>. MST detects this motion through the gradient by attached fluorophores in a very sensitive manner and can evaluate protein-protein or ligand-protein interactions (for more biophysical details: (Duhr & Braun, 2006a, 2006b; Jerabek-Willemsen, Wienken, Braun, Baaske, & Duhr, 2011; Seidel et al., 2013)). If binding is observed, the instrument can also measure the affinity of the titrated protein samples from the differences of the fluorescently labelled ligand movements in the temperature gradient <sup>156</sup>.

### 8.7.1 Synthesis of BODIPY-labelled RCZ12 and RCZ20

Since a fluorophore is required for performing MST analysis, it was firstly planned to tag **RCZ12** and **RCZ20** with a fluorescent tag. Previous studies in our groups highlighted the versatility and the ease of synthesis of the well-known fluorescent probe BODIPY <sup>161</sup>, a difluoro-bora-diaza-indacene dye widely used in biological assays (for reviews: <sup>162</sup>).

Once the compounds had their attached fluorophore, they could then be treated with

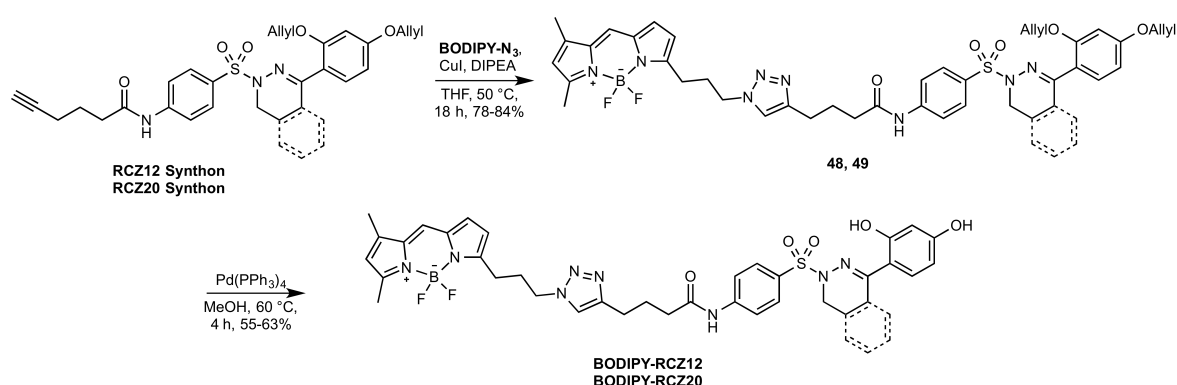


**Fig. 29: Synthetic route for BODIPY-labelled RCZ12 and RCZ20:** BODIPY-N<sub>3</sub> was obtained following previous protocols in our lab <sup>161</sup> and coupled with both RCZ synthons by means of a Huisgen 1,3-dipolar cycloaddition. Protected intermediates **48** and **49** were de-allylated in presence of tetrakis(triphenylphosphine)palladium in refluxing methanol <sup>142</sup>. BODIPY-labelled derivatives were afforded in 2 steps from the previously synthesised synthons.

titrated solution of whole cell lysate from *E. coli* O157 TUV 93-0 to detect their hypothesised interaction with EspD. BODIPY-N<sub>3</sub> was synthesised according to the research group protocols and reacted with both **RCZ12** and **RCZ20** synthons in a click reaction fashion in presence of catalytic amount of copper(I)iodide and DIPEA <sup>161</sup> (Fig. 29). Protected intermediates **48** and **49** were de-allylated in presence of tetrakis(triphenylphosphine)palladium following our previous conditions <sup>142</sup> to afford BODIPY-labelled **RCZ12** and **RCZ20**.

### 8.7.2 MST analysis with BODIPY-labelled **RCZ12** and **RCZ20**

MST experiment between our BODIPY-labelled **RCZ12** and **RCZ20** and a whole cell lysate solution from *E. coli* O157 TUV 93-0 were performed by means of a Nanotemper® Monolith NT115. The concentration of the fluorescent ligand was kept constant in all samples, while the whole cell solution was diluted with decreasing concentrations in order to detect the interaction and to calculate its possible affinity. Unfortunately, the buffer used resulted to be incompatible with our 2 BODIPY-labelled derivatives, which precipitated and lost fluorescence. After changing a variety of buffer systems, it was obvious that the components of the experiments were mismatched and especially the fluorescent probe was particularly sensitive to the aqueous media. An attempt to MST analysis was performed, but the fluorescent signal was found to be weak and not sufficient to carry out the experiment as expected.

After these discouraging findings, it was planned to install the fluorescence unit on EspD and to treat it with serial dilutions of **RCZ12** and **RCZ20**. This was chosen to detect the movements of EspD when in presence of our molecules. Since EspD purification and solubility showed to be problematic, the decision was made to try the MST analysis with a whole cell lysate solution with EspD-GFP replacing the wild-type virulence protein EspD.

### 8.7.3 Generation of $\Delta espD$ pRZ001 strain

EspD-GFP was designed and created to overcome the solubility and stability issues demonstrated by the BODIPY-labelled **RCZ12** and **RCZ20** during our first MST analysis attempt. The plasmid was constructed using pAJR70 as a backbone, a promoter-less plasmid containing the *gfp* gene, which encodes for the desired green fluorescent protein <sup>163</sup>. The *espD* gene was designed adjacent to a *tir* promoter (plasmid purchased from

GenScript®), expressed in a DH5- $\alpha$  strain and digested to extract the desired DNA portion. The purified DNA construct was then cloned directly upstream of the *gfp* gene in the pAJR70 backbone. Correct insertion was confirmed by diagnostic digestion (*Hind*III) and the new plasmid was named pRZ001. The purified plasmid was transformed into  $\Delta$ *espD* mutant in order to have only EspD-GFP expression inside the bacterial cell ( $\Delta$ *espD* pRZ001 strain). Fluorescence was assessed by measuring the absorbance of the GFP probe (480 nm) of chemically lysed  $\Delta$ *espD* pRZ001 cells grown in a T3SS-inducing media (Fig. 30). TUV 93-0 and EPEC *ptirGFP* strains were used as negative and positive controls respectively. RFUs were measured before and after treatment with the lysis buffer solution to display the maximum intensity for the EspD-GFP protein. Western blot analysis revealed that the new EspD-GFP was not detectable by the  $\alpha$ -EspD antibody, while the  $\alpha$ -GFP antibody showed a well-marked band at 65 kDa, the correct predicted molecular weight for the new fluorescent protein.

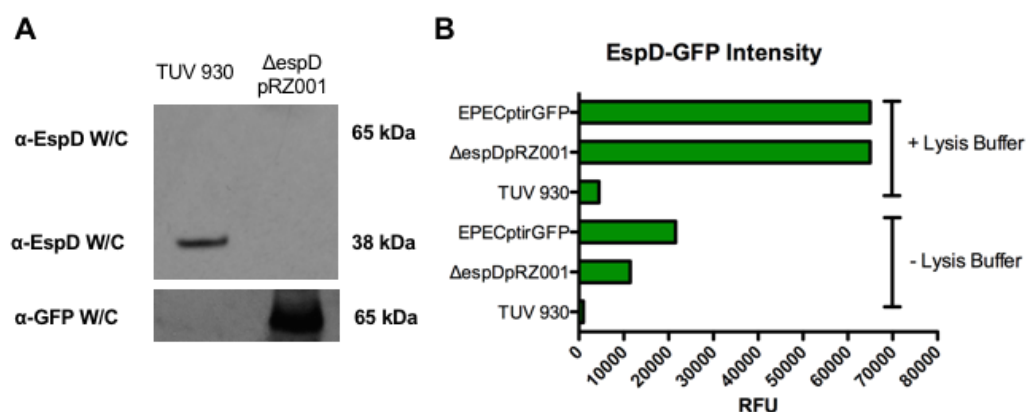


**Fig. 30: Western blot results for  $\alpha$ -EspD and  $\alpha$ -GFP antibodies (left) and GFP intensity of the  $\Delta$ *espD* pRZ001 strain (right):** Western blot analysis were carried out to confirm the expression of the new EspD-GFP protein (see Experimental Part for Ab dilution). EspD-GFP was not detected by means of the  $\alpha$ -EspD antibody, but a 65 kDa protein was identified when using the  $\alpha$ -GFP antibody, indication of the expression of EspD-GFP. Fluorescence intensity was measured through absorbance at 480 nm. Lysed cells from  $\Delta$ *espD* pRZ001 showed a maximum intensity when lysed with BugBuster mix. TUV 93-0 and EPEC *ptirGFP* strains were used as negative and positive controls respectively.

#### 8.7.4 MST analysis with EspD-GFP

A whole cell lysate solution from the  $\Delta$ *espD* pRZ001 strain, containing EspD-GFP, was used for the second attempt to MST experiments. Cells were grown under T3SS-inducing conditions, pelleted and lysed. The corresponding viscous solution was diluted by 1/1'000 in accordance with the protocols recommended by the instrument manufacturer and

aliquoted. Decreasing concentrations of both **RCZ12** and **RCZ20** were then added to the fluorescent protein solution. Even in this case, the two candidates demonstrated to be insoluble in the aqueous media and precipitated or formed emulsions according to their concentrations. Increasing percentages of DMSO were added in order to solubilise the compounds to a maximum of 20% on the total volume of the samples. MST analyses were performed, but no indications of interaction were detected by the instrument. The result of the experiment was considered inconclusive due to the high DMSO percentage.

The MST experiment highlighted the solubility issues of both our synthetic derivatives that proved to be incompatible with most of the biological buffers used for such analysis. Unlike the biotinylated derivatives, which easily solubilise in aqueous media, both BODIPY-labelled and the unlabelled **RCZ12** and **RCZ20** were found to be incompatible with the whole cell lysate media. The outcomes of the two experiments were affected by this incomplete solubilisation and mismatch of our molecules. To overcome this problem, increasing DMSO percentages were used up to 20% on the total volume of the samples. The clear solutions were tested, but revealed no evidence of binding. It is well-known that the presence of DMSO affects the folding, behaviour and binding abilities of the proteins<sup>164</sup>. Especially at high concentrations, as we employed, results could be tampered by the DMSO effects, which help the solubilisation of the compounds and, at the same time, alter the properties of the whole cell lysate proteins. In addition, it is possible that the bulk of the GFP protein could have hindered **RCZ12** and **RCZ20** binding site or compromised the intracellular folding of EspD, obstructing its “native” or chaperone-bound conformation. Indications of this obstruction were suggested by the western blot analysis performed on the *ΔespD* pRZ001 strain, where EspD-GFP was not recognised by the  $\alpha$ -EspD antibody, but only by the  $\alpha$ -GFP. Due to all these findings, the results obtained from the MST experiments had to be considered questionable and inconclusive.



### 8.7.5 Pull-down assay with EspD-GFP

MST analysis with  $\Delta espD$  pRZ001 whole cell lysate solution has clearly demonstrated the unsuitability of RCZ12 and RCZ20 in many different biological buffers. In addition, the GFP unit could have also played a key role in impeding the binding between the compounds and the protein.

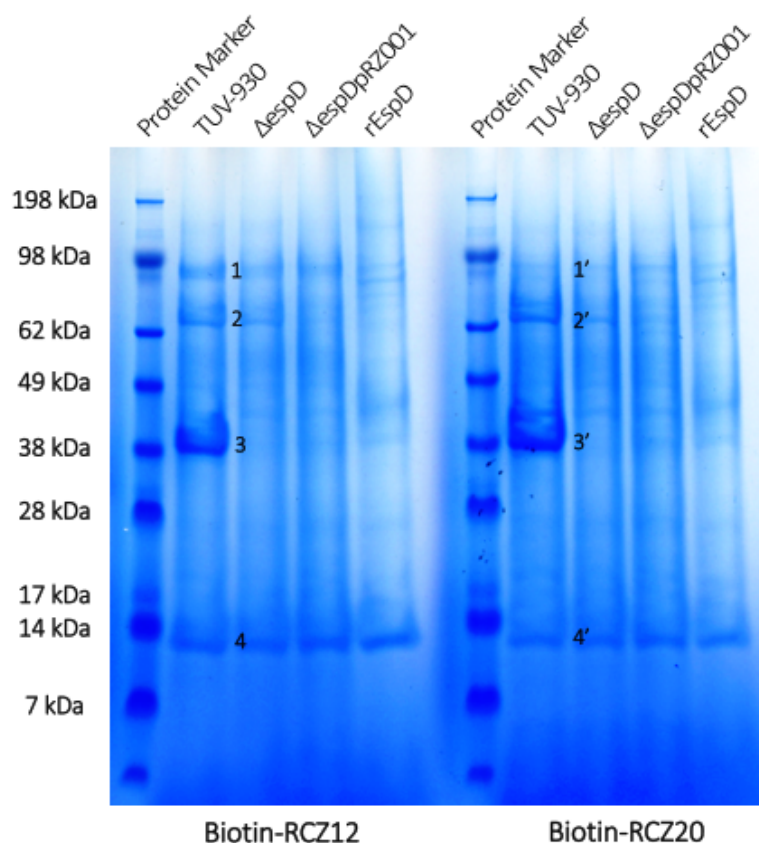


**Fig. 31: SDS-PAGE gel for the pull-down assay with  $\Delta espD$  pRZ001 strain:** Biotin-RCZ12 and biotin-RCZ20 pull-down assay with different bacterial strains is shown in the gel above (see Experimental Section). SDS wash lanes for each bacterial strain used are shown in the gel. The TUV 93-0 strain was used as positive control as both biotin-RCZ12 and biotin-RCZ20 bind to EspD, as previously shown (Fig.21, Paragraph 3.32), while the  $\Delta espD$  strain was employed as negative control for EspD. EspD-GFP ( $\Delta espD$  pRZ001 strain) wasn't detected in the gel when incubated with our biotinylated compounds. The result supports the hypothesis that the GFP core might hinder the binding site or change the conformational configuration of the virulence protein disabling the interaction with the compounds. In addition, a rEspD solution was also incubated with the biotin-labelled molecules and, interestingly, no binding was observed. This data corroborates the extremely difficult handling and the issue of solubilising this membrane protein in a "native-like" configuration.

To confirm this obstruction, a pull-down assay with  $\Delta espD$  pRZ001 whole cell lysate was performed. Whole cell lysate solution from *E. coli* O157 TUV 93-0 and  $\Delta espD$  strain were employed as positive and negative controls respectively and an rEspD solution was also

used to prove the binding of our molecules. As observed in our previous pull-down assay (Fig.27, Paragraph 8.4.2), both biotin-RCZ12 and biotin-RCZ20 bound to EspD (band 3 and 3') when treated with the TUV 93-0 cell lysate and showed to bind the same T3SS unrelated protein 2-oxo-glutarate dehydrogenase (1 and 1') (Fig. 31). Band 2 and 2' were detected for the first time and resulted to be the virulence protein EspB (MOWSE score/# peptide matched: 1154/77 for **RCZ12**). Since EspB has a molecular weight of 31 kDa, we assumed the interaction with our biotinylated compounds occurred in the homodimerised form, as the band appeared to have a molecular weight of 63 kDa. It is rather unusual to have homodimers after SDS treatment and thus, this band result was considered not reliable and unspecific, as it never appeared again in the SDS wash lane of other pull-down experiments. No EspD band was detected in both  $\Delta espD$  and  $\Delta espD$  pRZ001 strains lanes when the whole cell lysate solutions were incubated with biotin-RCZ12 and biotin-RCZ20. While the  $\Delta espD$  result was expected as no EspD is produced by the bacteria, the  $\Delta espD$  pRZ001 confirmed that EspD-GFP has less affinity for our compounds as the GFP unit modifies the conformational configuration of the virulence protein inside the cell. Also rEspD showed no interaction when incubated with the biotinylated compounds, corroborating the issues of EspD solubility and partially "native" configuration with the buffer used, which affected the outcome of the experiment. In addition, the rEspD displayed a poor level of purity as other bands in the SDS wash lane were detected in very low concentration.

## 8.8 Generation of truncated-EspD-HA strains

Validating EspD as the main protein target for **RCZ12** and **RCZ20** proved to be a difficult task due to issues associated with both the protein and the solubility of the compounds, as observed by the SPR and MST experiments. Metabolomics data verified the cellular uptake of our compounds by *E. coli*, supporting the intracellular interaction between the two derivatives and the T3SS protein EspD, hypothesised from the pull-down assay results. Unfortunately, the other binding techniques used failed to verify the result due to the aforementioned issues. To overcome these limitations, it was decided to generate a series of five truncates of EspD to then observe any possible variation or loss of activity by **RCZ12** and **RCZ20**. As mentioned before, EspD is a key virulence protein for the EHEC T3SS apparatus, which mediates the anchoring of the bacterium to the host cells and allows the injection of virulence effectors to start the infection<sup>32–34</sup>. It has been predicted that EspD

possesses 2 coiled-coil domains for host cell membrane anchoring and homo-oligomerisation, 2 transmembrane domains for insertion and two amphipatic regions thought to be involved in the secretion process of the protein and in chaperone recognition<sup>31,32,34</sup>. It was decided to delete these functional regions to validate EspD as main protein target of our derivatives and then to evaluate the inhibition of the secretion through western blot analysis. If EspD is the main protein target of **RCZ12** and **RCZ20**, key modifications in its structure would reverse the compounds effect on secretion. To allow immunoblotting of the new constructs, the truncated-EspD were tagged with an HA sequence at the carboxy-terminus.

### 8.8.1 Creation of TUV 93-0 EspD-HA

A new strain producing full length EspD-HA was firstly created as a starting point for further truncations and modifications. Generation of this strain was achieved by means of a process called allelic exchange, which it was optimised for EHEC by Emmerson *et al.*<sup>165</sup> (for more details refer to Experimental Part, Paragraph 13.2.14). This ensures that a single chromosomally encoded copy of the gene is integrated into the genome, overcoming the issues associated with plasmid based expression systems such as copy number and stability.

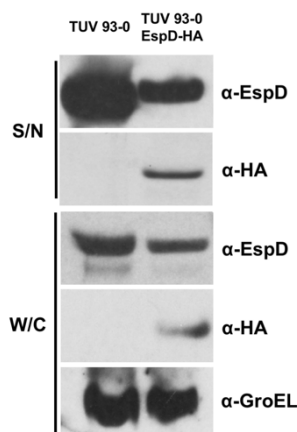


**Fig. 32: TUV 93-0 EspD-HA Western blot analysis:** Western blot analyses were carried out according to standard procedure (see Experimental Part for methods and Ab dilutions). Both supernatant proteins (S/N) and whole cell lysate solution (W/C) were analysed in repeats of three independent experiments. As expected, the new construct EspD-HA was recognised by both  $\alpha$ -EspD and  $\alpha$ -HA antibodies, which confirmed its correct expression and secretion of the new strain.

The *espD-HA* gene was flanked between the 3' and 5' homologous regions of the endogenous gene *espD* (purchased from GenScript®) and cloned into a temperature sensitive exchange plasmid (pIB307) to create the first allelic exchange plasmid pIB307-*LEE4-EspD-HA*. Generation of the second allelic exchange plasmid pIB307-*LEE4-sacB-kan* was achieved by *Bam*H1 digestion of pIB307-*LEE4-EspD-HA* and subsequent insertion of the *sacB-kan* cassette. pIB307-*LEE4-sacB-kan* was transformed into TUV 93-0 and the strain then underwent allelic exchange to yield TUV 93-0  $\Delta espD$  *sacB-kan*, intermediate strain where the endogenous gene *espD* was replaced by the *sacB-kan* cassette through homologous recombination. pIB307-*LEE4-EspD-HA* was then transformed into this intermediate strain and a second allelic exchange was performed to obtain the desired TUV 93-0 *EspD-HA* strain. The correct insertion of the gene was confirmed by PCR across the new *espD-HA* gene and western blot with both  $\alpha$ -*EspD* and  $\alpha$ -HA antibodies of the supernatant and whole cell lysate (Fig. 32). As expected, *EspD-HA* was correctly secreted and expressed by bacteria.

### 8.8.2 Creation of truncated-*EspD-HA* strains

To create the correct exchange plasmids for the truncated-*EspD-HA* strains, various regions of the *espD-HA* gene were amplified and then ligated together through a DNA assembly reaction with the pIB307 backbone. 8 *espD-HA* fragments were purified to assemble 4 temperature sensitive exchange plasmids: pIB307-*LEE4-EspD-HA* $_{\Delta 26-81}$ , pIB307-*LEE4-EspD-HA* $_{\Delta 138-171}$ , pIB307-*LEE4-EspD-HA* $_{\Delta 176-251}$  and pIB307-*LEE4-EspD-HA* $_{\Delta 333-356}$ . Plasmids were then transformed into the intermediate TUV 93-0  $\Delta espD$  *sacB-kan* strain and subjected to allelic exchange treatment to afford the corresponding 4 truncated-*EspD-HA* strains (Fig.23): TUV 93-0 *EspD-HA* $_{\Delta 26-81}$ , where the two predicted amphipathic regions 1 and 2 (Amph1/2) adjacent to the N-terminus were deleted, TUV 93-0 *EspD-HA* $_{\Delta 138-171}$ , where the coiled-coil domain 1 (COIL1) was deleted, TUV 93-0 *EspD-HA* $_{\Delta 176-251}$ , where the two transmembrane domains 1 and 2 (TMD1/2) were deleted, and TUV 93-0 *EspD-HA* $_{\Delta 333-356}$ , where the coiled-coil domain 2 (COIL2) was deleted. The new strains were confirmed by PCR across the new genes inserted and western blot analysis with  $\alpha$ -HA antibody of the supernatant and whole cell lysate to highlight the correct secretion of the constructs (Fig. 33).

All the new strains expressed and secreted the HA-labelled constructs beside TUV 93-0 EspD-HA $_{\Delta 26-81}$ , which did not express or secrete any construct. It has been postulated that the amphipathic region 2 (Amph2), predicted to be located between amino acids 66-83, functions as a recognition site for EspD chaperones CesD and CesD2, which maintain the virulence protein in a secretion competent conformation<sup>32,148,149</sup>. Therefore, deletion of this region produces a misfolded EspD which undergoes rapid degradation, since it cannot be secreted correctly<sup>32</sup>. Evidence of this has already been observed by Dasanayake *et al.* and verified by the fact that our new strain TUV 93-0 EspD-HA $_{\Delta 26-81}$  did not express and secrete any EspD construct according to the  $\alpha$ -HA Western blot.

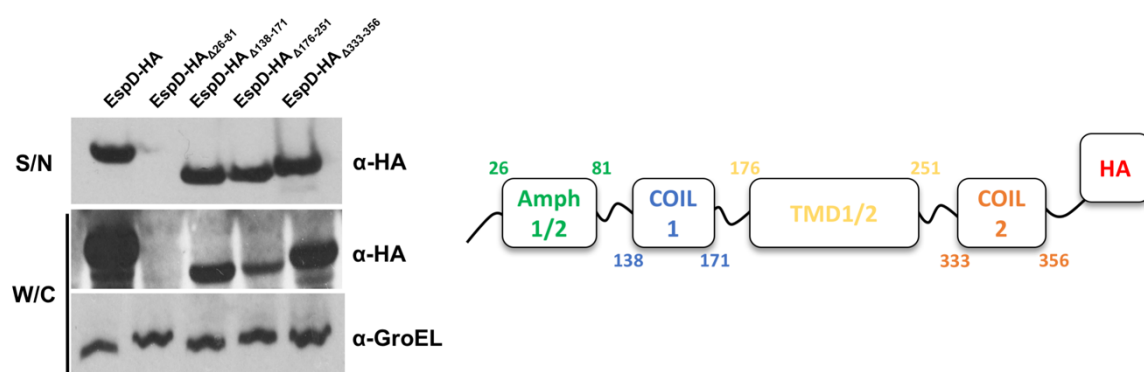


**Fig. 33: Western blots of the truncated-EspD-HA producing strains (left) and cartoon showing the 4 deleted functional regions of EspD (right):** Western blot analyses were carried out according to standard procedure (see Experimental Part for methods and Ab dilutions). Both supernatant proteins (S/N) and whole cell lysate solution (W/C) were analysed in repeats of three independent experiments. All the new strains demonstrated to express and secrete their truncated-EspD-HA constructs beside TUV 93-0 EspD-HA $_{\Delta 26-81}$ , which did not express any new construct. Deletion of the amphipathic region 2 (Amph 2) (aa. 63-88) in EspD resulted in the production of a misfolded protein, which is in a non-secretive competent conformation, due to the lack of the chaperone recognition site. Therefore, our new strain TUV 93-0 EspD-HA $_{\Delta 26-81}$  produced a construct which was rapidly degraded by the cell because of the lack of this recognition site. Despite no crystallographic data available for EspD, it has been predicted that this virulence protein contains 2 amphipathic regions (Amph1/2), two coiled-coil domains (COIL1 and COIL2) and two transmembrane domains (TMD1/2). Each truncated-EspD-HA strains produce a different EspD-HA construct with a specific deletion of the functional regions shown in the figure above. Unfortunately, when Amph2 is deleted, no production of the new construct has been detected by Western blot analyses due to rapid degradation.

### 8.8.3 Western blot analysis with RCZ12

Since we already assumed that our derivatives share the same mode of action against EHEC T3SS, it was decided to evaluate **RCZ12** against the new truncated-EspD-HA strains due to its potency and slightly better solubility in biological media (Fig. 34). The compound

showed total inhibition of EspD secretion at 200  $\mu$ M and this concentration was chosen for the western blot experiment. When TUV 93-0 EspD-HA was treated with **RCZ12**, a total inhibition of EspD-HA secretion was detected, indicating that the HA tag did not influence the compound's activity. Retention of total inhibition of the secretion was also observed for EspD-HA $_{\Delta 176-251}$  (25-fold inhibition) and EspD-HA $_{\Delta 333-356}$  (15-fold inhibition), even though in the latter case a slightly attenuated effect was registered. Secretion of EspD-HA $_{\Delta 138-171}$ , instead, was not affected by **RCZ12**, as equal amounts of the truncated protein were found in the untreated and treated samples, highlighting a complete loss of activity.

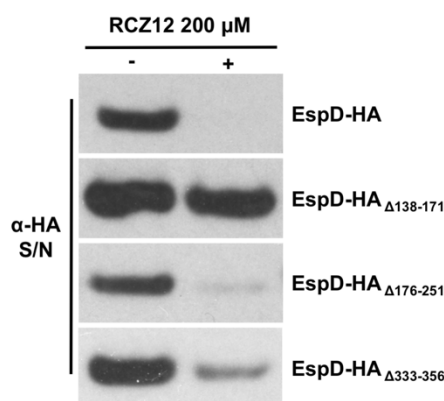


**Fig. 34: Western blot analyses of truncated-EspD-HA strains with and without RCZ12 treatment at 200  $\mu$ M:** Western blot analyses were carried out according to standard procedure (see Experimental Part for methods and Ab dilutions). Supernatant proteins (S/N) were analysed in repeats of three independent experiments for each strain. **RCZ12** showed retention of inhibition of EspD-HA, EspD-HA $_{\Delta 176-251}$  and EspD-HA $_{\Delta 333-356}$  at 200  $\mu$ M, while no activity was detected against EspD-HA $_{\Delta 138-171}$ . The results detected from this assay validated EspD as main target of both **RCZ12** and **RCZ20**, as **RCZ12** lost its activity when EspD structure was specifically modified. A complete loss of activity was registered against EspD-HA $_{\Delta 138-171}$ , which supports the pull-down assay findings confirming the direct interaction between our compounds and the virulence protein EspD. It can be speculated that **RCZ12** and **RCZ20** are likely to bind to EspD COIL1 region, since the loss of activity was only detected for EspD-HA $_{\Delta 138-171}$ . Attenuation of activity against EspD-HA $_{\Delta 333-356}$  suggests that COIL2 is also partially involved in the interaction or that the structural modifications induced by **RCZ12** and **RCZ20** influence this second coile-coil domain to stop the secretion.

These results confirmed the hypothesis proposed from the pull-down experiment in which **RCZ12** and **RCZ20** bind to EspD, consequently blocking its secretion. Various modifications of the virulence protein structure resulted in both retention and loss of activity by **RCZ12**. When the two TMD1/2 domains or COIL2 were deleted, inhibition of the corresponding constructs by our derivative was detected, while normal secretion was observed when COIL1 was absent in the structure. The fact that **RCZ12** lost its effect on secretion with a truncated version of EspD, confirms that the virulence protein is the main target of our

compounds and supports the major conclusion from the pull-down experiments. In addition, we can postulate that **RCZ12** and **RCZ20** are likely to bind to EspD in the COIL1 region, since only the deletion of this functional area resulted in a marked loss of activity. Attenuation of the compound's activity against EspD-HA<sub>Δ333-356</sub>, where the COIL2 is deleted, may indicate that both coiled-coil domains could be involved in the interaction or that the structural modifications induced by **RCZ12** and **RCZ20** also influence the COIL2 domain to stop the secretion.

## 8.9 Conclusions and future work

**RCZ12** and **RCZ20** demonstrated to be promising T3SS inhibitors, primarily blocking EspD secretion and acting also on Tir expression and secretion at 200 μM. Both compounds were designed and synthesised as ME0055 more stable derivatives, but displayed a distinct and more specific activity on EHEC T3SS than the SA compound. These encouraging results provided by the transcriptional and post-transcriptional experiments drove us to investigate in details the mode of action of these new active molecules. A new synthetic route was firstly planned and carried out to obtain **RCZ12** and **RCZ20** in good yields. Replacement of the methyl ethers with weaker *iso*-propyl ethers afforded a longer synthetic route, but faster and easier purification steps. Labelled derivatives of our compounds were designed in order to perform various binding techniques to identify the protein target. It was decided to install the tags onto the left-hand side of the molecule, since di-hydroxyl compounds resulted to be more active than di-methoxyl ones in our preliminary screening.

Following previous studies by our group<sup>125</sup>, it was decided to carry out a pull-down assay against a TUV 93-0 whole cell lysate to try and identify the bacterial protein specifically bound to our compounds. Biotinylated versions of **RCZ12** and **RCZ20** were obtained through a Huisgen copper-catalysed 1,3-dipolar cycloaddition in 5 steps starting from **RCZ12** and **RCZ20**. By means of streptavidin-coated magnetic beads, a pull-down experiment that identified EspD as the only bona fide T3SS-related protein target bound to both biotin-RCZ12 and biotin-RCZ20. Other proteins that were identified through this procedure could be eliminated as being involved in the mode of action as they were not related to T3SS apparatus and not consistent with the phenotype of accumulated EspD in the bacterial cytoplasm. From this result, we deduced that **RCZ12** and **RCZ20** shared the same mechanism of action and hypothesised that our new compounds are interacting with

the virulence protein EspD inside the cell to block its secretion. Metabolomics analysis demonstrated that the derivatives accumulated within the bacterial cytoplasm, consistent with the hypothesis that the compound-EspD interaction has to occur inside the cytosol. To further validate our hypothesis, other binding techniques were carried out. Surface plasmon resonance (SPR) with gold chips was attempted with both biotin-labelled and amino-labelled molecules, but it provided only inconclusive results due to dilution issues required for the instrument protocols. Microscale thermophoresis (MST) was also performed with BODIPY-labelled molecules against a TUV 93-0 whole cell lysate and with EspD-GFP whole cell lysate, but unfortunately highlighted the unsuitability of our compounds with most of the buffer systems used for the experiment. Both SPR and MST techniques were then considered inconclusive and underlined the problematic biological properties of EspD and the poor solubility of **RCZ12** and **RCZ20**. Generation of truncated-EspD-HA strains was carried out by means of allelic exchange, in order to create 4 different strains producing various EspD mutants labelled with HA. Once the strains were obtained, western blot analyses of the new clones were performed with and without the presence of **RCZ12** at 200  $\mu$ M to evaluate changing or loss of activity. Retention of a normal inhibition on the new constructs secretion was detected for all the new strains beside EspD-HA $\Delta$ <sub>138-171</sub>. Equal amounts of EspD-HA $\Delta$ <sub>138-171</sub> were found in the untreated and treated samples, indicating a complete loss of activity by **RCZ12**. The results showed how a selective modification in the EspD structure can affect our compound's activity, hence, confirming EspD as the main protein target for **RCZ12** and **RCZ20**. Furthermore, the experiment also suggested that our derivatives might bind to EspD in the COIL1 domain (138-171), since only the deletion of this functional region reverted **RCZ12** effect on secretion. This detail can only be fully confirmed by crystallographic data, which are still unavailable for this protein, but it is also a clear indication on **RCZ12** and **RCZ20** binding site. An attenuated inhibitory effect was also detected for the strain producing EspD-HA $\Delta$ <sub>333-356</sub>, where COIL2 was deleted. This also suggest that both coiled-coil domains are involved in the interaction or that our compounds induce conformational changes that also influence COIL2 to block EspD secretion.

From these experiments, we identified and validated EspD as the main protein target of both **RCZ12** and **RCZ20**. It is likely that our compounds cross *E. coli*'s membrane and directly interact with the protein either in its "native" or chaperone-bound conformation to block its correct secretion. Cellular accumulation was confirmed by metabolomics on *E.*



*coli* incubated with both **RCZ12** and **RCZ20**, while the EspD binding detected in the pull-down assay was validated by the western blot experiments on truncated-EspD-HA strains. The latter experiment also highlighted the possibility that the derivatives might bind to the coiled-coil domain (COIL1) of EspD to exhibit their effect against EHEC T3SS. In the future, efforts focused on purifying this challenging protein should be attempted in order to confirm the exact interaction site of **RCZ12** and **RCZ20** in EspD structure. Crystallographic data of the virulence protein EspD will also provide useful information for new and more potent compounds based on the THP and DHP scaffolds.

## 9 RCZ12 and RCZ20 Derivatives

### 9.1 Structural analysis on RCZ12 and RCZ20

Our THP and DHP derivatives demonstrated to possess selective activity against EHEC T3SS, especially blocking EspD secretion and down-regulating T3SS-related genes. The main protein target resulted to be the virulence protein EspD, which was firstly identified by pull-down experiments and then validated by western blot analyses on truncated-EspD-HA strains. It is thought that **RCZ12** and **RCZ20** are able to cross the bacterial membrane and directly interact with EspD to block its secretion. Despite the promising activity, our compounds also displayed poor solubility in biological media, which interfered with binding experiments during the investigation of the candidates' mode of action. However, **RCZ12** and **RCZ20** can be considered an excellent starting point for chemical optimisation, since they both include new biologically active scaffolds against T3SS.

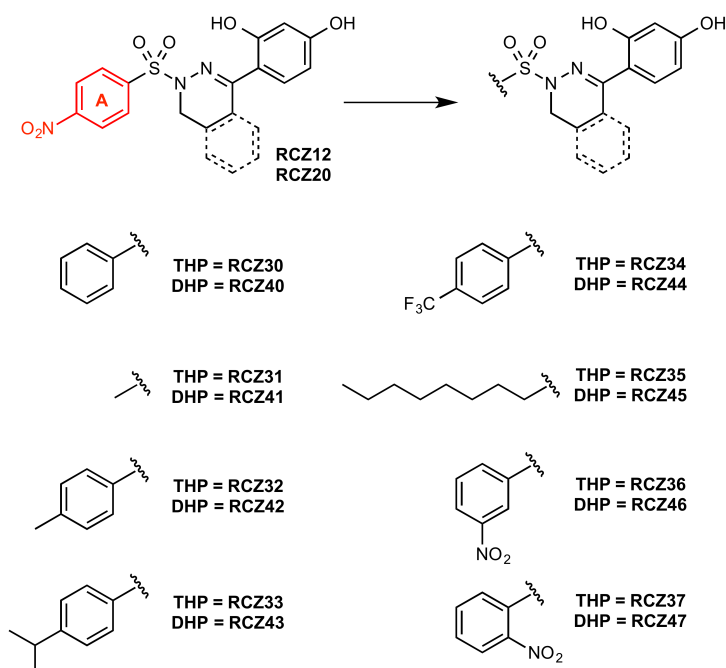


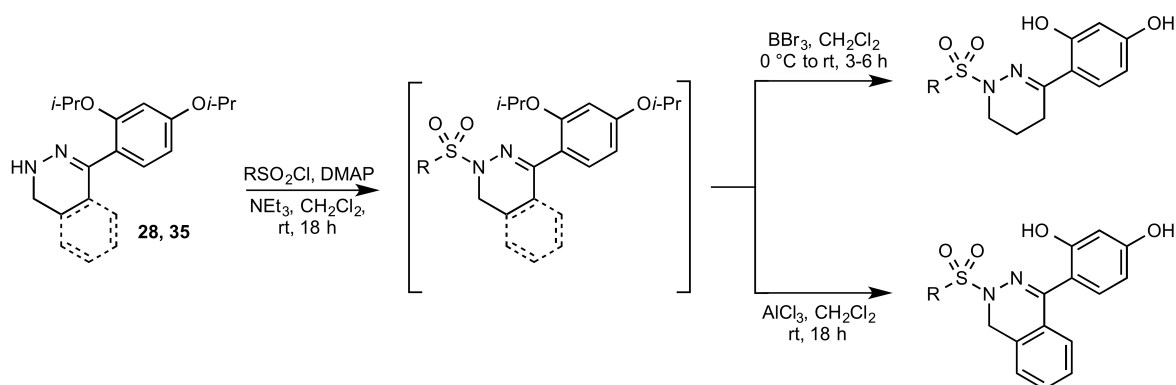
**Fig. 35: Rational design of RCZ12 and RCZ20 derivatives:** Due to our previous findings, the left-hand side phenyl ring A (red) was modified in order to build a small library focused on the THP and DHP scaffolds. Removal of the nitro group was first planned (**RCZ30** and **RCZ40**), then the whole phenyl ring was removed and replaced by a methyl group (**RCZ31** and **RCZ41**). Substitution with a small (methyl group) (**RCZ32** and **RCZ42**) and a bulky (*iso*-propyl group) (**RCZ33** and **RCZ43**) alkyl group was planned to evaluate the influence of electron-donating groups on ring A. A trifluoromethyl group (**RCZ34** and **RCZ44**) was then placed in the same position of the nitro group to have an inducing electron-withdrawing effect on the molecule. A long alkyl chain (**RCZ35** and **RCZ45**) was introduced instead of the whole ring A to investigate the impact of a more lipophilic derivative with a flexible carbon chain. At last, the nitro group was moved in *meta* (**RCZ36** and **RCZ46**) and in *ortho* (**RCZ37** and **RCZ47**) to assess the best position for this functional group in terms of activity against EspD secretion.

Our preliminary evaluation of the THP and DHP series (Paragraph 7.3.2) highlighted that the two hydroxyl groups on the right-hand side of the molecule were essential for activity against EspD secretion. Di-methoxyl derivatives showed a reduced activity against the virulence protein than the di-hydroxyl analogues, which suggested that the hydroxyl groups could take part in key hydrogen bond interactions with EspD. The geometry of the sulphone was also considered relevant for the activity, as the sulphonyl di-hydroxyl molecules were found to be more potent than the carbonyl di-hydroxyl counterpart. Due to these data, it was decided to modify the left-hand side phenyl ring (Fig. 35, ring A) of both **RCZ12** and **RCZ20**. This ring is thought to be the recognition site of the molecule and modification of the substituents could bring to more soluble and active derivatives against T3SS.

It was firstly planned to remove the nitro group from ring A (**RCZ30** and **RCZ40**), in order to observe the lack of the electron-withdrawing effect on the molecules' activity (Fig. 35). Removal of the whole ring A was designed and replaced with a simple methyl group (**RCZ31** and **RCZ41**) to investigate the relevance of this phenyl ring. We also wanted to evaluate electron-donating groups on this phenyl ring and how they could affect the activity against EspD. Therefore, the replacement of the nitro group with a small methyl group (**RCZ32** and **RCZ42**) was planned as well as the replacement with a bulky *iso*-propyl group (**RCZ33** and **RCZ43**). Both alkyl substituents induce an electron-donating effect on ring A and on the whole molecule, but differ in dimensions, which can be crucial for the EspD interaction. To compare different electron-withdrawing groups, it was opted to replace the nitro group with a trifluoromethyl group (**RCZ34** and **RCZ44**); in this case, this new functional group exhibit an inducing electron-withdrawing effect on ring A rather than a resonance electron-withdrawing effect like the nitro group. An alkyl chain was also introduced to substitute ring A (**RCZ35** and **RCZ45**) to confer more lipophilicity to the molecule and to assess the compounds' activity in the presence of a long and flexible alkyl chain. At last, it was also decided to move the nitro group around ring A in *meta* (**RCZ36** and **RCZ46**) and *ortho* (**RCZ37** and **RCZ47**) position to identified the most active position on this phenyl ring.

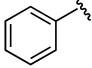
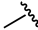
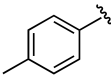
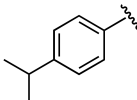
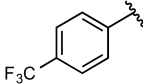
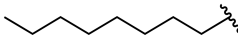
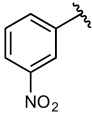
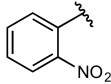
## 9.2 Synthesis of RCZ12 and RCZ20 derivatives

Synthesis of **RCZ12** derivatives started from the previously obtained amine **28** (Paragraph 7.2), which was sulphonylated with various sulphonyl chlorides following our standard conditions used before for the synthesis of the THP compound (Fig. 36). These protected intermediates were then immediately de-protected by  $\text{BBr}_3$  in DCM to afford the corresponding **RCZ12** analogues in moderate yield. **RCZ20** derivatives were synthesised in a similar way. Amine **35** was sulphonylated with different sulphonyl chlorides and the intermediates were treated with  $\text{AlCl}_3$  overnight to afford the corresponding **RCZ20** analogues.



**Fig. 36: Synthetic route for RCZ12 and RCZ20 derivatives:** Amine **28** and **35** were sulphonylated with different commercially available sulphonyl chlorides following our previous conditions. The intermediates thus obtained were immediately subjected to a de-protection step with  $\text{BBr}_3$  for THP analogues and with  $\text{AlCl}_3$  for DHP derivatives. The route proved to be fast and easy to create a moderate number of new compounds and it can be used to build extensive libraries based on the THP and DHP scaffold.

In both cases, the creation of the *ortho*-nitro (**RCZ37** and **RCZ47**) derivatives was found to be problematic as the protected intermediates were found to be extremely sensitive and decomposed during the de-protection step. For these reasons, we were unable to synthesise **RCZ37** and **RCZ47** (Table 9). However, the synthetic route proved to be fast and easy to generate a moderate number of derivatives from the two amines previously obtained, making this route ideal for the creation of extensive libraries based on the THP and DHP cores.

| R   | Entry (THP/DHP) | Yield (THP/DHP) |
|---|-----------------|-----------------|
|  | RCZ30/RCZ40     | 57%/49%         |
|  | RCZ31/RCZ41     | 31%/60%         |
|  | RCZ32/RCZ42     | 23%/55%         |
|  | RCZ33/RCZ43     | 22%/44%         |
|  | RCZ34/RCZ44     | 20%/34%         |
|  | RCZ35/RCZ45     | 33%/58%         |
|  | RCZ36/RCZ46     | 32%/24%         |
|  | RCZ37/RCZ47     | N/A             |

**Table 9: RCZ12 and RCZ20 derivatives yields:** The yields for the new **RCZ12** and **RCZ20** derivatives are listed above. All the yields are reported as an over two steps yield. **RCZ37** and **RCZ47** were not synthesised due to starting material decomposition.

### 9.3 Conclusions and future work

A total of 14 new **RCZ12** and **RCZ20** derivatives were synthesised in order to investigate the structure-activity relationship between the THP and DHP scaffold and EspD. Due to the results obtained in our preliminary screening, it was decided to modify the left-hand side phenyl ring (ring A), replacing it with small and long alkyl chains or introducing new substituents in place of the nitro group. The new series was afforded starting from the previously synthesised amines **28** and **35** and followed our standard protocols for sulphonylation and de-protection of the *iso*-propyl groups. The route was found to be fast and with easy purification steps. Unfortunately, intermediates for the synthesis of the *ortho*-nitro derivative (**RCZ37** and **RCZ47**) proved to be unstable and decomposed in the de-protection step. Other de-protecting agents were used, but they either displayed partial or unsuccessful de-protection. Both 2- and 4-nitrobenzenesulphonyl groups are extensively used as protecting groups for the preparation of secondary amines due to their selective cleavage<sup>166</sup>. Since the 2-nitrobenzenesulphonyl group is typically weaker than

the 4-nitrobenzenesulphonyl group, it is possible that our de-protection conditions were too harsh for this group and caused its removal.

This new series based on **RCZ12** and **RCZ20** structural features was designed and synthesised to obtain structure-activity relationship data from the compound-EspD interaction and it will be tested in the near future. The various substituents installed on the left-hand side of the molecule will provide new information of the intracellular interaction with EspD and their different chemical nature will evaluate which substituents is best-suited against EHEC T3SS. The series could also be evaluated against the truncated-EspD-HA strains to assess if a change in substituents or structure on the ring A affects the interaction site affinity. The biological evaluation of this series will provide essential information on the structure-activity relationship between **RCZ12/RCZ20**-EspD interaction and its influence on the T3SS apparatus.

## 10 [1,2,4]-Triazolo[4,3-b]pyridazine (TZP) Derivatives

### 10.1 Design and rationale of the TZP core

The inclusion of the hydrazide moiety in a hydrazine-containing heterocycle such as the THP and the DHP cores yielded stable and effective SA compounds derivatives. The THP and DHP derivatives resulted to be chemically more stable than the lead compound ME0055 and also showed a more selective effect on EHEC T3SS with no impact on bacterial growth, even at higher concentrations. In particular, **RCZ12** and **RCZ20** demonstrated a significant activity on the secretion of EspD, which caused intracellular retention of the virulence protein. A total inhibition of secretion was detected at 200  $\mu$ M, which proved to be the ideal concentrations for these compounds to block the assembly of the T3SS and the consequent colonisation. A significant down-regulation of T3SS-related genes was also detected and, in particular, Tir expression and secretion was found greatly reduced. The intracellular interaction between our derivatives and EspD was highlighted by pull-down analyses and confirmed by western blot using truncated-EspD-HA producing strains. Although both **RCZ12** and **RCZ20** displayed an improved chemical stability and a promising activity as anti-virulence compounds against *E. coli* O157 TUV 93-0, they also showed poor solubility when diluted in biological media for binding assay techniques such as MST and SPR, precipitating at high concentrations. ITC and NMR binding experiments were considered but not attempted due to this issue; although it should be noted that NMR chemical shift provided successful for investigating the interaction of the SA compounds with putative target proteins<sup>125</sup>.

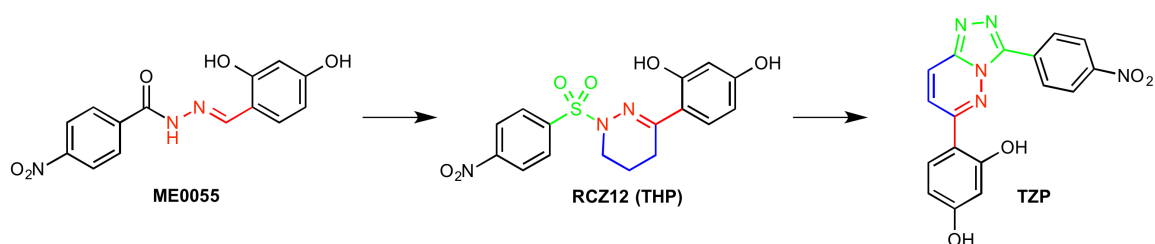


**Fig. 37: Design of the TZP core:** To improve the solubility of our compounds, it was decided to replace the sulphonyl motif of **RCZ12** with a [1,2,4]-triazolo[4,3-b]pyridazine (TZP) ring. The hydrazine moiety (highlighted in red) has been retained throughout both modifications (THP and TZP). The additional six-membered ring (blue), introduced in the THP scaffold, has been flattened by the new aromatic ring system TZP. The sulphonyl feature (green), which demonstrated to be essential for a significant activity, has been replaced by the triazole ring of the TZP core, preserving the hydrogen bond acceptor properties of the sulphonyl group.

To improve the solubility of our candidates, it was decided to further modify the central core of the structure of our hydrazine-containing heterocycles (Fig. 37). [1,2,4]-Triazolo[4,3-b]pyridazines (TZP) are well-known biologically active heterocycles and have been employed in the last decades in modern medicinal chemistry as successful bioisosteres for anti-tumoral and sedative activity<sup>167–169</sup>. It was opted to replace the sulphonyl motif of **RCZ12** with a TZP core in order to lower the lipophilicity of our scaffold. This *ortho*-fused ring system is more than optimal to enhance the hydrophilic nature of our candidate due to the high number of nitrogen, which provide interactions with protic solvents through hydrogen bonding. At the same time, the triazole ring mimics the geometric features of the sulphonyl group, which proved to be relevant for a marked activity in our first biological evaluation (Paragraph 7.3.2). The TZP core also flattens the original THP scaffold, since a fully aromatic ring system is introduced, leading to new potential pi-stacking interactions with EspD. All substituents on the left and right phenyl rings were retained, as in our previous modifications, in order to have a direct comparison between the candidates' effects. Only the **RCZ12** TZP analogue was firstly designed, while the **RCZ20** analogue was not considered, as an additional phenyl ring could increase the lipophilicity and bulk of the scaffold.

## 10.2 Synthesis of the TZP derivative

The synthesis of the TZP derivative started from the previously afforded 3-chloropyridazine intermediate **26** (Paragraph 8.3), which underwent condensation with 4-nitrobenzhydrazide in refluxing *n*-butanol<sup>170</sup> (Fig. 38).

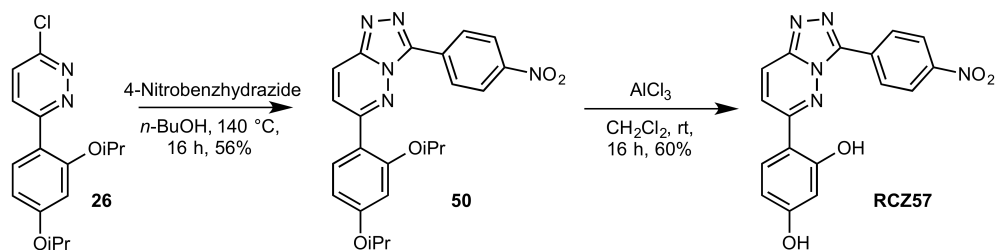


**Fig. 38: Synthetic route for the TZP derivative:** Starting from intermediate **26**, previously obtained for the synthesis of **RCZ12**, adduct **50** was obtained by means of condensation with 4-nitrobenzhydrazide in refluxing *n*-butanol. The protected TZP derivative underwent iso-propyl de-protection in the presence of aluminium trichloride to yield the desired TZP compound **RCZ57** in 4 steps from 3,6-dichloropyridazine and only 2 steps from intermediate **26**.



The protected [1,2,4]-triazolo[4,3-b]pyridazine adduct **50**, thus obtained, was easily de-protected with aluminium trichloride to yield the desired TZP analogue **RCZ57** in only 2 steps.

### 10.3 Biological evaluation of RCZ57

The biological evaluation of **RCZ57** was firstly compared against the SA compound ME0055 and it followed our previous experimental procedures used for the assessment of the THP and DHP derivatives. The target concentration of 200  $\mu$ M was chosen for all the preliminary tests, since **RCZ12** and **RCZ20** displayed an ideal inhibitory effect against T3SS at this concentration without affecting any other essential bacterial pathway or growth.

#### 10.3.1 Bacterial growth

*E. coli* O157 TUV 93-0 was cultured in the presence of **RCZ57** in order to evaluate any unwanted effects of the new candidate on the bacterial growth, as performed before for the THP and DHP derivatives. Optical density ( $OD_{600}$ ) was calculated hourly by means of a refractometer and the growth curve was then interpolated accordingly with the desired time-point (Fig. 39).

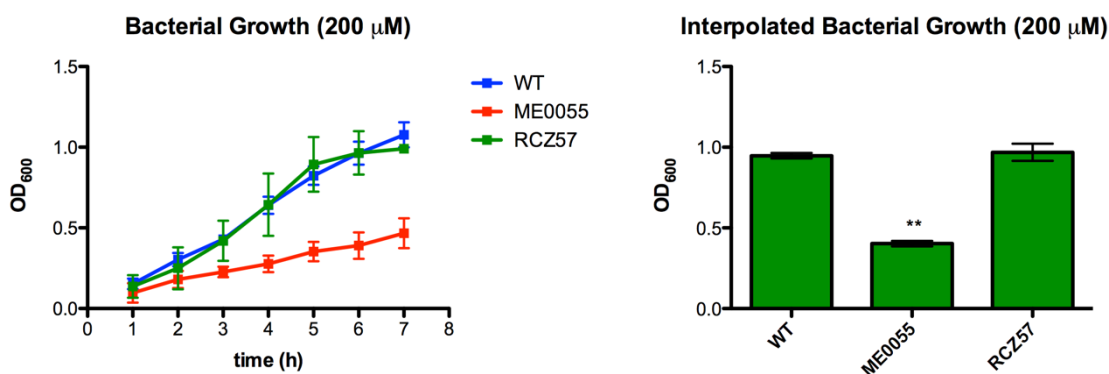


**Fig. 39: Bacterial growth evaluation:** Bacterial growth curves at 200  $\mu$ M are represented in the graph on the left. Standard deviation from the mean of each time point is shown by error bars. The curves thus obtained were analysed through linear regression interpolated with a determined time value (6 hours). Interpolated  $OD_{600}$  mean values are represented in the graph on the right. Standard deviation from the mean is shown by error bars.  $OD_{600}$  values of treated samples were compared to the control sample (WT) by Student's t-test for statistical significance ( $P$  value < 0.05). Significant samples are indicated by an asterisk. ME0055 bacterial growth inhibition resulted to be very statistically significant ( $P = 0.0046$ ), while RCZ57 did not affect the growth in a significant way.

As shown before, ME0055 affected the bacterial growth rate at a high concentration by 2.5-fold. **RCZ57** did not display any effects on *E. coli* O157 growth, demonstrating to be a suitable molecule for further biological evaluation.

### 10.3.2 RCZ57 vs. ME0055

**RCZ12** and **RCZ20** showed to inhibit the secretion of EspD, causing withholding of such virulence protein inside the bacterial cytosol, and to down-regulate Tir expression and secretion at 200  $\mu$ M. Since these effects are essential for the activity for our derivatives, Western blot experiments were carried out to evaluate **RCZ57** influence on the expression and secretion of T3SS proteins. ME0055 was firstly taken as a reference for direct comparison (Fig. 40).

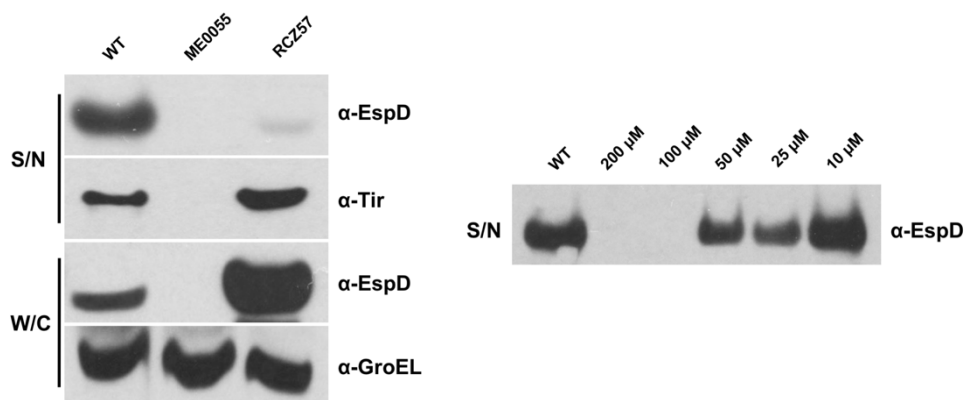


**Fig. 40:  $\alpha$ -EspD,  $\alpha$ -Tir and  $\alpha$ -GroEL Western blot for ME0055 and RCZ57 at 200  $\mu$ M (left) and  $\alpha$ -EspD Western blot with decreasing concentrations of RCZ57 (right):** Western blot analysis were carried out according to standard procedure (see Experimental Part for methods and Ab dilutions). Both supernatant proteins (S/N) and whole cell lysate solution (W/C) were analysed in repeats of three independent experiments. **RCZ57** demonstrated to inhibit EspD secretion with consequent retention of such protein inside the cell, while Tir secretion was not affected. Interestingly, our new TZP derivative did not influence other T3SS proteins, such as Tir, like **RCZ12** and **RCZ20** at 200  $\mu$ M. Withholding of EspD was also found to be well-marked, indicating accumulation of the protein into the cytosol. Decreasing concentrations of **RCZ57** showed a concentration-dependant effect on EspD secretion similar to the observed activity of **RCZ12** and **RCZ20**. In this case, **RCZ57** proved to very potent against the virulence protein even at 100  $\mu$ M, reducing its secretion by 20-fold. Weak activity was detected at 50 and 25  $\mu$ M, while the new compound was found completely inactive at 10  $\mu$ M.

At 200  $\mu$ M, ME0055 demonstrated to totally inhibit EspD secretion, as expected, and **RCZ57** encouragingly displayed a similar activity with a 25-fold reduction of EspD protein secretion. The phenotype of EspD retention inside the bacterial cells by **RCZ12** and **RCZ20** was also observed for **RCZ57**, while a total lack of such virulence protein was registered for

ME0055. Intracellular accumulation of EspD was also very clear for **RCZ57**, consistent with a retention of the protein into the cytosol. Tir secretion was also assessed by western blot in order to evaluate the selectivity of **RCZ57** with other T3SS protein of interest. ME0055 showed strong inhibition of Tir secretion, while our TZP derivative did not affect secretion of this protein. This result differed from what observed for **RCZ12** and **RCZ20** at 200  $\mu$ M, as the two derivatives inhibited both Tir secretion at high concentration. GroEL analyses were carried out as an experimental reference to confirm the selectivity of our new candidate. Bacteria were treated with decreasing concentrations of **RCZ57** and immunoblotted against GroEL to confirm the effect on EspD secretion. Total inhibition of EspD secretion was observed at 200  $\mu$ M, as previously evaluated. **RCZ57** demonstrated to block the secretion significantly also at 100  $\mu$ M (20-fold), while the molecule only had a very weak effect at 50  $\mu$ M (2-fold) and 25  $\mu$ M (1.5-fold). The new compound was found to be inactive against EspD secretion at 10  $\mu$ M. As previously reported for our THP and DHP derivatives, the new TZP compound showed a concentration-dependent effect on EspD secretion.

### 10.3.3 RCZ57 vs. RCZ12

**RCZ57** demonstrated to have a similar selective activity against EspD as previously reported for **RCZ12** and **RCZ20** beside its effect on Tir secretion. To directly compare our new candidate with the THP derivative, western blot analyses were also performed with **RCZ12** and **RCZ57** at 200  $\mu$ M to compare the ability of blocking EHEC T3SS apparatus (Fig. 41). As expected, both candidates showed a strong inhibition (approximately 25-fold reduction) of the virulence protein EspD, with the characteristic retention inside the bacterial cell. In this case, **RCZ57** displayed a marked accumulation of this protein with an EspD concentration 2-fold higher than the untreated wild type. As mentioned before, the new TZP derivative did not affect Tir secretion, while **RCZ12** exhibited a total inhibition of such protein secretion. Tir expression was also normal for **RCZ57**, while the THP compound down-regulated the transcription as previously observed (Paragraph 7.3.5). The structural modification applied to the TZP compound seemed to have improved the selectivity of the inhibitory effect on EspD, while reducing the transcriptional influence on T3SS-related genes. In addition, **RCZ57** demonstrated to cause a well-marked accumulation of EspD inside the bacterial cell at least 2-fold higher than the wild type. Inhibition of EspD

secretion still remained similar to **RCZ12** and **RCZ20** and, therefore, **RCZ57** can be considered an excellent derivative with enhanced solubility in biological media.

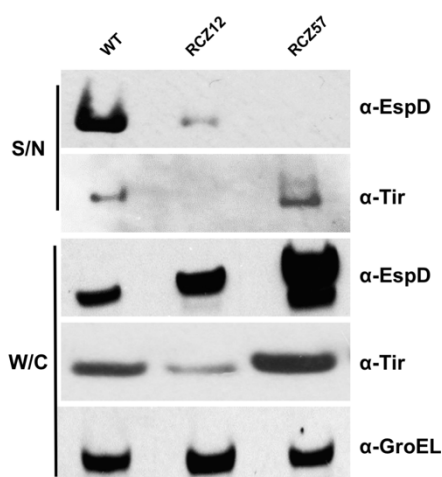


**Fig. 41:  $\alpha$ -EspD,  $\alpha$ -Tir and  $\alpha$ -GroEL Western blot for RCZ12 and RCZ57 at 200  $\mu$ M (left):** Western blot analysis were carried out according to standard procedure (see Experimental Part for methods and Ab dilutions). Both supernatant proteins (S/N) and whole cell lysate solution (W/C) were analysed in repeats of three independent experiments. **RCZ57** demonstrated to inhibit EspD secretion as **RCZ12** and to accumulate such protein in a more marked way than the THP molecule. Tir expression and secretion was found to be similar to the wild type when EHEC was treated with **RCZ57**, while **RCZ12** inhibit both expression and secretion as previously observed. It seems that the structural modification applied to **RCZ57** improved the selectivity of the activity on EspD secretion, while reducing the transcriptional effects on T3SS-related genes.

#### 10.3.4 Transcriptional effects of RCZ57

The effects of our new promising derivative on T3SS gene expression were also evaluated through a GFP reporter fusion assay, as previously performed for the THP and DHP compounds (Fig. 42). *LEE1:gfp* and *rpsM:gfp* were used in order to assess the global influence of **RCZ57** on T3SS-related and non T3SS-related genes transcription. It was already highlighted by the western blot results that **RCZ57** did not affect Tir expression at 200  $\mu$ M; therefore, it was opted to test the new compound against *LEE1* to confirm its selectivity. As previously shown, ME0055 demonstrated to significantly down-regulate both *rpsM* and *LEE1* promoter activity at 200  $\mu$ M. **RCZ57** did not show significant activity against the promoters of both genes, supporting the results shown in the previous western blot. From these data, it seems that the effects of our new compound were focused on EspD secretion at post-transcriptional level, without any side-effect on transcription.

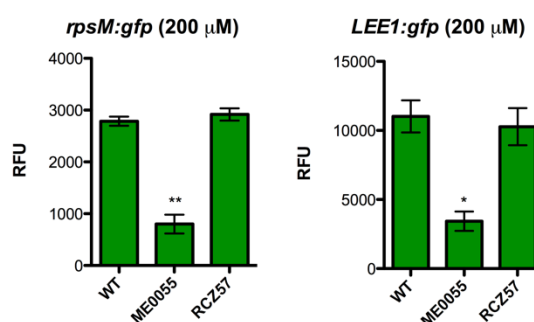


**Fig. 42: *rpsM:gfp* and *LEE1:gfp* promoter activity at OD<sub>600</sub> = 0.6 with ME0055 and RCZ57 at 200 μM:** GFP-reporter fusion assays analyses were carried out according to standard procedure (see Experimental Part for methods). The promoter activity was measured for every sample plotting fluorescence (RFU) against OD<sub>600</sub>. The curves thus obtained were analysed through linear regression interpolated with a determined OD<sub>600</sub> value (0.6). Interpolated RFU mean values are represented in the graphs above. Standard deviation from the mean is shown by error bars. RFU values of treated samples were compared to the control sample (WT) by Student's t-test for statistical significance (*P* value < 0.05). Significant samples are indicated by an asterisk, very significant samples by two asterisks and extremely significant samples by three asterisks. **RCZ57** did not show any significant influence on both *rpsM* and *LEE1* transcription, supporting the Western blot findings, where our new compound was found to selective inhibit EspD secretion, while no activity on Tir was detected. Unlike **RCZ12**, which also inhibited Tir at 200 μM, **RCZ57** demonstrated to be more selective for blocking EspD secretion.

### 10.3.5 Secreted protein profile

**RCZ57** exhibited a promising specific activity on EHEC T3SS similar to both THP and DHP derivatives. Total inhibition of EspD secretion, with characteristic intracellular accumulation, and no influence on Tir transcription were observed through western blot and GFP reporter fusion assays. To complete the biological characterisation of our TZP compound and investigate further its very specific effects on EspD, it was decided to examine the secreted proteins profile by SDS-PAGE electrophoresis. Once the secreted proteins were denatured in SDS, the samples were run on a SDS-PAGE gel and stained with Coomassie Brilliant Blue (Fig. 43). **RCZ57** showed a completely different protein profile than the wild type. As expected, EspD (39 kDa) was absent from the TZP compound profile, but high concentrations of unusual protein bands were also visualised. Some of these bands were removed and analysed by means of tandem mass spectrometry. Interestingly, all the unfamiliar secreted proteins were classified as either outer membrane or periplasmic proteins. Intimin (band number 1), the outer membrane protein responsible of intimate attachment to the host cell through Intimin-Tir interactions<sup>171</sup>, was detected in high amount in the secreted protein samples as well as the receptor for ferric enterobactin

and colicins B and D (band number 2), which is usually located in the outer membrane to allow the transport of enterobactin and colicins<sup>172</sup>. The outer membrane protein C, known as OmpC (band number 3), was also detected in the samples. OmpC is one of the main *E. coli* porins together with OmpF and regulates the passive diffusion of nutrients and antibiotics<sup>173–175</sup>.

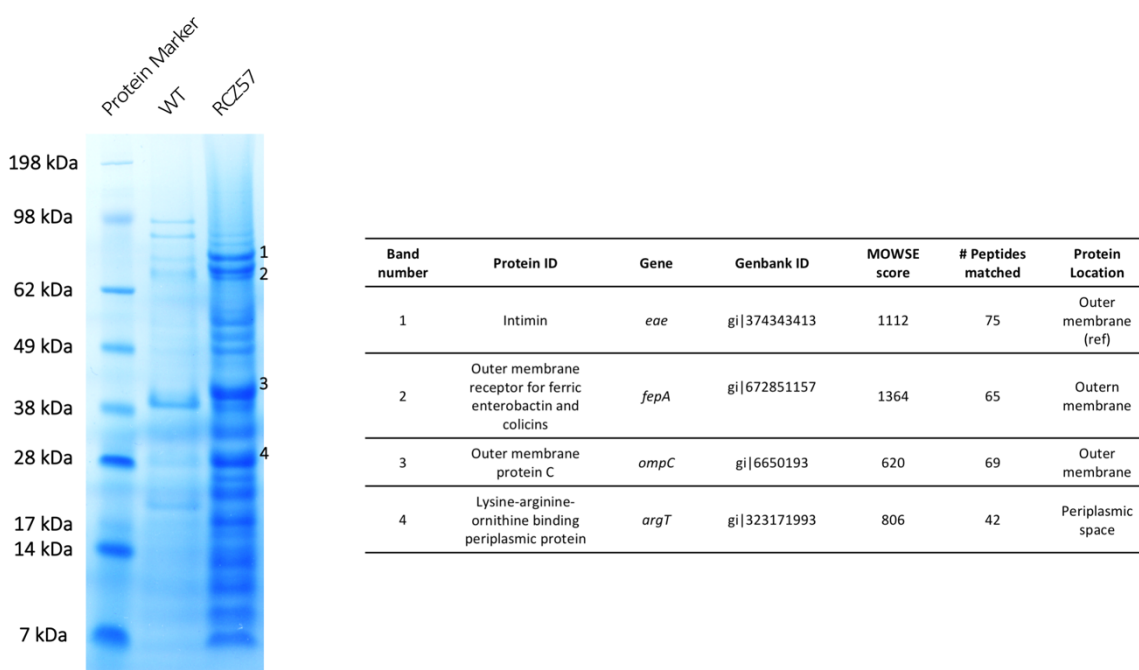


**Fig. 43: SDS-PAGE electrophoresis of secreted proteins (left) and the list of identified proteins by tandem mass spectrometry (right):** Many unusual protein bands were visualised by SDS-PAGE electrophoresis when *E. coli* was treated with **RCZ57** at 200  $\mu$ M. The most concentrated bands were excised and analysed by tandem mass-spectrometry to reveal the identity of 4 outer membranes proteins. This membrane protein shedding outside the cell can be linked to either vesicles formation or key changing in bacterial permeability. It is possible that **RCZ57** might bind to various permeability regulators, inducing porins over-expression and, therefore, enhancing the bacterium's permeability. Cell lysis was not included as a hypothesis as **RCZ57** did not inhibit bacterial growth. A list of the 4 outer membrane proteins visualised in the secreted protein samples. Protein Genbank ID, MOWSE score, number of peptides matched and gene of origin are listed in the table. All the entries were identified as either outer membrane or periplasmic proteins, which is rather unusual to find in the secretion media and, especially, in such high concentrations.

As the name infers, even this protein is always located in the outer membrane and its presence in the secreted protein samples is rather unusual. In addition, OmpC is a key protein for traditional antibiotics diffusion and it has been demonstrated that a lack of this porin is one of the main mechanism for the development of resistance<sup>176</sup> and also for enhancing the bacterium's sensitivity to acidic environments<sup>177</sup>. The lysine-arginine-ornithine binding protein (band number 4) was also identified in the secreted protein

samples, a portion of an ABC amino acids transporter, which is usually located in the periplasmic space between inner and outer membrane in the bacterium<sup>178,179</sup>. These are just some of the most abundant protein bands detected from the **RCZ57** treatment, but it is clear that many other outer membrane and periplasmic proteins were released into the media from the bacterial membrane, since the two secreted proteins profile did not match. It can be postulated that high concentrations of **RCZ57** might cause the formation and release of vesicles thereby resulting on the detection of the membrane proteins outside the cell. Modification of the bacterium's membrane permeability can also be associated with high concentrations of **RCZ57**, which can bind or interfere with regulators associated with osmotic control, EnvZ/OmpR, causing over-expression of porins and, therefore, shedding of proteins in the secretion media<sup>180,181</sup>. Cell lysis can, instead, be ruled out, since **RCZ57** does not affect bacterial growth at 200 µM, as lysis is always linked to growth inhibition.

#### 10.3.6 Transmission electron microscopy (TEM) analysis

The unusual shedding of outer membrane proteins was observed from the SDS-PAGE gel, when *E. coli* O157 TUV 93-0 was treated with **RCZ57** at 200 µM. To further investigate this effect, it was decided to analyse the bacterial membrane through transmission electron microscopy (TEM). Bacteria were treated with our TZP compound and untreated TUV 93-0 was employed as the negative control. Bacterial sections were analysed and resulted that **RCZ57** did not cause any vesicle formation or perturbation of the membranes, excluding the possibility of vesicle formation by high concentrations of the compound (see Appendix, Fig. 51). TEM analyses were also used to assess the ability of **RCZ57** to block the EspA filament formation, as performed for **RCZ12** and **RCZ20** (Paragraph 7.3.7). **RCZ12** was used as a direct comparison. **RCZ57** inhibited the formation of the EspA filaments by 5-fold as well as the THP derivative. This result suggested that the TZP compound might have the same mechanism of action as **RCZ12**.

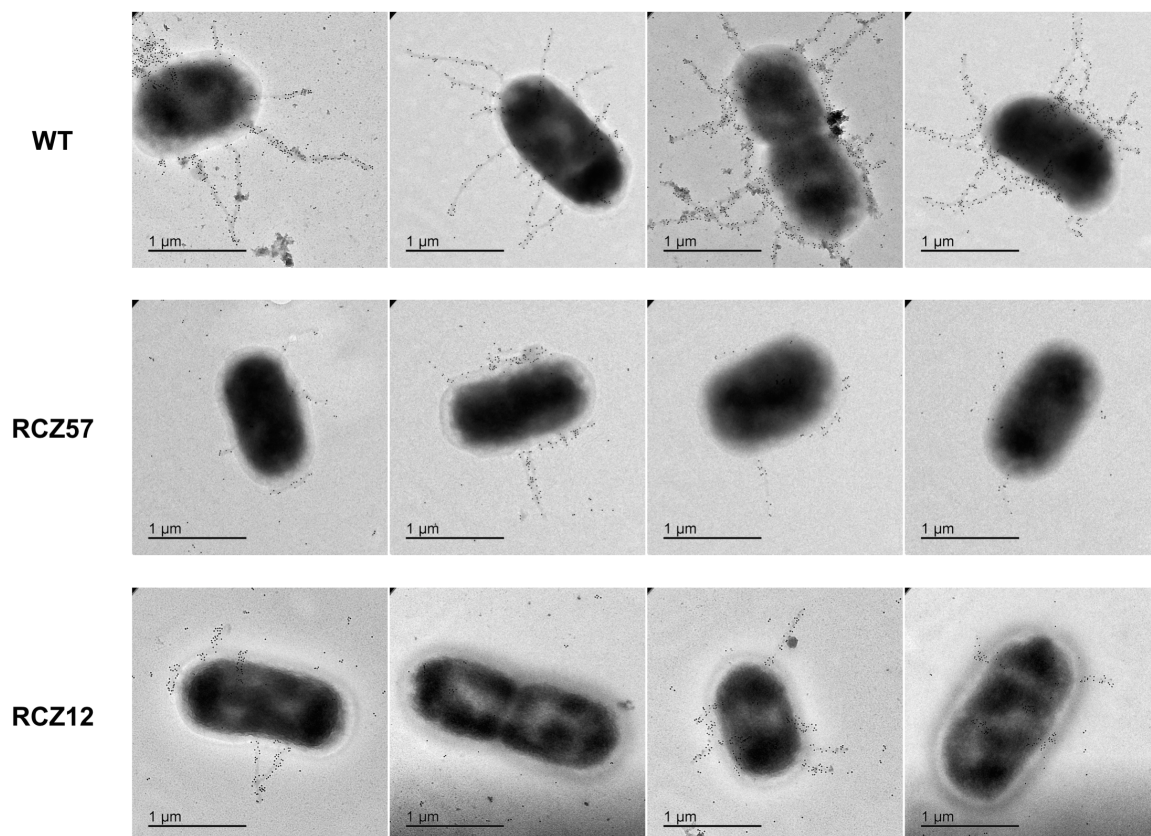


**Fig. 44: TEM images of EspA filaments with RCZ57:** Bacteria were grown in T3SS-inducing media and immobilised in paraformaldehyde. Before exposure on the microscope, the samples were incubated with a  $\alpha$ -EspA primary antibody and then with the corresponding secondary antibody conjugated with gold nanoparticle. The black dots on the images represents the gold particle, which specifically identify EspA. **RCZ12** and **RCZ57** demonstrated to reduce the correct EspA filament formation by 5-fold, causing a focal accumulation of the protein on the bacterium's surface.

#### 10.3.7 Metabolomics analysis for RCZ57

**RCZ57** displayed a similar activity profile to **RCZ12** on EspD at 200  $\mu$ M. The new compound also did not show any transcriptional effects, unlike the THP derivative which down-regulated T3SS-related genes. After these biological evaluation, we assumed that **RCZ57** mechanism of action might be analogous to both **RCZ12** and **RCZ20**; therefore, the TZP compound might directly bind to EspD to block its correct secretion. It was then opted to perform the previous metabolomics analysis (Paragraph 8.5) to confirm **RCZ57** uptake by *E. coli* O157 TUV 93-0 (Table 10). Even in this case, high concentrations of the molecule were found inside the cell pellets, clearly showing bacterial membrane crossing and supporting the hypothesis that our new analogue and **RCZ12** might have the same mode of action.



| Entry | Experimental Blank | Supernatant                           | Bacterial pellets                     |
|-------|--------------------|---------------------------------------|---------------------------------------|
| RCZ57 | 0                  | $1.14 \cdot 10^7 \pm 2.14 \cdot 10^6$ | $3.73 \cdot 10^9 \pm 5.76 \cdot 10^8$ |

**Table 10: Metabolomics data for RCZ12 and RCZ20 cellular uptake:** Average intensities of **RCZ57** and corresponding standard deviation in Supernatant and Bacterial pellets samples are represented in the table above. Experimental triplicates were prepared and analysed through hydrophilic interaction liquid chromatography (HILIC). A three magnitude increase of the compounds' concentration was registered for the Bacterial pellets samples, indicating a cellular uptake of both drugs inside the bacteria. This confirms that also **RCZ57** is taken up by the bacteria.

## 10.4 Synthesis of RCZ57 modular derivatives

**RCZ57** was found to be selectively active against EspD secretion, as **RCZ12** and **RCZ20**, with no significant transcriptional effect on T3SS-related genes. The new TZP derivative exhibited a strong inhibition of secretion (20- to 25-fold) at both 200 and 100  $\mu$ M with an obvious accumulation of the protein into the bacterial cytosol. No significant effect was observed on bacterial growth, other T3SS proteins of interests or essential cellular pathway. Due to these promising data, it was planned to synthesise few modular derivatives to investigate the structure-activity relationship of our new active compound.

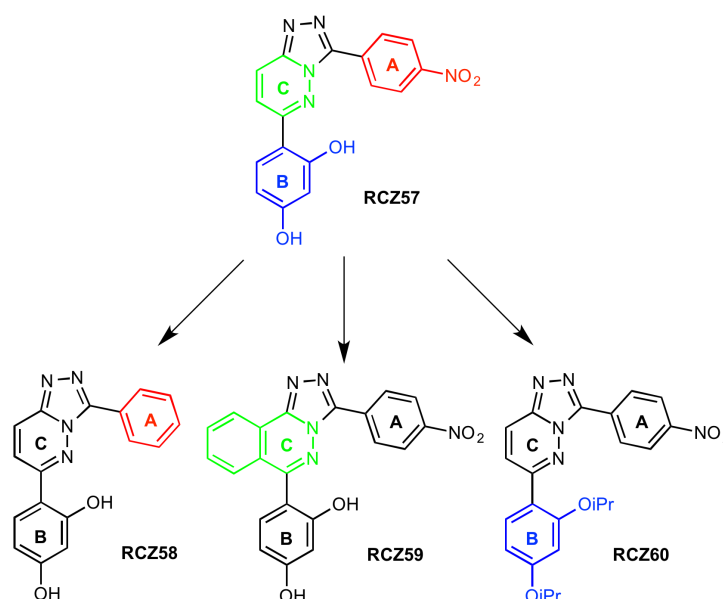


**Fig. 45: Structural design of RCZ57 modular derivatives:** Ring A, B and C were selected as **RCZ57** essential features for modular modifications. Firstly, the nitro group on ring A (red) was removed to investigate the activity of the compound with no substituents on the right-hand side of the molecule (**RCZ58**). An *ortho*-fused ring system was then introduced into **RCZ57** central ring C (green) to evaluate the bulk of this conjugated aromatic system and also the effects on solubility (**RCZ59**). Lastly, synthetic intermediate **41** was also employed in this modular series to assess the relevance of the two hydroxyl groups on ring B (blue) (**RCZ60**). In this case, the two *iso*-propyl groups eliminate the hydrogen bond acceptor properties of the hydroxyl groups and introduce bulk on ring B.

Three different structural features of **RCZ57** were selected: the nitro-bearing phenyl ring (Fig. 45, Ring A, red), the hydroxyl-bearing phenyl ring (Fig. 45, Ring B, blue) and the central pyridazine ring (Fig. 45, Ring C, green).

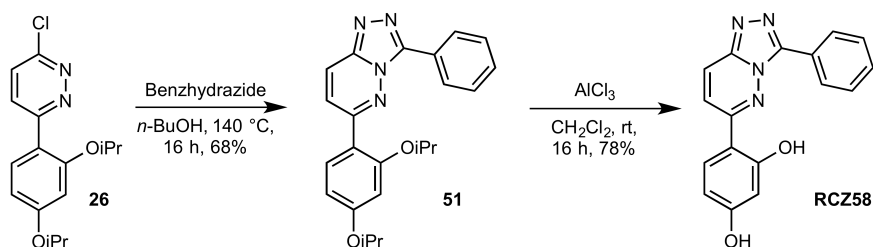


**Fig. 46: RCZ58 synthesis:** **RCZ58** synthesis follows our previous synthesis of **RCZ57**. In brief, intermediate **26** underwent condensation with benzhydrazide to obtain adduct **51**, which was consequently de-protected with aluminium trichloride in good yield.

Since the hydroxyl groups were previously found to be essential for **RCZ12** and **RCZ20** activity, it was firstly decided to use the *iso*-propyl protected intermediate **50** as a modification of ring B (**RCZ60**) to evaluate the two hydroxyl groups relevance in the inhibitory effect. The nitro group on ring A was then removed to investigate the lack of substituents on the right-hand side of the molecule (**RCZ58**) and to lower the electron-withdrawing effect of the nitro group on the whole structure. Finally, an *ortho*-fused phenyl ring was added to ring C to create the direct TZP derivative of **RCZ20** (**RCZ59**), introducing more bulk to the structure and decreasing the hydrophilicity of the compound.

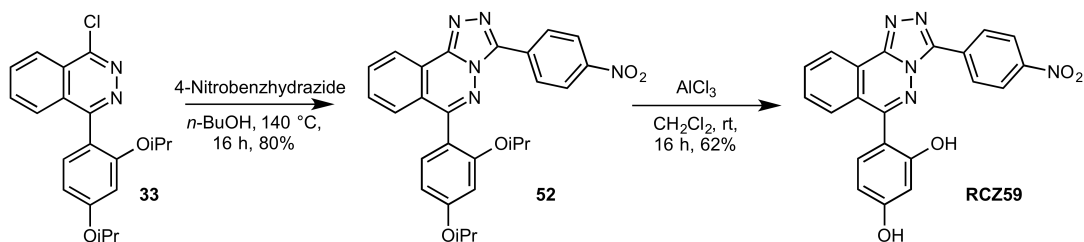


**Fig. 47: RCZ59 synthesis:** **RCZ59** synthesis follows our previous synthesis of **RCZ57**. In brief, intermediate **33** underwent condensation with 4-nitrobenzhydrazide to obtain adduct **52**, which was consequently de-protected with aluminium trichloride in good yield.

**RCZ58** synthesis started from the previously obtained intermediate **26**, which reacted with benzhydrazide in refluxing *n*-butanol to afford intermediate **51** in good yield<sup>170</sup> (Fig. 46). The adduct, thus obtained, was then treated with aluminium trichloride to yield **RCZ58** in only 2 steps from intermediate **26**. **RCZ59** synthesis was performed in a similar way starting from intermediate **33**, obtained for the alternative synthesis of **RCZ20** (see Paragraph 8.3) (Fig. 47). The chloro-pyridazine **33** underwent condensation with 4-nitrobenzhydrazide in

refluxing *n*-butanol to obtain intermediate **52**, which was consequently de-protected with aluminium trichloride to yield the desired compound.

### 10.5 Biological evaluation of RCZ57 modular derivatives

In order to overcome the solubility issues encountered during **RCZ12** and **RCZ20** biological evaluation, it was planned to design and synthesise a new more hydrophilic T3SS inhibitor, **RCZ57**. **RCZ57** showed a similar activity to the THP and DHP compounds, inhibiting EspD secretion and increasing the concentration of the T3SS protein inside the bacterium at 200  $\mu$ M and in a concentration-dependent manner. Modular derivatives of the TZP candidate were generated to investigate the structure-activity relationship of this new active scaffold.

#### 10.5.1 Bacterial growth

The ability of our modular analogues to interfere with the bacterial growth was firstly evaluated at 200  $\mu$ M as performed before with all our synthetic compounds (Fig. 48). **RCZ57** was taken as a reference. After 6 hours of incubation, none of our new molecules significantly affected *E. coli* O157 TUV 93-0 growth rate, making them suitable candidates for further testing.

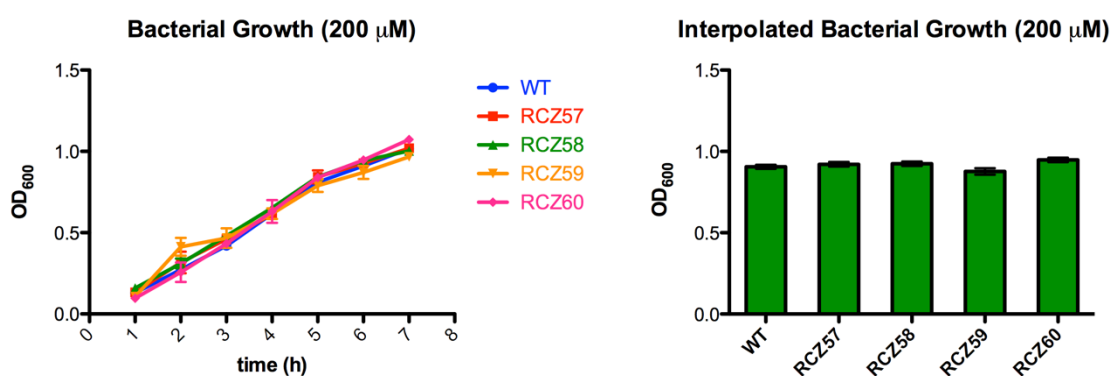


**Fig. 48: Bacterial growth evaluation:** Bacterial growth curves at 200  $\mu$ M are represented in the graph on the left. Standard deviation from the mean of each time point is shown by error bars. The curves thus obtained were analysed through linear regression interpolated with a determined time value (6 hours). Interpolated OD<sub>600</sub> mean values are represented in the graph on the right. Standard deviation from the mean is shown by error bars. OD<sub>600</sub> values of treated samples were compared to the control sample (WT) by Student's t-test for statistical significance ( $P$  value < 0.05). No statistically significant values were detected. None of the modular derivatives affected the bacterial growth in a significant way.

### 10.5.2 Virulence protein secretion

**RCZ57** was found to inhibit EspD secretion significantly at 200  $\mu$ M, while accumulating such virulence protein inside the bacterial cells. In order to further investigate this mode of action, all our modular derivatives were evaluated on their ability of blocking the secretion of T3SS proteins by means of western blot experiments. EspD concentrations were analysed in presence of our compounds at 200  $\mu$ M both outside and inside the cell (Fig. 49). **RCZ57** displayed a total inhibition of EspD secretion (more than 25-fold inhibition) and a 2-fold accumulation of the protein in the whole cell lysate, as previously obtained. **RCZ58** showed a moderate inhibitory activity (10-fold inhibition) with a slight increase of EspD concentration inside the cell (1.2-fold increase), while **RCZ59** demonstrated to have a very weak activity (1.5-fold reduction) and also a poor solubility in biological media. **RCZ60** did not affect the virulence protein secretion or expression. Western blot analyses were also performed for the translocated intimin receptor (Tir) in order to assess the selectivity of our modular compounds in inhibiting only EspD secretion. **RCZ57** did not affect Tir secretion, as evaluated before, even though a slight increased concentration of such virulence protein was found outside the cells. Despite its poor solubility and weak effect on EspD secretion, **RCZ59** proved to significantly increase (2-fold) Tir secretion, while **RCZ58** and **RCZ60** did not influence the secretion. The data highlighted the relevance of the two hydroxyl groups in **RCZ57** activity, as **RCZ60** resulted to be completely inactive against EspD secretion. **RCZ59** showed how modifications on the central ring C can influence the solubility of the molecule and, therefore, its effect on EspD. Removal of the nitro group on ring A (**RCZ58**) resulted in a compound with slightly attenuated activity probably due to the missing electron-withdrawing effect on the whole structure.

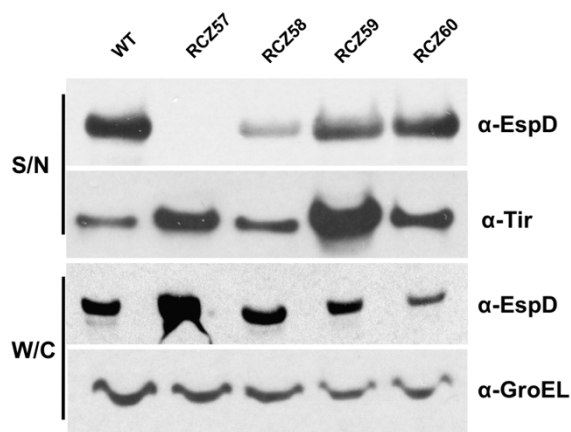


**Fig. 49:  $\alpha$ -EspD  $\alpha$ -Tir and  $\alpha$ -GroEL Western blot for RCZ57 modular derivatives RCZ58, RCZ59 and RCZ60 at 200  $\mu$ M:** Western blot analysis were carried out according to standard procedure (see Experimental Part for methods and Ab dilutions). Both supernatant proteins (S/N) and whole cell lysate solution (W/C) were analysed in repeats of three independent experiments. **RCZ58** demonstrated to have a similar activity to **RCZ57**, significantly reducing EspD secretion (10-fold), while retaining such virulence protein inside the cell. **RCZ59** had just a very weak effect on EspD secretion due to its very poor solubility in biological media, while **RCZ60** resulted to be completely inactive, highlighting the relevance of the two hydroxyl groups on the ring B of **RCZ57**.

### 10.5.3 Structure-activity relationship (SAR)

**RCZ58**, **RCZ59** and **RCZ60** were specifically designed and synthesise to evaluate **RCZ57** preliminary structure-activity relationship, in order to highlight the active features of the molecule. Western blot experiments were carried out to assess the effect of the new analogues on T3SS proteins of interest. In our previous biological tests, **RCZ57** displayed a very strong inhibition of EspD secretion (more than 25-fold inhibition) at 200  $\mu$ M and an obvious accumulation (2-fold) of the same protein inside the bacterial cytosol. No effect on growth was detected against *E. coli* O157:H7 and an interesting slight increase in Tir secretion was also observed from the western blot analyses.

Removal of the nitro group on ring A (**RCZ58**) produced an active compound against EspD secretion, which retained a good activity profile similar to **RCZ57**. A slight decrement in potency was detected compared to **RCZ57**; probably, due to the lack of the strong electron-withdrawing effects induced by the nitro group. In addition, **RCZ58** did not affect Tir secretion neither positively or negatively. These data suggest that ring A might be a recognition site, which gives selectivity to the compound, but it is not directly involved in the essential interactions.

Introduction of an *ortho*-fused phenyl ring on the pyridazine ring C (**RCZ59**) yielded a flat, bulky and non-polar **RCZ57** derivative, which resulted just slightly soluble in the western blot biological media. Due to this solubility issue, **RCZ59** activity was limited to a very weak effect on EspD secretion (1.5-fold reduction) and considered partially reliable. Tir analysis revealed an obvious increased concentration of the protein outside the bacterial cell than **RCZ57**. The pyridazine ring C cannot be considered as an essential feature for the TZP compound activity, but it surely plays a relevant role for the solubility in biological media. Addition of bulky and lipophilic substituents resulted in a decreased solubility and, therefore, in a barely active derivative. This site can be modified for achieving even more hydrophilic versions of **RCZ57** without influencing the activity of the compound.

Alkylation of the two hydroxyl groups on ring B (**RCZ60**) resulted in a completely inactive analogue. **RCZ60** did not affect EspD or Tir secretion. The data suggest that, whenever the hydroxyl groups on ring B are unable of interacting through hydrogen bond, **RCZ57** loses its activity against EspD secretion. Therefore, the hydroxyl groups are to be considered as the active site of the molecule as their inability of accepting/donating hydrogen bonds resulted in a total loss of activity.

## 10.6 Conclusions and future work

In order to overcome the solubility issues encountered during the investigation of **RCZ12** and **RCZ20** mode of action, it was planned to modify the THP core with a new hydrazine-containing heterocycles. Due to its well-known biological activity, a [1,2,4]-triazolo[4,3-b]pyridazine (TZP) core was installed in the central part of the molecule to generate a new TZP derivative (**RCZ57**). The synthesis of this new analogue started from the previously obtained chloro-pyridazine **26** and yielded the desired product in just 2 steps. **RCZ57** was firstly tested against ME0055 and then against **RCZ12** at 200  $\mu$ M. The TZP compound demonstrated to have the same activity against EspD secretion as **RCZ12** and to cause an even more marked characteristic EspD accumulation inside the cell. The new derivative also proved to be more potent than **RCZ12**, as it exhibited a strong 20-fold reduction of EspD at 100  $\mu$ M. In addition, **RCZ57** did not influence the transcription of T3SS-related genes, unlike observed for the THP compound at 200  $\mu$ M. Interestingly, analysis of the secreted protein profile revealed a totally different protein pattern for bacteria treated with **RCZ57**. Mass spectrometry identified at least 4 outer membrane and periplasmic proteins into the secreted media, indicating an unusual protein shedding outside the cell.

Microscopy visualisation excluded a plausible vesicles formation caused by high concentrations of the TZP compound. It can be speculated that, at 200  $\mu$ M, **RCZ57** may bind or interfere with osmolarity regulators and then modify the bacterium's permeability. An indication of this can be linked to the abnormal concentrations of the porin OmpC found in the secreted media samples, but it will have to be studied in more details in the future. Permeability modification can be evaluated through dye leakage assays and flow cytometry experiments.

To further investigate the structure-activity relationship of **RCZ57**, a small series of 3 derivatives was designed and synthesised modifying three TZP main structural features. **RCZ58** (modification on ring A), **RCZ59** (modification on ring C) and **RCZ60** (modification on the hydroxyl groups on ring B) were tested together with **RCZ57** through western blot analyses. From the data obtained from this experiment, we summarised that the two hydroxyl groups on ring B are essential for **RCZ57**, since **RCZ60** was found to be completely inactive. Modifications on ring A, instead, resulted in an active compound with a slightly attenuated activity against EspD secretion, while installation of another aromatic ring on ring C yielded an inactive compound due to its very poor solubility. Due to **RCZ57** relative ease of synthesis, an extensive library of analogues can be easily build to obtain relevant structure-activity relationship data and to optimise this very promising T3SS inhibitor in a more potent and “drug-like” compound. Furthermore, the synthesis of **RCZ57** labelled version will help to confirm that the TZP compound shares the same mode of action of **RCZ12** and **RCZ20**. Thanks to our preliminary structure-activity relationship investigation, the molecular probe can be installed on ring A without affecting the compound's inhibitory effects.

## 11 Final Discussion

*Escherichia coli* O157:H7 is considered one of the most dangerous serotype of the EHEC family<sup>9</sup>. Its infection can cause bloody diarrhoea, haemolytic colitis and haemolytic uremic syndrome (HUS), which can lead to death. The mode of action of bactericidal and bacteriostatic compounds to eradicate *E. coli* O157:H7 infections triggers bacterial SOS responses and results in an increased Shiga toxin release, worsening the clinical symptoms and leading to development of resistant clones. Consequently, traditional antibiotic treatments must be avoided for *E. coli* O157:H7 infections. Anti-virulence compounds are considered as a promising alternative to overcome this problem. These compounds selectively inhibit the virulence weapons of the bacterium, resulting in a mild evolutionary pressure and, therefore, leading to less chances to develop resistance<sup>182–184</sup>. Salicylidene acylhydrazide (SA) compounds were one of the first class of anti-virulence compounds with activity against the Type Three Secretion System (T3SS) in many Gram-negative bacteria<sup>114,118,185</sup>. Studies to identify the main protein target of SA compounds were made by Wang *et al.*, leading to the conclusion that the mode of action of these potent molecules was a result of a modulation of several metabolic pathways rather than a direct influence on T3SS<sup>125</sup>. This study aimed to modify the chemical structure of one of the best SA compounds against EHEC, ME0055, in order to overcome its limitation and to discover new potential T3SS inhibitors.

### 11.1 RCZ12 and RCZ20

The first design we applied to the ME0055 scaffold was to include the imine motif in a more stable heterocycle. Incorporating the hydrazine feature in a cycle strengthened the whole acylhydrazone structure, which was previously prone to hydrolysis. 1,4,5,6-tetrahydro-pyridazine (THP) and 1,2-dihydrophthalazine (DHP) cores were selected as main new scaffolds. A small library (8 compounds) based on these two heterocycles was synthesised and tested against EHEC T3SS with ME0055 for direct comparison. **RCZ12** and **RCZ20** resulted to have comparable activity to the SA compound inhibiting the secretion of the protein EspD. Further testing displayed that the two compounds were strongly active against the T3SS. At 200  $\mu$ M, both **RCZ12** and **RCZ20** blocked EspD secretion, causing retention of such protein inside the bacterial cells, and down-regulated T3SS-related genes as suggested by western blot analyses on Tir and by GFP reporter fusion assays. In



addition, the THP and DHP compounds did not show to interfere with the bacterial growth even at high concentrations, while ME0055 previously demonstrated to already influence the growth at 50  $\mu\text{M}$  <sup>118</sup>. The modifications applied for the THP and DHP resulted in two active compounds with slightly different effects on T3SS than the SA compound. While ME0055 showed to inhibit both transcription and secretion of T3SS proteins, **RCZ12** and **RCZ20** revealed to primarily block EspD secretion only and then to down-regulate the transcription of other T3SS proteins. The transcriptional effect of the new compounds, investigated by RNAseq and GFP reporter analyses, resulted to be weaker than the SA compound influence. Furthermore, **RCZ12** and **RCZ20** selectively down-regulated T3SS-related genes, while the data registered for ME0055 suggested a broader down-regulation of other non T3SS-related genes. It is easy to speculate that the retention of EspD inside the cell, caused by our compounds, could trigger a negative feedback circuit against T3SS-related genes. This signalling could stop the production of EspD and other T3SS proteins in order to avoid toxic levels of the accumulating protein. Evidences of this pathway were found using a *ΔespD tif:gfp* strain, which demonstrated to have an attenuated *tir* expression than the TUV 93-0 counterpart. However, both **RCZ12** and **RCZ20** showed to down-regulate the LEE even in the absence of the main target EspD, supporting the hypothesis of a transcriptional influence as a secondary effect. This feedback circuit could be investigated in the near future to elucidate the phenotype observed. Immuno-labelling microscope experiment (TEM) also highlighted the ability of our compounds to block the correct assembly of functioning EspA filaments, a phenotype already associated with EspD malfunction <sup>33</sup>.

Due to our findings, it was clear that our new THP and DHP compounds might act differently and more selectively on the T3SS than the SA compound. The enhanced degree of selectivity achieved by our chemical modifications onto ME0055 structure drove us to examine the mode of action of the THP and DHP derivatives. Following previous studies conducted by Wang *et al.*, labelled version of **RCZ12** and **RCZ20** were synthesised to perform affinity pull-down experiments <sup>125</sup>. EspD was identified as the only bona fide T3SS-related protein to specifically bound to our labelled compounds. The fact that the same virulence protein was found to be bound with both **RCZ12** and **RCZ20**, confirmed the hypothesis of a common mechanism of action by our molecules. In addition, the few non T3SS-related proteins bound to our compounds also confirmed the increased selectivity of our new derivatives. From these affinity experiments, we hypothesised a direct

intracellular interaction between our compounds and EspD. Metabolomics data supported this hypothesis, since high concentrations of the compounds were found inside the bacteria by hydrophilic interaction liquid chromatography. *E. coli* strains producing a truncated-EspD-HA constructs were generated by allelic exchange and then treated with **RCZ12** at 200  $\mu$ M. The experiment validated EspD as the main target of both THP and DHP compounds, since a modification in the protein structure lead to a complete loss of activity and restored a normal secretion of the construct outside the bacterium. In addition, from this analysis we postulated that **RCZ12** and **RCZ20** might bind to the predicted coiled-coil domain 1 (COIL1) of EspD, since only deletion of this region completely reversed the THP compound effect.

### 11.2 The future of RCZ12 and RCZ20

Our THP and DHP compounds demonstrated to be a promising class of EHEC T3SS inhibitors. The enhanced selective mode of action make them a more than optimal starting point for new structural optimisation to build more potent inhibitors against EspD. A small series based on **RCZ12** and **RCZ20** was also synthesised in a fast and efficient way. The modifications were mostly performed on the left-hand side phenyl ring, where different substituents were placed instead of the nitro group or the entire ring was exchanged with either a small or long alkyl chain. Testing of these new derivatives will be useful in terms of structure-activity relationship (SAR) data that could lead to more selective and active molecules. Due to the easy synthetic route, an expanded library focused on **RCZ12** and **RCZ20** can be built for extensive SAR information.

Attempting in crystallising EspD bound to our THP and DHP compounds should also be carried out in order to confirm the binding site of these molecules. Unfortunately, the biological properties of this membrane protein will provide several issues to the purification and crystallisation processes. Not surprisingly, all our efforts in purifying EspD failed due to its physical and biological properties and the protein itself resulted to be extremely hard to work with.

After our results, adhesion assays could be performed with **RCZ12** and **RCZ20** in order to verify the reduced intimate attachment of the bacterium to intestinal epithelial cells. Since EspD functions as an anchor for the bacteria colonisation, it is likely that treatment with our compounds will lead to a less invasive bacterial phenotype. The data obtained from the transmission electron microscope (TEM) already revealed a reduction of correctly

assembled EspA filaments, which will likely result in an impaired attachment to the host cells. The data gathered with the adhesion experiment will be completing the biological profile of **RCZ12** and **RCZ20** and will also encourage testing in infection mouse models for assessing the *in vivo* efficacy.

The THP and DHP compounds could also undergo testing against other Gram-negative bacterial strains that harbours the T3SS. Since this virulence weapon is highly conserved in more than 25 species of bacteria<sup>186</sup>, it is possible that **RCZ12** and **RCZ20** will also interact with the corresponding EspD homologue in other species such as *Salmonella* sp., *Yersinia* sp., *S. flexneri*, *P. aeruginosa* and *Chlamidya* sp. (see Appendix for EspD alignment). The possibility of activity against other bacterial strain is very attractive for the generation of broad-spectrum anti-virulence compounds and the scaffolds can be easily modified to achieved selective compounds for individual strains.

### 11.3 RCZ57

It was opted to install a new hydrazine-containing heterocycle into the ME0055 structure based on **RCZ12** and **RCZ20** features. A [1,2,4]-triazolo[4,3-b]pyridazine (TZP) ring was then introduced to create a new potential T3SS inhibitor, **RCZ57**. The synthesis of this molecule started from the previously obtained intermediate **28** and employed only 2 steps to yield the desired compound. **RCZ57** was tested against ME0055 and **RCZ12** and demonstrated to be an excellent T3SS inhibitor. At 200 µM, the TZP compound displayed a strong inhibition of EspD secretion with the characteristic intracellular retention and, surprisingly, did not show any significant effects on the transcription of T3SS-related genes. Further GFP reporter analyses confirmed the inactivity of **RCZ57** at transcriptional level and suggested an even more selective post-transcriptional effect on EspD. While investigating the secreted proteins profile, an unusual protein pattern was detected for the **RCZ57** treatment. Mass spectrometry analyses identified many outer membrane and periplasmic proteins shedding in the secretion media. This unusual behaviour was firstly linked to the possibility of vesicle formation by high concentration of **RCZ57**, but microscopy studies, focused on the morphology of the bacterial membrane, did not show any vesicle formation. It was hypothesised that the TZP compound might interfere with osmolarity regulators in order to over-express porins (such as OmpC) and, therefore, change the bacterial membrane's permeability. Evidence of this unusual effect will be investigated in the near future.

Modular analogues of **RCZ57** were also designed and synthesised for preliminary structure-activity relationship (SAR) studies. Western blot analysis confirmed the relevance of the two hydroxyl groups on ring B, since etherification of such groups lead to an inactive derivative, and also showed that the removal of the nitro group on ring A yielded another strong T3SS inhibitors. These preliminary results addressed future modifications of the TZP scaffold and suggested that, as for **RCZ12** and **RCZ20**, the hydroxyl groups are essential for interaction with EspD.

#### 11.4 The future of **RCZ57**

**RCZ57** demonstrated to be an excellent ME0055 derivative, with enhanced selectivity and solubility in biological media. The effects observed for this new molecule were all focused on blocking EspD secretion, while no transcriptional activity was detected by our experiments. After the data obtained, we hypothesised that the TZP derivative could share the same intracellular EspD interaction of both THP and DHP compounds and in a more selective manner. Metabolomics data confirmed the uptake of our new molecule inside the bacteria and supported such hypothesis. **RCZ57** labelled version should be synthesised in the future to replicate the pull-down assay against EHEC whole cell lysate in order to confirm EspD as target or to identify the compound's new mode of action.

Due to ease of synthesis, an expanded library of **RCZ57** derivatives could also be easily synthesised. Different substituents can be installed on ring A, which proved to be the recognition site of the molecule. In addition, it would be very useful to change the hydroxyl groups position across ring B in order to identify the most potent position and combination against EspD secretion.

Adhesion assays on epithelial cells should also be performed to evaluate the efficacy of this new molecule as well as *in vivo* experiment in infection mouse models.

The unusual outer membrane proteins shedding observed by SDS-PAGE could be investigated by dye leakage assays or by treatment of porins null mutant, such as  $\Delta ompC$ ,  $\Delta ompF$  and  $\Delta ompR$ , with **RCZ57** and analyses on the secreted protein profiles. This effect might be linked to a plausible interaction of the TZP compound with off-target proteins and could be confirmed by the pull-down assay against EHEC whole cell lysate solution.

## **11.5 Conclusion**

This study provided the synthesis and the biological evaluation of three new potential classes of anti-virulence compounds. The scaffold designed on ME0055 proved to be more selective and potent of the starting compound and lead to the discovery of EspD as the main protein target. The biological and chemical results obtained, yielded a solid framework for future research focused on the development of T3SS inhibitors.

## References

- (1) Eisen, J. a. (2000) Horizontal gene transfer among microbial genomes: new insights from complete genome analysis. *Curr. Opin. Genet. Dev.* 10, 606–611.
- (2) Didelot, X., Meric, G., Falush, D., and Darling, A. E. (2012) Impact of homologous and non-homologous recombination in the genomic evolution of *Escherichia coli*. *BMC Genomics* 13, 256.
- (3) Reid, S. D., Herbelin, C. J., Bumbaugh, a C., Selander, R. K., and Whittam, T. S. (2000) Parallel evolution of virulence in pathogenic *Escherichia coli*. *Nature* 406, 64–7.
- (4) Kaper, J. B., Nataro, J. P., and Mobley, H. L. T. (2004) Pathogenic *Escherichia coli*. *Nat. Rev. Microbiol.* 2, 123–140.
- (5) Marrs, C. F., Zhang, L., and Foxman, B. (2005) *Escherichia coli* mediated urinary tract infections: Are there distinct uropathogenic *E. coli* (UPEC) pathotypes? *FEMS Microbiol. Lett.*
- (6) Wiles, T. J., Kulesus, R. R., and Mulvey, M. A. (2008) Origins and virulence mechanisms of uropathogenic *Escherichia coli*. *Exp. Mol. Pathol.*
- (7) Cziráok, E., Milch, H., Madár, J., and Semjén, G. (1977) Characterization of *Escherichia coli* serogroups causing meningitis, sepsis and enteritis. I. Serological properties and animal pathogenicity of O18, O78 and O83 isolates. *Acta Microbiol. Acad. Sci. Hung.* 24, 115–26.
- (8) *Escherichia*, E. (2011) Media centre Enterohaemorrhagic *Escherichia coli* ( EHEC ). *Fruits* 1–4.
- (9) Organisation, W. H. (2011) Enterohaemorrhagic *E.coli* (EHEC).
- (10) Riley, L. W., Remis, R. S., Helgerson, S. D., McGee, H. B., Wells, J. G., Davis, B. R., Hebert, R. J., Olcott, E. S., Johnson, L. M., Hargrett, N. T., Blake, P. A., and Cohen, M. L. (1983) Hemorrhagic Colitis Associated with a Rare *Escherichia coli* Serotype — NEJM. *N. Engl. J. Med.* 308, 681–685.
- (11) Orskov F, Orskov I, V. J. (1987) CATTLE AS RESERVOIR OF VEROTOXIN-PRODUCING *ESCHERICHIA COLI* O157:H7. *Lancet* 276.
- (12) Naylor, S. W., Low, J. C., Besser, T. E., Mahajan, A., Gunn, G. J., Pearce, M. C., McKendrick, I. J., Smith, D. G. E., and Gally, D. L. (2003) Lymphoid follicle-dense mucosa at the terminal rectum is the principal site of colonization of enterohemorrhagic *Escherichia coli* O157:H7 in the bovine host. *Infect. Immun.* 71, 1505–1512.
- (13) Low, J. C., McKendrick, I. J., Fenlon, D., Naylor, S. W., Currie, C., Smith, D. G. E., Allison, L., Gally, D. L., Low, J. C., Mckendrick, I. J., Mckechnie, C., and Fenlon, D. (2005) Rectal Carriage of Enterohemorrhagic *Escherichia coli* O157 in Slaughtered Cattle Rectal Carriage

of Enterohemorrhagic *Escherichia coli* O157 in Slaughtered Cattle. *Appl. Environ. Microbiol.* 71, 93–97.

(14) Tilden, J., Young, W., McNamara, A. M., Custer, C., Boesel, B., Lambert-Fair, M. A., Majkowski, J., Vugia, D., Werner, S. B., Hollingsworth, J., and Morris, J. G. (1996) A new route of transmission for *Escherichia coli*: Infection from dry fermented salami. *Am. J. Public Health* 86, 1142–1145.

(15) Karmali, M. a., Petric, M., Steele, B. T., and Lim, C. (1983) Sporadic Cases of Haemolytic-Uraemic Syndrome Associated With FaecalCytotoxin and Cytotoxin-Producing *Escherichia coli* In Stools. *Lancet i*, 619–620.

(16) Karmali, M.A. Petric, M. Lim, C. Fleming, P.C. and Steele, B. T. (1983) *Escherichia coli* cytotoxin, haemolytic uraemic syndrome and haemolytic colitis. *Lancet* 1299–1300.

(17) Panos, G. Z., Betsi, G. I., and Falagas, M. E. (2006) Systematic review: Are antibiotics detrimental or beneficial for the treatment of patients with *Escherichia coli* O157:H7 infection? *Aliment. Pharmacol. Ther.* 24, 731–742.

(18) Coburn, B., Sekirov, I., and Finlay, B. B. (2007) Type III secretion systems and disease. *Clin Microbiol Rev* 20, 535–549.

(19) Moon, H. W., Whipp, S. C., Argenzio, R. A., Levine, M. M., and Giannella, R. A. (1983) Attaching and effacing activities of rabbit and human enteropathogenic *Escherichia coli* in pig and rabbit intestines. *Infect. Immun.* 41, 1340–1351.

(20) Jerse, a E., Yu, J., Tall, B. D., and Kaper, J. B. (1990) A genetic locus of enteropathogenic *Escherichia coli* necessary for the production of attaching and effacing lesions on tissue culture cells. *Proc. Natl. Acad. Sci. U. S. A.* 87, 7839–7843.

(21) Rothbaum, R., McAdams, A. J., Giannella, R., and Partin, J. C. (1982) A clinicopathologic study of enterocyte-adherent *Escherichia coli*: a cause of protracted diarrhea in infants. *Gastroenterology* 83, 441–454.

(22) Knutton, S., Lloyd, D. R., and McNeish, A. S. (1987) Adhesion of enteropathogenic *Escherichia coli* to human intestinal enterocytes and cultured human intestinal mucosa. *Infect. Immun.* 55, 69–77.

(23) Yip, C. K., and Strynadka, N. C. J. (2006) New structural insights into the bacterial type III secretion system. *Trends Biochem. Sci.*

(24) Deane, J. E., Abrusci, P., Johnson, S., and Lea, S. M. (2010) Timing is everything: The regulation of type III secretion. *Cell. Mol. Life Sci.*

(25) Zarivach, R., Vuckovic, M., Deng, W., Finlay, B. B., and Strynadka, N. C. J. (2007)



Structural analysis of a prototypical ATPase from the type III secretion system. *Nat. Struct. Mol. Biol.* 14, 131–137.

(26) Tree, J. J., Wolfson, E. B., Wang, D., Roe, A. J., and Gally, D. L. (2009) Controlling injection: regulation of type III secretion in enterohaemorrhagic *Escherichia coli*. *Trends Microbiol.*

(27) Wang, D., Roe, A. J., McAteer, S., Shipston, M. J., and Gally, D. L. (2008) Hierarchical type III secretion of translocators and effectors from *Escherichia coli* O157:H7 requires the carboxy terminus of SepL that binds to Tir. *Mol. Microbiol.* 69, 1499–1512.

(28) Lario, P. I., Pfuetzner, R. A., Frey, E. A., Creagh, L., Haynes, C., Maurelli, A. T., and Strynadka, N. C. J. (2005) Structure and biochemical analysis of a secretin pilot protein. *EMBO J.* 24, 1111–21.

(29) Wang, Y. A., Yu, X., Yip, C., Strynadka, N. C., and Egelman, E. H. (2006) Structural Polymorphism in Bacterial EspA Filaments Revealed by Cryo-EM and an Improved Approach to Helical Reconstruction. *Structure* 14, 1189–1196.

(30) Veenendaal, A. K. J., Hodgkinson, J. L., Schwarzer, L., Stabat, D., Zenk, S. F., and Blocker, A. J. (2007) The type III secretion system needle tip complex mediates host cell sensing and translocon insertion. *Mol. Microbiol.* 63, 1719–1730.

(31) Wachter, C., Beinke, C., Mattes, M., and Schmidt, M. A. (1999) Insertion of EspD into epithelial target cell membranes by infecting enteropathogenic *Escherichia coli*. *Mol. Microbiol.* 31, 1695–1707.

(32) Dasanayake, D., Richaud, M., Cyr, N., Caballero-Franco, C., Pittroff, S., Finn, R. M., Ausi, J., Luo, W., Donnenberg, M. S., and Jardim, A. (2011) The N-terminal amphipathic region of the *Escherichia coli* type III secretion system protein EspD is required for membrane insertion and function. *Mol. Microbiol.* 81, 734–750.

(33) Kresse, A. U., Rohde, M., and Guzmán, C. A. (1999) The EspD protein of enterohemorrhagic *Escherichia coli* is required for the formation of bacterial surface appendages and is incorporated in the cytoplasmic membranes of target cells. *Infect. Immun.* 67, 4834–4842.

(34) Chatterjee, A., Caballero-Franco, C., Bakker, D., Totten, S., and Jardim, A. (2015) Pore-forming activity of the *Escherichia coli* type III secretion system protein EspD. *J. Biol. Chem.* 290, 25579–25594.

(35) Troisfontaines, P., and Cornelis, G. R. (2005) Type III Secretion: More Systems Than You Think. *Physiology* 20, 326–339.

- (36) Wiles, S., Pickard, K. M., Peng, K., MacDonald, T. T., and Frankel, G. (2006) In vivo bioluminescence imaging of the murine pathogen *Citrobacter rodentium*. *Infect. Immun.* 74, 5391–5396.
- (37) Deng, W., Puente, J. L., Gruenheid, S., Li, Y., Vallance, B. A., Vázquez, A., Barba, J., Ibarra, J. A., O'Donnell, P., Metalnikov, P., Ashman, K., Lee, S., Goode, D., Pawson, T., and Finlay, B. B. (2004) Dissecting virulence: systematic and functional analyses of a pathogenicity island. *Proc. Natl. Acad. Sci. U. S. A.* 101, 3597–602.
- (38) McDaniel, T. K., Jarvis, K. G., Donnenberg, M. S., and Kaper, J. B. (1995) A genetic locus of enterocyte effacement conserved among diverse enterobacterial pathogens. *Proc. Natl. Acad. Sci. U. S. A.* 92, 1664–1668.
- (39) Perna, N. T., Plunkett 3rd, G., Burland, V., Mau, B., Glasner, J. D., Rose, D. J., Mayhew, G. F., Evans, P. S., Gregor, J., Kirkpatrick, H. A., Posfai, G., Hackett, J., Klink, S., Boutin, A., Shao, Y., Miller, L., Grotbeck, E. J., Davis, N. W., Lim, A., Dimalanta, E. T., Potamouisis, K. D., Apodaca, J., Anantharaman, T. S., Lin, J., Yen, G., Schwartz, D. C., Welch, R. A., and Blattner, F. R. (2001) Genome sequence of enterohaemorrhagic *Escherichia coli* O157:H7. *Nature* 409, 529–533.
- (40) Bustamante, V. H., Santana, F. J., Calva, E., and Puente, J. L. (2001) Transcriptional regulation of type III secretion genes in enteropathogenic *Escherichia coli*: Ler antagonizes H-NS-dependent repression. *Mol. Microbiol.* 39, 664–678.
- (41) Crane, J. K., McNamara, B. P., and Donnenberg, M. S. (2001) Role of EspF in host cell death induced by enteropathogenic *Escherichia coli*. *Cell. Microbiol.* 3, 197–211.
- (42) Knutton, S., Rosenshine, M., Pallen, M. J., Nisan, I., Neves, B. C., Bain, C., Wolff, C., Dougan, G., and Frankel, G. (1998) A novel EspA-associated surface organelle of enteropathogenic *Escherichia coli* involved in protein translocation into epithelial cells. *EMBO J.* 17, 2166–2176.
- (43) Sanchez-SanMartin, C., Bustamante, V. H., Calva, E., and Puente, J. L. (2001) Transcriptional regulation of the orf19 gene and the tir-cesT-eae operon of enteropathogenic *Escherichia coli*. *J. Bacteriol.* 183, 2823–2833.
- (44) Elliott, S. J., Wainwright, L. A., McDaniel, T. K., Jarvis, K. G., Deng, Y., Lai, L. C., McNamara, B. P., Donnenberg, M. S., and Kaper, J. B. (1998) The complete sequence of the locus of enterocyte effacement (LEE) from enteropathogenic *Escherichia coli* E2348/69. *Mol. Microbiol.* 28, 1–4.
- (45) Fang, F. C., and Rimsky, S. (2008) New insights into transcriptional regulation by H-NS.

- (46) Mellies, J. L., Elliott, S. J., Sperandio, V., Donnenberg, M. S., and Kaper, J. B. (1999) The Per regulon of enteropathogenic *Escherichia coli*: identification of a regulatory cascade and a novel transcriptional activator, the locus of enterocyte effacement (LEE)-encoded regulator (Ler). *Mol. Microbiol.* 33, 296–306.
- (47) Iyoda, S., Koizumi, N., Satou, H., Lu, Y., Saitoh, T., Ohnishi, M., and Watanabe, H. (2006) The GrlR-GrlA regulatory system coordinately controls the expression of flagellar and LEE-encoded type III protein secretion systems in enterohemorrhagic *Escherichia coli*. *J. Bacteriol.* 188, 5682–5692.
- (48) Hughes, D. T., Clarke, M. B., Yamamoto, K., Rasko, D. A., and Sperandio, V. (2009) The QseC Adrenergic Signaling Cascade in Enterohemorrhagic *E. coli* (EHEC). *PLoS Pathog* 5, e1000553.
- (49) Njoroge, J. W., Nguyen, Y., Curtis, M. M., Moreira, C. G., and Sperandio, V. (2012) Virulence meets metabolism: Cra and KdpE gene regulation in enterohemorrhagic *Escherichia coli*. *MBio* 3.
- (50) Zhang, L., Chaudhuri, R. R., Constantinidou, C., Hobman, J. L., Patel, M. D., Jones, A. C., Sarti, D., Roe, A. J., Vlisidou, I., Shaw, R. K., Falciani, F., Stevens, M. P., Gally, D. L., Knutton, S., Frankel, G., Penn, C. W., and Pallen, M. J. (2004) Regulators encoded in the *Escherichia coli* type III secretion system 2 gene cluster influence expression of genes within the locus for enterocyte effacement in enterohemorrhagic *E. coli* O157:H7. *Infect. Immun.* 72, 7282–7293.
- (51) Shakhnovich, E. A., Davis, B. M., and Waldor, M. K. (2009) Hfq negatively regulates type III secretion in EHEC and several other pathogens. *Mol. Microbiol.* 74, 347–363.
- (52) Kenny, B., DeVinney, R., Stein, M., Reinscheid, D. J., Frey, E. a, and Finlay, B. B. (1997) Enteropathogenic *E. coli* (EPEC) transfers its receptor for intimate adherence into mammalian cells. *Cell* 91, 511–520.
- (53) Kalman, D., Weiner, O. D., Goosney, D. L., Sedat, J. W., Finlay, B. B., Abo, A., and Bishop, J. M. (1999) Enteropathogenic *E. coli* acts through WASP and Arp2/3 complex to form actin pedestals. *Nat. Cell Biol.* 1, 389–91.
- (54) Kodama, T., Akeda, Y., Kono, G., Takahashi, A., Imura, K., Iida, T., and Honda, T. (2002) The EspB protein of enterohaemorrhagic *Escherichia coli* interacts directly with  $\beta$ -catenin. *Cell. Microbiol.* 4, 213–222.
- (55) Marchès, O., Batchelor, M., Shaw, R. K., Patel, A., Cummings, N., Nagai, T., Sasakawa,

- C., Carlsson, S. R., Lundmark, R., Cougoule, C., Caron, E., Knutton, S., Connerton, I., and Frankel, G. (2006) EspF of enteropathogenic *Escherichia coli* binds sorting nexin 9. *J. Bacteriol.* 188, 3110–3115.
- (56) Kenny, B., and Jepson, M. (2000) Targeting of an enteropathogenic *Escherichia coli* (EPEC) effector protein to host mitochondria. *Cell. Microbiol.* 2, 579–590.
- (57) Dean, P., and Kenny, B. (2009) The effector repertoire of enteropathogenic *E. coli*: ganging up on the host cell. *Curr. Opin. Microbiol.*
- (58) Fraser, M. E., Fujinaga, M., Cherney, M. M., Melton-Celsa, a R., Twiddy, E. M., O’Brien, a D., and James, M. N. (2004) Structure of shiga toxin type 2 (Stx2) from *Escherichia coli* O157:H7. *J Biol Chem* 279, 27511–27517.
- (59) Endo, Y., Tsurugi, K., Yutsude, T., Takeda, Y., Ogasawara, T., and Igarashi, K. (1988) Site of action of a Vero toxin (VT2) from *Escherichia coli* O157 : H7 and of Shiga toxin on eukaryotic ribosomes. *Eur. J. Biochem.* 171, 45–50.
- (60) Lindberg, A. A., Brown, J. E., Strömberg, N., Westling-Ryd, M., Schultz, J. E., and Karlsson, K. A. (1987) Identification of the carbohydrate receptor for Shiga toxin produced by *Shigella dysenteriae* type 1. *J. Biol. Chem.* 262, 1779–1785.
- (61) Johannes, L., and Römer, W. (2010) Shiga toxins--from cell biology to biomedical applications. *Nat. Rev. Microbiol.* 8, 105–116.
- (62) Pacheco, A. R., and Sperandio, V. (2012) Shiga toxin in enterohemorrhagic *E.coli*: regulation and novel anti-virulence strategies. *Front. Cell. Infect. Microbiol.* 2, 1–12.
- (63) Walterspiel, J. N., Morrow, A. L., Cleary, T. G., and Ashkenazi, S. (1992) Effect of subinhibitory concentrations of antibiotics on extracellular shiga-like toxin I. *Infection* 20, 25–29.
- (64) Acheson, D. W. K., and Donohue-Rolfe, a. (1989) Cancer associated hemolytic uremic syndrome: a possible role of Mitomycin C in relation to Shiga-like toxins. *J. Clin. Oncol.* 7, 1953.
- (65) Matsushiro, A., Sato, K., Miyamoto, H., Yamamura, T., and Honda, T. (1999) Induction of prophages of enterohemorrhagic *Escherichia coli* O157:H7 with norfloxacin. *J. Bacteriol.* 181, 2257–2260.
- (66) Takeda, T., Yoshino, K., Adachi, E., Sato, Y., and Yamagata, K. (1999) In vitro assessment of a chemically synthesized Shiga toxin receptor analog attached to chromosorb P (Synsorb Pk) as a specific absorbing agent of Shiga toxin 1 and 2. *Microbiol. Immunol.* 43, 331–337.

- (67) Trachtman, H., Cnaan, A., Christen, E., Gibbs, K., Zhao, S., Acheson, D. W. K., Weiss, R., Kaskel, F. J., Spitzer, A., and Hirschman, G. H. (2003) Effect of an Oral Shiga Toxin-Binding Agent on Diarrhea-Associated Hemolytic Uremic Syndrome in Children: A Randomized Controlled Trial. *J. Am. Med. Assoc.* 290, 1337–1344.
- (68) Zhu, C., Yu, J., Yang, Z., Davis, K., Rios, H., Wang, B., Glenn, G., and Boedeker, E. C. (2008) Protection against Shiga toxin-producing *Escherichia coli* infection by transcutaneous immunization with Shiga toxin subunit B. *Clin. Vaccine Immunol.* 15, 359–66.
- (69) Goldwater, P. N., and Bettelheim, K. a. (2012) Treatment of enterohemorrhagic *Escherichia coli* (EHEC) infection and hemolytic uremic syndrome (HUS). *BMC Med.* 10, 12.
- (70) Clarke, M. B., Hughes, D. T., Zhu, C., Boedeker, E. C., and Sperandio, V. (2006) The QseC sensor kinase: a bacterial adrenergic receptor. *Proc. Natl. Acad. Sci. U. S. A.* 103, 10420–5.
- (71) Hughes, D. T., and Sperandio, V. (2008) Inter-kingdom signalling: communication between bacteria and their hosts. *Nat.Rev.Microbiol.* 6, 111–120.
- (72) Sperandio, V., Torres, A. G., Jarvis, B., Nataro, J. P., and Kaper, J. B. (2003) Bacteria-host communication: The language of hormones. *Proc. Natl. Acad. Sci.* 100, 8951–8956.
- (73) Clarke, M. B., and Sperandio, V. (2005) Transcriptional autoregulation by quorum sensing *Escherichia coli* regulators B and C (QseBC) in enterohaemorrhagic *E. coli* (EHEC). *Mol. Microbiol.* 58, 441–455.
- (74) Rasko, D. A., Moreira, C. G., Li de, R., Reading, N. C., Ritchie, J. M., Waldor, M. K., Williams, N., Taussig, R., Wei, S., Roth, M., Hughes, D. T., Huntley, J. F., Fina, M. W., Falck, J. R., and Sperandio, V. (2008) Targeting QseC signaling and virulence for antibiotic development. *Science (80-. ).* 321, 1078–1080.
- (75) Lyte, M., Arulanandam, B. P., and Frank, C. D. (1996) Production of Shiga-like toxins by *Escherichia coli* O157:H7 can be influenced by the neuroendocrine hormone norepinephrine. *J. Lab. Clin. Med.* 128, 392–398.
- (76) Bearson, B. L., and Bearson, S. M. D. (2008) The role of the QseC quorum-sensing sensor kinase in colonization and norepinephrine-enhanced motility of *Salmonella enterica* serovar Typhimurium. *Microb. Pathog.* 44, 271–278.
- (77) Sauer, F. G., Remaut, H., Hultgren, S. J., and Waksman, G. (2004) Fiber assembly by the chaperone-usheer pathway. *Biochim. Biophys. Acta - Mol. Cell Res.*
- (78) Hung, D. L., Knight, S. D., Woods, R. M., Pinkner, J. S., and Hultgren, S. J. (1996)

Molecular basis of two subfamilies of immunoglobulin-like chaperones. *EMBO J* 15, 3792–3805.

(79) Roberts, J. A., Marklund, B. I., Ilver, D., Haslam, D., Kaack, M. B., Baskin, G., Louis, M., Möllby, R., Winberg, J., and Normark, S. (1994) The Gal(alpha 1-4)Gal-specific tip adhesin of *Escherichia coli* P-fimbriae is needed for pyelonephritis to occur in the normal urinary tract. *Proc. Natl. Acad. Sci. U. S. A.* 91, 11889–93.

(80) Dodson, K. W., Pinkner, J. S., Rose, T., Magnusson, G., Hultgren, S. J., and Waksman, G. (2001) Structural basis of the interaction of the pyelonephritic *E. coli* adhesin to its human kidney receptor. *Cell* 105, 733–743.

(81) Anderson, G. G., Palermo, J. J., Schilling, J. D., Roth, R., Heuser, J., and Hultgren, S. J. (2003) Intracellular bacterial biofilm-like pods in urinary tract infections. *Science* (80-. ). 301, 105–107.

(82) Justice, S. S., Hung, C., Theriot, J. A., Fletcher, D. A., Anderson, G. G., Footer, M. J., and Hultgren, S. J. (2004) Differentiation and developmental pathways of uropathogenic *Escherichia coli* in urinary tract pathogenesis. *Proc. Natl. Acad. Sci. U. S. A.* 101, 1333–1338.

(83) Bann, J. G., Pinkner, J. S., Frieden, C., and Hultgren, S. J. (2004) Catalysis of protein folding by chaperones in pathogenic bacteria. *Proc Natl Acad Sci U S A* 101, 17389–17393.

(84) Vetsch, M., Puorger, C., Spirig, T., Grauschopf, U., Weber-Ban, E. U., and Glockshuber, R. (2004) Pilus chaperones represent a new type of protein-folding catalyst. *Nature* 431, 329–333.

(85) Holmgren, A., and Branden, C. I. (1989) Crystal structure of chaperone protein PapD reveals an immunoglobulin fold. *Nature* 342, 248–251.

(86) Choudhury, D., Thompson, A., Stojanoff, V., Langermann, S., Pinkner, J., Hultgren, S. J., and Knight, S. D. (1999) X-ray structure of the FimC-FimH chaperone-adhesin complex from uropathogenic *Escherichia coli*. *Science* (80-. ). 285, 1061–1066.

(87) Sauer, F. G., Fütterer, K., Pinkner, J. S., Dodson, K. W., Hultgren, S. J., and Waksman, G. (1999) Structural basis of chaperone function and pilus biogenesis. *Science* 285, 1058–1061.

(88) Sauer, F. G., Pinkner, J. S., Waksman, G., and Hultgren, S. J. (2002) Chaperone priming of pilus subunits facilitates a topological transition that drives fiber formation. *Cell* 111, 543–551.

(89) Thanassi, D. G., Saulino, E. T., Lombardo, M. J., Roth, R., Heuser, J., and Hultgren, S. J. (1998) The PapC usher forms an oligomeric channel: implications for pilus biogenesis

across the outer membrane. *Proc. Natl. Acad. Sci. U. S. A.* 95, 3146–51.

(90) Dodson, K. W., Jacob-Dubuisson, F., Striker, R. T., and Hultgren, S. J. (1993) Outer-membrane PapC molecular usher discriminately recognizes periplasmic chaperone-pilus subunit complexes. *Proc. Natl. Acad. Sci.* 90, 3670–3674.

(91) Nishiyama, M., Horst, R., Eidam, O., Herrmann, T., Ignatov, O., Vetsch, M., Bettendorff, P., Jelesarov, I., Grütter, M. G., Wüthrich, K., Glockshuber, R., and Capitani, G. (2005) Structural basis of chaperone-subunit complex recognition by the type 1 pilus assembly platform FimD. *EMBO J.* 24, 2075–86.

(92) Ng, T. W., Akman, L., Osisami, M., and Thanassi, D. G. (2004) The usher N terminus is the initial targeting site for chaperone-subunit complexes and participates in subsequent pilus biogenesis events. *J. Bacteriol.* 186, 5321–5331.

(93) Barnhart, M. M., Pinkner, J. S., Soto, G. E., Sauer, F. G., Langermann, S., Waksman, G., Frieden, C., and Hultgren, S. J. (2000) PapD-like chaperones provide the missing information for folding of pilin proteins. *Proc. Natl. Acad. Sci. U. S. A.* 97, 7709–14.

(94) Remaut, H., Rose, R. J., Hannan, T. J., Hultgren, S. J., Radford, S. E., Ashcroft, A. E., and Waksman, G. (2006) Donor-Strand Exchange in Chaperone-Assisted Pilus Assembly Proceeds through a Concerted  $\beta$  Strand Displacement Mechanism. *Mol. Cell* 22, 831–842.

(95) Zavialov, A. V., Berglund, J., Pudney, A. F., Fooks, L. J., Ibrahim, T. M., MacIntyre, S., and Knight, S. D. (2003) Structure and biogenesis of the capsular F1 antigen from *Yersinia pestis*: Preserved folding energy drives fiber formation. *Cell* 113, 587–596.

(96) Svensson A, Larsson A, Emtenas H, Hedenstrom M, Fex T, Hultgren SJ, Pinkner JS, Almqvist F, K. J. (2001) Design and evaluation of pilicides: potential novel antibacterial agents directed against uropathogenic *Escherichia coli*. *Chembiochem* 915–918.

(97) Kuehn, M. J., Ogg, D. J., Kihlberg, J., Slonim, L. N., Flemmer, K., Bergfors, T., and Hultgren, S. J. (1993) Structural basis of pilus subunit recognition by the PapD chaperone. *Science*.

(98) Pinkner, J. S., Remaut, H., Buelens, F., Miller, E., Aberg, V., Pemberton, N., Hedenström, M., Larsson, A., Seed, P., Waksman, G., Hultgren, S. J., and Almqvist, F. (2006) Rationally designed small compounds inhibit pilus biogenesis in uropathogenic bacteria. *Proc. Natl. Acad. Sci. U. S. A.* 103, 17897–902.

(99) Cusumano, C. K., Pinkner, J. S., Han, Z., Greene, S. E., Ford, B. A., Crowley, J. R., Henderson, J. P., Janetka, J. W., and Hultgren, S. J. (2011) Treatment and prevention of urinary tract infection with orally active FimH inhibitors. *Sci. Transl. Med.* 3, 109ra115.

- (100) Chorell, E., Pinkner, J. S., Phan, G., Edvinsson, S., Buelens, F., Remaut, H., Waksman, G., Hultgren, S. J., and Almqvist, F. (2010) Design and synthesis of C-2 substituted thiazolo and dihydrothiazolo ring-fused 2-pyridones: Pilicides with increased antivirulence activity. *J. Med. Chem.* *53*, 5690–5695.
- (101) Viboud, G. I., and Bliska, J. B. (2005) Yersinia outer proteins: role in modulation of host cell signaling responses and pathogenesis. *Annu. Rev. Microbiol.* *59*, 69–89.
- (102) Linington, R. G., Robertson, M., Gauthier, A., Finlay, B. B., MacMillan, J. B., Molinski, T. F., Van Soest, R., and Andersen, R. J. (2006) Caminosides B-D, antimicrobial glycolipids isolated from the marine sponge *Caminus sphaeroconia*. *J. Nat. Prod.* *69*, 173–177.
- (103) Maehr, H., Leach, M., Williams, T. H., and Blount, J. F. (1980) The chemistry of aurodox and related antibiotics. *Can. J. Chem.* *58*, 501–526.
- (104) Kimura, K., Iwatsuki, M., Nagai, T., Matsumoto, A., Takahashi, Y., Shiomi, K., Omura, S., and Abe, A. (2011) A small-molecule inhibitor of the bacterial type III secretion system protects against in vivo infection with *Citrobacter rodentium*. *J. Antibiot. (Tokyo)*. *64*, 197–203.
- (105) Iwatsuki, M., Uchida, R., Yoshijima, H., Ui, H., Shiomi, K., Kim, Y. P., Hirose, T., Sunazuka, T., Abe, A., Tomoda, H., and Omura, S. (2008) Guadinomines, Type III secretion system inhibitors, produced by streptomyces sp K01-0509. *J. Antibiot. (Tokyo)*. *61*, 230–236.
- (106) Zetterström, C. E., Hasselgren, J., Salin, O., Davis, R. A., Quinn, R. J., Sundin, C., and Elofsson, M. (2013) The resveratrol tetramer (-)-hopeaphenol inhibits type III secretion in the gram-negative pathogens *Yersinia pseudotuberculosis* and *Pseudomonas aeruginosa*. *PLoS One* *8*.
- (107) Duncan, M. C., Wong, W. R., Dupzyk, A. J., Bray, W. M., Linington, R. G., and Auerbuch, V. (2014) An NF- $\kappa$ B-based high-throughput screen identifies piericidins as inhibitors of the *Yersinia pseudotuberculosis* type III secretion system. *Antimicrob. Agents Chemother.* *58*, 1118–1126.
- (108) Linington, R. G., Robertson, M., Gauthier, A., Finlay, B. B., Van Soest, R., and Andersen, R. J. (2002) Caminoside A, an antimicrobial glycolipid isolated from the marine sponge *Caminus sphaeroconia*. *Org. Lett.* *4*, 4089–4092.
- (109) Parmeggiani, A., and Swart, G. W. M. (1985) Mechanism of action of kirromycin-like antibiotics. *Annu. Rev. Microbiol.*
- (110) Pan, N. J., Brady, M. J., Leong, J. M., and Goguen, J. D. (2009) Targeting type III



secretion in *Yersinia pestis*. *Antimicrob. Agents Chemother.* 53, 385–392.

(111) Felise, H. B., Nguyen, H. V., Pfuetzner, R. A., Barry, K. C., Jackson, S. R., Blanc, M.-P., Bronstein, P. A., Kline, T., and Miller, S. I. (2008) An inhibitor of gram-negative bacterial virulence protein secretion. *Cell Host Microbe* 4, 325–336.

(112) Kline, T., Felise, H. B., Barry, K. C., Jackson, S. R., Nguyen, H. V., and Miller, S. I. (2008) Substituted 2-Imino-5-arylidenethiazolidin-4-one Inhibitors of Bacterial Type III Secretion. *J. Med. Chem.* 51, 7065–7074.

(113) Kauppi, A. M., Nordfelth, R., Uvell, H., Wolf-Watz, H., and Elofsson, M. (2003) Targeting bacterial virulence: Inhibitors of type III secretion in *Yersinia*. *Chem. Biol.* 10, 241–249.

(114) Wolf, K., Betts, H. J., Chellas-G??ry, B., Hower, S., Linton, C. N., and Fields, K. A. (2006) Treatment of *Chlamydia trachomatis* with a small molecule inhibitor of the *Yersinia* type III secretion system disrupts progression of the chlamydial developmental cycle. *Mol. Microbiol.* 61, 1543–1555.

(115) Muschiol, S., Bailey, L., Gylfe, A., Sundin, C., Hultenby, K., Bergstrom, S., Elofsson, M., Wolf-Watz, H., Normark, S., and Henriques-Normark, B. (2006) A small-molecule inhibitor of type III secretion inhibits different stages of the infectious cycle of *Chlamydia trachomatis*. *Proc Natl Acad Sci U S A* 103, 14566–14571.

(116) Hudson, D. L., Layton, A. N., Field, T. R., Bowen, A. J., Wolf-Watz, H., Elofsson, M., Stevens, M. P., and Galyov, E. E. (2007) Inhibition of Type III Secretion in *Salmonella enterica* Serovar Typhimurium by Small-Molecule Inhibitors. *Antimicrob. Agents Chemother.* 51, 2631–2635.

(117) Negrea, A., Bjur, E., Ygberg, S. E., Elofsson, M., Wolf-Watz, H., and Rhen, M. (2007) Salicylidene acylhydrazides that affect type III protein secretion in *Salmonella enterica* serovar typhimurium. *Antimicrob. Agents Chemother.* 51, 2867–2876.

(118) Tree, J. J., Wang, D., McNally, C., Mahajan, A., Layton, A., Houghton, I., Elofsson, M., Stevens, M. P., Gally, D. L., and Roe, A. J. (2009) Characterization of the effects of salicylidene acylhydrazide compounds on type III secretion in *Escherichia coli* O157:H7. *Infect. Immun.* 77, 4209–4220.

(119) Veenendaal, A. K. J., Sundin, C., and Blocker, A. J. (2009) Small-molecule type III secretion system inhibitors block assembly of the shigella type III secretion. *J. Bacteriol.* 191, 563–570.

(120) Hillgren, J. M., Dahlgren, M. K., To, T. M., and Elofsson, M. (2010) Synthesis of [4-(2-

hydroxyphenyl)thiazol-2-yl]methanones as potential bioisosteres of salicylidene acylhydrazides. *Molecules* 15, 6019–6034.

(121) Dahlgren, M. K., Oeberg, C. T., Wallin, E. A., Janson, P. G., and Elofsson, M. (2010) Synthesis of 2-(2-aminopyrimidine)-2,2-difluoroethanols as potential bioisosters of salicylidene acylhydrazides. *Molecules* 15, 4423–4438.

(122) Slepénkin, A., Enquist, P. A., Högglund, U., De La Maza, L. M., Elofsson, M., and Peterson, E. M. (2007) Reversal of the antichlamydial activity of putative type III secretion inhibitors by iron. *Infect. Immun.* 75, 3478–3489.

(123) Layton, A. N., Hudson, D. L., Thompson, A., Hinton, J. C. D., Stevens, J. M., Galyov, E. E., and Stevens, M. P. (2010) Salicylidene acylhydrazide-mediated inhibition of type III secretion system-1 in *Salmonella enterica* serovar Typhimurium is associated with iron restriction and can be reversed by free iron. *FEMS Microbiol. Lett.* 302, 114–122.

(124) Martínez-Argudo, I., Veenendaal, A. K. J., Liu, X., Roehrich, A. D., Ronessen, M. C., Franzoni, G., van Rietschoten, K. N., Morimoto, Y. V., Saijo-Hamano, Y., Avison, M. B., Studholme, D. J., Namba, K., Minamino, T., and Blocker, A. J. (2013) Isolation of *Salmonella* Mutants Resistant to the Inhibitory Effect of Salicylidene acylhydrazides on Flagella-Mediated Motility. *PLoS One* 8.

(125) Wang, D., Zetterström, C. E., Gabrielsen, M., Beckham, K. S. H., Tree, J. J., Macdonald, S. E., Byron, O., Mitchell, T. J., Gally, D. L., Herzyk, P., Mahajan, A., Uvell, H., Burchmore, R., Smith, B. O., Elofsson, M., and Roe, A. J. (2011) Identification of bacterial target proteins for the salicylidene acylhydrazide Class of virulence-blocking compounds. *J. Biol. Chem.* 286, 29922–29931.

(126) Baker, L. M. S., and Poole, L. B. (2003) Catalytic Mechanism of Thiol Peroxidase from *Escherichia coli*. *J. Biol. Chem.* 278, 9203–9211.

(127) Patridge, E. V., and Ferry, J. G. (2006) WrbA from *Escherichia coli* and *Archaeoglobus fulgidus* Is an NAD(P) H:Quinone Oxidoreductase. *J. Bacteriol.* 188, 3498–3506.

(128) Beckham, K. S. H., Byron, O., Roe, A. J., and Gabrielsen, M. (2012) The structure of an orthorhombic crystal form of a “forced reduced” thiol peroxidase reveals lattice formation aided by the presence of the affinity tag. *Acta Crystallogr. Sect. F Struct. Biol. Cryst. Commun.* 68, 522–526.

(129) Gabrielsen, M., Zetterström, C. E., Wang, D., Beckham, K. S. H., Elofsson, M., Isaacs, N. W., and Roe, A. J. (2010) Expression, purification, crystallization and initial X-ray diffraction analysis of thiol peroxidase from *Yersinia pseudotuberculosis*. *Acta Crystallogr.*

*Sect. F Struct. Biol. Cryst. Commun.* **66**, 1606–1609.

(130) Gabrielsen, M., Beckham, K. S. H., Cogdell, R. J., Byron, O., and Roe, A. J. (2012) FolX from *Pseudomonas aeruginosa* is octameric in both crystal and solution. *FEBS Lett.*

(131) Gabrielsen, M., Beckham, K. S. H., Feher, V. A., Zetterström, C. E., Wang, D., Müller, S., Elofsson, M., Amaro, R. E., Byron, O., and Roe, A. J. (2012) Structural characterisation of Tpx from yersinia pseudotuberculosis reveals insights into the binding of salicylidene acylhydrazide compounds. *PLoS One* **7**.

(132) Beckham, K. S. H., Connolly, J. P. R., Ritchie, J. M., Wang, D., Gawthorne, J. A., Tahoun, A., Gally, D. L., Burgess, K., Burchmore, R. J., Smith, B. O., Beatson, S. A., Byron, O., Wolfe, A. J., Douce, G. R., and Roe, A. J. (2014) The metabolic enzyme AdhE controls the virulence of *Escherichia coli* O157: H7. *Mol. Microbiol.* **93**, 199–211.

(133) Wermuth, C. G. (2011) Are pyridazines privileged structures? *Medchemcomm* **2**, 935.

(134) Papeo, G., Casale, E., Montagnoli, A., and Cirila, A. (2013) Review PARP inhibitors in cancer therapy : an update. *Expert Opin. Ther. Pat.* **23**, 503–514.

(135) Combs, D. W., Reese, K., and Phillips, A. (1995) Nonsteroidal progesterone receptor ligands. 1. 3-Aryl-1-benzoyl-1,4,5,6- tetrahydropyridazines. *J. Med. Chem.* **38**, 4878–4879.

(136) Blocker, A. J., Deane, J. E., Veenendaal, A. K. J., Roversi, P., Hodgkinson, J. L., Johnson, S., and Lea, S. M. (2008) What's the point of the type III secretion system needle? *Proc. Natl. Acad. Sci. U. S. A.* **105**, 6507–6513.

(137) Pal, M., Batchu, V. R., Parasuraman, K., and Yeleswarapu, K. R. (2003) Aluminum chloride-induced heteroarylation of arenes and heteroarenes. 2. A new synthesis of 4-substituted phthalazin-1(2H)-ones. *J. Org. Chem.* **68**, 6806–6809.

(138) Sun, X.-Y., Hu, C., Deng, X.-Q., Wei, C.-X., Sun, Z.-G., and Quan, Z.-S. (2010) Synthesis and anti-inflammatory activity evaluation of some novel 6-alkoxy(phenoxy)-[1,2,4]triazolo[3,4-a]phthalazine-3-amine derivatives. *Eur. J. Med. Chem.* **45**, 4807–4812.

(139) Sousa, C., and Silva, P. J. (2013) BBr<sub>3</sub>-assisted cleavage of most ethers does not follow the commonly assumed mechanism. *European J. Org. Chem.* 5195–5199.

(140) Yu, W. L., Guizzunti, G., Foley, T. L., Burkart, M. D., and La Clair, J. J. (2010) An optimized immunoaffinity fluorescent method for natural product target elucidation. *J. Nat. Prod.* **73**, 1659–1666.

(141) Yu, F., Wang, Q., Zhang, Z., Peng, Y., Qiu, Y., Shi, Y., Zheng, Y., Xiao, S., Wang, H., Huang, X., Zhu, L., Chen, K., Zhao, C., Zhang, C., Yu, M., Sun, D., Zhang, L., and Zhou, D. (2013) Development of oleanane-type triterpenes as a new class of HCV entry inhibitors. *J.*

*Med. Chem.* 56, 4300–4319.

(142) Vutukuri, D. R., Bharathi, P., Yu, Z., Rajasekaran, K., Tran, M. H., and Thayumanavan, S. (2003) A mild deprotection strategy for allyl-protecting groups and its implications in sequence specific dendrimer synthesis. *J. Org. Chem.* 68, 1146–1149.

(143) Lai, L. C., Wainwright, L. A., Stone, K. D., and Donnenberg, M. S. (1997) A third secreted protein that is encoded by the enteropathogenic *Escherichia coli* pathogenicity island is required for transduction of signals and for attaching and effacing activities in host cells. *Infect. Immun.* 65, 2211–2217.

(144) Kenny, B., Lai, L. C., Finlay, B. B., and Donnenberg, M. S. (1996) EspA, a protein secreted by enteropathogenic *Escherichia coli*, is required to induce signals in epithelial cells. *Mol. Microbiol.* 20, 313–23.

(145) Bunik, V. I., and Degtyarev, D. (2008) Structure-function relationships in the 2-oxo acid dehydrogenase family: Substrate-specific signatures and functional predictions for the 2-oxoglutarate dehydrogenase-like proteins. *Proteins Struct. Funct. Genet.* 71, 874–890.

(146) Weijland, A., Harmark, K., Cool, R. H., Anborgh, P. H., and Parmeggiani, A. (1992) Elongation factor Tu: a molecular switch in protein biosynthesis. *Mol. Microbiol.* 6, 683–8.

(147) Lucas-Lenard, J., and Lipmann, F. (1966) Separation of three microbial amino acid polymerization factors. *Proc. Natl. Acad. Sci. U. S. A.* 55, 1562–6.

(148) Wainwright, L. A., and Kaper, J. B. (1998) EspB and EspD require a specific chaperone for proper secretion from enteropathogenic *Escherichia coli*. *Mol. Microbiol.* 27, 1247–1260.

(149) Neves, B. C., Mundy, R., Petrovska, L., Dougan, G., Knutton, S., and Frankel, G. (2003) CesD2 of Enteropathogenic *Escherichia coli* Is a Second Chaperone for the Type III Secretion Translocator Protein EspD CesD2 of Enteropathogenic *Escherichia coli* Is a Second Chaperone for the Type III Secretion Translocator Protein EspD 71, 2130–2141.

(150) Liedberg, B., Nylander, C., and Lundström, I. (1983) Surface plasmon resonance for gas detection and biosensing. *Sensors and Actuators* 4, 299–304.

(151) Liedberg, B., Nylander, C., and Lundström, I. (1995) Biosensing with surface plasmon resonance--how it all started. *Biosens. Bioelectron.* 10, i–ix.

(152) Homola, J., Yee, S. S., and Gauglitz, G. (1999) Surface plasmon resonance sensors: review. *Sensors Actuators B Chem.* 54, 3–15.

(153) Lofas, S. (2004) Optimizing the hit-to-lead process using SPR analysis. *Assay Drug Dev Technol* 2, 407–415.

- (154) Beld, J., Cang, H., and Burkart, M. D. (2014) Visualizing the chain-flipping mechanism in Fatty-Acid biosynthesis. *Angew. Chem. Int. Ed. Engl.* 53, 14456–61.
- (155) Ludwig, C. (1856) Diffusion zwischen ungleich erwärmten Orten gleich zusammengesetzter Lösungen, in *itzungber Bayer Akad Wiss Wien Math- Naturwiss Kl*, p vol. 20.
- (156) Jerabek-Willemsen, M., Andr??, T., Wanner, R., Roth, H. M., Duhr, S., Baaske, P., and Breitsprecher, D. (2014) MicroScale Thermophoresis: Interaction analysis and beyond. *J. Mol. Struct.* 1077, 101–113.
- (157) Seidel, S. A. I., Dijkman, P. M., Lea, W. A., van den Bogaart, G., Jerabek-Willemsen, M., Lazic, A., Joseph, J. S., Srinivasan, P., Baaske, P., Simeonov, A., Katritch, I., Melo, F. A., Ladbury, J. E., Schreiber, G., Watts, A., Braun, D., and Duhr, S. (2013) Microscale thermophoresis quantifies biomolecular interactions under previously challenging conditions. *Methods* 59, 301–315.
- (158) Jerabek-Willemsen, M., Wienken, C. J., Braun, D., Baaske, P., and Duhr, S. (2011) Molecular interaction studies using microscale thermophoresis. *Assay Drug Dev. Technol.* 9, 342–53.
- (159) Duhr, S., and Braun, D. (2006) Why molecules move along a temperature gradient. *Proc. Natl. Acad. Sci. U. S. A.* 103, 19678–82.
- (160) Duhr, S., and Braun, D. (2006) Thermophoretic depletion follows boltzmann distribution. *Phys. Rev. Lett.* 96, 1–4.
- (161) Hansen, A. M., Sewell, A. L., Pedersen, R. H., Long, D. L., Gadegaard, N., and Marquez, R. (2013) Tunable BODIPY derivatives amenable to “click” and peptide chemistry. *Tetrahedron* 69, 8527–8533.
- (162) Loudet, A., and Burgess, K. (2007) BODIPY Dyes and Their Derivatives: Syntheses and Spectroscopic Properties. *Chem. Rev.* 107, 4891–4932.
- (163) Cormack, B. P., Valdivia, R. H., and Falkow, S. (1996) FACS-optimized mutants of the green fluorescent protein (GFP). *Gene* 173, 33–38.
- (164) Tjernberg, A. (2005) DMSO-Related Effects in Protein Characterization. *J. Biomol. Screen.* 11, 131–137.
- (165) Emmerson, J. R., Gally, D. L., and Roe, A. J. (2006) Generation of gene deletions and gene replacements in Escherichia coli O157:H7 using a temperature sensitive allelic exchange system. *Biol. Proced. Online* 8, 153–162.
- (166) Tohru Fukuyama, Chung-Kuang Jow, M. C. (1995) 2- and 4-

Nitrobenzenesulfonamides: Exceptionally versatile means for preparation of secondary amines and protection of amines. *Tetrahedron Lett.* 36, 6373–6374.

(167) Noguchi, H., Kitazumi, K., Mori, M., and Shiba, T. (2002) Binding and neuropharmacological profile of zaleplon, a novel nonbenzodiazepine sedative / hypnotic. *Eur. J. Pharmacol.* 434, 21–28.

(168) Carling, R. W., Madin, A., Guiblin, A., Russell, M. G. N., Moore, K. W., Mitchinson, A., Sohal, B., Pike, A., Cook, S. M., Ragan, I. C., Mckernan, R. M., Quirk, K., Ferris, P., Marshall, G., Thompson, S. A., Wafford, K. A., Dawson, G. R., Attack, J. R., Harrison, T., Castro, L., and Street, L. J. (2005) 7-(1,1-Dimethylethyl)-6-(2-ethyl-2H-1,2,4-triazol-3-ylmethoxy)-3-(2-fluorophenyl)-1,2,4-triazolo[4,3-b]pyridazine: A Functionally Selective  $\gamma$ -Aminobutyric AcidA (GABAA)  $\alpha 2/\alpha 3$ -Subtype Selective Agonist That Exhibits Potent Anxiolytic Activity but Is Not. *J Med Chem* 48.

(169) Rakib, E. M., Abouricha, S., Hannioui, A., Benchat, N., Ait, L. M., and Zyad, A. (2006) Synthesis and in vitro Cytotoxicity Studies of Novel Triazolo[4,3-b]pyridazinones. *Iran. Chem. Soc.* 3, 272–276.

(170) Albright, J. D., Moran, D. B., Wright Jr., W. B., Collins, J. B., Beer, B., Lippa, A. S., and Greenblatt, E. N. (1981) Synthesis and anxiolytic activity of 6-(substituted-phenyl)-1,2,4-triazolo[4,3-b]pyridazines. *J Med Chem* 24, 592–600.

(171) Adu-Bobie, J., Frankel, G., Bain, C., Goncalves, A. G., Trabulsi, L. R., Douce, G., Knutton, S., and Dougan, G. (1998) Detection of intimins  $\alpha$ ,  $\beta$ ,  $\gamma$ , and  $\delta$ , four intimin derivatives expressed by attaching and effacing microbial pathogens. *J. Clin. Microbiol.* 36, 662–668.

(172) Ecker, D. J., Matzanke, B. F., and Raymond, K. N. (1986) Recognition and transport of ferric enterobactin in Escherichia coli. *J. Bacteriol.* 167, 666–673.

(173) Nikaido, H., Luckey, M., and Rosenberg, E. Y. (1980) Nonspecific and Specific Diffusion Channels in the Outer Membrane of Escherichia coli. *J. Supramol. Struct.* 13, 305–313.

(174) Nikaido, H.; Varra, M. (1985) Molecular basis of bacterial outer membrane permeability. *Microbiol Mol Biol Rev* 67, 593–656.

(175) Nikaido, H., Rosenberg, E. Y., and Foulds, J. (1983) Porin channels in Escherichia coli: studies with beta-lactams in intact cells. *J Bacteriol* 153, 232–240.

(176) Jaffe, A., Chabbert, Y. A., and Semonin, O. (1982) Role of porin proteins OmpF and OmpC in the permeation of  $\beta$ -lactams. *Antimicrob. Agents Chemother.* 22, 942–948.

- (177) Bekhit, A., Fukamachi, T., Saito, H., and Kobayashi, H. (2011) The Role of OmpC and OmpF in Acidic Resistance in *Escherichia coli*. *Biol. Pharm. Bull.* 34, 330–334.
- (178) Kustu, S. G., McFarland, N. C., Hui, S. P., Esmon, B., and Ames, G. F.-L. (1979) Nitrogen control in *Salmonella typhimurium*: Co-regulation of synthesis of glutamine synthetase and amino acid transport systems. *J. Bacteriol.* 138, 218–234.
- (179) Nikaido, K., and Ames, G.-L. (1992) Purification and characterization of the periplasmic lysine-arginine-ornithine-binding protein (LAO) from *Salmonella typhimurium*. *J. Biol. Chem* 267, 20706–20712.
- (180) Cai, S. J., and Inouye, M. (2002) EnvZ-OmpR interaction and osmoregulation in *Escherichia coli*. *J. Biol. Chem.* 277, 24155–24161.
- (181) Forst, S., Delgado, J., and Inouye, M. (1989) Phosphorylation of OmpR by the osmosensor EnvZ modulates expression of the ompF and ompC genes in *Escherichia coli*. *Proc. Natl. Acad. Sci. U. S. A.* 86, 6052–6056.
- (182) Werner, G., Strommenger, B., and Witte, W. (2008) Acquired vancomycin resistance in clinically relevant pathogens. *Future Microbiol.* 3, 547–562.
- (183) Rasko, D. a, and Sperandio, V. (2010) Anti-virulence strategies to combat bacteria-mediated disease. *Nat. Rev. Drug Discov.* 9, 117–28.
- (184) Zambelloni, R., Marquez, R., and Roe, A. J. (2015) Development of antivirulence compounds: A biochemical review. *Chem. Biol. Drug Des.* 85, 43–55.
- (185) Nordfelth, R., Kauppi, A. M., Norberg, H. A., Wolf-Watz, H., and Elofsson, M. (2005) Small-molecule inhibitors specifically targeting type III secretion. *Infect. Immun.* 73, 3104–3114.
- (186) Cornelis, G. R., and Van Gijsegem, F. (2000) Assembly and function of type III secretory systems. *Annu Rev Microbiol* 54, 735–774.
- (187) Pal, M., Batchu, V. R., and Parasuraman, K. (2003) Heteroarylation of Arenes and Heteroarenes . 2 . A New Synthesis of 4-Substituted Phthalazin-1 ( 2H ) -ones †, 1 4-Substituted 2H-phthalazin-1-ones of structure A ( Figure 1 ) are of considerable interest due to their useful intermediates for the synthesis 1, 6806–6809.
- (188) Zabrodski, T., Baskin, M., Kaniraj, P., and Maayan, G. (2014) Click To Bind: Microwave-Assisted Solid-Phase Synthesis of Peptoids Incorporating Pyridine–Triazole Ligands and Their Copper(II) Complexes. *Synlett* 26, 461–466.
- (189) Barnard, A., Long, K., Martin, H. L., Miles, J. A., Edwards, T. A., Tomlinson, D. C., Macdonald, A., and Wilson, A. J. (2015) Selective and potent proteomimetic inhibitors of

- intracellular protein-protein interactions. *Angew. Chemie - Int. Ed.* 54, 2960–2965.
- (190) Campellone, K. G., Robbins, D., and Leong, J. M. (2004) EspFU is a translocated EHEC effector that interacts with Tir and N-WASP and promotes Nck-independent actin assembly. *Dev. Cell* 7, 217–228.
- (191) Roe, A. J., Yull, H., Naylor, S. W., Woodward, M. J., Smith, D. G. E., and Gally, D. L. (2003) Heterogeneous surface expression of EspA translocon filaments by *Escherichia coli* O157:H7 is controlled at the posttranscriptional level. *Infect. Immun.* 71, 5900–5909.
- (192) Blomfield, I. C., Vaughn, V., Rest, R. F., and Eisenstein, B. I. (1991) Allelic exchange in *Escherichia coli* using the *Bacillus subtilis* *sacB* gene and a temperature-sensitive pSC101 replicon. *Mol. Microbiol.* 5, 1447–57.
- (193) Shevchenko, A., Tomas, H., Havlis, J., Olsen, J. V., and Mann, M. (2006) In-gel digestion for mass spectrometric characterization of proteins and proteomes. *Nat. Protoc.* 1, 2856–2860.
- (194) Pappin, D. J. C., Hojrup, P., and Bleasby, A. J. (1993) Rapid identification of proteins by peptide-mass fingerprinting. *Curr. Biol.* 3, 327–332.
- (195) Creek, D. J., Jankevics, A., Breitling, R., Watson, D. G., Barrett, M. P., and Burgess, K. E. V. (2011) Toward global metabolomics analysis with hydrophilic interaction liquid chromatography-mass spectrometry: Improved metabolite identification by retention time prediction. *Anal. Chem.* 83, 8703–8710.
- (196) Robinson, M. D., McCarthy, D. J., and Smyth, G. K. (2009) edgeR: A Bioconductor package for differential expression analysis of digital gene expression data. *Bioinformatics* 26, 139–140.
- (197) Tree, J. J., Roe, A. J., Flockhart, A., Mcateer, S. P., Xu, X., Shaw, D., Mahajan, A., Beatson, S. A., Best, A., Lotz, S., Woodward, M. J., La Ragione, R., Murphy, K. C., Leong, J. M., and Gally, D. L. (2011) Transcriptional regulators of the GAD acid stress island are carried by effector protein-encoding prophages and indirectly control type III secretion in enterohemorrhagic *Escherichia coli* O157:H7. *Mol. Microbiol.* 80, 1349–1365.
- (198) Chaudhuri, R. R., Khan, A. M., and Pallen, M. J. (2004) coliBASE: an online database for *Escherichia coli*, *Shigella* and *Salmonella* comparative genomics. *Nucleic Acids Res.* 32, D296–D299.
- (199) Büttner, D. (2012) Protein export according to schedule: architecture, assembly, and regulation of type III secretion systems from plant- and animal-pathogenic bacteria. *Microbiol. Mol. Biol. Rev.* 76, 262–310.



- (200) Wong, A. R. C., Pearson, J. S., Bright, M. D., Munera, D., Robinson, K. S., Lee, S. F., Frankel, G., and Hartland, E. L. (2011) Enteropathogenic and enterohaemorrhagic *Escherichia coli*: Even more subversive elements. *Mol. Microbiol.*
- (201) Mellies, J. L., Barron, A. M. S., and Carmona, A. M. (2007) Enteropathogenic and enterohemorrhagic *Escherichia coli* virulence gene regulation. *Infect. Immun.* 75, 4199–4210.

## Appendix

| Band number | Protein ID                   | Gene          | Genbank ID  | MOWSE score | # peptides matched |
|-------------|------------------------------|---------------|-------------|-------------|--------------------|
| 1           | 2-Oxoglutarate dehydrogenase | <i>sucA</i>   | gi 15800430 | 1716        | 106                |
| 2           | Elongation factor Tu         | <i>tufA/B</i> | gi 26110363 | 745         | 75                 |
| 3           | EspD                         | <i>espD</i>   | gi 15804216 | 1266        | 45                 |
| 3'          | EspD                         | <i>espD</i>   | gi 15804216 | 1174        | 40                 |
| 4           | 30S Ribosomal subunit        | <i>rpsJ</i>   | gi 15803848 | 235         | 10                 |

**Table 11: List of protein identified by the first pull-down assay with biotin-RCZ12 and biotin-RCZ20:** The protein identified by tandem mass spectrometry for the pull-down assay (Paragraph 8.4.2) is listed above. Band numbers refer to Fig.17 of the Results and Discussion section.

| Band number | Protein ID                   | Gene        | Genbank ID   | MOWSE score | # peptides matched |
|-------------|------------------------------|-------------|--------------|-------------|--------------------|
| 1           | 2-Oxoglutarate dehydrogenase | <i>sucA</i> | gi 15800430  | 481         | 57                 |
| 2           | EspB                         | <i>espB</i> | gi 188016858 | 1154        | 78                 |
| 3           | EspD                         | <i>espD</i> | gi 15804216  | 672         | 55                 |
| 4           | 30S Ribosomal subunit        | <i>rpsJ</i> | gi 15803848  | 173         | 15                 |

**Table 12: List of protein identified by the second pull-down assay with biotin-RCZ12 and biotin-RCZ20:** The protein identified by tandem mass spectrometry for the pull-down assay (Paragraph 8.7.5) is listed above. Band numbers refer to Fig.21 of the Results and Discussion section.

| Gene        | Log <sup>2</sup> fold change | P value  | Function  |
|-------------|------------------------------|----------|---|
| <i>torC</i> | 15.97                        | 8.48E-13 | Cytochrome C-type protein   |
| <i>torA</i> | 13.44                        | 3.01E-35 | Trimethylamine-N-oxide reductase                                      |
| <i>yjiY</i> | 6.64                         | 6.93E-20 | Carbon starvation protein CstA  |
| <i>metF</i> | 4.83                         | 4.38E-12 | 5,10-Methylenetetrahydrofolate reductase                              |
| <i>bssR</i> | 4.51                         | 5.43E-09 | Biofilm regulator BssR  |
| Z2427       | 2.64                         | 2.01E-19 | Amidohydrolase  |
| <i>metE</i> | 2.61                         | 4.25E-19 | 5-Methyltetrahydropteroyltriglutamate- homocysteine methyltransferase |
| <i>yhiW</i> | 2.48                         | 5.54E-06 | DNA-binding transcriptional activator                                 |
| <i>ydaJ</i> | 2.38                         | 1.36E-18 | Putative aminohydrolase   |
| <i>yhfC</i> | 2.37                         | 7.00E-10 | Hypothetical protein  |
| Z2428       | 2.12                         | 5.09E-10 | Anion permease ArsB/NhaD  |

|               |       |          |   |
|---------------|-------|----------|---|
| <i>ycfS</i>   | 1.89  | 2.94E-04 | Hypothetical protein  |
| <i>htrL</i>   | 1.79  | 7.26E-04 | Putative lipopolysaccharide biosynthesis protein                                |
| <i>metK</i>   | 1.75  | 1.53E-07 | S-Adenosylmethionine synthetase   |
| <i>ydeA</i>   | 1.75  | 8.08E-04 | Putative substrate translocation pore   |
| <i>yjbA</i>   | 1.75  | 7.44E-05 | Phosphate-starvation-inducible protein PsiE                                     |
| <i>gcd</i>    | 1.72  | 1.23E-06 | Glucose dehydrogenase   |
| <i>metN</i>   | 1.71  | 5.91E-04 | DL-Methionine transporter subunit   |
| <i>yihE</i>   | 1.66  | 8.37E-06 | Serine/threonine protein kinase   |
| <i>yojH</i>   | 1.64  | 3.17E-06 | Malate:quinone oxidoreductase   |
| <i>cpxP</i>   | 1.62  | 7.57E-06 | Periplasmic repressor CpxP  |
| <i>dps</i>    | 1.6   | 1.23E-06 | DNA protection during starvation conditions                                     |
| <i>yfiA</i>   | 1.57  | 2.75E-06 | Translation inhibitor protein RaiA  |
| <i>folE</i>   | 1.57  | 8.17E-05 | GTP cyclohydrolase I  |
| <i>ompC</i>   | 1.52  | 2.35E-04 | Outer membrane protein C, porin   |
| <i>ompX</i>   | 1.52  | 5.90E-06 | Outer membrane protein X  |
| <i>Z2779</i>  | 1.38  | 2.47E-04 | Arginine succinyltransferase  |
| <i>ydjS</i>   | 1.38  | 3.61E-04 | Succinylglutamate desuccinylase   |
| <i>Z2777</i>  | 1.37  | 2.39E-04 | Succinylarginine dihydrolase  |
| <i>astD</i>   | 1.37  | 2.30E-04 | Succinylglutamic semialdehyde dehydrogenase                                     |
| <i>argD_1</i> | 1.35  | 3.33E-04 | Bifunctional succinylornithine transaminase/acetylornithine transaminase        |
| <i>ptsH</i>   | -1.4  | 2.41E-04 | Phosphohistidinoprotein-hexose phosphotransferase component of PTS system (Hpr) |
| <i>Z1824</i>  | -1.4  | 2.13E-04 | Hypothetical protein  |
| <i>Z5137</i>  | -1.53 | 6.46E-04 | Hypothetical protein  |
| <i>Z5125</i>  | -1.53 | 3.24E-04 | Hypothetical protein  |
| <i>Z6020</i>  | -1.54 | 6.78E-04 | Hypothetical protein  |
| <i>Z5115</i>  | -1.59 | 7.15E-05 | Hypothetical protein  |
| <i>Z3920</i>  | -1.59 | 8.01E-06 | Hypothetical protein  |
| <i>Z5352</i>  | -1.6  | 1.25E-04 | Esterases and lipases   |
| <i>Z3644</i>  | -1.6  | 7.36E-05 | Aspartate aminotransferase  |
| <i>ptsG</i>   | -1.63 | 1.40E-07 | Phosphotransferase system, EIIC   |
| <i>Z5123</i>  | -1.65 | 4.13E-05 | Hypothetical protein  |
| <i>Z3071</i>  | -1.66 | 2.51E-05 | Hypothetical protein  |
| <i>manZ</i>   | -1.71 | 1.03E-08 | Mannose-specific PTS system protein IID   |
| <i>Z5102</i>  | -1.72 | 4.03E-05 | Hypothetical protein  |
| <i>manY</i>   | -1.75 | 1.54E-08 | PTS system sorbose-specific iic component                                       |
| <i>Z5129</i>  | -1.75 | 2.12E-05 | Negative regulator GrIR   |

|              |       |          |   |
|--------------|-------|----------|---|
| <i>Z0955</i> | -1.76 | 4.77E-07 | Hypothetical protein  |
| <i>Z4326</i> | -1.79 | 3.69E-04 | ShET2 enterotoxin   |
| <i>manX</i>  | -1.88 | 1.27E-11 | PTS system, mannose-specific IIB component  |
| <i>Z5142</i> | -1.9  | 8.39E-06 | Hypothetical protein  |
| <i>rcaA</i>  | -1.94 | 9.40E-08 | Response regulator containing a CheY-like receiver domain and an HTH DNA-binding domain |
| <i>Z5128</i> | -1.95 | 1.42E-07 | Hypothetical protein  |
| <i>Z5138</i> | -1.97 | 1.01E-05 | Hypothetical protein  |
| <i>gcvH</i>  | -2    | 6.07E-04 | Glycine cleavage system protein H   |
| <i>rrsE</i>  | -2.02 | 7.62E-06 | 16S ribosomal RNA   |
| <i>Z5136</i> | -2.04 | 4.19E-10 | Hypothetical protein  |
| <i>ssrS</i>  | -2.28 | 1.14E-07 | 6S RNA  |
| <i>Z5143</i> | -2.31 | 2.80E-04 | Hypothetical protein  |
| <i>wcaI</i>  | -2.4  | 2.03E-04 | Putative glycosyl transferase   |
| <i>Z5139</i> | -2.42 | 2.14E-09 | Hypothetical protein  |
| <i>wcaD</i>  | -2.47 | 3.77E-04 | Putative colanic acid biosynthesis protein  |
| <i>fruA</i>  | -2.49 | 7.70E-10 | Fructose-specific PTS system IIBC component   |
| <i>cpsB</i>  | -2.54 | 8.22E-05 | Mannose-1-phosphate guanylttransferase  |
| <i>wcaG</i>  | -2.67 | 3.23E-07 | Putative nucleotide di-P-sugar epimerase or dehydratase                                 |
| <i>Z3921</i> | -2.74 | 1.93E-05 | Hypothetical protein  |
| <i>Z2151</i> | -2.79 | 3.35E-05 | Hypothetical protein  |
| <i>fruK</i>  | -3.15 | 1.89E-06 | 1-Phosphofructokinase   |
| <i>Z2339</i> | -3.16 | 1.28E-05 | Hypothetical protein  |
| <i>gmd</i>   | -3.39 | 3.63E-13 | GDP-D-mannose dehydratase   |
| <i>Z6024</i> | -3.52 | 1.14E-14 | Hypothetical protein  |
| <i>fruB</i>  | -3.75 | 3.65E-11 | Bifunctional fructose-specific PTS IIA/HPr protein                                      |
| <i>wcaH</i>  | -4.26 | 4.24E-05 | GDP-mannose mannosyl hydrolase  |
| <i>ffs</i>   | -4.73 | 3.72E-04 | 4.5S RNA, component of ribonucleoprotein  |

**Table 13: List of additional genes influenced by RCZ20 at 50  $\mu$ M:** The list of the non-LEE-related genes influenced by RCZ20 at 50  $\mu$ M is listed above.

A

|   |  |
|---|--|
| gi   155533   gb   Y.pseudotuberculosis | -----  |
| gi   975295   gb   S.typhimurium        | MVNDASSISRSRGYTQNPRLAEAAFGVVRKNTDFLKAADKAFKDVVATKAGDLKAGTKSGE  |
| gi   1041718008   gb   EHEC             | -----  |
| gi   194415512   gb   EPEC              | -----  |
| gi   15723935   gb   C.rodentium        | -----  |
| gi   155533   gb   Y.pseudotuberculosis | -----  |
| gi   975295   gb   S.typhimurium        | SAINTVGLKPPDAAREKLSSEGLTLLGKMLTLLGDVSLSQLESRLAVVQAMIESQKE      |
| gi   1041718008   gb   EHEC             | -----MLN-----  |
| gi   194415512   gb   EPEC              | -----MLN-----  |
| gi   15723935   gb   C.rodentium        | -----MLN-----  |
| gi   155533   gb   Y.pseudotuberculosis | -----MSALITHDRSTPV   |
| gi   975295   gb   S.typhimurium        | MGIQVSKEFQTALGEAEATDLYEASIKKTDIAKSVYDAATKKLTQAQNKLSLDPADP-     |
| gi   1041718008   gb   EHEC             | -----VNNDTLVSTSGVNTASGT--SGITQSETG-----LSLDLQLVKSMNSS          |
| gi   194415512   gb   EPEC              | -----VNSDIQSMRSGASAATAT--SGINQPEVT-----SALDLQLVKSTAPS          |
| gi   15723935   gb   C.rodentium        | -----VNSNIQSIKSGASAATAI--SGINQPEVT-----SGLDLQLVKSFAPS          |
| gi   155533   gb   Y.pseudotuberculosis | -----  |
| gi   975295   gb   S.typhimurium        | TGSLLPYVETPA-PAPLQTQQ--VAGELKDKN-GGVSSQGV---QLPAPLAVVASQVTEG   |
| gi   1041718008   gb   EHEC             | -----GYAQAEA-AVEQAGKEATEAKEALDKATDATVKAGTDAKAKAKADNILTQFGGT    |
| gi   194415512   gb   EPEC              | A-----GWTESSPLPTPPAGHS-----LVTPSAAEDVLSKLFEGG                  |
| gi   15723935   gb   C.rodentium        | A-----SWTESTALPTPPAGHS-----LVTPSVAEDVLSKLFEGG                  |
| gi   155533   gb   Y.pseudotuberculosis | -----  |
| gi   975295   gb   S.typhimurium        | QQQEVTKLES--VTRGAAGSQLISNYVSVLTKFTLASPDTFE-----IELGKLV--SNL    |
| gi   1041718008   gb   EHEC             | ANAAASQNGV-----SQGE-----Q---DNLS---NVARLTMLMAMFIEIVGKNT---E    |
| gi   194415512   gb   EPEC              | ISGEVTSRTTEAEPPQR-----TSYPYLSQVN---TVDPQMM---MVTLLSLDTSQAKV    |
| gi   15723935   gb   C.rodentium        | ISGEVRSRTTEGPQRSTQNASSGYPYLSQVN---NVDPQAMM---MVTLLSLDASAQKV    |
| gi   155533   gb   Y.pseudotuberculosis | ISGDVINRRTAGTEPERGTQNTSSGYPYLSQVN---NVDPQAMM---MVTQLSLNTSAQKV  |
| gi   155533   gb   Y.pseudotuberculosis | -----  |
| gi   975295   gb   S.typhimurium        | EEVRKDIKIADI--QRLHEQ--NMKKIEENQEKIKETEENAKQVKKSGIASKIFGWSAIAIS |
| gi   1041718008   gb   EHEC             | ESLQNDLALFNALQEGRQAEMEKSAEFQ---EETRKAEETNRIMCGICIKVLGALLTIVS   |
| gi   194415512   gb   EPEC              | SSLKNSNEIY---MDGQTKALENKTEYKQLEEQKAEKSKQSKIVGVQFVGLGVAIT       |
| gi   15723935   gb   C.rodentium        | ASMKNSNEIY---TDGQNKALDNKLEFFKQLEEQKAEKSKQSKILGVQFVGLGVAIT      |
| gi   155533   gb   Y.pseudotuberculosis | ASMKDSNEIY---TAGQNALENKLEFFKQLEEQKAEKSKQSKIVGVQFVGLGVAIT       |
| gi   155533   gb   Y.pseudotuberculosis | -----  |
| gi   975295   gb   S.typhimurium        | VIVGAIMVASG--VGAVAGAMVASGVIGMANMAVQAAEDGLISQEMKILGPILTAIE      |
| gi   1041718008   gb   EHEC             | VVAAVFTGGASLALAAVGLAVMVADEIVK-----AATGVSFIIQQA---LNPIMEHVL     |
| gi   194415512   gb   EPEC              | AVAAVFNPALW--AVVAIGATAMALQ-----AATGVSFIIQQA---LNPIMEHVL        |
| gi   15723935   gb   C.rodentium        | AIAAIFNPALW--AVVAISATAMALQ-----AIAAFFNPALW--AVVAISATAMALQ      |
| gi   155533   gb   Y.pseudotuberculosis | -----  |
| gi   975295   gb   S.typhimurium        | VALTVVSTVM-TFGGSALKCLANIGAKL-----GANTASLAAKGAESAKVAQIS         |
| gi   1041718008   gb   EHEC             | -----KPLMELIGKAITKALEGLGVDDKTAEMAGSIVGAIVAAIAM--VAVIVVAVVG     |
| gi   194415512   gb   EPEC              | -----TAVDVMGENAPQGLKTAQVFGGISMAASILTAVGVG-----VSSLLSKFG        |
| gi   15723935   gb   C.rodentium        | -----TAVDVMGDKAPQALKTAQVFGGVSIAASILTAVGIG-----VSSLMSKVG        |
| gi   155533   gb   Y.pseudotuberculosis | -----TAVDVMGDKAPQALKTAQAFGGLSLAAGILTAVGLG-----VSSLMSKVG        |
| gi   155533   gb   Y.pseudotuberculosis | -----  |
| gi   975295   gb   S.typhimurium        | TGISNTVGSVAVTKLGGSFAGLTMSHAIRTGSAAT-----QVA-----VGVGSGITQ      |
| gi   1041718008   gb   EHEC             | KGAALKGNALSKMMGETIKKLVNVLKQLAQNGSKLFTQGMQRITSGLNVGSKMGLQT      |
| gi   194415512   gb   EPEC              | -NVANKIGSSVVVKVVEKAAEALVKNVFAKISTVAE-----G---VTNGIRSGITG-----  |
| gi   15723935   gb   C.rodentium        | -DVANKVGSNIVKTVTKLADVFNENNVSKVAATAN-----G---FTTSARSIGTT-----   |
| gi   155533   gb   Y.pseudotuberculosis | -DVAGKVGSNIVKTVTKLADVFNENIASKVSAN-----G---LTTSTRSIGTT-----     |
| gi   155533   gb   Y.pseudotuberculosis | -----  |
| gi   975295   gb   S.typhimurium        | TINNKKQAD-----LQHNNADLALNKAAMALQS                              |
| gi   1041718008   gb   EHEC             | NALSKELVGNTLNKVALGMEVTNTAAQSAGGVAEVGFINKASEALDFMLARFAMDQIQQ    |
| gi   194415512   gb   EPEC              | -ALNNEA-----AQLQMLSQLAAFAVQN                                   |
| gi   15723935   gb   C.rodentium        | -VLNND-----AQYSILAQLSAYAVQN                                    |
| gi   155533   gb   Y.pseudotuberculosis | -VLNND-----ANHNVLQSISAFVVEN                                    |
| gi   155533   gb   Y.pseudotuberculosis | -----  |
| gi   975295   gb   S.typhimurium        | IIDRLKEELSHLSESHQVMEIQQMINAKG-----DML-----HNLAGRPH             |
| gi   1041718008   gb   EHEC             | WLKQSVEI---FGENQKVTAELOKAMSSAVQQ---NADSRFILRQSR-----           |
| gi   194415512   gb   EPEC              | L--TRQSES---LGESAKL---ELDKAASELQNASYLSQVSLMSDSARVNSRIVSGRI--   |
| gi   15723935   gb   C.rodentium        | L--TRQSEN---LGESAKV---ELDKAAELRNQASYLQNASQLISDSARVNSRIVSGRV--  |
| gi   155533   gb   Y.pseudotuberculosis | L--TRQSEQ---LSQSAKA---ELDKAADELQNASYMSQASQLISDSARVNSRIVSGRV--  |
| gi   155533   gb   Y.pseudotuberculosis | V  |
| gi   975295   gb   S.typhimurium        | -  |
| gi   1041718008   gb   EHEC             | -  |
| gi   194415512   gb   EPEC              | -  |
| gi   15723935   gb   C.rodentium        | -  |

B

|  |        |        |        |        |        |
|--|--------|--------|--------|--------|--------|
| 1: gi   155533   gb   Y.pseudotuberculosis | 100.00 | 22.16  | 20.54  | 20.13  | 19.14  |
| 2: gi   975295   gb   S.typhimurium        | 22.16  | 100.00 | 24.85  | 24.42  | 23.26  |
| 3: gi   1041718008   gb   EHEC             | 20.54  | 24.85  | 100.00 | 75.13  | 70.86  |
| 4: gi   194415512   gb   EPEC              | 20.13  | 24.42  | 75.13  | 100.00 | 85.00  |
| 5: gi   15723935   gb   C.rodentium        | 19.14  | 23.26  | 70.86  | 85.00  | 100.00 |

**Fig. 51: Alignment of EspD amino acid sequence from EHEC, EPEC, *C. rodentium*, *Y. pseudotuberculosis* and *S. typhimurium* and calculated percentage of homology: A)** EspD sequence alignment. Amino acids sequences were obtained from NCBI and Colibase and the alignment was performed by Clustal Omega. Asterisks (\*) underneath determined amino acids indicate a fully conserved site, colon (:) specify a conservation between groups of very similar properties and period (.) mean conservation between groups of different properties. Amino acids in the sequence are colour coded according to their chemical nature: red, small and aromatic amino acids; blue, acidic amino acids; green, hydroxyl-, sulfhydryl- and amine-bearing amino acids; magenta, basic amino acids. A dash (-) indicates a gap in the sequence. **B)** Homology percentage calculated by Clustal Omega. A strong sequence homology was detected for EspD in EHEC, EPEC and *C. rodentium* of 75% and 70%, while a poor homology was found between EHEC EspD and YopB and SipB (20% and 24% homology respectively).

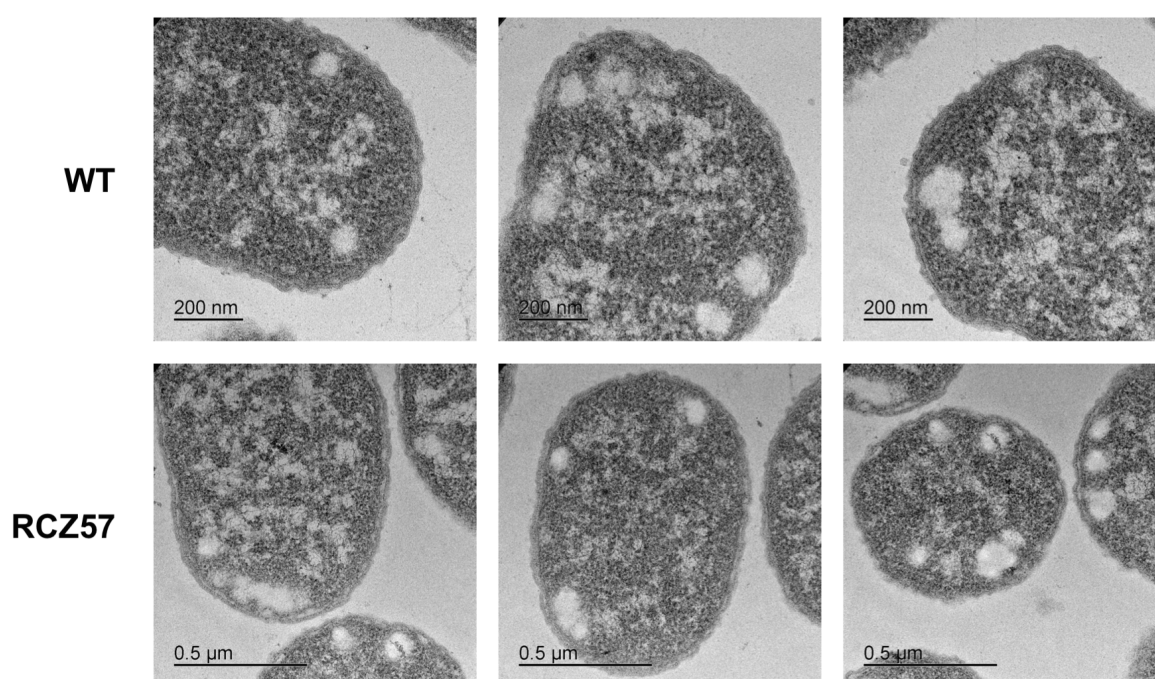


**Fig. 50: TEM images of sectioned bacteria treated with RCZ57:** Bacterial membrane were analysed to assess any perturbances or vesicle formation in the presence of **RCZ57** at 200 uM. No substantial differences were observed between the treated and untreated samples, indicating that the TZP derivative did not promote vesicle formation on the bacterial membrane.

| Sample | n° EspA filaments (>500 nm) | SD      | N  |
|--------|-----------------------------|---------|----|
| WT     | 5.600                       | ± 2.345 | 25 |
| RCZ12  | 1.320                       | ± 1.249 | 25 |
| RCZ57  | 0.960                       | ± 0.935 | 25 |

**Table 14: Functioning EspA filaments (>500 nm) for the TEM experiment with RCZ57:** The average number of EspA filaments (>500 nm) for the TEM samples is shown in the table above. The values have been calculated from 25 different images taken from 5 independent experiments. Standard deviation from the mean value is also shown in the table.

## Experimental Part

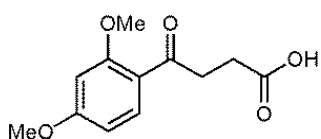


## 12 Chemistry experimental part

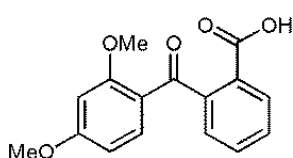
All chemicals used in this study were purchased from Sigma-Aldrich<sup>®</sup>, Acros Organics<sup>®</sup>, Fisher Scientific<sup>®</sup> and Life Technologies<sup>®</sup> and used as sold. All reactions were performed under a dry argon atmosphere, unless otherwise stated, and monitored using aluminum TLC pre-coated with silica (Merck<sup>®</sup>), visualised under UV light at 256 nm. Proton NMR spectra were recorded on a Bruker AM-400 and carbon NMR spectra on a Bruker AM-500. All chemical shifts ( $\delta$ ) are reported in parts per million (ppm). IR spectra were recorded on a Shimadzu FT-IR 8000S<sup>®</sup> with neat samples. Uncorrected melting points were performed with a Stuart Scientific Melting Point SMP1. All flash columns chromatography were performed using Merck<sup>®</sup> Silica.

### 12.1 Procedure for Friedel-Crafts acylation:

The desired anhydride (48 mmol) was dissolved in dry DCE (100 mL) and anhydrous aluminium chloride (61 mmol) was added at 0 °C in one portion. After being stirred for 15 minutes, 1,3-dimethoxybenzene (43 mmol) was added dropwise at 0 °C through 30 minutes. The ice bath was removed and the reaction mixture was stirred at room temperature for 5 hours. Water (200 mL) was added carefully at 0 °C to quench the aluminium chloride and the aqueous layer was extracted with DCM (3x100 mL), dried over Na<sub>2</sub>SO<sub>4</sub>, filtered and concentrated. The product was purified through flash column chromatography.



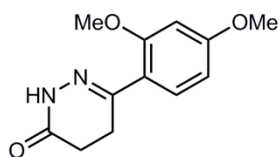
**4-(2,4-Dimethoxy-phenyl)-4-oxo-butanoic acid (18):** The product was purified through flash column chromatography (2% methanol in DCM) to afford an off-white solid (6.8 g, 29 mmol from 6 g, 43 mmol of **17**) in 65% yield. m.p. 138 °C. <sup>1</sup>H-NMR (CDCl<sub>3</sub> 400 MHz)  $\delta$  7.81 (1H, d,  $J$  = 8.8 Hz, C(CO)CHCH), 6.45 (1H, dd,  $J$  = 8.8 Hz, 2.3 Hz, CHCHC(OMe)), 6.38 (1H, d,  $J$  = 2.3 Hz, C(OMe)CHC(OMe)), 3.83 (3H, s, OCH<sub>3</sub>), 3.78 (3H, s, OCH<sub>3</sub>), 3.22 (2H, t,  $J$  = 6.6 Hz, COCH<sub>2</sub>), 2.66 (2H, t,  $J$  = 6.6 Hz, COOHCH<sub>2</sub>). <sup>13</sup>C-NMR (CDCl<sub>3</sub> 126 MHz)  $\delta$  197.5 (CO), 178.7 (COOH), 161.2 (CHC(OMe)CH), 155.6 (C(CO)C(OMe)CH), 132.9 (C(CO)CHH), 108.3 (C(CO)), 105.2 (C(CO)CHCH), 98.3 (C(OMe)CHC(OMe)), 55.5 (OCH<sub>3</sub>), 55.4 (OCH<sub>3</sub>), 38.4 (COCH<sub>2</sub>), 28.7 (COOHCH<sub>2</sub>). IR (neat)  $\nu_{\text{max}}$ : 2878, 1606, 1498, 1100, 998 cm<sup>-1</sup>. HRMS (ESI) calcd for C<sub>12</sub>H<sub>14</sub>NaO<sub>5</sub> [M+Na]<sup>+</sup> 261.0733 m/z found 261.0728 m/z.



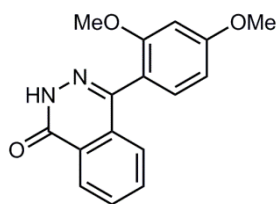
**2-(2,4-Dimethoxy-benzoyl)-benzoic acid (19):** The product was purified through flash column chromatography (5% methanol in DCM) to afford an off-white solid (5.1 g, 18 mmol from 4.5 g, 32 mmol of **17**) in 54% yield. m.p. 134 °C.  $^1\text{H-NMR}$  ( $\text{CDCl}_3$  400 MHz)  $\delta$  7.93 (1H, d,  $J$  = 6.7 Hz, C(COOH)CH), 7.67 (1H, d,  $J$  = 8.1 Hz, C(OMe)C(CO)CH), 7.50 (1H, t,  $J$  = 6.7 Hz, C(COOH)CHCHCH), 7.39 (1H, t,  $J$  = 7.5 Hz, C(COOH)CHCH), 7.21 (1H, d,  $J$  = 7.4 Hz, C(COOH)C(CO)CH), 6.44 (1H, d,  $J$  = 8.0 Hz, C(CO)CHCH), 6.30 (1H, s, C(OMe)CHC(OMe)), 3.77 (3H, s,  $\text{OCH}_3$ ), 3.47 (3H, s,  $\text{OCH}_3$ ).  $^{13}\text{C-NMR}$  ( $\text{CDCl}_3$  126 MHz)  $\delta$  194.6 (CO), 170.9 (COOH), 165.0 (CHC(OMe)CH), 161.3 (C(CO)C(OMe)), 145.8 (CHC(CO)C(COOH)), 133.9 (C(COOH)), 133.1 (C(OMe)C(CO)CH), 130.2 (C(COOH)CHCHCH), 128.5 (C(COOH)CHCH), 127.4 (C(COOH)C(CO)CH), 126.8 (C(COOH)CH), 120.0 (C(OMe)C(CO)), 105.2 (CHC(OMe)CH), 98.6 (C(OMe)CHC(OMe)), 55.5 ( $\text{OCH}_3$ ), 55.4 ( $\text{OCH}_3$ ). IR (neat)  $\nu_{\text{max}}$ : 3001, 1721, 1595, 1261, 1122  $\text{cm}^{-1}$ . HRMS (ESI) calcd for  $\text{C}_{16}\text{H}_{13}\text{O}_5$   $[\text{M-H}]^-$  285.0768 m/z found 285.0755 m/z.

## 12.2 Procedure for hydrazine coupling:

The desired carboxylic acid (9 mmol) was suspended in absolute ethanol (25 mL) and hydrazine hydrate (17 mmol) was added via syringe. The reaction mixture was refluxed at 100 °C until total consumption of the starting material, monitored by TLC (normally 3-4 hours). The solvent was then removed and the product was dried under vacuum pump to obtain the desired product in excellent purity.



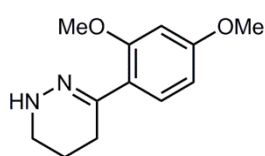
**6-(2,4-Dimethoxy-phenyl)-4,5-dihydro-2H-pyridazin-3-one (20):** The product was obtained as a yellowish solid in 96% yield in 2 hours (470 mg, 2 mmol from 500 mg, 2 mmol of **18**). m.p. 121 °C.  $^1\text{H-NMR}$  ( $\text{CDCl}_3$  400 MHz)  $\delta$  8.60 (1H, s, NH), 7.33 (1H, d,  $J$  = 8.4 Hz, C(CN)CH), 6.44 (1H, dd,  $J$  = 8.4 Hz, 2.4 Hz, C(OMe)CHCH), 6.40 (1H, d,  $J$  = 2.3 Hz, C(OMe)CHC(OMe)), 3.76 (6H, s,  $\text{OCH}_3$ ), 2.86 (2H, t,  $J$  = 8.2 Hz, CONHCH<sub>2</sub>), 2.44 (2H, t,  $J$  = 8.4 Hz, CONHCH<sub>2</sub>CH<sub>2</sub>).  $^{13}\text{C-NMR}$  ( $\text{CDCl}_3$  126 MHz)  $\delta$  168.2 (CONH), 162.2 (C(OMe)CHC(OMe)), 158.6 (C(CN)C(OMe)CH), 153.5 (CNNH), 130.0 (C(CN)CH), 118.9 (C(CN)), 104.8 (C(CN)CHCH), 98.7 (C(OMe)CHC(OMe)), 55.5 ( $\text{OCH}_3$ ), 55.4 ( $\text{OCH}_3$ ), 26.6 (CONHCH<sub>2</sub>), 25.7 (CONHCH<sub>2</sub>CH<sub>2</sub>). IR (neat)  $\nu_{\text{max}}$ : 3274, 2935, 1672, 1334, 1207  $\text{cm}^{-1}$ . HRMS (ESI) calcd for  $\text{C}_{12}\text{H}_{17}\text{N}_2\text{O}_2$   $[\text{M+H}]^+$  221.1285 m/z found 221.1282 m/z.



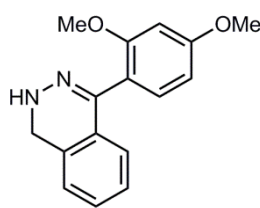
**4-(2,4-Dimethoxy-phenyl)-2H-phthalazin-1-one (21):** The product was obtained as an off-white solid (2 g, 7 mmol from 2.5 g, 9 mmol of **19**) in 85% yield in 4 hours. m.p. 256 °C.  $^1\text{H-NMR}$  ( $\text{CDCl}_3$  400 MHz)  $\delta$  10.43 (1H, s, NH), 8.40 (1H, dd,  $J$  = 7.5 Hz, 1.8 Hz, C(CO)CCH), 7.70 - 7.65 (2H, m, ArH, ArH), 7.32 (1H, dd,  $J$  = 7.6 Hz, 1.8 Hz, C(CN)CCH), 7.21 (1H, d,  $J$  = 8.2 Hz, C(CN)CH), 6.55 (1H, dd,  $J$  = 8.2 Hz, 2.3 Hz, C(CN)CHCH), 6.52 (1H, d,  $J$  = 2.3 Hz, C(OMe)CHC(OMe)), 3.81 (3H, s, OCH<sub>3</sub>), 3.63 (3H, s, OCH<sub>3</sub>).  $^{13}\text{C-NMR}$  ( $\text{CDCl}_3$  126 MHz)  $\delta$  162.0 (CONH), 160.4 (C(CN)C(OMe)CH), 158.6 (C(OMe)CHC(OMe)), 146.6 (C(NNH)), 133.0 (Ar-CC), 131.8 (Ar-CC), 131.2 (Ar-CH), 130.8 (Ar-CH), 127.9 (Ar-CH), 127.4 (Ar-CH), 126.3 (Ar-CH), 116.7 (C(CN)C(OMe)), 104.8 (C(CN)CHCH), 98.8 (C(OMe)CHC(OMe)), 55.5 (OCH<sub>3</sub>), 55.4 (OCH<sub>3</sub>). IR (neat)  $\nu_{\text{max}}$ : 3142, 2922, 1676, 1208, 1157  $\text{cm}^{-1}$ . HRMS (ESI) calcd for  $\text{C}_{16}\text{H}_{14}\text{N}_2\text{NaO}_3$   $[\text{M}+\text{Na}]^+$  305.0897 m/z found 305.0895 m/z.

### 12.3 Procedure for $\text{LiAlH}_4$ reduction <sup>135</sup>:

$\text{LiAlH}_4$  (6 mmol) was suspended in dry THF (10 mL) and a solution of the desired amide (2 mmol) in dry THF (10 mL) was added dropwise at room temperature. The reaction mixture was refluxed at 80 °C for 5 hours. Water (20 mL) was added very carefully at 0 °C to quench the excess of  $\text{LiAlH}_4$  and the aqueous layer was extracted with ethyl acetate (3x30 mL), dried over  $\text{Na}_2\text{SO}_4$ , filtered and concentrated. The desired products were pure enough (by NMR) and were used in the next step without any further purification.



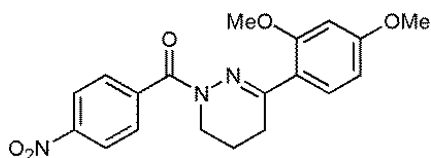
**3-(2,4-Dimethoxy-phenyl)-1,4,5,6-tetrahydro-pyridazine (22):** The product was obtained as a yellow thick oil (360 mg, 2 mmol from 500 mg, 2 mmol of **20**) in 81% yield and it was used without any further purification.  $^1\text{H-NMR}$  ( $\text{CDCl}_3$  400 MHz)  $\delta$  7.30 (1H, d,  $J$  = 8.4 Hz, C(CN)CH), 6.50 (1H, dd,  $J$  = 8.3 Hz, 2.4 Hz, C(CN)CHCH), 6.47 (1H, d,  $J$  = 2.4 Hz, C(OMe)CHC(OMe)), 3.84 (3H, s, OCH<sub>3</sub>), 3.83 (3H, s, OCH<sub>3</sub>), 3.18 (2H, t,  $J$  = 5.5 Hz, NHCH<sub>2</sub>), 2.60 (2H, t,  $J$  = 6.8 Hz, C(CN)CH<sub>2</sub>), 2.03 (2H, dddd,  $J$  = 6.7 Hz, 6.7 Hz, 5.5 Hz, 5.5 Hz, NHCH<sub>2</sub>CH<sub>2</sub>).  $^{13}\text{C-NMR}$  ( $\text{CDCl}_3$  126 MHz)  $\delta$  162.0 (CHC(OMe)CH), 160.4 (C(CN)C(OMe)), 158.6 (C(NNH)), 146.6 (C(CN)CHCH), 116.7 (C(CN)), 104.8 (C(CN)CHCH), 98.8 (C(OMe)CHC(OMe)), 55.5 (OCH<sub>3</sub>), 55.4 (OCH<sub>3</sub>), 45.6 (NHCH<sub>2</sub>), 25.5 (C(CN)CH<sub>2</sub>), 19.1 (NHCH<sub>2</sub>CH<sub>2</sub>). IR (neat)  $\nu_{\text{max}}$ : 3366, 2935, 1609, 1206, 919  $\text{cm}^{-1}$ . HRMS (ESI) calcd for  $\text{C}_{12}\text{H}_{14}\text{N}_2\text{NaO}_3$   $[\text{M}+\text{Na}]^+$  257.0897 m/z found 257.0897 m/z.



**4-(2,4-Dimethoxy-phenyl)-1,2-dihydro-phthalazine (23):** The product was obtained as a yellowish solid (627 mg, 2 mmol from 700 mg, 2 mmol of **21**) in 94% yield and with excellent purity. m.p. 124 °C. <sup>1</sup>H-NMR (CDCl<sub>3</sub> 400 MHz) δ 7.37 (1H, d, J = 8.3 Hz, C(CN)CH), 7.34 (1H, t, J = 7.5 Hz, CNCCHCH), 7.21 (1H, t, J = 7.7 Hz, NHCH<sub>2</sub>CCHCH), 7.15 (1H, d, J = 7.5 Hz, CNCCH), 6.89 (1H, d, J = 7.7 Hz, NHCH<sub>2</sub>CCH), 6.60 (1H, dd, J = 8.3 Hz, 2.3 Hz, C(CN)CHCH), 6.56 (1H, d, J = 2.3 Hz, C(OMe)CHC(OMe)), 6.06 (1H, s, NH), 4.31 (2H, s, NHCH<sub>2</sub>), 3.88 (3H, s, OCH<sub>3</sub>), 3.72 (3H, s, OCH<sub>3</sub>). <sup>13</sup>C-NMR (CDCl<sub>3</sub> 126 MHz) δ 161.2 (CHC(OMe)CH), 158.8 (C(CN)C(OMe)), 147.8 (CNNH), 131.5 (Ar-CC), 131.4 (C(CN)CH), 129.8 (Ar-CC), 127.5 (Ar-CH), 127.4 (2xAr-CH), 124.8 (Ar-CH), 118.6 (C(CN)), 104.6 (C(CN)CHCH), 98.8 (C(OMe)CHC(OMe)), 55.5 (OCH<sub>3</sub>), 55.4 (OCH<sub>3</sub>), 45.6 (NHCH<sub>2</sub>). IR (neat) ν<sub>max</sub>: 3364, 2936, 1608, 1207, 826 cm<sup>-1</sup>. HRMS (ESI) calcd for C<sub>16</sub>H<sub>17</sub>N<sub>2</sub>O<sub>2</sub> [M+H]<sup>+</sup> 269.1285 m/z found 269.1279 m/z.

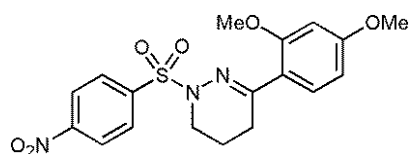
#### 12.4 Procedure for acylation/sulphonylation:

The desired amine derivatives (1.63 mmol) was dissolved in dry DCM (10 mL) and TEA (3.42 mmol) and DMAP (0.16 mmol) were added subsequently. After 5 minutes, the desired acid/sulphonyl chloride (1.79 mmol) was added and the reaction mixture was stirred at room temperature until the starting material was no longer detectable by TLC (2-16 hours). The solvent was then removed and the crude material was purified through direct flash column chromatography.



**[3-(2,4-Dimethoxy-phenyl)-5,6-dihydro-4H-pyridazin-1-yl]-(4-nitro-phenyl)-methanone (RCZ09):** The product was purified with direct flash column chromatography (from 10% to 20% ethyl acetate in petroleum ether) to afford a yellow solid (361 mg, 0.97 mmol from 360 mg, 1.63 mmol of **22**) in 60% yield. m.p. 152 °C. <sup>1</sup>H-NMR (CDCl<sub>3</sub> 400 MHz) δ 8.13 (2H, d, J = 8.8 Hz, 2xC(NO<sub>2</sub>)CH), 7.78 (2H, d, J = 8.9 Hz, 2xC(CO)CH), 7.06 (1H, d, J = 8.2 Hz, C(CN)CH), 6.35 (1H, d, J = 2.4 Hz, C(OMe)CHC(OMe)), 6.34 (1H, dd, J = 8.3 Hz, 2.4 Hz, C(CN)CHCH), 3.93 (2H, t, J = 5.9 Hz, NCH<sub>2</sub>), 3.72 (3H, s, OCH<sub>3</sub>), 3.71 (3H, s, OCH<sub>3</sub>), 2.65 (2H, t, J = 6.3 Hz, CNCH<sub>2</sub>), 1.95 (2H, dddd, J = 6.3 Hz, 6.3 Hz, 5.7 Hz, 5.7 Hz, NCH<sub>2</sub>CH<sub>2</sub>). <sup>13</sup>C-NMR (CDCl<sub>3</sub> 126 MHz) δ 168.2

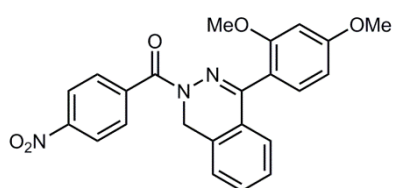
(CON), 161.7 (CHC(OMe)CH), 158.8 (C(CN)C(OMe)), 151.2 (C(NO<sub>2</sub>)), 148.2 (CNNCO), 141.9 (C(CO)), 130.5 (C(CN)CH), 129.7 (2xC(CO)CH), 122.5 (2xC(NO<sub>2</sub>)CH), 120.3 (C(CN)CH), 104.6 (C(CN)CHCH), 98.8 (C(OMe)CHC(OMe)), 55.4 (OCH<sub>3</sub>), 55.3 (OCH<sub>3</sub>), 40.1 (NCH<sub>2</sub>), 26.8 (CNCH<sub>2</sub>), 17.6 (NCH<sub>2</sub>CH<sub>2</sub>). IR (neat)  $\nu_{\text{max}}$ : 2838, 1647, 1520, 1344, 1160 cm<sup>-1</sup>. HRMS (ESI) calcd for C<sub>19</sub>H<sub>19</sub>N<sub>3</sub>NaO<sub>5</sub> [M+Na]<sup>+</sup> 392.1217 m/z found 392.1200 m/z.



**3-(2,4-Dimethoxy-phenyl)-1-(4-nitro-benzenesulphonyl)-**

**1,4,5,6-tetrahydro-pyridazine (RCZ11):** The product was purified with direct flash column chromatography (20%

ethyl acetate in petroleum ether) to afford a brownish solid (310 mg, 0.76 mmol from 250 mg, 1.13 mmol of **22**) in 67% yield. m.p. 168 °C. <sup>1</sup>H-NMR (CDCl<sub>3</sub> 400 MHz)  $\delta$  8.27 (2H, d, J = 9.0 Hz, 2xC(NO<sub>2</sub>)CH), 8.04 (2H, d, J = 8.9 Hz, 2xC(CO)CH), 7.15 (1H, d, J = 8.5 Hz, C(CN)CH), 6.40 (1H, dd, J = 8.4 Hz, 2.3 Hz, C(CN)CHCH), 6.34 (1H, d, J = 2.3 Hz, C(OMe)CHC(OMe)), 3.75 (3H, s, OCH<sub>3</sub>), 3.66 (3H, s, OCH<sub>3</sub>), 3.39 (2H, t, J = 5.6 Hz, NCH<sub>2</sub>), 2.49 (2H, t, J = 6.6 Hz, CNCH<sub>2</sub>), 1.97 (2H, dddd, J = 6.6 Hz, 6.6 Hz, 5.6 Hz, 5.6 Hz, NCH<sub>2</sub>CH<sub>2</sub>). <sup>13</sup>C-NMR (CDCl<sub>3</sub> 126 MHz)  $\delta$  161.8 (C(OMe)CHC(OMe)), 158.6 (C(CN)C(OMe)), 154.7 (CNNSO<sub>2</sub>), 150.2 (C(NO<sub>2</sub>)), 142.0 (C(SO<sub>2</sub>)), 130.4 (C(CN)CH), 129.7 (2xC(SO<sub>2</sub>)CH), 123.8 (2xC(NO<sub>2</sub>)CH), 120.1 (C(CN)), 104.6 (C(CN)CHCH), 98.7 (C(OMe)CHC(OMe)), 55.4 (OCH<sub>3</sub>), 55.3 (OCH<sub>3</sub>), 43.1 (NCH<sub>2</sub>), 25.1 (CNCH<sub>2</sub>), 19.0 (NCH<sub>2</sub>CH<sub>2</sub>). IR (neat)  $\nu_{\text{max}}$ : 2925, 1606, 1527, 1308, 1172 cm<sup>-1</sup>. HRMS (ESI) calcd for C<sub>18</sub>H<sub>19</sub>N<sub>3</sub>NaO<sub>6</sub>S [M+Na]<sup>+</sup> 428.0887 m/z found 428.0892 m/z.

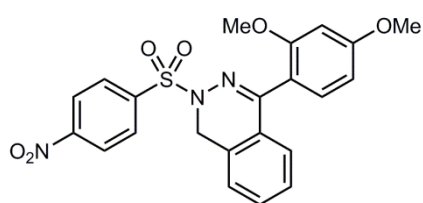


**[4-(2,4-Dimethoxy-phenyl)-1H-phthalazin-2-yl]-(4-nitro-**

**phenyl)-methanone (RCZ17):** The product was purified with direct flash column chromatography (20% ethyl acetate in petroleum ether) to give a bright yellow solid

(212 mg, 0.50 mmol from 250 mg, 0.93 mmol of **23**) in 54% yield. m.p. 183 °C. <sup>1</sup>H-NMR (CDCl<sub>3</sub> 400 MHz)  $\delta$  8.26 (2H, d, J = 9.1 Hz, 2xC(NO<sub>2</sub>)CH), 7.96 (2H, d, J = 9.1 Hz, 2xC(CO)CH), 7.50 (1H, t, J = 7.5 Hz, NCH<sub>2</sub>CCHCH), 7.33 (1H, t, J = 7.5 Hz, CNCCHCH), 7.32 (1H, d, J = 7.8 Hz, NCH<sub>2</sub>CCH), 7.20 (1H, d, J = 8.2 Hz, C(CN)CH), 7.06 (1H, d, J = 7.8 Hz, CNCCH), 6.58 (1H, dd, J = 8.1 Hz, 2.3 Hz, C(CN)CHCH), 6.55 (1H, d, J = 2.3 Hz, C(OMe)CHC(OMe)), 5.20 (2H, s, NCH<sub>2</sub>), 3.87 (3H, s, OCH<sub>3</sub>), 3.75 (3H, s, OCH<sub>3</sub>). <sup>13</sup>C-NMR (CDCl<sub>3</sub> 126 MHz)  $\delta$  168.5 (CON), 162.1 (C(OMe)CHC(OMe)), 158.9 (C(CN)C(OMe)), 151.8 (C(NO<sub>2</sub>)), 148.7 (CNN), 140.6 (C(CO)), 131.6 (C(CN)CH), 131.2 (Ar-CC), 131.0 (2xC(CO)CH), 130.3 (Ar-CC), 128.0 (Ar-CH),

127.3 (Ar-CH), 126.8 (Ar-CH), 125.9 (Ar-CH), 122.6 (2xC(NO<sub>2</sub>)CH), 116.6 (C(CN)), 104.8 (C(CN)CHCH), 98.9 (C(OMe)CHC(OMe)), 55.5 (OCH<sub>3</sub>), 55.4 (OCH<sub>3</sub>), 42.7 (NCH<sub>2</sub>). IR (neat)  $\nu_{\max}$ : 2926, 1651, 1520, 1344, 1209 cm<sup>-1</sup>. HRMS (ESI) calcd for C<sub>23</sub>H<sub>19</sub>N<sub>3</sub>NaO<sub>5</sub> [M+Na]<sup>+</sup> 440.1217 m/z found 440.1202 m/z.



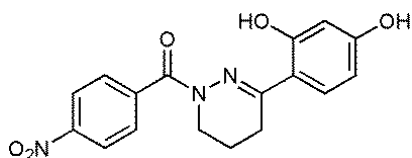
**4-(2,4-Dimethoxy-phenyl)-2-(4-nitro-benzenesulphonyl)-1,2-dihydro-phthalazine (RCZ19):**

The product was purified by direct flash column chromatography (20% ethyl acetate in petroleum ether)

to afford a bright yellow solid (235 mg, 0.51 mmol from 250 mg, 0.93 mmol of **23**) in 75% yield. m.p. 186 °C. <sup>1</sup>H-NMR (CDCl<sub>3</sub> 400 MHz)  $\delta$  8.38 (2H, d, J = 8.9 Hz, 2xC(NO<sub>2</sub>)CH), 8.21 (2H, d, J = 8.9 Hz, 2xC(CO)CH), 7.44 (1H, t, J = 7.4 Hz, NCH<sub>2</sub>CCHCH), 7.42 (1H, d, J = 8.4 Hz, C(CN)CH), 7.27 (1H, t, J = 7.4 Hz, CNCCHCH), 7.25 (1H, d, J = 7.4 Hz, NCH<sub>2</sub>CCH), 6.98 (1H, d, J = 7.4 Hz, CNCCH), 6.62 (1H, dd, J = 8.4 Hz, 2.4 Hz, C(CN)CHCH), 6.51 (1H, d, J = 2.4 Hz, C(OMe)CHC(OMe)), 4.53 (2H, s, NCH<sub>2</sub>), 3.90 (3H, s, OCH<sub>3</sub>), 3.60 (3H, s, OCH<sub>3</sub>). <sup>13</sup>C-NMR (CDCl<sub>3</sub> 126 MHz)  $\delta$  162.3 (C(OMe)CHCC(OMe)), 158.8 (C(CN)C(OMe)), 154.3 (CNN), 150.4 (C(NO<sub>2</sub>)), 141.3 (C(SO<sub>2</sub>)), 132.0 (Ar-CC), 131.4 (C(CN)CH), 130.3 (Ar-CC), 130.0 (2xC(NO<sub>2</sub>)CH), 128.2 (Ar-CH), 126.6 (Ar-CH), 126.1 (Ar-CH), 125.5 (Ar-CH), 123.9 (2xC(SO<sub>2</sub>)CH), 116.6 (C(CN)), 104.9 (C(CN)CHCH), 98.8 (C(OMe)CHC(OMe)), 55.5 (OCH<sub>3</sub>), 55.3 (OCH<sub>3</sub>), 45.8 (NCH<sub>2</sub>). IR (neat)  $\nu_{\max}$ : 2936, 1608, 1348, 1177, 738 cm<sup>-1</sup>. HRMS (ESI) calcd for C<sub>22</sub>H<sub>20</sub>N<sub>3</sub>O<sub>6</sub>S [M+H]<sup>+</sup> 454.0995 m/z found 454.0999 m/z.

### 12.5 Procedure for de-methylation:

The desired di-methoxyl analogue (**RCZ09**, **RCZ11**, **RCZ17** or **RCZ19**) (0.24 mmol) was dissolved in dry DCM (6 mL) and a 1 M solution of BBr<sub>3</sub> in DCM (2.4 mmol) was added dropwise at 0 °C. The reaction mixture was then heated to 40 °C until starting material was consumed (ca. 3-36 hours), as monitored by TLC. After cooling to room temperature, the excess of BBr<sub>3</sub> was quenched with careful addition of water (20 mL) and the organic and aqueous layers were separated. The aqueous layer was then washed with DCM (2x20 mL) and the combined organic layers were dried over Na<sub>2</sub>SO<sub>4</sub>, filtered and concentrated. The crude was purified through flash column chromatography to give the desired product.

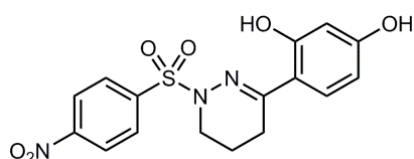


**[3-(2,4-Dihydroxy-phenyl)-5,6-dihydro-4H-pyridazin-1-yl]-**

**(4-nitro-phenyl)-methanone (RCZ10):**

The product was purified through flash column chromatography (1% methanol in DCM) to give a yellow solid (45 mg, 0.13

mmol from 90 mg, 0.24 mmol of **RCZ09**) in 55% yield. m.p. 231 °C. <sup>1</sup>H-NMR (DMSO 400 MHz) δ 10.60 (1H, s, COH), 9.83 (1H, s, COH), 8.33 (2H, d, J = 8.6 Hz, 2xC(NO<sub>2</sub>)CH), 7.79 (2H, d, J = 8.6 Hz, 2xC(CO)CH), 7.33 (1H, d, J = 8.8 Hz, C(CN)CH), 6.27 (1H, dd, J = 8.8 Hz, 2.2 Hz, C(CN)CHCH), 6.03 (1H, d, J = 2.2 Hz, C(OH)CHC(OH)), 3.91 (2H, t, J = 5.7 Hz, NCH<sub>2</sub>), 2.76 (2H, t, J = 6.9 Hz, CNCH<sub>2</sub>), 2.04 (2H, dddd, J = 6.8 Hz, 6.8 Hz, 5.7 Hz, 5.7 Hz, NCH<sub>2</sub>CH<sub>2</sub>). <sup>13</sup>C-NMR (DMSO 126 MHz) δ 167.1 (CON), 160.1 (C(OH)CHC(OH)), 158.7 (C(CN)C(OH)), 153.8 (C(NO<sub>2</sub>)), 147.8 (CNN), 142.2 (C(CO)), 128.9 (C(CN)CH), 128.8 (2xC(NO<sub>2</sub>)CH), 123.6 (2xC(CO)CH), 110.9 (C(CN)), 107.1 (C(CN)CHCH), 102.7 (C(OH)CHC(OH)), 44.1 (NCH<sub>2</sub>), 22.7 (CNCH<sub>2</sub>), 16.8 (NCH<sub>2</sub>CH<sub>2</sub>). IR (neat) ν<sub>max</sub>: 3385, 2359, 1627, 1518, 1349 cm<sup>-1</sup>. HRMS (ESI) calcd for C<sub>17</sub>H<sub>15</sub>N<sub>3</sub>NaO<sub>5</sub> [M+Na]<sup>+</sup> 364.0904 m/z found 364.0890 m/z.

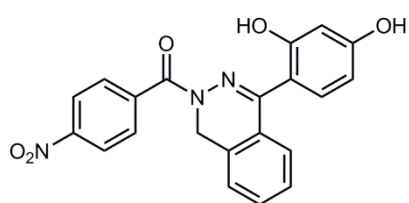


**4-[1-(4-Nitro-benzenesulphonyl)-1,4,5,6-tetrahydro-**

**pyridazin-3-yl]-benzene-1,3-diol (RCZ12):**

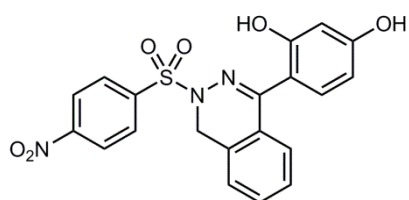
The product was purified through flash column chromatography (50% ethyl acetate in petroleum ether) to afford a bright

yellow foam (14 mg, 0.036 mmol from 100 mg, 0.24 mmol of **23**) in 15%. <sup>1</sup>H-NMR (CDCl<sub>3</sub> 400 MHz) δ 11.79 (1H, s, COH), 8.30 (2H, d, J = 9.0 Hz, 2xC(NO<sub>2</sub>)CH), 8.01 (2H, d, J = 9.0 Hz, 2xC(SO<sub>2</sub>)CH), 7.08 (1H, d, J = 8.7 Hz, C(CN)CH), 6.36 (1H, d, J = 2.5 Hz, C(OH)CHC(OH)), 6.27 (1H, dd, J = 8.5 Hz, 2.5 Hz, C(CN)CHCH), 4.98 (1H, s, COH), 3.40 (2H, t, J = 6.9 Hz, NCH<sub>2</sub>), 2.51 (2H, t, J = 6.7 Hz, CNCH<sub>2</sub>), 2.11 (2H, dddd, J = 6.9 Hz, 6.9 Hz, 6.7 Hz, 6.7 Hz, NCH<sub>2</sub>CH<sub>2</sub>). <sup>13</sup>C-NMR (CDCl<sub>3</sub> 126 MHz) δ 161.8 (C(OH)CHC(OH)), 158.6 (C(CN)C(OH)), 154.7 (CNN), 150.2 (C(NO<sub>2</sub>)), 142.0 (C(SO<sub>2</sub>)), 130.4 (C(CN)CH), 129.7 (C(NO<sub>2</sub>)CH), 123.8 (C(SO<sub>2</sub>)CH), 120.1 (C(CN)), 104.6 (C(CN)CHCH), 98.7 (C(OH)CHC(OH)), 43.1 (NCH<sub>2</sub>), 25.1 (CNCH<sub>2</sub>), 19.0 (NCH<sub>2</sub>CH<sub>2</sub>). IR (neat) ν<sub>max</sub>: 3431, 2924, 1627, 1530, 1349 cm<sup>-1</sup>. HRMS (ESI) calcd for C<sub>16</sub>H<sub>15</sub>N<sub>3</sub>O<sub>6</sub>S [M+H]<sup>+</sup> 378.0743 m/z found 378.0723 m/z.



**[4-(2,4-Dihydroxy-phenyl)-1H-phthalazin-2-yl]-(4-nitro-phenyl)-methanone (RCZ18):** The product was purified through flash column chromatography (1% methanol in DCM) to give an bright yellow solid (87 mg, 0.22 mmol

from 127 mg, 0.30 mmol of **RCZ17**) in 74% yield. m.p. 253 °C.  $^1\text{H-NMR}$  (DMSO 400 MHz)  $\delta$  9.60 (1H, s, COH), 9.51 (1H, s, COH), 8.28 (2H, d,  $J$  = 8.7 Hz,  $2\times\text{C}(\text{NO}_2)\text{CH}$ ), 7.93 (2H, d,  $J$  = 8.9 Hz,  $2\times\text{C}(\text{CO})\text{CH}$ ), 7.53 (1H, t,  $J$  = 7.6 Hz,  $\text{NCH}_2\text{CCHCH}$ ), 7.49 (1H, d,  $J$  = 7.2 Hz,  $\text{NCH}_2\text{CCH}$ ), 7.36 (1H, t,  $J$  = 7.7 Hz,  $\text{CNCCHCH}$ ), 7.07 (1H, d,  $J$  = 7.2 Hz,  $\text{CNCCH}$ ), 7.05 (1H, d,  $J$  = 8.3 Hz,  $\text{C}(\text{CN})\text{CH}$ ), 6.35 (1H, d,  $J$  = 2.3 Hz,  $\text{C}(\text{OH})\text{CHC}(\text{OH})$ ), 6.29 (1H, dd,  $J$  = 8.3 Hz, 2.3 Hz,  $\text{C}(\text{CN})\text{CHCH}$ ), 5.09 (2H, s,  $\text{NCH}_2$ ).  $^{13}\text{C-NMR}$  ( $\text{CDCl}_3$  126 MHz)  $\delta$  167.8 (CON), 159.5 ( $\text{C}(\text{OH})\text{CHC}(\text{OH})$ ), 156.8 ( $\text{C}(\text{CN})\text{C}(\text{OH})$ ), 151.8 ( $\text{C}(\text{NO}_2)$ ), 148.0 (CNN), 140.8 ( $\text{C}(\text{CO})$ ), 131.4 (Ar-CC), 131.2 ( $\text{C}(\text{CN})\text{CH}$ ), 130.7 ( $2\times\text{C}(\text{NO}_2)\text{CH}$ ), 130.4 (Ar-CC), 127.9 (Ar-CH), 126.7 (Ar-CH), 126.1 (Ar-CH), 125.3 (Ar-CH), 122.7 ( $2\times\text{C}(\text{CO})\text{CH}$ ), 112.7 ( $\text{C}(\text{CN})$ ), 106.8 ( $\text{C}(\text{CN})\text{CHCH}$ ), 102.5 ( $\text{C}(\text{OH})\text{CHC}(\text{OH})$ ), 42.1 ( $\text{NCH}_2$ ). IR (neat)  $\nu_{\text{max}}$ : 2931, 2355, 1622, 1348, 1103  $\text{cm}^{-1}$ . HRMS (ESI) calcd for  $\text{C}_{21}\text{H}_{14}\text{N}_3\text{O}_5$   $[\text{M-H}]^-$  388.0939 m/z found 388.0931 m/z.

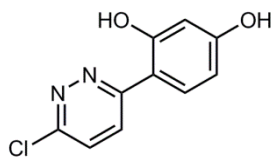


**4-[3-(4-Nitro-benzenesulphonyl)-3,4-dihydro-phthalazin-1-yl]-benzene-1,3-diol (RCZ20):** The product was purified through flash column chromatography (1% methanol in DCM) to afford a yellow foam (15 mg, 0.035 mmol from

70 mg, 0.15 mmol of **RCZ19**) in 25% yield.  $^1\text{H-NMR}$  ( $\text{CDCl}_3$  400 MHz)  $\delta$  10.34 (1H, s, COH), 8.33 (2H, d,  $J$  = 8.7 Hz,  $2\times\text{C}(\text{NO}_2)\text{CH}$ ), 8.09 (2H, d,  $J$  = 8.7 Hz,  $2\times\text{C}(\text{SO}_2)\text{CH}$ ), 7.48 (1H, t,  $J$  = 7.5 Hz,  $\text{NCH}_2\text{CCHCH}$ ), 7.43 (1H, d,  $J$  = 7.5 Hz,  $\text{NCH}_2\text{CCH}$ ), 7.35 (1H, t,  $J$  = 7.7 Hz,  $\text{CNCCHCH}$ ), 7.26 (1H, d,  $J$  = 7.7 Hz,  $\text{CNCCH}$ ), 7.18 (1H, d, 8.5 Hz,  $\text{C}(\text{CN})\text{CH}$ ), 6.50 (1H, d, 2.3 Hz,  $\text{C}(\text{OH})\text{CHC}(\text{OH})$ ), 6.33 (1H, dd,  $J$  = 8.5 Hz, 2.3 Hz,  $\text{C}(\text{CN})\text{CHCH}$ ), 5.10 (1H, s, COH), 4.29 (2H, s,  $\text{NCH}_2$ ).  $^{13}\text{C-NMR}$  ( $\text{CDCl}_3$  126 MHz)  $\delta$  161.5 ( $\text{C}(\text{OH})\text{CHC}(\text{OH})$ ), 160.3 ( $\text{C}(\text{CN})\text{C}(\text{OH})$ ), 157.7 (CNN), 152.0 ( $\text{C}(\text{NO}_2)$ ), 140.9 ( $\text{C}(\text{SO}_2)$ ), 134.0 (Ar-CC), 133.3 (Ar-CC), 133.0 ( $2\times\text{C}(\text{NO}_2)\text{CH}$ ), 131.9 ( $\text{C}(\text{CN})\text{CH}$ ), 129.3 (Ar-CH), 128.6 (Ar-CH), 127.4 (Ar-CH), 125.5 (Ar-CH), 125.4 ( $2\times\text{C}(\text{SO}_2)\text{CH}$ ), 110.5 ( $\text{C}(\text{CN})$ ), 108.0 ( $\text{C}(\text{CN})\text{CHCH}$ ), 104.6 ( $\text{C}(\text{OH})\text{CHC}(\text{OH})$ ), 47.3 ( $\text{NCH}_2$ ). IR (neat)  $\nu_{\text{max}}$ : 3122, 2926, 2363, 1356, 652  $\text{cm}^{-1}$ . HRMS (ESI) calcd for  $\text{C}_{20}\text{H}_{15}\text{N}_3\text{NaO}_6\text{S}$   $[\text{M}+\text{Na}]^+$  448.0574 m/z found 448.0563 m/z.

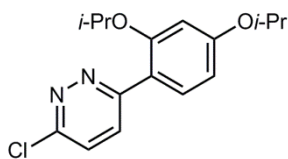


## 12.6 Alternative synthesis of RCZ12 and RCZ20



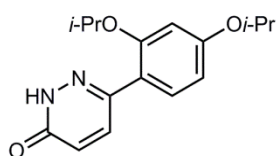
### 4-(6-Chloro-pyridazin-3-yl)-benzene-1,3-diol <sup>187</sup> (25):

3,6-Dichloropyridazine (**24**) (2.9 g, 19.98 mmol) was dissolved in dry DCE (70 mL) and resorcinol (2.0 g, 18.16 mmol) and anhydrous aluminium trichloride (3.39 g, 25.42 mmol) were added subsequently. The reaction mixture was refluxed (80 °C) for 18 hours. The mixture was then poured into a stirring 3 M solution of HCl and crushed ice. The yellow solid thus formed was collected through suction filtration, washed with water (3x100 mL) and dried under high vacuum to afford a yellow solid (3.7 g, 16.66 mmol, 93%). Characterisation data matched with the results previously reported <sup>187</sup>. <sup>1</sup>H-NMR (DMSO 500 MHz)  $\delta$  8.38 (1H, d, J = 9.3 Hz, ClCNCH), 7.95 (1H, d, J = 9.3 Hz, CNCH), 7.82 (1H, d, J = 9.3 Hz, C(CN)CH), 6.47 - 6.40 (2H, m, C(CN)CHCH, C(OH)CHC(OH)). <sup>13</sup>C-NMR (DMSO 126 MHz)  $\delta$  161.8 (C(OH)CHC(OH)), 159.8 (CNN), 159.7 (C(CN)C(OH)), 153.5 (ClCN), 130.4 (ClCNCH), 129.9 (CNCH), 128.8 (C(CN)CH), 110.3 (C(CN)), 108.5 (C(CN)CHCH), 103.8 (C(OH)CHC(OH)).



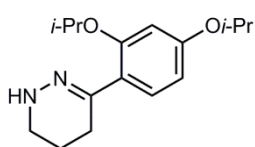
### 3-Chloro-6-(2,4-diisopropoxy-phenyl)-pyridazine (26):

4-(6-Chloro-pyridazin-3-yl)-benzene-1,3-diol (222 mg, 1.00 mmol) was dissolved in dry DMF (10 mL) and anhydrous potassium carbonate (552 mg, 4.00 mmol) was added. After 15 minutes, 2-bromo propane (375  $\mu$ L, 4.00 mmol) was added slowly to the reaction, which was stirred at 50 °C for 18 hours. Water (25 mL) was added and extracted with ether (3x50 mL). The organic phase was then washed with brine (5x50 mL), dried over Na<sub>2</sub>SO<sub>4</sub>, filtered and concentrated to yield the desired compound as a white paste (261 mg, 0.85 mmol, 85%). <sup>1</sup>H-NMR (CDCl<sub>3</sub> 400 MHz)  $\delta$  8.07 (1H, d, J = 9.0 Hz, ClCNCH), 7.98 (1H, d, J = 8.7 Hz, C(CN)CH), 7.45 (1H, d, J = 9.0 Hz, CNCH), 6.65 (1H, dd, J = 8.8 Hz, 2.3 Hz, C(CN)CHCH), 6.55 (1H, d, J = 2.3 Hz, C(OiPr)CHC(OiPr)), 4.70 - 4.55 (2H, m, 2xCH<sub>3</sub>CHCH<sub>3</sub>), 1.40 (6H, d, J = 6.1 Hz, 2xCHCH<sub>3</sub>), 1.34 (6H, d, J = 6.1 Hz, 2xCHCH<sub>3</sub>). <sup>13</sup>C-NMR (CDCl<sub>3</sub> 126 MHz)  $\delta$  160.9 (C(OiPr)CHC(OiPr)), 158.0 (CNN), 156.7 (C(CN)C(OiPr)), 154.1 (ClCN), 132.1 (ClCNCH), 130.2 (C(CN)CH), 126.7 (CNCH), 118.0 (C(CN)), 107.2 (C(CN)CHCH), 102.5 (C(OiPr)CHC(OiPr)), 71.0 (CH<sub>3</sub>CH), 70.1 (CH<sub>3</sub>CH), 22.1 (2xCHCH<sub>3</sub>), 22.0 (2xCHCH<sub>3</sub>). IR (neat)  $\nu_{\text{max}}$ : 2980, 1605, 1399, 1192, 840 cm<sup>-1</sup>. HRMS (ESI) calcd for C<sub>16</sub>H<sub>19</sub>N<sub>2</sub>NaO<sub>2</sub><sup>35</sup>Cl [M+Na]<sup>+</sup> 329.1027 m/z found 329.1012 m/z.



**6-(2,4-Diisopropoxy-phenyl)-2H-pyridazin-3-one**<sup>187</sup> (27): 3-

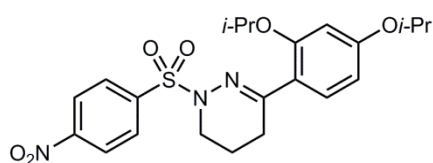
Chloro-6-(2,4-diisopropoxy-phenyl)-pyridazine (26) (657 mg, 2.14 mmol) was dissolved in glacial acetic acid (20 mL) and sodium acetate (352 mg, 4.29 mmol) was added one pot. The reaction mixture was stirred at 110 °C for 18 hours. Water (50 mL) was added to the mixture and the aqueous phase was washed with DCM (3x50 mL), dried over Na<sub>2</sub>SO<sub>4</sub>, filtered and concentrated. The residue was further dried under high vacuum to afford the desired product with excellent purity (by NMR) as a white solid (585 mg, 2.03 mmol, 94%). m.p. 155 °C. <sup>1</sup>H-NMR (CDCl<sub>3</sub> 500 MHz) δ 10.39 (1H, s, NH), 7.80 (1H, d, J = 9.9 Hz, ClCNCH), 7.49 (1H, d, J = 8.5 Hz, C(CN)CH), 6.92 (1H, d, J = 9.9 Hz, CNCH), 6.57 (1H, dd, J = 8.6 Hz, 2.3 Hz, C(CN)CHCH), 6.51 (1H, d, J = 2.2 Hz, C(OiPr)CHC(OiPr)), 4.66 - 4.51 (2H, m, 2xCH<sub>3</sub>CH), 1.38 (6H, d, J = 6.1 Hz, 2xCHCH<sub>3</sub>), 1.35 (6H, d, J = 6.1 Hz, 2xCHCH<sub>3</sub>). <sup>13</sup>C-NMR (CDCl<sub>3</sub> 126 MHz) δ 160.5 (CON), 160.4 (C(OiPr)CHC(OiPr)), 156.5 (C(CN)C(OiPr)), 145.8 (CNN), 136.0 (CNCH), 130.7 (CONHCH), 128.2 (C(CN)CH), 117.5 (C(CN)), 107.1 (C(CN)CHCH), 102.6 (C(OiPr)CHC(OiPr)), 70.9 (CH<sub>3</sub>CH), 70.1 (CH<sub>3</sub>CH), 22.0 (4xCHCH<sub>3</sub>). IR (neat) ν<sub>max</sub>: 3079, 1524, 1282, 1109, 949 cm<sup>-1</sup>. HRMS (ESI) calcd for C<sub>16</sub>H<sub>20</sub>N<sub>2</sub>NaO<sub>3</sub> [M+Na]<sup>+</sup> 311.1366 m/z found 311.1348 m/z.



**3-(2,4-Diisopropoxy-phenyl)-1,4,5,6-tetrahydro-pyridazine**<sup>135</sup> (28):

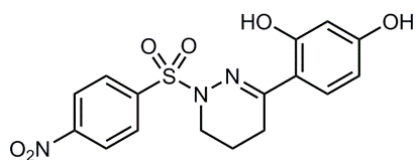
6-(2,4-Diisopropoxy-phenyl)-2H-pyridazin-3-one (27) (250 mg, 0.86 mmol) was dissolved in dry THF (30 mL) and LiAlH<sub>4</sub> (263 mg, 8.63 mmol) was added portion-wise. The reaction mixture was refluxed at 80 °C for 18 hours. Water (60 mL) was added carefully at 0 °C to quench the excess of LiAlH<sub>4</sub> and the mixture was then extracted with DCM (3x100 mL), dried over Na<sub>2</sub>SO<sub>4</sub>, filtered and concentrated. The desired amine was obtained as thick greenish oil with excellent purity (by NMR) and it was used without any further purification (214 mg, 0.77 mmol, 90%). <sup>1</sup>H-NMR (CDCl<sub>3</sub> 500 MHz) δ 7.18 (1H, d, J = 9.6 Hz, C(CN)CH), 6.38 (1H, dd, J = 8.5 Hz, 2.3 Hz, C(CN)CHCH), 6.34 (1H, d, J = 2.3 Hz, C(OiPr)CHC(OiPr)), 4.51 - 4.38 (2H, m, 2xCH<sub>3</sub>CH), 3.10 - 3.04 (2H, m, NHCH<sub>2</sub>), 2.53 (2H, t, J = 6.9 Hz, CNCH<sub>2</sub>), 1.95 - 1.87 (2H, m, NHCH<sub>2</sub>CH<sub>2</sub>), 1.25 (12H, d, J = 6.1 Hz, 4xCHCH<sub>3</sub>). <sup>13</sup>C-NMR (CDCl<sub>3</sub> 126 MHz) δ 158.7 (C(OiPr)CHC(OiPr)), 156.5 (C(CN)C(OiPr)), 148.5 (CNN), 129.9 (C(CN)CH), 123.6 (C(CN)), 106.7 (C(CN)CHCH), 102.9 (C(OiPr)CHC(OiPr)), 70.4 (CH<sub>3</sub>CH), 69.9 (CH<sub>3</sub>CH), 42.2 (NHCH<sub>2</sub>), 25.8 (CNCH<sub>2</sub>), 22.1 (2xCHCH<sub>3</sub>), 22.0 (2xCHCH<sub>3</sub>), 20.1 (NHCH<sub>2</sub>CH<sub>2</sub>). IR (neat) ν<sub>max</sub>: 3122, 1452, 1327, 1167, 872

cm<sup>-1</sup>. IR (neat)  $\nu_{\text{max}}$ : 2999, 1715, 1346, 1018, 789 cm<sup>-1</sup>. HRMS (ESI) calcd for C<sub>16</sub>H<sub>20</sub>N<sub>2</sub>NaO<sub>2</sub> [M+Na]<sup>+</sup> 311.1366 m/z found 311.1348 m/z.



**3-(2,4-Diisopropoxy-phenyl)-1-(4-nitro-benzenesulphonyl)-1,4,5,6-tetrahydro-pyridazine (29):**

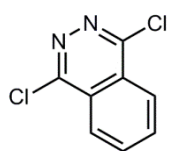
3-(2,4-Diisopropoxy-phenyl)-1,4,5,6-tetrahydro-pyridazine (**28**) (200 mg, 0.72 mmol) was dissolved in dry DCM (10 mL) and TEA (200  $\mu$ L, 1.44 mmol) and DMAP (1 mg, 0.072 mmol) were added subsequently. After 5 minutes, 4-nitrobenzenesulphonyl chloride (192 mg, 0.86 mmol) was added and the reaction mixture was stirred at room temperature until the starting material was no longer detectable by TLC (16 hours). The solvent was then removed and the product was purified by direct flash column chromatography (30% ethyl acetate in petroleum ether) to afford a yellow oil (206 mg, 0.44 mmol) in 62% yield. <sup>1</sup>H-NMR (CDCl<sub>3</sub> 400 MHz)  $\delta$  8.37 (2H, d, J = 9.1 Hz, 2xC(NO<sub>2</sub>)CH), 8.14 (2H, d, J = 9.1 Hz, 2xC(SO<sub>2</sub>)CH), 7.19 (1H, d, J = 8.6 Hz, C(CN)CH), 6.45 (1H, dd, J = 8.5 Hz, 2.2 Hz, C(CN)CHCH), 6.39 (1H, d, J = 2.2 Hz, C(OiPr)CHC(OiPr)), 4.56 (1H, dt, J = 12.6 Hz, 6.0 Hz, CH<sub>3</sub>CH), 4.49 (1H, dt, J = 12.5 Hz, 6.0 Hz, CH<sub>3</sub>CH), 3.49 (2H, t, J = 5.6 Hz, NCH<sub>2</sub>), 2.60 (2H, t, J = 6.7 Hz, CNCH<sub>2</sub>), 2.04 (2H, dddd, J = 6.8 Hz, 6.8 Hz, 5.7 Hz, 5.7 Hz, NCH<sub>2</sub>CH<sub>2</sub>), 1.36 (6H, d, J = 6.1 Hz, 2xCHCH<sub>3</sub>), 1.27 (6H, d, J = 6.1 Hz, 2xCHCH<sub>3</sub>). <sup>13</sup>C-NMR (CDCl<sub>3</sub> 126 MHz)  $\delta$  160.0 (C(OiPr)CHC(OiPr)), 157.0 (C(CN)C(OiPr)), 155.4 (CNN), 150.4 (C(NO<sub>2</sub>)), 142.1 (C(SO<sub>2</sub>)), 130.4 (C(CN)CH), 129.7 (2xC(NO<sub>2</sub>)CH), 123.8 (2xC(SO<sub>2</sub>)CH), 120.7 (C(CN)), 106.3 (C(CN)CHCH), 102.3 (C(OiPr)CHC(OiPr)), 70.4 (CH<sub>3</sub>CH), 70.0 (CH<sub>3</sub>CH), 43.2 (NCH<sub>2</sub>), 26.0 (CNCH<sub>2</sub>), 22.1 (2xCHCH<sub>3</sub>), 22.0 (2xCHCH<sub>3</sub>), 19.0 (NCH<sub>2</sub>CH<sub>2</sub>). IR (neat)  $\nu_{\text{max}}$ : 2977, 1606, 1570, 1372, 1188 cm<sup>-1</sup>. HRMS (ESI) calcd for C<sub>22</sub>H<sub>27</sub>N<sub>3</sub>O<sub>6</sub>S [M+H]<sup>+</sup> 462.1616 m/z found 462.1634 m/z.



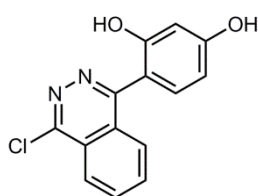
**4-[1-(4-Nitro-benzenesulphonyl)-1,4,5,6-tetrahydro-pyridazin-3-yl]-benzene-1,3-diol (RCZ12):** 3-(2,4-Diisopropoxy-phenyl)-1-(4-nitro-benzenesulphonyl)-

1,4,5,6-tetrahydro-pyridazine (**29**) (100 mg, 0.21 mmol) was dissolved in dry DCM (6 mL) and a 1 M solution of BBr<sub>3</sub> in DCM (1.68 mL, 1.68 mmol) was added slowly at 0 °C. The reaction mixture was stirred at 0 °C for 30 minutes and then at room temperature for 3 hours. Water (20 mL) was added and the layers separated. The aqueous phase was extracted with DCM (2x15 mL). The combined organic phases were dried over Na<sub>2</sub>SO<sub>4</sub>,

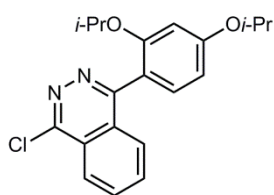
filtered and concentrated. The product was purified through flash column chromatography (40% ethyl acetate in petroleum ether) to afford **RCZ12** as a yellow foam (50 mg, 0.132 mmol, 58%). NMR, IR and mass spectrometry matches with the compound previously obtained.



**1,4-Dichloro-phthalazine (31):** The synthesis of this compound was achieved through a modified known protocol <sup>138</sup>. An oven dried round bottom flask was loaded with phthalhydrazide (**30**) (5 g, 30.86 mmol) and POCl<sub>3</sub> (30 mL). The reaction mixture was stirred for 4 hours at 110 °C under argon atmosphere. The mixture was then added dropwise to stirring solution of crushed ice and saturated NaHCO<sub>3</sub> (500 mL) to quench the POCl<sub>3</sub> excess. The pH was then adjusted to 8/9 with a 3 M solution of NaOH (200 mL) and the aqueous solution was extracted with DCM (3x250 mL), dried over Na<sub>2</sub>SO<sub>4</sub>, filtered and concentrated to afford the product as a yellowish solid (5.4 g, 27.13 mmol) in 87% yield. The product was used without any further purification. Characterisation data matched with the results previously reported <sup>138</sup>. <sup>1</sup>H-NMR (CDCl<sub>3</sub> 400 MHz) δ 8.39 - 8.32 (2H, m), 8.14 - 8.08 (2H, m). <sup>13</sup>C-NMR (CDCl<sub>3</sub> 126 MHz) δ 155.0, 134.4, 127.3, 125.9.

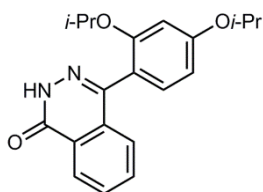


**4-(4-Chloro-phthalazin-1-yl)-benzene-1,3-diol <sup>187</sup> (32):** 1,4-Dichloro-phthalazine (**31**) (1.5 g, 7.53 mmol) was dissolved in dry DCE (35 mL) and resorcinol (753 mg, 6.85 mmol) and anhydrous aluminium trichloride (1.22 g, 9.59 mmol) were added subsequently. The reaction mixture was refluxed (80 °C) for 18 hours. The mixture was then poured into a stirring 3 M solution of HCl and crushed ice. The yellow solid thus formed was collected through suction filtration, washed with water (3x50 mL) and dried under high vacuum to afford a yellow/orange solid (1.61 g, 5.91 mmol, 78%). Characterisation data matched with the results previously reported <sup>187</sup>. <sup>1</sup>H-NMR (DMSO 500 MHz) δ 8.37 (1H, d, J = 8.1 Hz, ClCNCH), 8.20 (1H, t, J = 8.2 Hz, ClCNCHCH), 8.12 (1H, t, J = 7.1 Hz, CNCCHCH), 7.91 (1H, d, J = 7.2 Hz, CNCCH), 7.22 (1H, d, J = 8.3 Hz, C(CN)CH), 6.58 (1H, d, J = 2.2 Hz, C(OH)CHC(OH)), 6.47 (1H, dd, J = 8.3 Hz, 2.2 Hz, C(CN)CHCH). <sup>13</sup>C-NMR (DMSO 126 MHz) δ 161.1 (C(OH)CHC(OH)), 159.8 (CNN), 157.0 (C(CN)CH), 154.1 (ClCN), 135.4 (Ar-CC), 134.6 (Ar-CC), 132.7 (C(CN)CH), 129.1 (Ar-CH), 128.3 (Ar-CH), 125.9 (Ar-CH), 125.2 (Ar-CH), 111.3 (C(CN)), 107.7 (C(CN)CHCH), 103.2 (C(OH)CHC(OH)).



**1-Chloro-4-(2,4-diisopropoxy-phenyl)-phthalazine (33):**

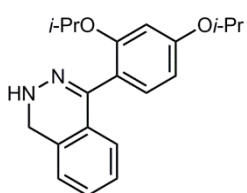
4-(4-Chloro-phthalazin-1-yl)-benzene-1,3-diol (**32**) (1.35 g, 4.77 mmol) was dissolved in dry DMF (35 mL) and anhydrous potassium carbonate (2.60 g, 19.11 mmol) was added. After 15 minutes, 2-bromo propane (1.7 mL, 19.11 mmol) was added slowly to the reaction, which was stirred at 50 °C for 18 hours. Water (70 mL) was added and extracted with ether (3x80 mL). The organic phase was then washed with brine (5x80 mL), dried over Na<sub>2</sub>SO<sub>4</sub>, filtered and concentrated to yield the desired compound as a colourless paste (1.68 g, 4.71 mmol, 98%). <sup>1</sup>H-NMR (CDCl<sub>3</sub> 500 MHz) δ 8.33 (1H, d, J = 8.3 Hz, ClCNCH), 8.00 - 7.91 (1H, m, ClCNCHCH), 7.87 - 7.80 (2H, m, CNCCH, CNCCHCH), 7.43 (1H, d, J = 8.4 Hz, C(CN)CH), 6.67 (1H, dd, J = 8.4 Hz, 2.2 Hz, C(CN)CHCH), 6.59 (1H, d, J = 2.2 Hz, C(OiPr)CHC(OiPr)), 4.66 (1H, dt, J = 12.1 Hz, 6.0 Hz, CH<sub>3</sub>CH), 4.44 (1H, dt, J = 12.1 Hz, 6.1 Hz, CH<sub>3</sub>CH), 1.46 - 1.35 (6H, m, CHCH<sub>3</sub>) 1.11 - 1.07 (6H, m, CHCH<sub>3</sub>). <sup>13</sup>C-NMR (CDCl<sub>3</sub> 126 MHz) δ 160.5 (C(OiPr)CHC(OiPr)), 159.4 (C(CN)C(OiPr)), 156.7 (CNN), 154.3 (ClCN), 132.7 (Ar-CC), 132.4 (Ar-CC), 132.1 (C(CN)CH), 128.3 (Ar-CH), 128.2 (Ar-CH), 125.6 (Ar-CH), 124.8 (Ar-CH), 118.2 (C(CN)), 107.0 (C(CN)CHCH), 102.6 (C(OiPr)CHC(OiPr)), 70.7 (CH<sub>3</sub>CH), 70.1 (CH<sub>3</sub>CH), 22.1 (2xCHCH<sub>3</sub>), 21.7 (2xCHCH<sub>3</sub>). IR (neat) ν<sub>max</sub>: 2977, 1606, 1382, 1287, 1007 cm<sup>-1</sup>. HRMS (ESI) calcd for C<sub>20</sub>H<sub>21</sub>N<sub>2</sub>NaO<sub>2</sub><sup>35</sup>Cl [M+Na]<sup>+</sup> 379.1184 m/z found 379.1169 m/z.



**4-(2,4-Diisopropoxy-phenyl)-2H-phthalazin-1-one <sup>187</sup> (34):**

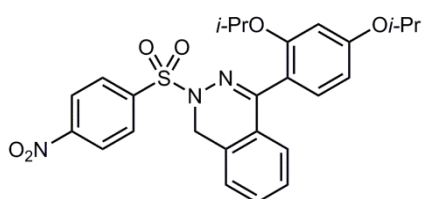
1-Chloro-4-(2,4-diisopropoxy-phenyl)-phthalazine (**33**) (500 mg, 1.40 mmol) was dissolved in glacial acetic acid (40 mL) and sodium acetate (230 mg, 2.80 mmol) was added one pot. The reaction mixture was stirred at 110 °C for 18 hours. Water (70 mL) was added to the mixture and the aqueous phase was washed with DCM (3x70 mL), dried over Na<sub>2</sub>SO<sub>4</sub>, filtered and concentrated. The residue was further dried under high vacuum to afford the product in excellent purity as a white solid (455 mg, 1.34 mmol, 96%). m.p. 182 °C. <sup>1</sup>H-NMR (CDCl<sub>3</sub> 500 MHz) δ 9.94 (1H, s, NH), 8.47 (1H, d, J = 7.9 Hz, CONHCCH), 7.82 - 7.67 (2H, m, CONHCCHCH, CNCCHCH), 7.50 (1H, d, J = 6.9 Hz, CNCCH), 7.29 (1H, d, J = 8.3 Hz, C(CN)CH) (solvent peak overlap), 6.62 (1H, dd, J = 8.4 Hz, 2.3 Hz, C(CN)CHCH), 6.57 (1H, d, J = 2.2 Hz, C(OiPr)CHC(OiPr)), 4.64 (1H, dt, J = 12.1 Hz, 6.1 Hz, CH<sub>3</sub>CH), 4.47 (1H, dt, J = 12.1 Hz, 6.1 Hz, CH<sub>3</sub>CH), 1.41 (6H, d, J = 5.4 Hz, 2xCHCH<sub>3</sub>), 1.11 (6H, d, J = 5.9 Hz, 2xCHCH<sub>3</sub>). <sup>13</sup>C-NMR

(CDCl<sub>3</sub> 126 MHz)  $\delta$  168.3 (CONH), 160.2 (C(OiPr)CHC(OiPr)), 157.0 (C(CN)C(OiPr)), 154.7 (CNNH), 132.7 (Ar-CC), 131.7 (C(CN)CH), 131.1 (Ar-CC), 130.7 (Ar-CH), 128.0 (Ar-CH), 127.7 (Ar-CH), 126.1 (Ar-CH), 117.5 (C(CN)), 106.7 (C(CN)CHCH), 102.6 (C(OiPr)CHC(OiPr)), 70.6 (CH<sub>3</sub>CH), 70.1 (CH<sub>3</sub>CH), 22.1 (CHCH<sub>3</sub>), 22.0 (CHCH<sub>3</sub>), 21.9 (CHCH<sub>3</sub>), 21.6 (CHCH<sub>3</sub>). IR (neat)  $\nu_{\max}$ : 3130, 1658, 1506, 1193, 950 cm<sup>-1</sup>. HRMS (ESI) calcd for C<sub>20</sub>H<sub>22</sub>N<sub>2</sub>NaO<sub>3</sub> [M+Na]<sup>+</sup> 361.1523 m/z found 361.1505 m/z.



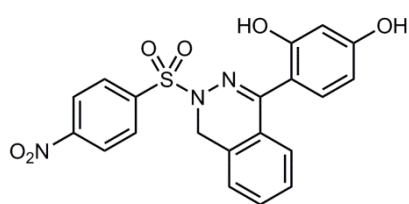
**4-(2,4-Diisopropoxy-phenyl)-1,2-dihydro-phthalazine** <sup>135</sup> **(35)**: 4-(2,4-Diisopropoxy-phenyl)-2H-phthalazin-1-one **(34)** (500 mg, 1.47 mmol) was dissolved in dry THF (30 mL) and LiAlH<sub>4</sub> (168 mg, 4.43 mmol) was added portion-wise. The reaction mixture was refluxed at 80 °C for 3

hours. Water (60 mL) was added carefully at 0 °C to quench the excess of LiAlH<sub>4</sub> and the mixture was then extracted with DCM (3x100 mL), dried over Na<sub>2</sub>SO<sub>4</sub>, filtered and concentrated. The desired amine was obtained as yellowish oil with excellent purity and it was used without any further purification (444 mg, 1.37 mmol, 93%). <sup>1</sup>H-NMR (CDCl<sub>3</sub> 500 MHz)  $\delta$  7.37 (1H, d, J = 8.4 Hz, C(CN)CH), 7.32 (1H, td, J = 7.5 Hz, 1.2 Hz, NHCH<sub>2</sub>CCHCH), 7.19 (1H, td, J = 7.6 Hz, 1.1 Hz, CNCCHCH), 7.14 (1H, d, J = 7.4 Hz, CNCCH), 6.95 (1H, d, J = 7.7 Hz, NHCH<sub>2</sub>CCH), 6.58 (1H, dd, J = 8.4 Hz, 2.3 Hz, C(CN)CHCH), 6.50 (1H, d, J = 2.3 Hz, C(OiPr)CHC(OiPr)), 6.00 (1H, s, NH), 4.60 (1H, dt, J = 12.1 Hz, 6.1 Hz, CH<sub>3</sub>CH), 4.40 (1H, dt, J = 12.1 Hz, 6.0 Hz, CH<sub>3</sub>CH), 4.26 (2H, s, NHCH<sub>2</sub>), 1.39 (6H, d, J = 6.1 Hz, 2xCHCH<sub>3</sub>), 1.08 (6H, d, J = 6.0 Hz, 2xCHCH<sub>3</sub>). <sup>13</sup>C-NMR (CDCl<sub>3</sub> 126 MHz)  $\delta$  159.4 (C(OiPr)CHC(OiPr)), 157.1 (C(CN)C(OiPr)), 157.1 (CNNH), 131.6 (Ar-CC), 131.4 (C(CN)CH), 131.3 (Ar-CC), 129.7 (Ar-CH), 127.1 (Ar-CH), 125.4 (Ar-CH), 124.5 (Ar-CH), 115.5 (C(CN)), 107.1 (C(CN)CHCH), 103.4 (C(OiPr)CHC(OiPr)), 70.6 (CH<sub>3</sub>CH), 69.9 (CH<sub>3</sub>CH), 45.7 (NHCH<sub>2</sub>), 22.1 (2xCHCH<sub>3</sub>), 21.8 (2xCHCH<sub>3</sub>). IR (neat)  $\nu_{\max}$ : 2976, 2365, 1618, 1173, 1095 cm<sup>-1</sup>. HRMS (ESI) calcd for C<sub>20</sub>H<sub>24</sub>N<sub>2</sub>NaO<sub>2</sub> [M+Na]<sup>+</sup> 347.1301 m/z found 347.1307 m/z.



**4-(2,4-Diisopropoxy-phenyl)-2-(4-nitro-benzenesulphonyl)-1,2-dihydro-phthalazine** **(36)**: 4-(2,4-Diisopropoxy-phenyl)-1,2-dihydro-phthalazine **(35)** (150 mg, 0.46 mmol) was dissolved in dry DCM (8 mL) and

TEA (128  $\mu$ L, 0.92 mmol) and DMAP (1 mg, 0.046 mmol) were added subsequently. After 5 minutes, 4-nitrobenzenesulphonyl chloride (112 mg, 0.50 mmol) was added and the reaction mixture was stirred at room temperature until the starting material was no longer detectable by TLC (16 hours). The solvent was then removed and the product was purified by direct flash column chromatography (20% ethyl acetate in petroleum ether) to afford a yellow foam (150 mg, 0.29 mmol) in 64% yield. The product was purified by direct flash column chromatography (20% ethyl acetate in petroleum ether) to afford a yellow oil in 64% yield.  $^1\text{H-NMR}$  ( $\text{CDCl}_3$  400 MHz)  $\delta$  8.40 (2H, d,  $J$  = 8.7 Hz,  $2\times\text{C}(\text{NO}_2)\text{CH}$ ), 8.26 (2H, d,  $J$  = 8.8 Hz,  $2\times\text{C}(\text{SO}_2)\text{CH}$ ), 7.47 (1H, t,  $J$  = 7.5 Hz,  $\text{NCH}_2\text{CCHCH}$ ), 7.48 (1H, d,  $J$  = 8.6 Hz,  $\text{C}(\text{CN})\text{CH}$ ), 7.31 (1H, t,  $J$  = 7.5 Hz,  $\text{CNCCHCH}$ ), 7.27 (1H, d,  $J$  = 7.6 Hz,  $\text{NCH}_2\text{CCH}$ ), 7.02 (1H, d,  $J$  = 7.6 Hz,  $\text{CNCCH}$ ), 6.68 (1H, dd,  $J$  = 2.3 Hz, 8.4 Hz,  $\text{C}(\text{CN})\text{CHCH}$ ), 6.55 (1H, d,  $J$  = 2.3 Hz,  $\text{C}(\text{OiPr})\text{CHC}(\text{OiPr})$ ), 4.65 (1H, dt,  $J$  = 13.1 Hz, 6.1 Hz,  $\text{CH}_3\text{CH}$ ), 4.53 (2H, s,  $\text{NCH}_2$ ), 4.42 (1H, dt,  $J$  = 12.8 Hz, 6.0 Hz,  $\text{CH}_3\text{CH}$ ), 1.33 (6H, d,  $J$  = 6.0 Hz,  $2\times\text{CHCH}_3$ ), 1.27 (6H, d,  $J$  = 6.0 Hz,  $2\times\text{CHCH}_3$ ).  $^{13}\text{C-NMR}$  ( $\text{CDCl}_3$  126 MHz)  $\delta$  159.6 ( $\text{C}(\text{OiPr})\text{CHC}(\text{OiPr})$ ), 158.7 ( $\text{C}(\text{CN})\text{C}(\text{OiPr})$ ), 156.9 ( $\text{CNN}$ ), 150.8 ( $\text{C}(\text{NO}_2)$ ), 140.2 ( $\text{C}(\text{SO}_2)$ ), 132.4 ( $2\times\text{Ar-CC}$ ), 132.0 ( $2\times\text{C}(\text{NO}_2)\text{CH}$ ), 130.0 ( $\text{C}(\text{CN})\text{CH}$ ), 128.6 ( $\text{Ar-CH}$ ), 128.1 ( $\text{Ar-CH}$ ), 126.5 ( $\text{Ar-CH}$ ), 124.5 ( $\text{Ar-CH}$ ), 124.4 ( $2\times\text{C}(\text{SO}_2)\text{CH}$ ), 110.0 ( $\text{C}(\text{CN})$ ), 106.9 ( $\text{C}(\text{CN})\text{CH}$ ), 104.4 ( $\text{C}(\text{OiPr})\text{CHC}(\text{OiPr})$ ), 65.8 ( $2\times\text{CH}_3\text{CH}$ ), 46.4 ( $\text{NCH}_2$ ), 15.2 ( $4\times\text{CHCH}_3$ ). IR (neat)  $\nu_{\text{max}}$ : 2979, 1648, 1522, 1374, 1136  $\text{cm}^{-1}$ . HRMS (ESI) calcd for  $\text{C}_{26}\text{H}_{27}\text{N}_3\text{NaO}_6\text{S}$   $[\text{M}+\text{Na}]^+$  532.1513  $m/z$  found 532.1504  $m/z$ .



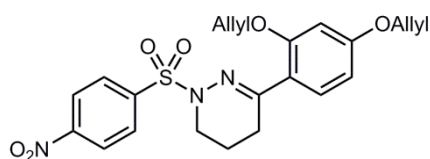
**4-[3-(4-Nitro-benzenesulphonyl)-3,4-dihydro-phthalazin-1-yl]-benzene-1,3-diol (RCZ20):**

4-(2,4-Diisopropoxyphenyl)-2-(4-nitro-benzenesulphonyl)-1,2-dihydro-phthalazine (**36**) (100 mg, 0.19 mmol) was dissolved in dry DCM (6 mL) and aluminium trichloride (157 mg, 1.17 mmol) was added. The reaction mixture was stirred at room temperature overnight. The solvent was then evaporated off under reduced pressure and the product was purified through direct flash column chromatography (50% ethyl acetate in petroleum ether) to afford **RCZ20** as a yellow foam (62 mg, 0.145 mmol, 75%). NMR, IR and mass spectrometry matches with the compound previously obtained.



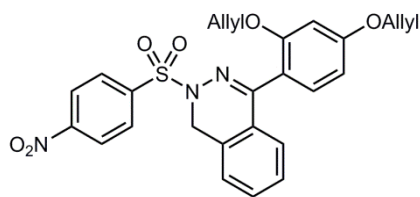
### 12.7 Procedure for allylation:

**RCZ12** or **RCZ20** (0.26 mmol) were dissolved in dry DMF (12 mL) and anhydrous potassium carbonate (0.78 mmol) was added. After 15 minutes, allyl bromide (1.06 mmol) was added slowly to the reaction, which was stirred at room temperature overnight. Water (10 mL) was added and extracted with ether (3x15 mL). The organic phase was then washed with brine (5x30 mL), dried over Na<sub>2</sub>SO<sub>4</sub>, filtered and concentrated. The product thus obtained was used in the next step without further purification.



#### **3-(2,4-Bis-allyloxy-phenyl)-1-(4-nitro-benzenesulphonyl)-1,4,5,6-tetrahydro-pyridazine (37):**

The product was obtained as a yellow oil (106 mg, 0.231 mmol, 89%). <sup>1</sup>H-NMR (CDCl<sub>3</sub> 400 MHz) δ 8.27 (2H, d, J = 8.9 Hz, 2xC(NO<sub>2</sub>)CH), 8.03 (2H, d, J = 8.9 Hz, 2xC(SO<sub>2</sub>)CH), 7.14 (1H, d, J = 8.4 Hz, C(CN)CH), 6.41 (1H, dd, J = 8.4 Hz, 2.3 Hz, C(CN)CHCH), 6.36 (1H, d, J = 2.2 Hz, C(OAllyl)CHC(OAllyl)), 5.97 (1H, ddt, J = 17.2 Hz, 10.6 Hz, 5.2 Hz, OCH<sub>2</sub>CHCH<sub>2</sub>), 5.87 (1H, ddt, J = 17.2 Hz, 10.1 Hz, 5.3 Hz, OCH<sub>2</sub>CHCH<sub>2</sub>), 5.35 (1H, dd, J = 17.2 Hz, 1.5 Hz, OCH<sub>2</sub>CHCHH (trans)), 5.23 (1H, dd, J = 9.8 Hz, 1.2 Hz, OCH<sub>2</sub>CHCHH (cis)), 5.22 (1H, dd, J = 15.6 Hz, 1.3 Hz, OCH<sub>2</sub>CHCHH (trans)), 5.15 (1H, dd, J = 10.4 Hz, 1.2 Hz, OCH<sub>2</sub>CHCHH (cis)), 4.46 (2H, dt, J = 5.4 Hz, 1.4 Hz, OCH<sub>2</sub>CHCH<sub>2</sub>), 4.39 (2H, dt, J = 5.2 Hz, 1.5 Hz, OCH<sub>2</sub>CHCH<sub>2</sub>), 3.40 (2H, t, J = 5.6 Hz, NCH<sub>2</sub>), 2.51 (2H, t, J = 6.6 Hz, CNCH<sub>2</sub>), 1.97 (2H, dddd, J = 6.6 Hz, 6.6 Hz, 5.7 Hz, 5.7 Hz, NCH<sub>2</sub>CH<sub>2</sub>). <sup>13</sup>C-NMR (CDCl<sub>3</sub> 126 MHz) δ 160.7 (C(OAllyl)CHC(OAllyl)), 157.4 (C(CN)C(OAllyl)), 154.7 (CNN), 150.3 (C(NO<sub>2</sub>)), 142.1 (C(SO<sub>2</sub>)), 132.8 (OCH<sub>2</sub>CHCH<sub>2</sub>), 132.7 (OCH<sub>2</sub>CHCH<sub>2</sub>), 130.3 (C(CN)CH), 129.7 (2xC(NO<sub>2</sub>)CH), 123.8 (2xC(SO<sub>2</sub>)CH), 118.2 (OCH<sub>2</sub>CHCH<sub>2</sub>), 117.7 (OCH<sub>2</sub>CHCH<sub>2</sub>), 105.8 (C(CN)CHCH), 100.6 (C(OAllyl)CHC(OAllyl)), 69.1 (OCH<sub>2</sub>CHCH<sub>2</sub>), 68.9 (OCH<sub>2</sub>CHCH<sub>2</sub>), 43.1 (NCH<sub>2</sub>), 26.0 (CNCH<sub>2</sub>), 18.9 (NCH<sub>2</sub>CH<sub>2</sub>). IR (neat) ν<sub>max</sub>: 2359, 1607, 1529, 1349, 930 cm<sup>-1</sup>. HRMS (ESI) calcd for C<sub>22</sub>H<sub>23</sub>N<sub>3</sub>NaO<sub>6</sub>S [M+Na]<sup>+</sup> 480.1216 m/z found 480.1231 m/z.



#### **4-(2,4-Bis-allyloxy-phenyl)-2-(4-nitro-benzenesulphonyl)-1,2-dihydro-phthalazine (38):**

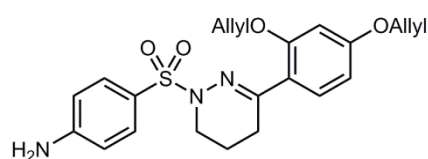
The product was obtained as a yellow oil (89 mg, 0.176 mmol, 99%). <sup>1</sup>H-NMR (CDCl<sub>3</sub> 400 MHz) δ 8.27 (2H, d, J = 9.0 Hz, 2xC(NO<sub>2</sub>)CH), 8.10 (2H, d, J = 9.0 Hz, 2xC(SO<sub>2</sub>)CH), 7.35 (1H, d, J = 8.5 Hz, C(CN)CH),



7.33 (1H, t, J = 7.7 Hz, CNCCHCH), 7.15 (2H, m, NCH<sub>2</sub>CCH, NCH<sub>2</sub>CCHCH), 6.92 (1H, d, J = 7.6 Hz, CNCCH), 6.54 (1H, dd, J = 8.5 Hz, 2.3 Hz, C(CN)CHCH), 6.42 (1H, d, J = 2.3 Hz, C(OAllyl)CHC(OAllyl)), 6.01 (1H, ddt, J = 17.2 Hz, 10.6 Hz, 5.4 Hz, OCH<sub>2</sub>CHCH<sub>2</sub>), 5.51 (1H, ddt, J = 17.1 Hz, 10.6 Hz, 4.4 Hz, OCH<sub>2</sub>CHCH<sub>2</sub>), 5.38 (1H, dq, J = 17.1 Hz, 1.5 Hz, OCH<sub>2</sub>CHCHH (trans)), 5.27 (1H, dq, J = 10.5 Hz, 1.5 Hz, OCH<sub>2</sub>CHCHH (cis)), 4.83 (1H, dq, J = 10.8 Hz, 1.6 Hz, OCH<sub>2</sub>CHCHH (cis)), 4.69 (1H, dq, J = 17.2 Hz, 1.6 Hz, OCH<sub>2</sub>CHCHH (trans)), 4.51 (2H, dt, J = 5.2 Hz, 1.5 Hz, OCH<sub>2</sub>CHCH<sub>2</sub>), 4.41 (2H, s, NCH<sub>2</sub>), 4.24 (2H, dt, J = 4.4 Hz, 1.5 Hz, OCH<sub>2</sub>CHCH<sub>2</sub>). <sup>13</sup>C-NMR (CDCl<sub>3</sub> 126 MHz) δ 161.2 (C(OAllyl)CHC(OAllyl)), 157.7 (C(CN)C(OAllyl)), 157.6 (CNN), 148.4 (C(NO<sub>2</sub>)), 141.3 (C(SO<sub>2</sub>)), 132.9 (Ar-CC), 132.3 (Ar-CC), 131.9 (OCH<sub>2</sub>CHCH<sub>2</sub>), 131.8 (OCH<sub>2</sub>CHCH<sub>2</sub>), 131.4 (C(CN)CH), 130.3 (2xC(NO<sub>2</sub>)CH), 130.1 (Ar-CH), 128.2 (Ar-CH), 127.5 (Ar-CH), 126.7 (Ar-CH), 125.4 (2xC(SO<sub>2</sub>)CH), 123.9 (C(CN)), 118.0 (OCH<sub>2</sub>CHCH<sub>2</sub>), 116.3 (OCH<sub>2</sub>CHCH<sub>2</sub>), 106.1 (C(CN)CHCH), 100.6 (C(OAllyl)CHC(OAllyl)), 69.0 (OCH<sub>2</sub>CHCH<sub>2</sub>), 68.6 (OCH<sub>2</sub>CHCH<sub>2</sub>), 45.8 (NCH<sub>2</sub>). IR (neat) ν<sub>max</sub>: 2359, 1608, 1356, 1171, 1029 cm<sup>-1</sup>. HRMS (ESI) calcd for C<sub>26</sub>H<sub>23</sub>N<sub>3</sub>NaO<sub>6</sub>S [M+Na]<sup>+</sup> 528.1200 m/z found 528.1186 m/z.

## 12.8 Procedure for nitro reduction:

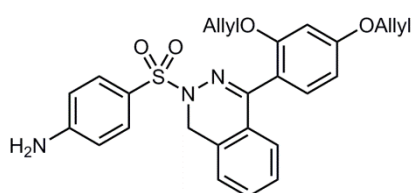
The desired bis-allyloxy derivative (0.23 mmol) was dissolved in absolute ethanol (12 mL) and iron powder (0.92 mmol) was added. A saturated solution of ammonium chloride (4 mL) was subsequently added until a white precipitate formed. The reaction mixture was then refluxed at 80 °C for 16 hours. After cooling to room temperature, the red/brown solution was filtered through a short pad of Celite and the residue washed with ethanol (25 mL) and ethyl acetate (25 mL). The solution was concentrated to dryness under reduced pressure, a mixture of DCM/water (30 mL) was added to the solid and the phases were separated. The aqueous phase was extracted with DCM (2x15 mL) and the combined organic phases were dried over Na<sub>2</sub>SO<sub>4</sub>, filtered and concentrated. The product thus obtained was used in the next step without further purification.



### 4-[3-(2,4-Bis-allyloxy-phenyl)-5,6-dihydro-4H-pyridazine-1-sulphonyl]-phenylamine (39):

The product was afforded as a yellow/brown oil (75 mg, 0.175 mmol, 85%). <sup>1</sup>H-NMR (CDCl<sub>3</sub> 400 MHz) δ 7.63 (2H, d, J = 8.7 Hz, 2xC(SO<sub>2</sub>)CH), 7.16 (1H, d, J = 8.5 Hz, C(CN)CH), 6.61 (2H, d, J = 8.7 Hz, 2xC(NH<sub>2</sub>)CH), 6.38 (1H, dd, J = 8.5 Hz, 2.3 Hz, C(CN)CHCH), 6.35 (1H, d, J = 2.3 Hz, C(OAllyl)CHC(OAllyl)), 6.01 - 5.86 (2H, m,

2xOCH<sub>2</sub>CHCH<sub>2</sub>), 5.33 (1H, dd, J = 17.2 Hz, 1.6 Hz, OCH<sub>2</sub>CHCHH (trans)), 5.25 (1H, dd, J = 16.4 Hz, 1.4 Hz, OCH<sub>2</sub>CHCHH (trans)), 5.22 (1H, dd, J = 10.4 Hz, 1.4 Hz, OCH<sub>2</sub>CHCHH (cis)), 5.17 (1H, dd, J = 10.5 Hz, 1.5 Hz, OCH<sub>2</sub>CHCHH (cis)), 4.45 (2H, dt, J = 6.5 Hz, 1.4 Hz, OCH<sub>2</sub>CHCH<sub>2</sub>), 4.39 (2H, dt, J = 5.0 Hz, 1.4 Hz, OCH<sub>2</sub>CHCH<sub>2</sub>), 4.03 (2H, s, NH<sub>2</sub>), 3.29 (2H, t, J = 5.6 Hz, NCH<sub>2</sub>), 2.48 (2H, t, J = 6.7 Hz, CNCH<sub>2</sub>), 1.94 (2H, dddd, J = 6.7 Hz, 6.7 Hz, 5.6 Hz, 5.6 Hz, NCH<sub>2</sub>CH<sub>2</sub>). <sup>13</sup>C-NMR (CDCl<sub>3</sub> 126 MHz) δ 160.3 (C(OAllyl)CHC(OAllyl)), 157.6 (C(CN)C(OAllyl)), 153.3 (CNN), 150.6 (C(NH<sub>2</sub>)), 133.0 (OCH<sub>2</sub>CHCH<sub>2</sub>), 132.9 (OCH<sub>2</sub>CHCH<sub>2</sub>), 130.7 (C(SO<sub>2</sub>)), 130.6 (2xC(SO<sub>2</sub>)CH), 121.4 (C(CN)CH), 117.8 (OCH<sub>2</sub>CHCH<sub>2</sub>), 117.6 (OCH<sub>2</sub>CHCH<sub>2</sub>), 113.9 (C(CN)), 113.7 (2xC(NH<sub>2</sub>)CH), 105.9 (C(CN)CHCH), 100.6 (C(OAllyl)CHC(OAllyl)), 69.3 (OCH<sub>2</sub>CHCH<sub>2</sub>), 68.9 (OCH<sub>2</sub>CHCH<sub>2</sub>), 43.1 (NCH<sub>2</sub>), 25.8 (CNCH<sub>2</sub>), 19.2 (NCH<sub>2</sub>CH<sub>2</sub>). IR (neat) ν<sub>max</sub>: 3451, 2390, 1616, 1189, 1054 cm<sup>-1</sup>. HRMS (ESI) calcd for C<sub>22</sub>H<sub>25</sub>N<sub>3</sub>NaO<sub>4</sub>S [M+Na]<sup>+</sup> 450.1554 m/z found 450.1576 m/z.



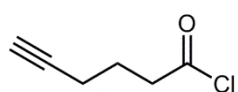
#### 4-[4-(2,4-Bis-allyloxy-phenyl)-1H-phthalazine-2-

sulphonyl]-phenylamine (40): The product was afforded

as a yellow/brown oil (81 mg, 0.170 mmol, 99%). <sup>1</sup>H-NMR (CDCl<sub>3</sub> 400 MHz) δ 7.67 (2H, d, J = 8.6 Hz,

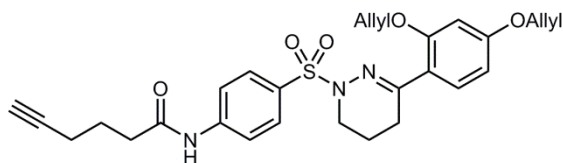
2xC(SO<sub>2</sub>)CH), 7.37 (1H, d, J = 8.3 Hz, C(CN)CH), 7.28 (1H, t, J = 7.4 Hz, NCH<sub>2</sub>CCHCH), 7.17 - 7.11 (2H, m, NCH<sub>2</sub>CCH, CNCCHCH), 6.89 (1H, d, J = 7.6 Hz, CNCCH), 6.58 (2H, d, J = 8.7 Hz, 2xC(NH<sub>2</sub>)CH), 6.52 (1H, dd, J = 8.3 Hz, 2.3 Hz, C(CN)CHCH), 6.42 (1H, d, J = 2.3 Hz, C(OAllyl)CHC(OAllyl)), 6.01 (1H, ddt, J = 17.1 Hz, 10.5 Hz, 5.6 Hz, OCH<sub>2</sub>CHCH<sub>2</sub>), 5.54 (1H, ddt, J = 17.2 Hz, 10.6 Hz, 4.8 Hz, OCH<sub>2</sub>CHCH<sub>2</sub>), 5.37 (1H, dd, J = 17.2 Hz, 1.4 Hz, OCH<sub>2</sub>CHCHH (trans)), 5.25 (1H, dd, J = 10.5 Hz, 1.4 Hz, OCH<sub>2</sub>CHCHH (cis)), 4.85 (1H, dd, J = 10.6 Hz, 1.6 Hz, OCH<sub>2</sub>CHCHH (cis)), 4.75 (1H, dd, J = 17.2 Hz, 1.5 Hz, OCH<sub>2</sub>CHCHH (trans)), 4.50 (2H, dt, J = 5.4 Hz, 1.4 Hz, OCH<sub>2</sub>CHCH<sub>2</sub>), 4.30 (2H, s, NCH<sub>2</sub>), 4.25 (2H, dt, J = 4.5 Hz, 1.4 Hz, OCH<sub>2</sub>CHCH<sub>2</sub>), 4.03 (2H, s, NH<sub>2</sub>). <sup>13</sup>C-NMR (CDCl<sub>3</sub> 126 MHz) δ 160.8 (C(OAllyl)CHC(OAllyl)), 157.7 (C(CN)C(OAllyl)), 152.7 (CNN), 150.9 (C(NH<sub>2</sub>)), 133.0 (Ar-CC), 132.5 (2xC(SO<sub>2</sub>)CH), 132.1 (OCH<sub>2</sub>CHCH<sub>2</sub>), 131.2 (OCH<sub>2</sub>CHCH<sub>2</sub>), 130.9 (C(SO<sub>2</sub>)), 130.8 (Ar-CC), 127.7 (Ar-CH), 126.6 (Ar-CH), 126.3 (Ar-CH), 125.3 (Ar-CH), 118.0 (OCH<sub>2</sub>CHCH<sub>2</sub>), 117.9 (OCH<sub>2</sub>CHCH<sub>2</sub>), 116.4 (C(CN)), 113.8 (2xC(NH<sub>2</sub>)CH), 106.1 (C(CN)CHCH), 100.8 (C(OAllyl)CHC(OAllyl)), 69.0 (OCH<sub>2</sub>CHCH<sub>2</sub>), 68.8 (OCH<sub>2</sub>CHCH<sub>2</sub>), 45.7 (NCH<sub>2</sub>). IR (neat) ν<sub>max</sub>: 3374, 2359, 1623, 1594, 1163 cm<sup>-1</sup>. HRMS (ESI) calcd for C<sub>26</sub>H<sub>25</sub>N<sub>3</sub>NaO<sub>4</sub>S [M+Na]<sup>+</sup> 498.1458 m/z found 498.1444 m/z.

### 12.9 Procedure for hex-5-ynoyl chloride coupling:



**Hex-5-ynoyl Chloride:** Hex-5-ynoic acid (0.495 mL, 4.45 mmol) was dissolved in dry DCM (20 mL) and two drops of dry DMF were added. Oxalyl chloride (0.421 mL, 4.90 mmol) was added drop-wise at 0 °C through 10 minutes. The reaction mixture was then allowed to stir at room temperature until the carbon dioxide bubbling ceased (2 hours). The solution was then concentrated under reduced pressure to afford a red oil which was used immediately for the next step.

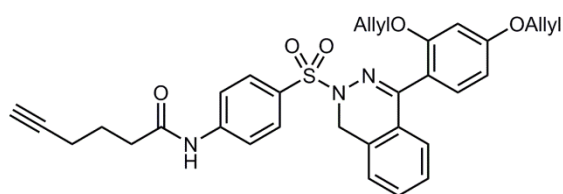
The desired aniline derivative (0.60 mmol) was dissolved in dry DCM (10 mL) and anhydrous pyridine (0.64 mmol) was added. After 10 minutes, a freshly prepared solution of hex-5-ynoyl chloride (0.32 mmol) in dry DCM (3 mL) was added slowly. The reaction mixture was allowed to stir at room temperature for 3 hours. The solvent was evaporated off under reduced pressure and the product was purified through direct flash column chromatography.



**Hex-5-ynoic acid {4-[3-(2,4-bis-allyloxy-phenyl)-5,6-dihydro-4H-pyridazine-1-sulphonyl]-phenyl}-amide (RCZ12 Synthon):**

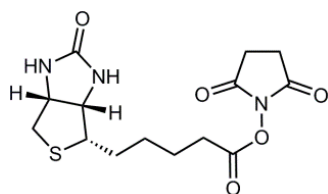
The product was purified through direct flash column chromatography (30% ethyl acetate in petroleum ether) to afford a colourless oil (75 mg, 0.143 mmol, 89%). <sup>1</sup>H-NMR (CDCl<sub>3</sub> 400 MHz) δ 7.90 (2H, d, J = 8.6 Hz, 2xC(CONH)CH), 7.69 (2H, d, J = 8.6 Hz, 2xC(SO<sub>2</sub>)CH), 7.39 (1H, s, CONH), 7.23 (1H, d, J = 8.5 Hz, C(CN)CH), 6.48 (1H, dd, J = 8.5 Hz, 2.3 Hz, C(CN)CHCH), 6.44 (1H, d, J = 2.3 Hz, C(OAllyl)CHC(OAllyl)), 6.06 (1H, ddt, J = 15.8 Hz, 10.6 Hz, 5.6 Hz, OCH<sub>2</sub>CHCH<sub>2</sub>), 5.98 (1H, ddt, J = 15.9 Hz, 10.8 Hz, 5.6 Hz, OCH<sub>2</sub>CHCH<sub>2</sub>), 5.42 (1H, dd, J = 17.2 Hz, 1.5 Hz, OCH<sub>2</sub>CHCHH (trans)), 5.33 (1H, dd, J = 17.2 Hz, 1.5 Hz, OCH<sub>2</sub>CHCHH (trans)), 5.30 (1H, dd, J = 10.6 Hz, 1.5 Hz, OCH<sub>2</sub>CHCHH (cis)), 5.25 (1H, dd, J = 10.5 Hz, 1.3 Hz, OCH<sub>2</sub>CHCHH (cis)), 4.55 (2H, dt, J = 5.5 Hz, 1.3 Hz, OCH<sub>2</sub>CHCH<sub>2</sub>), 4.48 (2H, dt, J = 5.2 Hz, 1.3 Hz, OCH<sub>2</sub>CHCH<sub>2</sub>), 3.42 (2H, t, J = 5.6 Hz, NCH<sub>2</sub>), 2.67 (2H, t, J = 7.4 Hz, CONHCH<sub>2</sub>), 2.54 (2H, t, J = 7.3 Hz, CNCH<sub>2</sub>), 2.05 - 1.95 (5H, m, CCH, CHCCH<sub>2</sub>, CHCCH<sub>2</sub>CH<sub>2</sub>), 1.89 (2H, dddd, J = 7.3 Hz, 7.3 Hz, 5.9 Hz, 5.9 Hz, NCH<sub>2</sub>CH<sub>2</sub>). <sup>13</sup>C-NMR (CDCl<sub>3</sub> 126 MHz) δ 166.8 (CONH), 160.7 (C(OAllyl)CHC(OAllyl)), 160.4 (C(CN)C(OAllyl)), 157.8 (CNN), 153.8 (C(CONH)), 149.4

(C(SO<sub>2</sub>)), 133.0 (OCH<sub>2</sub>CHCH<sub>2</sub>), 132.8 (OCH<sub>2</sub>CHCH<sub>2</sub>), 130.6 (2xC(SO<sub>2</sub>)CH), 129.8 (C(CN)CH), 118.9 (OCH<sub>2</sub>CHCH<sub>2</sub>), 117.9 (OCH<sub>2</sub>CHCH<sub>2</sub>), 117.6 (2xC(CONH)CH), 105.9 (C(CN)CHCH), 100.6 (C(OAllyl)CHC(OAllyl)), 91.1 (CHCCH<sub>2</sub>), 69.2 (OCH<sub>2</sub>CHCH<sub>2</sub>), 68.9 (OCH<sub>2</sub>CHCH<sub>2</sub>), 60.5 (CHCCH<sub>2</sub>), 43.1 (NCH<sub>2</sub>), 31.8 (CONHCH<sub>2</sub>), 25.9 (CNCH<sub>2</sub>), 23.6 (CONHCH<sub>2</sub>CH<sub>2</sub>), 23.3 (CHCCH<sub>2</sub>), 17.7 (NCH<sub>2</sub>CH<sub>2</sub>). IR (neat)  $\nu_{\text{max}}$ : 3209, 2357, 1701, 1590, 1166 cm<sup>-1</sup>. HRMS (ESI) calcd for C<sub>28</sub>H<sub>31</sub>N<sub>3</sub>NaO<sub>5</sub>S [M+Na]<sup>+</sup> 544.1919 m/z found 544.1922 m/z.



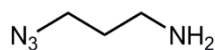
**Hex-5-ynoic acid [4-[4-(2,4-bis-allyloxy-phenyl)-1H-phthalazine-2-sulphonyl]-phenyl]-amide (RCZ20 Synthone):** The product

was purified through direct flash column chromatography (30% ethyl acetate in petroleum ether) to afford a colourless oil (61 mg, 0.107 mmol, 73%). <sup>1</sup>H-NMR (CDCl<sub>3</sub> 400 MHz)  $\delta$  7.94 (2H, d, J = 8.8 Hz, 2xC(CONH)CH), 7.68 (2H, d, J = 8.8 Hz, 2xC(SO<sub>2</sub>)CH), 7.51 (1H, s, NH), 7.45 (1H, d, J = 8.1 Hz, C(CN)CH), 7.40 (1H, t, J = 7.2 Hz, NCH<sub>2</sub>CCHCH), 7.23 (2H, m, NCH<sub>2</sub>CCH, CNCCHCH), 7.00 (1H, d, J = 7.2 Hz, CNCCH), 6.62 (1H, dd, J = 8.3 Hz, 2.1 Hz, C(CN)CHCH), 6.51 (1H, d, J = 2.1 Hz, C(OAllyl)CHC(OAllyl)), 6.11 (1H, ddt, J = 17.2 Hz, 10.6 Hz, 5.4 Hz, OCH<sub>2</sub>CHCH<sub>2</sub>), 5.62 (1H, ddt, J = 17.2 Hz, 10.5 Hz, 4.7 Hz, OCH<sub>2</sub>CHCH<sub>2</sub>), 5.48 (1H, dq, J = 17.3 Hz, 1.6 Hz, OCH<sub>2</sub>CHCHH (trans)), 5.36 (1H, dq, J = 10.5 Hz, 1.4 Hz, OCH<sub>2</sub>CHCHH (cis)), 4.94 (1H, dq, J = 10.6 Hz, 1.6 Hz, OCH<sub>2</sub>CHCHH (cis)), 4.82 (1H, dq, J = 17.2 Hz, 1.6 Hz, OCH<sub>2</sub>CHCHH (trans)), 4.60 (2H, dt, J = 5.6 Hz, 1.4 Hz, OCH<sub>2</sub>CHCH<sub>2</sub>), 4.45 (2H, s, NCH<sub>2</sub>), 4.34 (2H, dt, J = 4.7 Hz, 1.6 Hz, OCH<sub>2</sub>CHCH<sub>2</sub>), 2.57 (2H, t, J = 7.2 Hz, CONHCH<sub>2</sub>), 2.34 (2H, dt, J = 6.7 Hz, 2.7 Hz, CHCCH<sub>2</sub>), 2.03 (1H, t, J = 2.6 Hz, CCH), 1.96 (2H, quint., J = 7.0 Hz, CONHCH<sub>2</sub>CH<sub>2</sub>). <sup>13</sup>C-NMR (CDCl<sub>3</sub> 126 MHz)  $\delta$  170.9 (CONH), 160.9 (C(OAllyl)CHC(OAllyl)), 157.7 (C(CN)C(OAllyl)), 153.5 (CNN), 142.4 (C(CONH)), 133.0 (C(SO<sub>2</sub>)), 132.4 (C(CN)CH), 132.0 (Ar-CC), 131.1 (OCH<sub>2</sub>CHCH<sub>2</sub>), 130.6 (OCH<sub>2</sub>CHCH<sub>2</sub>), 130.3 (2xC(SO<sub>2</sub>)CH), 130.0 (Ar-CC), 127.9 (Ar-CH), 126.5 (Ar-CH), 126.4 (Ar-CH), 125.3 (Ar-CH), 119.0 (C(CN)), 118.0 (OCH<sub>2</sub>CHCH<sub>2</sub>), 117.6 (OCH<sub>2</sub>CHCH<sub>2</sub>), 116.4 (2xC(CONH)CH), 106.0 (C(CN)CHCH), 100.7 C(OAllyl)CHC(OAllyl)), 83.2 (CHCCH<sub>2</sub>), 69.5 (OCH<sub>2</sub>CHCH<sub>2</sub>), 69.0 (OCH<sub>2</sub>CHCH<sub>2</sub>), 68.7 (CHCCH<sub>2</sub>), 45.8 (NCH<sub>2</sub>), 35.9 (CONHCH<sub>2</sub>), 23.6 (CHCCH<sub>2</sub>), 17.7 (CONHCH<sub>2</sub>CH<sub>2</sub>). IR (neat)  $\nu_{\text{max}}$ : 3298, 2924, 2360, 1606, 1166 cm<sup>-1</sup>. HRMS (ESI) calcd for C<sub>32</sub>H<sub>31</sub>N<sub>3</sub>NaO<sub>5</sub>S [M+Na]<sup>+</sup> 592.1877 m/z found 592.1854 m/z.



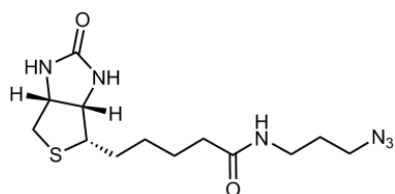
**(+)-Biotin N-succinimidyl ester**<sup>140</sup> **(41)**: (+)-Biotin (600 mg, 2.45 mmol) was dissolved in dry DMF (10 mL) and EDC (370 mg, 3.68 mmol) and NHS (424 mg, 3.68 mmol) were added subsequently. The reaction mixture was allowed to stir at room

temperature overnight. The solution was then poured into ice and the white precipitate formed was filtered by suction filtration. The solid thus obtained was dried under high vacuum to afford an off-white powder (520 mg, 1.52 mmol, 62%), which matched all the analytical data of previously reported characterisation<sup>140</sup>. <sup>1</sup>H-NMR (MeOD 400 MHz)  $\delta$  4.52 (1H, dd,  $J$  = 8.0 Hz, 5.1 Hz), 4.35 (1H, dd,  $J$  = 7.8 Hz, 4.9 Hz), 3.27 - 3.22 (1H, m), 2.96 (1H, dd,  $J$  = 12.5 Hz, 4.7 Hz), 2.86 (4H, s), 2.73 (1H, d,  $J$  = 12.5 Hz), 2.69 (2H, t,  $J$  = 6.8 Hz), 1.86 - 1.78 (3H, m), 1.68 - 1.56 (3H, m). <sup>13</sup>C-NMR (MeOD 126 MHz)  $\delta$ , 170.6, 169.1, 163.1, 61.8, 59.7, 55.6, 31.4, 28.9, 28.1, 25.0, 24.1.



**3-Azidopropylamine**<sup>188</sup> **(43)**: 3-Chloropropylamine hydrochloride **(42)** (1.12 g, 8.62 mmol) was dissolved in water (25 mL) and sodium azide

(1.68 g, 25.8 mmol) was added at room temperature. The reaction mixture was stirred at 80 °C overnight and then sodium hydroxide (pellets) (5 g) was added to basify the solution. The basic aqueous layer was extracted with diethyl ether (3x30 mL) and the organic phase was dried over Na<sub>2</sub>SO<sub>4</sub>, filtered and concentrated, to afford 3-azidopropylamine as a yellowish liquid (450 mg, 4.510 mmol, 52%). <sup>1</sup>H-NMR (CDCl<sub>3</sub> 400 MHz)  $\delta$  3.30 (2H, t,  $J$  = 6.4 Hz), 2.73 (2H, t,  $J$  = 6.4 Hz), 1.66 (2H, quint.,  $J$  = 6.4 Hz). <sup>13</sup>C-NMR (CDCl<sub>3</sub> 126 MHz)  $\delta$  49.1, 39.3, 32.4.



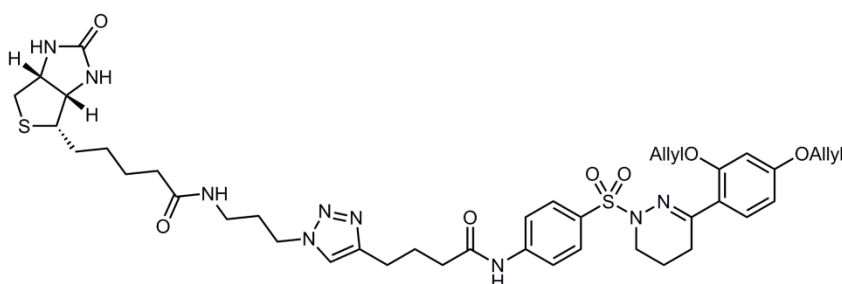
**5-(2-Oxo-hexahydro-thieno[3,4-d]imidazol-4-yl)-pentanoic acid (3-azido-propyl)-amide (Biotin Synthon)**: 3-Azidopropylamine **(43)** (112 mg, 1.12 mmol) was dissolved in dry methanol (8 mL). TEA (0.234 mL, 1.68 mmol) was

added at room temperature and then (+)-biotin N-succinimidyl ester (200 mg, 0.56 mmol) was added one pot. The reaction mixture was stirred at room temperature for 24 hours. The solvent was removed under reduced pressure and the residue was directly

chromatographed (from 0% to 10% methanol in ethyl acetate) to afford a white solid (185 mg, 0.567 mmol, 91%). The compound obtained matched the known characterisation data previously reported <sup>189</sup>. <sup>1</sup>H-NMR (MeOD 400 MHz)  $\delta$  4.50 (1H, dd, J = 7.8 Hz, 4.9 Hz, CONHCH), 4.32 (1H, dd, J = 8.0 Hz, 4.5 Hz, CONHCH), 3.37 (2H, t, J = 6.7 Hz, CONHCH<sub>2</sub>), 3.26 (2H, t, J = 6.7 Hz, N<sub>3</sub>CH<sub>2</sub>), 3.22 - 3.19 (1H, m, SCH), 2.94 (1H, dd, J = 12.6 Hz, 4.9 Hz, SCHH), 2.72 (1H, d, J = 12.6 Hz, SCHH), 2.22 (2H, t, J = 7.5 Hz, CONHCH<sub>2</sub>), 1.80 - 1.58 (6H, m, N<sub>3</sub>CH<sub>2</sub>CH<sub>2</sub>, SCHCH<sub>2</sub>, SCHCH<sub>2</sub>CH<sub>2</sub>), 1.45 (2H, quint., J = 7.5 Hz, CONHCH<sub>2</sub>CH<sub>2</sub>). <sup>13</sup>C-NMR (MeOD 126 MHz)  $\delta$  175.2 (CONH), 172.6 (CONH), 61.8 (CONHCH), 59.9 (CONHCH), 55.3 (SCH), 51.3 (CONHCH<sub>2</sub>), 39.9 (SCH<sub>2</sub>), 38.2 (CONHCH<sub>2</sub>), 35.6 (N<sub>3</sub>CH<sub>2</sub>), 28.7 (N<sub>3</sub>CH<sub>2</sub>CH<sub>2</sub>), 28.0 (SCHCH<sub>2</sub>), 25.4 (SCHCH<sub>2</sub>CH<sub>2</sub>), 24.7 (CONHCH<sub>2</sub>CH<sub>2</sub>). IR (neat)  $\nu_{\text{max}}$ : 3025, 2359, 2100, 1678, 1465 cm<sup>-1</sup>. HRMS (ESI) calcd for C<sub>13</sub>H<sub>22</sub>N<sub>6</sub>NaO<sub>2</sub>S [M+Na]<sup>+</sup> 349.1417 m/z found 349.1415 m/z.

#### 12.10 Procedure for click reaction (Biotin Labelling):

Oxo-hexahydro-thieno[3,4-d]imidazol-4-yl)-pentanoic acid (3-azido-propyl)-amide (**Biotin Synthron**) (0.09 mmol) and the desired alkyne derivative (**RCZ Synthron**) (0.11 mmol) were dissolved in a 3:1 mixture of THF:H<sub>2</sub>O (4 mL) and copper(II)sulfate (0.10 mmol) and sodium-(L)-ascorbate (0.21 mmol) were added subsequently to the solution. The reaction mixture was stirred at 50 °C for 18 hours. Solvents were removed under reduced pressure and the crude was purified through flash column chromatography

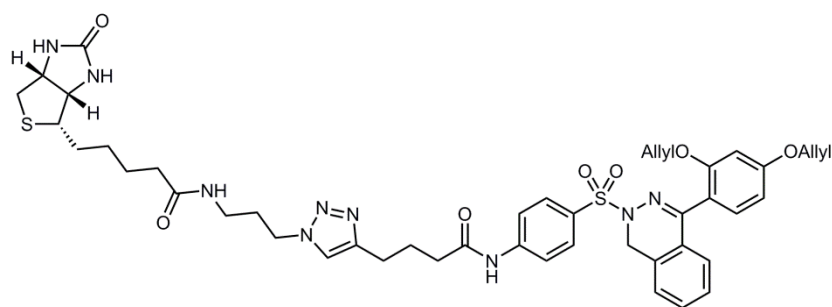


5-(2-Oxo-hexahydro-thieno[3,4-d]imidazol-4-yl)-pentanoic acid {3-[4-(3-{4-[3-(2,4-bis-allyloxy-phenyl)-5,6-

dihydro-4H-pyridazine-1-sulphonyl]-phenylcarbamoyl)-propyl)-[1,2,3]triazol-1-yl]-propyl)-

amide (**44**): The product was purified through flash column chromatography (from 0% to 5% methanol in DCM) to afford a colourless foam (69 mg, 0.081 mmol, 90%). <sup>1</sup>H-NMR (MeOD 400 MHz)  $\delta$  7.80 (5H, m, 2xC(CONH)CH, 2xC(SO<sub>2</sub>)CH, NCHC), 7.10 (1H, d, J = 8.2 Hz,

C(CN)CH), 6.54 - 6.51 (2H, m, C(CN)CHCH, C(OAllyl)CHC(OAllyl)), 6.06 (1H, ddt,  $J = 17.3$  Hz, 10.5 Hz, 5.2 Hz, OCH<sub>2</sub>CHCH<sub>2</sub>), 5.98 (1H, ddt,  $J = 17.2$  Hz, 10.4 Hz, 5.1 Hz, OCH<sub>2</sub>CHCH<sub>2</sub>), 5.40 (1H, dq,  $J = 17.2$  Hz, 1.5 Hz, OCH<sub>2</sub>CHCHH (trans)), 5.30 (1H, dq,  $J = 17.2$  Hz, 1.6 Hz, OCH<sub>2</sub>CHCHH (trans)), 5.27 (1H, dq,  $J = 10.5$  Hz, 1.5 Hz, OCH<sub>2</sub>CHCHH (cis)), 5.21 (1H, dq,  $J = 10.6$  Hz, 1.6 Hz, OCH<sub>2</sub>CHCHH (cis)), 4.55 (2H, dt,  $J = 5.2$  Hz, 1.6 Hz, OCH<sub>2</sub>CHCH<sub>2</sub>), 4.50 (2H, dt,  $J = 5.0$  Hz, 1.5 Hz, OCH<sub>2</sub>CHCH<sub>2</sub>), 4.48 (1H, dd,  $J = 7.8$  Hz, 4.2 Hz, CONHCH), 4.40 (2H, t,  $J = 6.8$  Hz, NNNCH<sub>2</sub>), 4.29 (1H, dd,  $J = 7.7$  Hz, 4.3 Hz, CONHCH), 3.38 (2H, t,  $J = 5.6$  Hz, CONHCH<sub>2</sub>), 3.21 - 3.16 (3H, m, NCH<sub>2</sub>, SCH), 2.91 (1H, dd,  $J = 12.7$  Hz, 4.9 Hz, SCHH), 2.80 (2H, t,  $J = 7.3$  Hz, NNNCCH<sub>2</sub>), 2.70 (1H, d,  $J = 12.7$  Hz, SCHH), 2.54 (2H, t,  $J = 6.6$  Hz, COCH<sub>2</sub>), 2.47 (2H, t,  $J = 7.3$  Hz, CNCH<sub>2</sub>), 2.21 (2H, t,  $J = 7.3$  Hz, COCH<sub>2</sub>), 2.11 - 1.98 (4H, m, NCH<sub>2</sub>CH<sub>2</sub>, COCH<sub>2</sub>CH<sub>2</sub>), 1.75 - 1.55 (6H, m, 3xCH<sub>2</sub>CH<sub>2</sub>CH<sub>2</sub>), 1.44 (2H, quint.,  $J = 7.5$  Hz, CONHCH<sub>2</sub>CH<sub>2</sub>). <sup>13</sup>C-NMR (MeOD 126 MHz)  $\delta$  174.7 (CONH), 172.8 (CONH), 164.6 (CONH), 160.6 (C(OAllyl)CHC(OAllyl)), 157.4 (C(CN)C(OAllyl)), 155.1 (CNN), 143.4 (C(CONH)), 133.3 (OCH<sub>2</sub>CHCH<sub>2</sub>), 133.0 (OCH<sub>2</sub>CHCH<sub>2</sub>), 129.9 (C(SO<sub>2</sub>)), 129.7 (NNNCHCCH<sub>2</sub>), 129.2 (2xC(SO<sub>2</sub>)CH), 128.9 (NNNCHCCH<sub>2</sub>), 122.2 (C(CN)CH), 120.9 (2xC(CONH)CH), 118.8 (C(CN)), 116.3 (OCH<sub>2</sub>CHCH<sub>2</sub>), 116.2 (OCH<sub>2</sub>CHCH<sub>2</sub>), 106.0 (C(CN)CHCH), 100.2 (C(OAllyl)CHC(OAllyl)), 68.9 (OCH<sub>2</sub>CHCH<sub>2</sub>), 68.5 (OCH<sub>2</sub>CHCH<sub>2</sub>), 61.9 (CONHCH), 60.2 (CONHCH), 55.5 (SCH), 43.2 (NCH<sub>2</sub>), 39.6 (SCH<sub>2</sub>), 35.9 (NNNCH<sub>2</sub>), 35.7 (CONHCH<sub>2</sub>), 35.3 (CONHCH<sub>2</sub>), 29.6 (SCHCH<sub>2</sub>), 28.3 (NNNCCH<sub>2</sub>), 28.0 (SCHCH<sub>2</sub>CH<sub>2</sub>), 25.8 (CH<sub>2</sub>CH<sub>2</sub>CH<sub>2</sub>), 25.3 (CH<sub>2</sub>CH<sub>2</sub>CH<sub>2</sub>), 24.8 (CH<sub>2</sub>CH<sub>2</sub>CH<sub>2</sub>), 24.2 (CNCH<sub>2</sub>), 18.6 (NCH<sub>2</sub>CH<sub>2</sub>). IR (neat)  $\nu_{\max}$ : 3311, 2391, 2060, 1684, 1162 cm<sup>-1</sup>. HRMS (ESI) calcd for C<sub>41</sub>H<sub>53</sub>N<sub>9</sub>NaO<sub>7</sub>S<sub>2</sub> [M+Na]<sup>+</sup> 870.3402 m/z found 870.3380 m/z.



**5-(2-Oxo-hexahydro-thieno[3,4-d]imidazol-4-yl)-pentanoic acid {3-[4-(3-[4-(4-(2,4-bis-allyloxy-phenyl)-1H-phthalazine-2-**

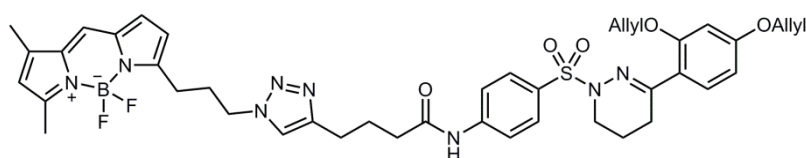
**sulphonyl]-phenylcarbamoyl}-propyl)-[1,2,3]triazol-1-yl)-propyl)-amide (45):** The product was purified through flash column chromatography (from 0% to 5% methanol in DCM) to afford a colourless foam (40 mg, 0.044 mmol, 45%). <sup>1</sup>H-NMR (Acetone 400 MHz)  $\delta$  9.95 (1H, s, CONH), 7.92 (2H, d,  $J = 9.0$  Hz, 2xC(CONH)CH), 7.88 (2H, d,  $J = 8.9$  Hz, 2xC(SO<sub>2</sub>)CH),

7.80 (1H, s, NNNCH), 7.49 (1H, t, J = 7.3 Hz, NCH<sub>2</sub>CCHCH), 7.44 (1H, d, J = 7.1 Hz, NCH<sub>2</sub>CCH), 7.39 (1H, d, J = 8.2 Hz, C(CN)CH), 7.32 (1H, t, J = 7.5 Hz, CNCCHCH), 7.00 (1H, d, J = 7.5 Hz, CNCCH), 6.73 (1H, dd, J = 8.2 Hz, 2.3 Hz, C(CN)CHCH), 6.67 (1H, d, J = 2.2 Hz, C(OAllyl)CHC(OAllyl)), 6.14 (1H, ddt, J = 17.2 Hz, 10.5 Hz, 5.2 Hz, OCH<sub>2</sub>CHCH<sub>2</sub>), 5.99 (1H, s, CONH), 5.78 (1H, s, CONH), 5.63 (1H, ddt, J = 17.2 Hz, 10.8 Hz, 4.7 Hz, OCH<sub>2</sub>CHCH<sub>2</sub>), 5.48 (1H, dq, J = 17.2 Hz, 1.6 Hz, OCH<sub>2</sub>CHCHH (trans)), 5.31 (1H, dq, J = 10.5 Hz, 1.6 Hz, OCH<sub>2</sub>CHCHH (cis)), 4.88 (1H, dq, J = 10.6 Hz, 1.7 Hz, OCH<sub>2</sub>CHCHH (cis)), 4.82 (1H, dq, J = 17.3 Hz, 1.8 Hz, OCH<sub>2</sub>CHCHH (trans)), 4.68 (2H, dt, J = 5.4 Hz, 1.6 Hz, OCH<sub>2</sub>CHCH<sub>2</sub>), 4.54 - 4.50 (1H, m, CONHCH), 4.47 (2H, s, NCH<sub>2</sub>), 4.44 - 4.39 (4H, m, OCH<sub>2</sub>CHCH<sub>2</sub>, NNNCH<sub>2</sub>), 4.37 - 4.32 (1H, m, CONHCH), 3.23 - 3.15 (5H, m, NCH<sub>2</sub>, SCH, CONHCH<sub>2</sub>), 2.94 (1H, dd, J = 12.5 Hz, 4.9 Hz, SCHH), 2.75 (2H, t, J = 7.1 Hz, NNNCCH<sub>2</sub>), 2.71 (1H, d, J = 12.5 Hz, SCHH), 2.45 (2H, t, J = 7.3 Hz, COCH<sub>2</sub>), 2.22 (2H, t, J = 7.0 Hz, COCH<sub>2</sub>), 2.03 (2H, quint., J = 7.0 Hz, COCH<sub>2</sub>CH<sub>2</sub>), 1.86 - 1.40 (8H, m, 3xCH<sub>2</sub>CH<sub>2</sub>CH<sub>2</sub>, CONHCH<sub>2</sub>CH<sub>2</sub>). <sup>13</sup>C-NMR (Acetone 126 MHz) δ 172.8 (CONH), 171.6 (CONH), 164.0 (CONH), 161.1 (C(OAllyl)CHC(OAllyl)), 157.8 (C(CN)C(OAllyl)), 156.9 (CNN), 146.4 (C(CONH)), 146.2 (NNNCCH<sub>2</sub>), 144.4 (Ar-CC), 133.6 (C(SO<sub>2</sub>)), 132.8 (NNNCH), 131.5 (C(CN)CH), 131.2 (OCH<sub>2</sub>CHCH<sub>2</sub>), 131.1 (OCH<sub>2</sub>CHCH<sub>2</sub>), 129.9 (2xC(SO<sub>2</sub>)CH), 128.8 (Ar-CC), 128.0 (Ar-CH), 126.5 (Ar-CH), 126.0 (Ar-CH), 125.5 (Ar-CH), 121.9 (C(CONH)CH), 118.5 (OCH<sub>2</sub>CHCH<sub>2</sub>), 118.4 (OCH<sub>2</sub>CHCH<sub>2</sub>), 116.7 (C(CONH)CH), 115.6 (C(CN)), 106.5 (C(CN)CHCH), 100.4 (C(OAllyl)CHC(OAllyl)), 68.6 (OCH<sub>2</sub>CHCH<sub>2</sub>), 68.4 (OCH<sub>2</sub>CHCH<sub>2</sub>), 61.4 (CONHCH), 60.0 (CONHCH), 55.4 (SCH), 47.1 (SCH<sub>2</sub>), 45.9 (NCH<sub>2</sub>), 40.1 (NNNCH<sub>2</sub>), 35.8 (CONHCH<sub>2</sub>), 35.7 (CONHCH<sub>2</sub>), 35.3 (SCHCH<sub>2</sub>), 30.1 (NNNCCH<sub>2</sub>), 28.0 (SCHCH<sub>2</sub>CH<sub>2</sub>), 25.4 (CH<sub>2</sub>CH<sub>2</sub>CH<sub>2</sub>), 24.8 (CH<sub>2</sub>CH<sub>2</sub>CH<sub>2</sub>), 24.4 (CH<sub>2</sub>CH<sub>2</sub>CH<sub>2</sub>). IR (neat) ν<sub>max</sub>: 3288, 2359, 1692, 1590, 1166 cm<sup>-1</sup>. HRMS (ESI) calcd for C<sub>45</sub>H<sub>53</sub>N<sub>9</sub>NaO<sub>7</sub>S<sub>2</sub> [M+Na]<sup>+</sup> 918.3433 m/z found 918.3476 m/z.

### 12.11 Procedure for click reaction (BODIPY Labelling):

The desired alkyne derivative (0.02 mmol) was dissolved in dry THF (2 mL) and BODIPY azide (0.03 mmol) <sup>161</sup> was added one pot. Copper iodide and DIPEA were added subsequently in catalytic amount and the reaction mixture was stirred at 50 °C for 18 hours. The solvent was removed under reduced pressure and the residue was purified through flash column chromatography.

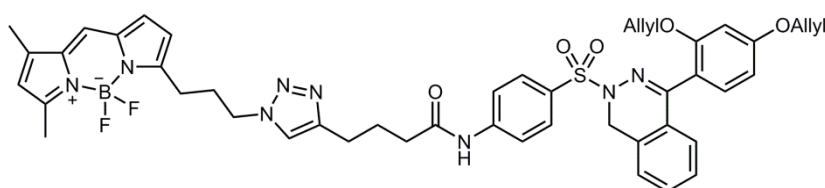




**BODIPY-Allyl-RCZ12 (48):**

The product was purified through flash column

chromatography (from 0% to 1% methanol in DCM) to afford an orange oil (18 mg, 0.021 mmol, 84%).  $^1\text{H-NMR}$  ( $\text{CDCl}_3$  400 MHz)  $\delta$  9.39 (1H, s, CONH), 7.74 (2H, d,  $J$  = 8.9 Hz, 2x(CONH)CH), 7.66 (2H, d,  $J$  = 8.8 Hz, 2x(C(SO<sub>2</sub>)CH), 7.34 (1H, s, C(CH<sub>3</sub>)C(N)CHC(N)CH), 7.14 (1H, d,  $J$  = 8.6 Hz, C(CN)CH), 7.02 (1H, s, NNNCHCH<sub>2</sub>), 6.81 (1H, d,  $J$  = 4.0 Hz, C(N)CH), 6.40 (1H, dd,  $J$  = 8.4 Hz, 2.2 Hz, C(CN)CHCH), 6.34 (1H, d,  $J$  = 2.2 Hz, C(OAllyl)CHC(OAllyl)), 6.18 (1H, d,  $J$  = 3.9 Hz, C(N)CH), 6.01 (1H, s, C(CH<sub>3</sub>)CHC(CH<sub>3</sub>)), 5.96 (1H, ddt,  $J$  = 17.0 Hz, 10.5 Hz, 5.2 Hz, OCH<sub>2</sub>CHCH<sub>2</sub>), 5.87 (1H, ddt,  $J$  = 17.0 Hz, 10.4 Hz, 5.1 Hz, OCH<sub>2</sub>CHCH<sub>2</sub>), 5.33 (1H, dd,  $J$  = 17.2 Hz, 1.5 Hz, OCH<sub>2</sub>CHCHH (trans)), 5.23 (1H, dd,  $J$  = 17.1 Hz, 1.5 Hz, OCH<sub>2</sub>CHCHH (trans)), 5.22 (1H, dd,  $J$  = 10.5 Hz, 1.5 Hz, OCH<sub>2</sub>CHCHH (cis)), 5.15 (1H, dd,  $J$  = 10.5 Hz, 1.3 Hz, OCH<sub>2</sub>CHCHH (trans)), 4.45 (2H, dt,  $J$  = 5.3 Hz, 1.5 Hz, OCH<sub>2</sub>CHCH<sub>2</sub>), 4.38 (4H, m, NNNCH<sub>2</sub>, OCH<sub>2</sub>CHCH<sub>2</sub>), 3.31 (2H, t,  $J$  = 5.5 Hz, NCH<sub>2</sub>), 2.90 (2H, t,  $J$  = 7.3 Hz, C(N)CH<sub>2</sub>), 2.89 - 2.78 (2H, m, CONHCH<sub>2</sub>), 2.48 (2H, t,  $J$  = 6.8 Hz, CNCH<sub>2</sub>), 2.43 (3H, s, CCH<sub>3</sub>), 2.45 - 2.34 (4H, m, CH<sub>2</sub>CH<sub>2</sub>CH<sub>2</sub>, NNNCH<sub>2</sub>), 2.18 (3H, s, CCH<sub>3</sub>), 2.02 - 1.92 (4H, m, CH<sub>2</sub>CH<sub>2</sub>CH<sub>2</sub>, NCH<sub>2</sub>CH<sub>2</sub>).  $^{13}\text{C-NMR}$  ( $\text{CDCl}_3$  126 MHz)  $\delta$  170.2 (CONH), 161.9 (C(OAllyl)CHC(OAllyl)), 157.4 (C(CN)C(OAllyl)), 156.2 (CNN), 146.1 (C(CONH)), 145.1 (NNNCCH<sub>2</sub>), 144.7 (NNNCHCCH<sub>2</sub>), 139.3 (C(SO<sub>2</sub>)), 134.5 (Ar-CC), 133.0 (Ar-CC), 131.9 (OCH<sub>2</sub>CHCH<sub>2</sub>), 131.8 (OCH<sub>2</sub>CHCH<sub>2</sub>), 130.6 (C(CN)CH), 129.6 (2x(C(SO<sub>2</sub>)CH), 126.7 (Ar-CC), 125.8 (Ar-CC), 123.1 (Ar-CC), 121.5 (Ar-CH), 120.9 (Ar-CH), 118.7 (C(CN)), 117.7 (OCH<sub>2</sub>CHCH<sub>2</sub>), 117.5 (OCH<sub>2</sub>CHCH<sub>2</sub>), 115.9 (Ar-CH), 115.2 (Ar-CH), 110.0 (C(OAllyl)CHC(OAllyl)), 105.9 (C(CN)CHCH), 69.2 (OCH<sub>2</sub>CHCH<sub>2</sub>), 68.9 (OCH<sub>2</sub>CHCH<sub>2</sub>), 50.3 (NNNCH<sub>2</sub>), 42.5 (NCH<sub>2</sub>), 35.3 (NNNCH<sub>2</sub>CH<sub>2</sub>), 35.2 (CONHCH<sub>2</sub>), 31.8 (NNNCCH<sub>2</sub>), 25.3 (CH<sub>2</sub>CH<sub>2</sub>CH<sub>2</sub>), 23.1 (CH<sub>2</sub>CH<sub>2</sub>CH<sub>2</sub>), 21.0 (CNCH<sub>2</sub>), 17.5 (NCH<sub>2</sub>CH<sub>2</sub>), 15.0 (CCH<sub>3</sub>), 11.3 (CCH<sub>3</sub>). IR (neat)  $\nu_{\text{max}}$ : 3033, 2489, 1604, 1166, 974  $\text{cm}^{-1}$ . HRMS (ESI) calcd for  $\text{C}_{42}\text{H}_{47}\text{F}_2\text{N}_8\text{NaO}_5\text{S}^{10}\text{B}$   $[\text{M}+\text{Na}]^+$  846.3380  $m/z$  found 846.3347  $m/z$ .



**BODIPY-Allyl-RCZ20 (49):**

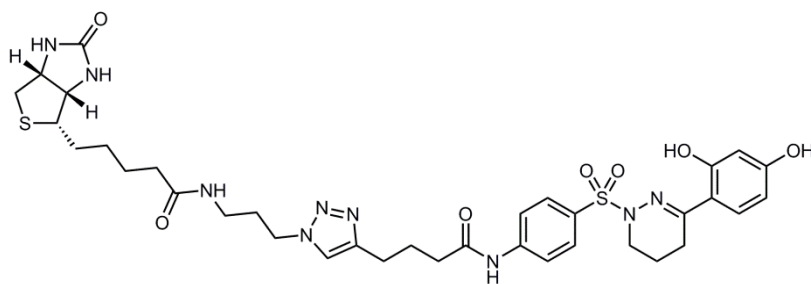
The product was purified through flash column chromatography (from

0% to 1% methanol in DCM) to afford an orange oil (48 mg, 0.055 mmol, 78%).  $^1\text{H-NMR}$

(Acetone 400 MHz)  $\delta$  9.59 (1H, s, NH), 7.88 (4H, s, 2xC(CONH)CH, 2xC(SO<sub>2</sub>)CH), 7.78 (1H, s, C(N)CHC(N)), 7.54 (1H, s, NNNCH), 7.49 (1H, t, J = 7.5 Hz, NCH<sub>2</sub>CCHCH), 7.44 (1H, d, J = 7.0 Hz, NCH<sub>2</sub>CCH), 7.39 (1H, d, J = 8.3 Hz, C(CN)CH), 7.32 (1H, t, J = 7.5 Hz, CNCCHCH), 7.07 (1H, d, J = 3.8 Hz, C(N)CH), 7.00 (1H, d, J = 7.5 Hz, CNCCH), 6.72 (1H, dd, J = 8.3 Hz, 2.3 Hz, C(CN)CHCH), 6.66 (1H, d, J = 2.3 Hz, C(OAllyl)CHC(OAllyl)), 6.42 (1H, d, J = 3.9 Hz, C(N)CH), 6.25 (1H, s, C(CH<sub>3</sub>)CHC(CH<sub>3</sub>)), 6.13 (1H, ddt, J = 17.1 Hz, 10.4 Hz, 5.4 Hz, OCH<sub>2</sub>CHCH<sub>2</sub>), 5.62 (1H, ddt, J = 17.3 Hz, 10.4 Hz, 4.7 Hz, OCH<sub>2</sub>CHCH<sub>2</sub>), 5.48 (1H, dq, J = 17.3 Hz, 1.7 Hz, OCH<sub>2</sub>CHCHH (trans)), 5.30 (1H, dq, J = 10.5 Hz, 1.5 Hz, OCH<sub>2</sub>CHCHH (cis)), 4.87 (1H, dq, J = 10.6 Hz, 1.6 Hz, OCH<sub>2</sub>CHCHH (cis)), 4.82 (1H, dq, J = 17.2 Hz, 1.7 Hz, OCH<sub>2</sub>CHCHH (trans)), 4.67 (2H, dt, J = 5.6 Hz, 1.5 Hz, OCH<sub>2</sub>CHCH<sub>2</sub>), 4.49 (2H, t, J = 7.0 Hz, NNNCH<sub>2</sub>), 4.45 (2H, s, NCH<sub>2</sub>), 4.41 (2H, dt, J = 4.6 Hz, 1.6 Hz, OCH<sub>2</sub>CHCH<sub>2</sub>), 2.99 (2H, t, J = 7.6 Hz, C(N)CH<sub>2</sub>), 2.75 (2H, t, J = 7.3 Hz, NNNCH<sub>2</sub>), 2.51 (3H, s, CCH<sub>3</sub>), 2.47 (2H, t, J = 7.3 Hz, CONHCH<sub>2</sub>), 2.35 (2H, quint., J = 7.3 Hz, CH<sub>2</sub>CH<sub>2</sub>CH<sub>2</sub>), 2.30 (3H, s, CCH<sub>3</sub>), 2.03 (2H, quint., J = 7.4 Hz, CH<sub>2</sub>CH<sub>2</sub>CH<sub>2</sub>). <sup>13</sup>C-NMR (Acetone 126 MHz)  $\delta$  171.4 (CONH), 161.1 (C(OAllyl)CHC(OAllyl)), 159.8 (C(CN)C(OAllyl)), 157.8 (CNN), 146.6 (C(CONH)), 144.3 (NNNCCH<sub>2</sub>), 144.0 (NNNCHCCH<sub>2</sub>), 135.0 (C(SO<sub>2</sub>)), 133.6 (Ar-CC), 133.4 (Ar-CC), 132.8 (Ar-CC), 131.5 (C(CN)CH), 131.2 (OCH<sub>2</sub>CHCH<sub>2</sub>), 131.1 (OCH<sub>2</sub>CHCH<sub>2</sub>), 129.9 (2xC(SO<sub>2</sub>)CH), 128.9 (Ar-CC), 128.5 (Ar-CH), 128.0 (Ar-CH), 126.6 (Ar-CH), 126.0 (Ar-CH), 125.5 (Ar-CH), 124.8 (Ar-CH), 121.3 (Ar-CH), 120.2 (Ar-CH), 118.4 (Ar-CC), 118.3 (2xC(CONH)CH), 117.4 (Ar-CC), 116.7 (OCH<sub>2</sub>CHCH<sub>2</sub>), 116.5 (OCH<sub>2</sub>CHCH<sub>2</sub>), 115.5 (C(CN)), 106.5 (C(CN)CHCH), 100.4 (C(OAllyl)CHC(OAllyl)), 68.6 (OCH<sub>2</sub>CHCH<sub>2</sub>), 68.4 (OCH<sub>2</sub>CHCH<sub>2</sub>), 49.1 (NNNCH<sub>2</sub>), 45.9 (NCH<sub>2</sub>), 35.9 (NNNCH<sub>2</sub>CH<sub>2</sub>), 35.7 (CONHCH<sub>2</sub>), 25.3 (NNNCCH<sub>2</sub>), 24.9 (CH<sub>2</sub>CH<sub>2</sub>CH<sub>2</sub>), 24.5 (CH<sub>2</sub>CH<sub>2</sub>CH<sub>2</sub>), 13.9 (CCH<sub>3</sub>), 10.3 (CCH<sub>3</sub>). IR (neat)  $\nu_{\text{max}}$ : 2389, 1615, 1187, 1011, 789 cm<sup>-1</sup>. HRMS (ESI) calcd for C<sub>46</sub>H<sub>47</sub>F<sub>2</sub>N<sub>8</sub>NaO<sub>5</sub>S<sup>10</sup>B [M+Na]<sup>+</sup> 894.3380 m/z found 894.3351 m/z.

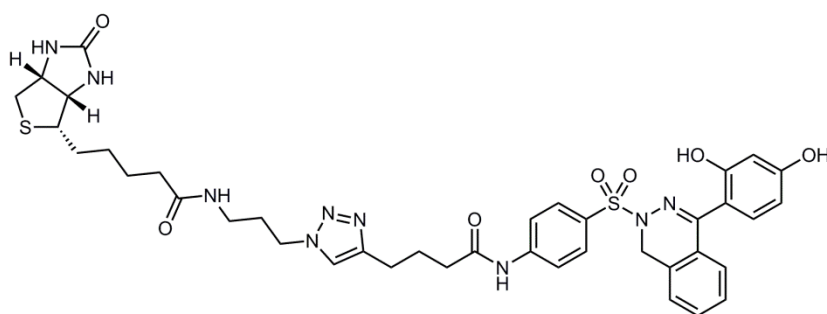
### 12.12 Procedure for de-allylation:

The desired labelled bis-allyloxy derivative (0.07 mmol) was dissolved in dry methanol (5 mL) and a catalytic amount of tetrakis(triphenylphosphine)palladium was added. The reaction mixture was stirred at 60 °C until total consumption of the starting material (2-3 hours). After cooling to room temperature, the solvent was removed under reduced pressure and the product was purified through flash column chromatography.



5-(2-Oxo-hexahydro-thieno[3,4-d]imidazol-4-yl)-pentanoic acid {3-[4-(3-{4-[3-(2,4-dihydroxy-phenyl)-5,6-dihydro-4H-pyridazine-1-sulphonyl]-

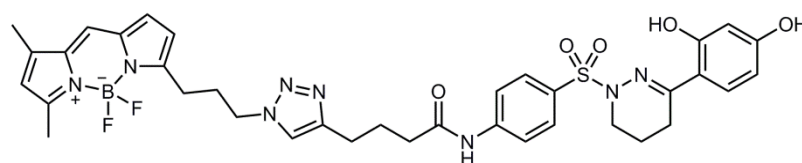
phenylcarbamoyl]-propyl)-[1,2,3]triazol-1-yl]-propyl}-amide (Biotin-RCZ12): The product was purified through flash column chromatography (from 0% to 7% methanol in DCM) to afford a white paste (28 mg, 0.035 mmol, 42%).  $^1\text{H-NMR}$  (MeOD 400 MHz)  $\delta$  7.80 (5H, m,  $2\times\text{C}(\text{CONH})\text{CH}$ ,  $2\times\text{C}(\text{SO}_2)\text{CH}$ , NNNCH), 7.24 (1H, d,  $J = 9.2$  Hz,  $\text{C}(\text{CN})\text{CH}$ ), 6.32 - 6.30 (2H, m,  $\text{C}(\text{CN})\text{CHCH}$ ,  $\text{C}(\text{OH})\text{CHC}(\text{OH})$ ), 4.61 (1H, s), 4.48 (1H, dd,  $J = 7.6$  Hz, 4.4 Hz, CONHCH), 4.38 (2H, t,  $J = 6.8$  Hz, NNNCH<sub>2</sub>), 4.28 (1H, dd,  $J = 7.8$  Hz, 4.4 Hz, CONHCH), 3.38 (2H, t,  $J = 5.4$  Hz, CONHCH<sub>2</sub>), 3.20 - 3.17 (3H, m, NCH<sub>2</sub>, SCH), 2.90 (1H, dd,  $J = 12.8$  Hz, 5.0 Hz, SCHH), 2.78 (2H, t,  $J = 7.4$  Hz, NNNCH<sub>2</sub>), 2.69 (2H, d,  $J = 12.9$  Hz, SCHH), 2.60 (2H, t,  $J = 6.6$  Hz, SCHCH<sub>2</sub>), 2.44 (2H, t,  $J = 7.4$  Hz, CNCH<sub>2</sub>), 2.21 (2H, t,  $J = 7.4$  Hz, CONHCH<sub>2</sub>), 2.14 - 2.02 (4H, m, NCH<sub>2</sub>CH<sub>2</sub>, SCHCH<sub>2</sub>CH<sub>2</sub>), 1.76 - 1.55 (4H, m,  $2\times\text{CH}_2\text{CH}_2\text{CH}_2$ ), 1.43 (2H, quint.,  $J = 7.6$  Hz,  $\text{CH}_2\text{CH}_2\text{CH}_2$ ).  $^{13}\text{C-NMR}$  (MeOD 126 MHz)  $\delta$  174.8 (CONH), 174.0 (CONH), 172.8 (CONH), 160.1 ( $\text{C}(\text{OH})\text{CHC}(\text{OH})$ ), 159.9 ( $\text{C}(\text{CN})\text{C}(\text{OH})$ ), 155.4 (CNN), 146.8 ( $\text{C}(\text{CONH})$ ), 143.7 ( $\text{C}(\text{SO}_2)$ ), 134.5 (NNNCCH<sub>2</sub>), 128.9 ( $2\times\text{C}(\text{SO}_2)\text{CH}$ ), 127.9 (NNNCH), 125.8( $\text{C}(\text{CN})\text{CH}$ ), 122.2 ( $2\times\text{C}(\text{CONH})\text{CH}$ ), 119.1 ( $\text{C}(\text{CN})$ ), 106.7 ( $\text{C}(\text{CN})\text{CHCH}$ ), 102.9 ( $\text{C}(\text{OH})\text{CHC}(\text{OH})$ ), 61.9 (CONHCH), 60.2 (CONHCH), 55.5 (SCH), 49.8 (CONHCH<sub>2</sub>), 42.9 (NCH<sub>2</sub>), 39.6 (SCH<sub>2</sub>), 35.9 (CONHCH<sub>2</sub>), 35.5 (CONHCH<sub>2</sub>), 35.3 (NNNCCH<sub>2</sub>), 29.5 (SCHCH<sub>2</sub>), 28.3 (NNNCH<sub>2</sub>CH<sub>2</sub>), 28.0 (SCHCH<sub>2</sub>CH<sub>2</sub>), 25.3 ( $\text{CH}_2\text{CH}_2\text{CH}_2$ ), 24.7 ( $\text{CH}_2\text{CH}_2\text{CH}_2$ ), 24.2 (CNCH<sub>2</sub>), 21.5 ( $\text{CH}_2\text{CH}_2\text{CH}_2$ ), 18.2 (NCH<sub>2</sub>CH<sub>2</sub>). IR (neat)  $\nu_{\text{max}}$ : 3283, 2932, 2359, 1676, 1355  $\text{cm}^{-1}$ . HRMS (ESI) calcd for  $\text{C}_{35}\text{H}_{45}\text{N}_9\text{NaO}_7\text{S}_2$   $[\text{M}+\text{Na}]^+$  790.2776  $m/z$  found 790.2737  $m/z$ .



5-(2-Oxo-hexahydro-thieno[3,4-d]imidazol-4-yl)-pentanoic acid {3-[4-(3-{4-[4-(2,4-dihydroxy-phenyl)-1H-phthalazine-2-sulphonyl]-

phenylcarbamoyl]-propyl)-[1,2,3]triazol-1-yl]-propyl}-amide (Biotin-RCZ20): The product

was purified through flash column chromatography (from 0% to 7% methanol in DCM) to afford a white paste (8 mg, 0.009 mmol, 47%).  $^1\text{H-NMR}$  (MeOD 400 MHz)  $\delta$  7.91 (2H, d,  $J$  = 9.1 Hz, 2xC(CONH)CH), 7.83 (2H, d,  $J$  = 8.9 Hz, 2xC(SO<sub>2</sub>)CH), 7.79 (1H, s, NNNCH), 7.57 - 7.54 (1H, m, NCH<sub>2</sub>CCHCH), 7.45 - 7.41 (3H, m, CNCCH, CNCCHCH, NCH<sub>2</sub>CCH), 7.26 (1H, d,  $J$  = 8.6 Hz, C(CN)CH), 6.44 (1H, d,  $J$  = 2.3 Hz, C(OH)CHC(OH)), 6.39 (1H, dd,  $J$  = 8.5 Hz, 2.3 Hz, C(CN)CHCH), 4.47 (1H, dd,  $J$  = 7.8 Hz, 4.2 Hz, CONHCH), 4.37 (2H, t,  $J$  = 7.0 Hz, NNNCH<sub>2</sub>), 4.31 (2H, s, NCH<sub>2</sub>), 4.28 (1H, dd,  $J$  = 8.0 Hz, 4.4 Hz, CONHCH), 3.20 - 3.15 (3H, m, SCH, CONHCH<sub>2</sub>), 2.90 (1H, dd,  $J$  = 12.6 Hz, 4.8 Hz, SCHH), 2.78 (2H, t,  $J$  = 7.4 Hz, NNNCCH<sub>2</sub>), 2.68 (1H, d,  $J$  = 12.6 Hz, SCHH), 2.45 (2H, t,  $J$  = 7.4 Hz, COCH<sub>2</sub>), 2.20 (2H, t,  $J$  = 7.4 Hz, COCH<sub>2</sub>), 2.04 (2H, quint.,  $J$  = 6.9 Hz, COCH<sub>2</sub>CH<sub>2</sub>), 1.75 - 1.55 (6H, m, CONHCH<sub>2</sub>CH<sub>2</sub>, 2xCH<sub>2</sub>CH<sub>2</sub>CH<sub>2</sub>), 1.43 (2H, quint.,  $J$  = 7.1 Hz, CH<sub>2</sub>CH<sub>2</sub>CH<sub>2</sub>).  $^{13}\text{C-NMR}$  (MeOD 126 MHz)  $\delta$  172.7 (CONH), 171.6 (CONH), 163.3 (CONH), 160.3 (C(OH)CHC(OH)), 157.8 (C(CN)C(OH)), 155.7 (CNN), 147.4 (C(CONH)), 146.2 (NNNCCH<sub>2</sub>), 144.9 (Ar-CC), 133.5 (C(SO<sub>2</sub>)), 132.1 (NNNCH), 131.8 (C(CN)CH), 129.8 (2xC(SO<sub>2</sub>)CH), 128.2 (Ar-CC), 127.4 (Ar-CH), 126.5 (Ar-CH), 125.8 (Ar-CH), 124.7 (Ar-CH), 122.0 (2xC(CONH)CH), 118.4 (C(CN)), 106.9 (C(CN)CHCH), 103.7 (C(OH)CHC(OH)), 61.3 (CONHCH), 60.3 (CONHCH), 55.4 (SCH), 47.0 (SCH<sub>2</sub>), 46.4 (NCH<sub>2</sub>), 40.0 (NNNCH<sub>2</sub>), 35.8 (CONHCH<sub>2</sub>), 35.6 (CONHCH<sub>2</sub>), 35.3 (SCHCH<sub>2</sub>), 30.0 (NNNCCH<sub>2</sub>), 29.2 (SCHCH<sub>2</sub>CH<sub>2</sub>), 25.4 (CH<sub>2</sub>CH<sub>2</sub>CH<sub>2</sub>), 24.7 (CH<sub>2</sub>CH<sub>2</sub>CH<sub>2</sub>), 24.4 (CH<sub>2</sub>CH<sub>2</sub>CH<sub>2</sub>). IR (neat)  $\nu_{\text{max}}$ : 3263, 2929, 2361, 1629, 1166 cm<sup>-1</sup>. HRMS (ESI) calcd for C<sub>39</sub>H<sub>45</sub>N<sub>9</sub>NaO<sub>7</sub>S<sub>2</sub> [M+Na]<sup>+</sup> 838.2891 m/z found 838.2911 m/z.

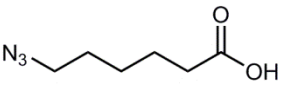


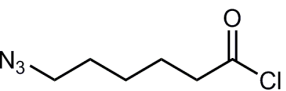
**BODIPY-RCZ12:** The product was purified through flash column

chromatography (from 0% to 1% methanol in DCM) to afford a red oil (12 mg, 0.016 mmol, 63%).  $^1\text{H-NMR}$  (CDCl<sub>3</sub> 500 MHz)  $\delta$  12.19 (1H, s, COH), 9.39 (1H, s, CONH), 7.79 - 7.66 (4H, m, 2xC(CONH)CH, 2xC(SO<sub>2</sub>)CH), 7.42 (1H, s, C(N)CHC(N)), 7.16 - 7.09 (2H, m, C(CN)CH, NNNCH), 6.90 (1H, d,  $J$  = 4.0 Hz, C(N)CH), 6.69 (1H, s, COH), 6.46 (1H, d,  $J$  = 2.4 Hz, C(OH)CHC(OH)), 6.36 (1H, dd,  $J$  = 8.6, 2.4 Hz, C(CN)CHCH), 6.27 (1H, d,  $J$  = 3.9 Hz, C(N)CH), 6.13 (1H, s, C(CH<sub>3</sub>)CHC(CH<sub>3</sub>)), 4.44 (2H, t,  $J$  = 6.5 Hz, NNNCH<sub>2</sub>), 3.42 - 3.33 (2H, m, NCH<sub>2</sub>), 2.98 (2H, t,  $J$  = 7.3 Hz, C(N)CH<sub>2</sub>), 2.85 - 2.72 (2H, m, CONHCH<sub>2</sub>), 2.53 (3H, s, CCH<sub>3</sub>), 2.47 - 2.33 (4H, m, CNCH<sub>2</sub>, CH<sub>2</sub>CH<sub>2</sub>CH<sub>2</sub>), 2.28 (3H, s, CCH<sub>3</sub>), 2.18 - 2.10 (2H, m, CH<sub>2</sub>CH<sub>2</sub>CH<sub>2</sub>), 2.10 -

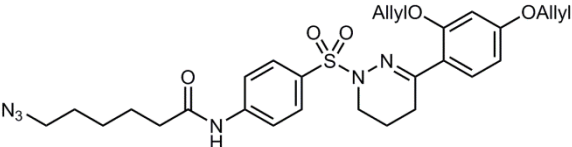


### 12.13 Procedure for 6-azido-hexanoyl chloride coupling:

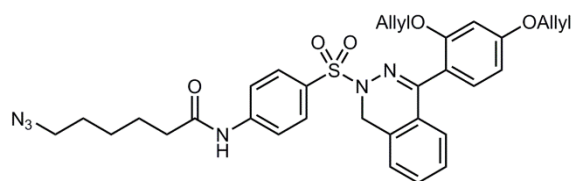
 **6-Azido-hexanoic acid** <sup>154</sup>: 6-Bromo-hexanoic acid (3 g, 15.38 mmol) was dissolved in dry DMF (30 mL) and sodium azide (2 g, 30.76 mmol) was then added. The reaction mixture was allowed to stir at 80 °C for 18 hours. A 0.1 M solution of HCl (100 mL) and ethyl acetate (100 mL) were added to the mixture and the aqueous phase was discarded. The organic phase was washed with a 0.1 M solution of HCl (2x100 mL) and brine (5x100 mL), dried over Na<sub>2</sub>SO<sub>4</sub>, filtered and concentrated to afford the desired compounds as a colourless oil (2.28 g, 14.52 mmol) in 94% yield with excellent purity. Characterisation data matched the ones previously reported. <sup>1</sup>H-NMR (CDCl<sub>3</sub> 400 MHz) δ 11.56 (1H, bs); 3.31 (2H, t, J = 6.9 Hz); 2.40 (2H, t, J = 7.4 Hz), 1.73 - 1.61 (4H, m), 1.50 - 1.42 (2H, m). <sup>13</sup>C NMR (CDCl<sub>3</sub> 126 MHz) δ 179.6, 51.2, 33.8, 28.5, 26.1, 24.1.

 **6-Azido-hexanoyl chloride**: 6-Azido-hexanoic acid (66 mg, 0.42 mmol) was dissolved in dry DCM (8 mL) and two drops of dry DMF were added. Oxalyl chloride (50 µL, 0.50 mmol) was added dropwise at 0 °C through 10 minutes. The reaction mixture was then allowed to stir at room temperature until the carbon dioxide bubbling ceased (2 hours). The solution was then concentrated under reduced pressure to afford a red oil which was used immediately for the next step.

The desired aniline derivative (**39** or **40**) (0.21 mmol) was dissolved in dry DCM (10 mL) and anhydrous pyridine (0.84 mmol) was added. After 10 minutes, a freshly prepared solution of 6-azido-hexanoyl chloride (0.42 mmol) in dry DCM (4 mL) was added slowly. The reaction mixture was allowed to stir at room temperature for 18 hours. The solvent was evaporated off under reduced pressure and the product was purified through direct flash column chromatography.

 **6-Azido-hexanoic acid {4-[3-(2,4-bis-allyloxy-phenyl)-5,6-dihydro-4H-pyridazine-1-sulphonyl]-phenyl}-amide (46)**: The product was purified through direct flash column chromatography (20% ethyl acetate in petroleum ether) to afford a yellow oil (122 mg, 0.21 mmol) in 56% (98% brsm) yield. <sup>1</sup>H-

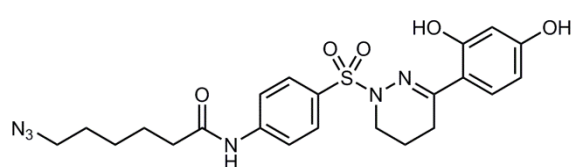
NMR (CDCl<sub>3</sub> 400 MHz)  $\delta$  7.79 (2H, d, J = 8.8 Hz, 2xC(CONH)CH), 7.60 (2H, d, J = 8.8 Hz, 2xC(SO<sub>2</sub>)CH), 7.40 (1H, s, CONH), 7.12 (1H, d, J = 8.5 Hz, C(CN)CH), 6.38 (1H, dd, J = 8.5 Hz, 2.3 Hz, C(CN)CHCH), 6.35 (1H, d, J = 2.3 Hz, C(OAllyl)CHC(OAllyl)), 6.04 - 5.83 (2H, m, 2xOCH<sub>2</sub>CHCH<sub>2</sub>), 5.34 (1H, ddd, J = 17.3 Hz, 3.1 Hz, 1.6 Hz, OCH<sub>2</sub>CHCHH (trans)), 5.27 - 5.20 (2H, m, OCH<sub>2</sub>CHCHH (trans), OCH<sub>2</sub>CHCHH (cis)), 5.16 (1H, ddd, J = 10.5 Hz, 2.7 Hz, 1.3 Hz, OCH<sub>2</sub>CHCHH (cis)), 4.45 (2H, dt, J = 5.3 Hz, 1.5 Hz, OCH<sub>2</sub>CHCH<sub>2</sub>), 4.39 (2H, dt, J = 5.2 Hz, 1.5 Hz, OCH<sub>2</sub>CHCH<sub>2</sub>), 3.36 - 3.29 (2H, m, NNNCH<sub>2</sub>), 3.22 (2H, t, J = 6.8 Hz, NCH<sub>2</sub>), 2.49 (2H, t, J = 6.7 Hz, CNCH<sub>2</sub>), 2.34 (2H, t, J = 7.4 Hz, CONHCH<sub>2</sub>), 1.95 (2H, dt, J = 12.8 Hz, 6.1 Hz, CNCH<sub>2</sub>CH<sub>2</sub>), 1.69 (2H, dt, J = 15.2 Hz, 7.5 Hz, NNNCH<sub>2</sub>CH<sub>2</sub>), 1.62 - 1.53 (2H, m, CH<sub>2</sub>CH<sub>2</sub>CH<sub>2</sub>), 1.45 - 1.34 (2H, m, CH<sub>2</sub>CH<sub>2</sub>CH<sub>2</sub>). <sup>13</sup>C-NMR (CDCl<sub>3</sub> 126 MHz)  $\delta$  171.2 (CONH), 160.4 (C(OAllyl)CHC(OAllyl)), 157.6 (C(CN)C(OAllyl)), 154.0 (CNN), 142.1 (C(SO<sub>2</sub>)), 132.9 (OCH<sub>2</sub>CHCH<sub>2</sub>), 132.8 (OCH<sub>2</sub>CHCH<sub>2</sub>), 130.7 (C(CONH)), 130.5 (C(CN)CH), 129.7 (2xC(SO<sub>2</sub>)CH), 121.0 (2xC(CONH)CH), 118.9 (C(CN)), 117.9 (OCH<sub>2</sub>CHCH<sub>2</sub>), 117.6 (OCH<sub>2</sub>CHCH<sub>2</sub>), 105.8 (C(CN)CHCH), 100.5 (C(OAllyl)CHC(OAllyl)), 69.2 (OCH<sub>2</sub>CHCH<sub>2</sub>), 68.9 (OCH<sub>2</sub>CHCH<sub>2</sub>), 51.2 (NNNCH<sub>2</sub>), 43.2 (NCH<sub>2</sub>), 37.4 (CONHCH<sub>2</sub>), 28.6 (NNNCH<sub>2</sub>CH<sub>2</sub>), 26.3 (CH<sub>2</sub>CH<sub>2</sub>CH<sub>2</sub>), 25.9 (CH<sub>2</sub>CH<sub>2</sub>CH<sub>2</sub>), 24.7 (CNCH<sub>2</sub>), 19.1 (CNCH<sub>2</sub>CH<sub>2</sub>). IR (neat)  $\nu_{\text{max}}$ : 2927, 2096, 1591, 1352, 1166 cm<sup>-1</sup>. HRMS (ESI) calcd for C<sub>28</sub>H<sub>34</sub>N<sub>6</sub>NaO<sub>5</sub>S [M+Na]<sup>+</sup> 589.2204 m/z found 589.2185 m/z.



**6-Azido-hexanoic acid {4-[4-(2,4-bis-allyloxy-phenyl)-1H-phthalazine-2-sulphonyl]-phenyl}-amide (47):** The product was purified through direct flash column

chromatography (40% ethyl acetate in petroleum ether) to afford a yellow oil (125 mg, 0.20 mmol) in 96% yield. <sup>1</sup>H-NMR (CDCl<sub>3</sub> 500 MHz)  $\delta$  7.94 (2H, d, J = 8.8 Hz, 2xC(CONH)CH), 7.68 (2H, d, J = 8.8 Hz, 2xC(SO<sub>2</sub>)CH), 7.45 (1H, d, J = 8.4 Hz, C(CN)CH), 7.42 - 7.37 (2H, m, NCH<sub>2</sub>CCH, NCH<sub>2</sub>CCHCH), 7.23 (1H, m, CNCCHCH), 7.00 (1H, d, J = 7.1 Hz, CNCCH), 6.61 (1H, dd, J = 8.4 Hz, 2.3 Hz, C(CN)CHCH), 6.51 (1H, d, J = 2.3 Hz, C(OAllyl)CHC(OAllyl)), 6.11 (1H, ddt, J = 17.2 Hz, 10.6 Hz, 5.4 Hz, OCH<sub>2</sub>CHCH<sub>2</sub>), 5.62 (1H, ddt, J = 17.2 Hz, 10.6 Hz, 4.7 Hz, OCH<sub>2</sub>CHCH<sub>2</sub>), 5.47 (1H, ddd, J = 17.3 Hz, 3.0 Hz, 1.5 Hz, OCH<sub>2</sub>CHCHH (trans)), 5.35 (1H, ddd, J = 10.5 Hz, 2.6 Hz, 1.3 Hz, OCH<sub>2</sub>CHCHH (cis)), 4.93 (1H, ddd, J = 10.7 Hz, 3.0 Hz, 1.5 Hz, OCH<sub>2</sub>CHCHH (cis)), 4.81 (1H, ddd, J = 17.2 Hz, 3.3 Hz, 1.7 Hz, OCH<sub>2</sub>CHCHH (trans)), 4.60

(2H, dt,  $J = 5.4$  Hz,  $1.4$  Hz,  $\text{OCH}_2\text{CHCH}_2$ ),  $4.45$  (2H, s,  $\text{NCH}_2$ ),  $4.36 - 4.31$  (2H, m,  $\text{OCH}_2\text{CHCH}_2$ ),  $3.30$  (2H, t,  $J = 6.8$  Hz,  $\text{NNNCH}_2$ ),  $2.42$  (2H, t,  $J = 7.4$  Hz,  $\text{CONHCH}_2$ ),  $1.77$  (2H, dt,  $J = 15.3$  Hz,  $7.5$  Hz,  $\text{CH}_2\text{CH}_2\text{CH}_2$ ),  $1.69 - 1.61$  (2H, m,  $\text{CH}_2\text{CH}_2\text{CH}_2$ ),  $1.47$  (2H, dt,  $J = 15.2$  Hz,  $7.6$  Hz,  $\text{CH}_2\text{CH}_2\text{CH}_2$ ).  $^{13}\text{C}$ -NMR ( $\text{CDCl}_3$   $126$  MHz)  $\delta$   $171.2$  ( $\text{CONH}$ ),  $160.9$  ( $\text{C}(\text{OAllyl})\text{CHC}(\text{OAllyl})$ ),  $157.7$  ( $\text{C}(\text{CN})\text{C}(\text{OAllyl})$ ),  $153.5$  ( $\text{CNN}$ ),  $142.3$  ( $\text{C}(\text{SO}_2)$ ),  $132.9$  ( $\text{C}(\text{CONH})$ ),  $132.4$  ( $\text{OCH}_2\text{CHCH}_2$ ),  $132.0$  ( $\text{OCH}_2\text{CHCH}_2$ ),  $131.1$  ( $\text{Ar-CC}$ ),  $130.6$  ( $\text{C}(\text{CN})\text{CH}$ ),  $130.4$  ( $\text{Ar-CC}$ ),  $130.0$  ( $2\times\text{C}(\text{SO}_2)\text{CH}$ ),  $129.4$  ( $\text{Ar-CC}$ ),  $127.9$  ( $\text{Ar-CH}$ ),  $126.5$  ( $\text{Ar-CH}$ ),  $125.4$  ( $\text{Ar-CH}$ ),  $118.9$  ( $\text{Ar-CH}$ ),  $118.0$  ( $\text{OCH}_2\text{CHCH}_2$ ),  $117.9$  ( $\text{OCH}_2\text{CHCH}_2$ ),  $117.6$  ( $2\times\text{C}(\text{CONH})\text{CH}$ ),  $116.4$  ( $\text{C}(\text{CN})$ ),  $106.0$  ( $\text{C}(\text{CN})\text{CHCH}$ ),  $100.6$  ( $\text{C}(\text{OAllyl})\text{CHC}(\text{OAllyl})$ ),  $69.0$  ( $\text{OCH}_2\text{CHCH}_2$ ),  $68.6$  ( $\text{OCH}_2\text{CHCH}_2$ ),  $51.2$  ( $\text{NNNCH}_2$ ),  $45.8$  ( $\text{NCH}_2$ ),  $37.4$  ( $\text{CONHCH}_2$ ),  $28.6$  ( $\text{CH}_2\text{CH}_2\text{CH}_2$ ),  $26.2$  ( $\text{CH}_2\text{CH}_2\text{CH}_2$ ),  $24.7$  ( $\text{CH}_2\text{CH}_2\text{CH}_2$ ). IR (neat)  $\nu_{\text{max}}$ :  $2998$ ,  $2095$ ,  $1698$ ,  $1590$ ,  $1167$   $\text{cm}^{-1}$ . HRMS (ESI) calcd for  $\text{C}_{32}\text{H}_{34}\text{N}_6\text{NaO}_5\text{S}$   $[\text{M}+\text{Na}]^+$   $637.2204$   $m/z$  found  $637.2186$   $m/z$ .

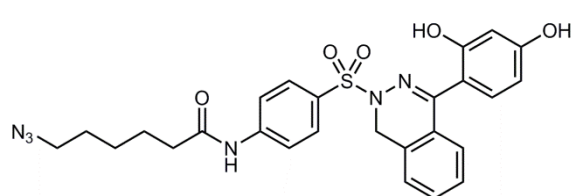


**6-Azido-hexanoic acid {4-[3-(2,4-dihydroxyphenyl)-5,6-dihydro-4H-pyridazine-1-sulphonyl]-phenyl}-amide:**

The product was obtained following Procedure 12.12 and

purified through direct flash column chromatography (50% ethyl acetate in petroleum ether) to afford a colourless oil (40 mg, 0.082 mmol) in 43% yield.  $^1\text{H}$ -NMR (Acetone 400 MHz)  $\delta$   $12.03$  (1H, s, COH),  $9.49$  (1H, s, COH),  $7.75$  (2H, d,  $J = 9.0$  Hz,  $2\times\text{C}(\text{SO}_2)\text{CH}$ ),  $7.69 - 7.63$  (2H, m,  $2\times\text{C}(\text{CONH})\text{CH}$ ),  $7.10$  (1H, d,  $J = 8.6$  Hz,  $\text{C}(\text{CN})\text{CH}$ ),  $6.28 - 6.14$  (2H, m,  $\text{C}(\text{CN})\text{CHCH}$ ,  $\text{C}(\text{OH})\text{CHC}(\text{OH})$ ),  $3.29 - 3.23$  (2H, m,  $\text{NNNCH}_2$ ),  $3.19$  (2H, t,  $J = 6.9$  Hz,  $\text{NCH}_2$ ),  $2.50$  (2H, t,  $J = 6.7$  Hz,  $\text{CONHCH}_2$ ),  $2.28$  (2H, t,  $J = 7.4$  Hz,  $\text{CNCH}_2$ ),  $2.05 - 1.96$  (2H, m,  $\text{CNCH}_2\text{CH}_2$ ),  $1.56$  (2H, dt,  $J = 15.0$  Hz,  $7.4$  Hz,  $\text{CH}_2\text{CH}_2\text{CH}_2$ ),  $1.51 - 1.42$  (2H, m,  $\text{CH}_2\text{CH}_2\text{CH}_2$ ),  $1.34 - 1.25$  (2H, m,  $\text{CH}_2\text{CH}_2\text{CH}_2$ ).  $^{13}\text{C}$ -NMR (Acetone 101 MHz)  $\delta$   $171.6$  ( $\text{CONH}$ ),  $160.5$  ( $\text{C}(\text{OH})\text{CHC}(\text{OH})$ ),  $160.2$  ( $\text{C}(\text{CN})\text{C}(\text{OH})$ ),  $155.4$  ( $\text{CNN}$ ),  $144.3$  ( $\text{C}(\text{SO}_2)$ ),  $131.9$  ( $\text{C}(\text{CONH})$ ),  $131.7$  ( $\text{C}(\text{CN})\text{CH}$ ),  $129.2$  ( $2\times\text{C}(\text{SO}_2)\text{CH}$ ),  $118.7$  ( $2\times\text{C}(\text{CONH})\text{CH}$ ),  $111.5$  ( $\text{C}(\text{CN})$ ),  $106.7$  ( $\text{C}(\text{CN})\text{CHCH}$ ),  $103.4$  ( $\text{C}(\text{OH})\text{CHC}(\text{OH})$ ),  $50.9$  ( $\text{NNNCH}_2$ ),  $43.0$  ( $\text{NCH}_2$ ),  $36.6$  ( $\text{CONHCH}_2$ ),  $28.1$  ( $\text{CH}_2\text{CH}_2\text{CH}_2$ ),  $26.0$  ( $\text{CH}_2\text{CH}_2\text{CH}_2$ ),  $24.5$  ( $\text{CH}_2\text{CH}_2\text{CH}_2$ ),  $21.7$  ( $\text{CNCH}_2$ ),  $18.4$  ( $\text{CNCH}_2\text{CH}_2$ ). IR (neat)  $\nu_{\text{max}}$ :  $3209$ ,  $2350$ ,  $1653$ ,  $1233$ ,  $1080$   $\text{cm}^{-1}$ . HRMS (ESI) calcd for  $\text{C}_{22}\text{H}_{26}\text{N}_6\text{NaO}_5\text{S}$   $[\text{M}+\text{Na}]^+$   $509.1578$   $m/z$  found  $509.1561$   $m/z$ .





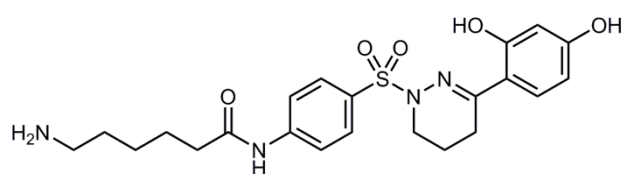
**6-Azido-hexanoic acid {4-[4-(2,4-dihydroxy-phenyl)-1H-phthalazine-2-sulphonyl]-phenyl}-amide:**

The product was obtained following Procedure 12.12 and purified

through direct flash column chromatography (40% ethyl acetate in petroleum ether) to afford a white paste (40 mg, 0.074 mmol) in 37% yield.  $^1\text{H-NMR}$  (Acetone 400 MHz)  $\delta$  10.52 (1H, s, COH), 9.45 (1H, s, COH), 7.84 - 7.71 (4H, m,  $2\times\text{C}(\text{CONH})\text{CH}$ ,  $2\times\text{C}(\text{SO}_2)\text{CH}$ ), 7.53 - 7.45 (1H, m,  $\text{NCH}_2\text{CCHCH}$ ), 7.44 - 7.32 (3H, m,  $\text{NCH}_2\text{CCH}$ ,  $\text{CNCCH}$ ,  $\text{CNCCCHCH}$ ), 7.16 (1H, d,  $J = 8.6$  Hz,  $\text{C}(\text{CN})\text{CH}$ ), 6.38 (1H, d,  $J = 2.4$  Hz,  $\text{C}(\text{OH})\text{CHC}(\text{OH})$ ), 6.31 (1H, dd,  $J = 8.6$  Hz, 2.5 Hz,  $\text{C}(\text{CN})\text{CHCH}$ ), 4.24 (2H, s,  $\text{NCH}_2$ ), 3.19 (2H, t,  $J = 6.9$  Hz,  $\text{NNNCH}_2$ ), 2.29 (2H, t,  $J = 7.4$  Hz,  $\text{CONHCH}_2$ ), 1.57 (2H, dt,  $J = 15.0$  Hz, 7.4 Hz,  $\text{CH}_2\text{CH}_2\text{CH}_2$ ), 1.48 (2H, dt,  $J = 14.5$  Hz, 7.1 Hz,  $\text{CH}_2\text{CH}_2\text{CH}_2$ ), 1.34 - 1.26 (2H, m,  $\text{CH}_2\text{CH}_2\text{CH}_2$ ).  $^{13}\text{C-NMR}$  (Acetone 126 MHz)  $\delta$  171.6 (CONH), 160.3 ( $\text{C}(\text{OH})\text{CHC}(\text{OH})$ ), 159.7 ( $\text{C}(\text{CN})\text{C}(\text{OH})$ ), 155.8 (CNN), 144.6 ( $\text{C}(\text{SO}_2)$ ), 133.5 ( $\text{C}(\text{CONH})$ ), 132.1 (Ar-CC), 131.9 ( $\text{C}(\text{CN})\text{CH}$ ), 129.9 ( $2\times\text{C}(\text{SO}_2)\text{CH}$ ), 128.2 (Ar-CC), 127.9 (Ar-CH), 127.4 (Ar-CH), 126.6 (Ar-CH), 124.7 (Ar-CH), 118.7 ( $2\times\text{C}(\text{CONH})\text{CH}$ ), 109.5 ( $\text{C}(\text{CN})$ ), 106.9 ( $\text{C}(\text{CN})\text{CHCH}$ ), 103.7 ( $\text{C}(\text{OH})\text{CHC}(\text{OH})$ ), 50.9 ( $\text{NNNCH}_2$ ), 46.4 ( $\text{NCH}_2$ ), 36.6 ( $\text{CONHCH}_2$ ), 36.5 ( $\text{NNNCH}_2\text{CH}_2$ ), 26.0 ( $\text{CH}_2\text{CH}_2\text{CH}_2$ ), 24.5 ( $\text{CH}_2\text{CH}_2\text{CH}_2$ ). IR (neat)  $\nu_{\text{max}}$ : 3170, 2099, 1589, 1167, 1025  $\text{cm}^{-1}$ . HRMS (ESI) calcd for  $\text{C}_{26}\text{H}_{26}\text{N}_6\text{NaO}_5\text{S}$   $[\text{M}+\text{Na}]^+$  557.1578  $m/z$  found 557.1562  $m/z$ .

#### 12.14 Procedure for Staudinger reaction:

The desired diol derivative (0.082 mmol) was dissolved in THF:H<sub>2</sub>O (10:1) (5 mL) and polymer bound triphenylphosphine (0.41 mmol) was added. The reaction mixture was allowed to stir for 18 hours at 50 °C and then filtered through a sinter funnel. The beads were further washed with methanol (25 mL) and with a 7 N solution of NH<sub>3</sub> in methanol (10 mL). The solution thus obtained was evaporated to dryness under reduced pressure and the residue was purified through flash column chromatography.

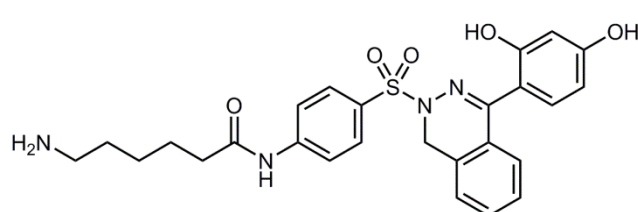


**6-Amino-hexanoic acid {4-[3-(2,4-dihydroxy-phenyl)-5,6-dihydro-4H-pyridazine-1-sulphonyl]-phenyl}-amide**

(NH<sub>2</sub>-RCZ12): The product was purified

through direct flash column chromatography (5% methanol in DCM) to afford a colourless

paste (15 mg, 0.032 mmol) in 40% yield.  $^1\text{H-NMR}$  (Acetone 400 MHz)  $\delta$  12.03 (1H, s, COH), 9.49 (1H, s, COH), 7.76 (2H, d,  $J$  = 8.9 Hz,  $2\times\text{C}(\text{CONH})\text{CH}$ ), 7.66 (2H, d,  $J$  = 8.9 Hz,  $2\times\text{C}(\text{SO}_2)\text{CH}$ ), 7.10 (1H, d,  $J$  = 8.6 Hz,  $\text{C}(\text{CN})\text{CH}$ ), 6.25 - 6.14 (2H, m,  $\text{C}(\text{CN})\text{CHCH}$ ,  $\text{C}(\text{OH})\text{CHC}(\text{OH})$ ), 3.29 - 3.22 (2H, m,  $\text{NCH}_2$ ), 2.95 (2H, dd,  $J$  = 12.4 Hz, 6.6 Hz,  $\text{NH}_2\text{CH}_2$ ), 2.50 (2H, t,  $J$  = 6.7 Hz,  $\text{CONHCH}_2$ ), 2.24 (2H, t,  $J$  = 7.4 Hz,  $\text{CNCH}_2$ ), 2.05 - 1.96 (2H, m,  $\text{NCH}_2\text{CH}_2$ ), 1.60 - 1.46 (4H, m,  $2\times\text{CH}_2\text{CH}_2\text{CH}_2$ ), 1.31 (2H, dt,  $J$  = 13.9 Hz, 7.1 Hz,  $\text{CH}_2\text{CH}_2\text{CH}_2$ ).  $^{13}\text{C-NMR}$  (Acetone 101 MHz)  $\delta$  171.9 (CONH), 160.3 ( $\text{C}(\text{OH})\text{CHC}(\text{OH})$ ), 160.0 ( $\text{C}(\text{CN})\text{CH}$ ), 155.4 (CNN), 144.4 ( $\text{C}(\text{SO}_2)$ ), 129.2 ( $2\times\text{C}(\text{SO}_2)\text{CH}$ ), 128.4 ( $\text{C}(\text{CONH})$ ), 128.2 ( $\text{C}(\text{CN})\text{CH}$ ), 118.7 ( $2\times\text{C}(\text{CONH})\text{CH}$ ), 111.5 ( $\text{C}(\text{CN})$ ), 106.7 ( $\text{C}(\text{CN})\text{CHCH}$ ), 103.3 ( $\text{C}(\text{OH})\text{CHC}(\text{OH})$ ), 43.0 ( $\text{NCH}_2$ ), 39.4 ( $\text{NH}_2\text{CH}_2$ ), 36.8 ( $\text{CONHCH}_2$ ), 29.9 ( $\text{NH}_2\text{CH}_2\text{CH}_2$ ), 26.0 ( $\text{CH}_2\text{CH}_2\text{CH}_2$ ), 24.7 ( $\text{CH}_2\text{CH}_2\text{CH}_2$ ), 21.7 ( $\text{CNCH}_2$ ), 18.4 ( $\text{CNCH}_2\text{CH}_2$ ). IR (neat)  $\nu_{\text{max}}$ : 3453, 3347, 1663, 1437, 1042  $\text{cm}^{-1}$ . HRMS (ESI) calcd for  $\text{C}_{22}\text{H}_{28}\text{N}_4\text{NaO}_5\text{S}$   $[\text{M}+\text{Na}]^+$  483.4511  $m/z$  found 483.4523  $m/z$ .

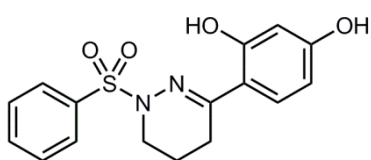


**6-Amino-hexanoic acid {4-[4-(2,4-dihydroxy-phenyl)-1H-phthalazine-2-sulphonyl]-phenyl}-amide ( $\text{NH}_2\text{-RCZ20}$ ):**

The product was purified through direct flash column chromatography (5% methanol in DCM) to afford a colourless oil (7 mg, 0.013 mmol) in 19% yield.  $^1\text{H-NMR}$  (Acetone 400 MHz)  $\delta$  10.51 (1H, s, COH), 9.50 (1H, s, COH), 7.81 (2H, d,  $J$  = 9.0 Hz,  $2\times\text{C}(\text{SO}_2)\text{CH}$ ), 7.76 (2H, d,  $J$  = 9.0 Hz,  $2\times\text{C}(\text{CONH})\text{CH}$ ), 7.52 - 7.44 (1H, m,  $\text{NCH}_2\text{CCHCH}$ ), 7.44 - 7.31 (3H, m,  $\text{NCH}_2\text{CCH}$ ,  $\text{CNCCH}$ ,  $\text{CNCCHCH}$ ), 7.15 (1H, d,  $J$  = 8.6 Hz,  $\text{C}(\text{CN})\text{CH}$ ), 6.37 (1H, d,  $J$  = 2.4 Hz,  $\text{C}(\text{OH})\text{CHC}(\text{OH})$ ), 6.30 (1H, dd,  $J$  = 8.6 Hz, 2.5 Hz,  $\text{C}(\text{CN})\text{CHCH}$ ), 4.24 (2H, s,  $\text{NCH}_2$ ), 2.94 (2H, dd,  $J$  = 12.4 Hz, 6.6 Hz,  $\text{NH}_2\text{CH}_2$ ), 2.24 (2H, t,  $J$  = 7.4 Hz,  $\text{CONHCH}_2$ ), 1.58 - 1.42 (4H, m,  $2\times\text{CH}_2\text{CH}_2\text{CH}_2$ ), 1.32 - 1.22 (2H, m,  $\text{CH}_2\text{CH}_2\text{CH}_2$ ).  $^{13}\text{C-NMR}$  (Acetone 126 MHz)  $\delta$  172.0 (CONH), 160.3 ( $\text{C}(\text{OH})\text{CHC}(\text{OH})$ ), 159.5 ( $\text{C}(\text{CN})\text{C}(\text{OH})$ ), 155.3 (CNN), 143.9 ( $\text{C}(\text{SO}_2)$ ), 132.7 ( $\text{C}(\text{CONH})$ ), 132.1 (Ar-CC), 131.9 (Ar-CC), 129.4 ( $2\times\text{C}(\text{SO}_2)\text{CH}$ ), 128.2 ( $\text{C}(\text{CN})\text{CH}$ ), 127.9 (Ar-CH), 127.1 (Ar-CH), 125.6 (Ar-CH), 124.7 (Ar-CH), 118.9 ( $2\times\text{C}(\text{CONH})\text{CH}$ ), 109.5 ( $\text{C}(\text{CN})$ ), 106.9 ( $\text{C}(\text{CN})\text{CHCH}$ ), 103.7 ( $\text{C}(\text{OH})\text{CHC}(\text{OH})$ ), 46.4 ( $\text{NCH}_2$ ), 36.9 ( $\text{NH}_2\text{CH}_2$ ), 36.5 ( $\text{CONHCH}_2$ ), 29.5 ( $\text{NH}_2\text{CH}_2\text{CH}_2$ ), 26.0 ( $\text{CH}_2\text{CH}_2\text{CH}_2$ ), 24.5 ( $\text{CH}_2\text{CH}_2\text{CH}_2$ ). IR (neat)  $\nu_{\text{max}}$ : 3295, 2919, 1590, 1167, 1025  $\text{cm}^{-1}$ . HRMS (ESI) calcd for  $\text{C}_{26}\text{H}_{28}\text{N}_4\text{NaO}_5\text{S}$   $[\text{M}+\text{Na}]^+$  531.4965  $m/z$  found 531.4958  $m/z$ .

### 12.15 General Procedure for sulphonylation/de-protection:

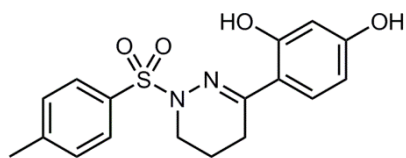
3-(2,4-Diisopropoxy-phenyl)-1,4,5,6-tetrahydro-pyridazine (0.7 mmol) was dissolved in dry DCM (10 mL) and TEA (1.54 mmol) and DMAP (0.07 mmol) were added subsequently. After 5 minutes, the desired sulphonyl chloride (0.9 mmol) was added and the reaction mixture was allowed to stir overnight. The mixture was washed with a 3 M solution of HCl (1x25 mL), a 5 M solution of NaOH (1x25 mL) and with water (2x25 mL). The organic phase was then dried over Na<sub>2</sub>SO<sub>4</sub>, filtered and concentrated. The residue was loaded onto a short pad of silica and filtered with a 20% ethyl acetate in petroleum ether solution to yield a yellow oil. The crude product was dried under high vacuum and used without further purification. The crude (0.4 mmol) was dissolved in dry DCM (8 mL) and a 1 M solution of BBr<sub>3</sub> (2.6 mmol) was added slowly at 0 °C. The reaction mixture was stirred for 30 minutes at 0 °C and then at room temperature until starting material consumption, monitored by TLC (3-6 hours). Water (50 mL) was added to quench the excess of BBr<sub>3</sub> and the layers were separated. The aqueous phase was back-extracted with DCM (2x50 mL) and the combined organic phases were dried over Na<sub>2</sub>SO<sub>4</sub>, filtered and concentrated. The residue was purified by flash column chromatography to afford the desired final product.



#### 4-(1-Benzenesulphonyl-1,4,5,6-tetrahydro-pyridazin-3-yl)-benzene-1,3-diol (RCZ30):

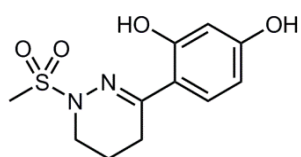
The product was purified by flash column chromatography (40% ethyl acetate in petroleum ether) to obtain a brownish oil (150 mg, 0.45 mmol) in 57% yield over two steps.

<sup>1</sup>H-NMR (Acetone 400 MHz) δ 12.17 (1H, s, COH), 9.35 (1H, s, COH), 7.90 (2H, d, J = 7.1 Hz, 2xC(SO<sub>2</sub>)CH), 7.75 (2H, m, C(CN)CH, Ar-CH), 7.67 (2H, t, J = 7.5 Hz, 2xC(SO<sub>2</sub>)CHCH), 6.56 (2H, m, C(CN)CHCH, C(OH)CHC(OH)), 3.50 - 3.42 (2H, m, NCH<sub>2</sub>), 2.69 (2H, t, J = 6.7 Hz, CNCH<sub>2</sub>), 2.24 - 2.12 (2H, m, NCH<sub>2</sub>CH<sub>2</sub>). <sup>13</sup>C-NMR (Acetone 101 MHz) δ 159.1 (C(OH)CHC(OH)), 156.0 (C(CN)C(OH)), 154.4 (CNN), 135.2 (C(SO<sub>2</sub>)), 133.7 (Ar-CH), 130.9 (C(CN)CH), 129.4 (2xC(SO<sub>2</sub>)CH), 127.9 (2xC(SO<sub>2</sub>)CHCH), 113.3 (C(CN)), 104.1 (C(CN)CHCH), 98.7 (C(OH)CHC(OH)), 42.9 (NCH<sub>2</sub>), 21.6 (CNCH<sub>2</sub>), 18.2 (NCH<sub>2</sub>CH<sub>2</sub>). IR (neat) ν<sub>max</sub>: 3031, 2564, 1620, 1383, 1016 cm<sup>-1</sup>. HRMS (ESI) calcd for C<sub>16</sub>H<sub>16</sub>N<sub>2</sub>NaO<sub>4</sub>S [M+Na]<sup>+</sup> 355.0421 m/z found 355.0444 m/z.



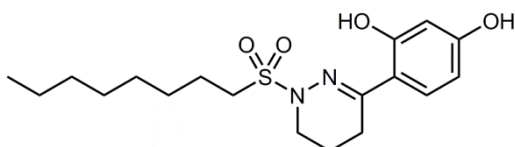
**4-[1-(Toluene-4-sulphonyl)-1,4,5,6-tetrahydro-pyridazin-3-yl]-benzene-1,3-diol (RCZ32):** The product was purified by flash column chromatography (40% ethyl acetate in petroleum ether) to obtain a beige solid (51 mg, 0.14

mmol) in 23% yield over two steps. m.p. 186 °C.  $^1\text{H-NMR}$  (Acetone 400 MHz)  $\delta$  12.18 (1H, s, COH), 7.78 (2H, d,  $J$  = 8.3 Hz,  $2\times\text{C}(\text{SO}_2)\text{CH}$ ), 7.45 (2H, d,  $J$  = 8.0 Hz,  $2\times\text{C}(\text{CH}_3)\text{CH}$ ), 7.26 (1H, d,  $J$  = 8.6 Hz,  $\text{C}(\text{CN})\text{CH}$ ), 6.39 - 6.31 (2H, m,  $\text{C}(\text{CN})\text{CHCH}$ ,  $\text{C}(\text{OH})\text{CHC}(\text{OH})$ ), 5.64 (1H, s, COH), 3.44 - 3.38 (2H, m,  $\text{NCH}_2$ ), 2.65 (2H, t,  $J$  = 6.7 Hz,  $\text{CNCH}_2$ ), 2.42 (3H, s,  $\text{CCH}_3$ ), 2.16 (2H, dt,  $J$  = 11.4 Hz, 6.7 Hz,  $\text{NCH}_2\text{CH}_2$ ).  $^{13}\text{C-NMR}$  (Acetone 126 MHz)  $\delta$  160.3 ( $\text{C}(\text{OH})\text{CHC}(\text{OH})$ ), 160.1 ( $\text{C}(\text{CN})\text{C}(\text{OH})$ ), 155.4 (CNN), 144.6 ( $\text{C}(\text{SO}_2)$ ), 132.2 ( $\text{C}(\text{CN})\text{CH}$ ), 129.8 ( $2\times\text{C}(\text{SO}_2)\text{CH}$ ), 128.2 ( $\text{C}(\text{CH}_3)$ ), 128.0 ( $2\times\text{C}(\text{CH}_3)\text{CH}$ ), 111.5 ( $\text{C}(\text{CN})$ ), 106.7 ( $\text{C}(\text{CN})\text{CHCH}$ ), 103.3 ( $\text{C}(\text{OH})\text{CHC}(\text{OH})$ ), 43.0 ( $\text{NCH}_2$ ), 21.7 ( $\text{CNCH}_2$ ), 20.5 ( $\text{CCH}_3$ ), 18.4 ( $\text{NCH}_2\text{CH}_2$ ). IR (neat)  $\nu_{\text{max}}$ : 3387, 2917, 1627, 1356, 1185  $\text{cm}^{-1}$ . HRMS (ESI) calcd for  $\text{C}_{17}\text{H}_{18}\text{N}_2\text{NaO}_4\text{S}$   $[\text{M}+\text{Na}]^+$  369.0879  $m/z$  found 369.0862  $m/z$ .



**4-(1-Methanesulphonyl-1,4,5,6-tetrahydro-pyridazin-3-yl)-benzene-1,3-diol (RCZ31):** The product was purified by flash

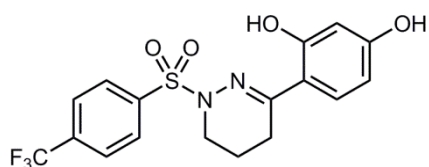
column chromatography (40% ethyl acetate in petroleum ether) to obtain a white solid (41 mg, 0.15 mmol) in 31% yield over two steps. m.p. 141 °C.  $^1\text{H-NMR}$  (Acetone 500 MHz)  $\delta$  11.95 (1H, s, COH), 8.75 (1H, s, COH), 7.37 (1H, d,  $J$  = 8.7 Hz,  $\text{C}(\text{CN})\text{CH}$ ), 6.40 (1H, dd,  $J$  = 9.3 Hz, 1.8 Hz,  $\text{C}(\text{CN})\text{CHCH}$ ), 6.36 (1H, d,  $J$  = 2.5 Hz,  $\text{C}(\text{OH})\text{CHC}(\text{OH})$ ), 3.69 - 3.55 (2H, m,  $\text{NCH}_2$ ), 3.01 (3H, s,  $\text{CCH}_3$ ), 2.78 (2H, t,  $J$  = 6.7 Hz,  $\text{CNCH}_2$ ), 2.21 (2H, dt,  $J$  = 13.5 Hz, 6.7 Hz,  $\text{NCH}_2\text{CH}_2$ ).  $^{13}\text{C-NMR}$  (Acetone 126 MHz)  $\delta$  160.3 ( $\text{C}(\text{OH})\text{CHC}(\text{OH})$ ), 160.1 ( $\text{C}(\text{CN})\text{C}(\text{OH})$ ), 154.9 (CNN), 128.3 ( $\text{C}(\text{CN})\text{CH}$ ), 111.7 ( $\text{C}(\text{CN})$ ), 106.7 ( $\text{C}(\text{CN})\text{CHCH}$ ), 103.3 ( $\text{C}(\text{OH})\text{CHC}(\text{OH})$ ), 42.4 ( $\text{NCH}_2$ ), 33.5 ( $\text{SO}_2\text{CH}_3$ ), 21.8 ( $\text{CNCH}_2$ ), 18.6 ( $\text{NCH}_2\text{CH}_2$ ). IR (neat)  $\nu_{\text{max}}$ : 3043, 1627, 1351, 1257, 970  $\text{cm}^{-1}$ . HRMS (ESI) calcd for  $\text{C}_{11}\text{H}_{14}\text{N}_2\text{NaO}_4\text{S}$   $[\text{M}+\text{Na}]^+$  293.0566  $m/z$  found 293.0562  $m/z$ .



**4-[1-(Octane-1-sulphonyl)-1,4,5,6-tetrahydro-pyridazin-3-yl]-benzene-1,3-diol (RCZ35):** The

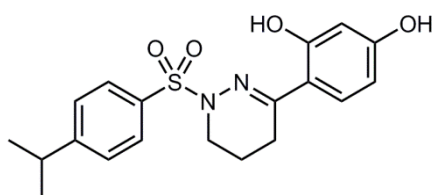
product was purified by flash column chromatography (40% ethyl acetate in petroleum ether) to obtain a colourless oil (90 mg, 0.24 mmol) in 33% yield over two steps.

$^1\text{H}$ -NMR ( $\text{CDCl}_3$  500 MHz)  $\delta$  11.81 (1H, s, COH), 7.14 (1H, d,  $J$  = 8.7 Hz, C(CN)CH), 6.35 (1H, d,  $J$  = 2.5 Hz, C(OH)CHC(OH)), 6.31 (1H, dd,  $J$  = 8.7 Hz, 2.6 Hz, C(CN)CHCH), 5.53 (1H, s, COH), 3.61 - 3.48 (2H, m,  $\text{NCH}_2$ ), 3.10 - 2.98 (2H, m,  $\text{SO}_2\text{CH}_2$ ), 2.60 (2H, t,  $J$  = 6.7 Hz,  $\text{CNCH}_2$ ), 2.14 - 2.05 (2H, m,  $\text{NCH}_2\text{CH}_2$ ), 1.83 - 1.70 (2H, m,  $\text{CH}_2\text{CH}_2\text{CH}_2$ ), 1.33 (2H, dt,  $J$  = 15.0 Hz, 7.3 Hz,  $\text{CH}_2\text{CH}_2\text{CH}_2$ ), 1.25 - 1.10 (8H, m, 4x  $\text{CH}_2\text{CH}_2\text{CH}_2$ ), 0.79 (3H, t,  $J$  = 7.0 Hz,  $\text{CH}_2\text{CH}_3$ ).  $^{13}\text{C}$ -NMR ( $\text{CDCl}_3$  126 MHz)  $\delta$  159.9 (C(OH)CHC(OH)), 158.4 (C(CN)C(OH)), 153.4 (CNN), 127.8 (C(CN)CH), 112.4 (C(CN)), 106.9 (C(CN)CHCH), 104.0 (C(OH)CHC(OH)), 49.1 ( $\text{SO}_2\text{CH}_2$ ), 42.2 ( $\text{NCH}_2$ ), 31.6 ( $\text{SO}_2\text{CH}_2\text{CH}_2$ ), 28.9 ( $\text{CH}_2\text{CH}_2\text{CH}_2$ ), 28.9 ( $\text{CH}_2\text{CH}_2\text{CH}_2$ ), 28.3 ( $\text{CH}_2\text{CH}_2\text{CH}_2$ ), 22.8 ( $\text{CH}_2\text{CH}_2\text{CH}_2$ ), 22.5 ( $\text{CH}_2\text{CH}_2\text{CH}_2$ ), 22.2 ( $\text{CNCH}_2$ ), 18.9 ( $\text{NCH}_2\text{CH}_2$ ), 14.0 ( $\text{CH}_2\text{CH}_3$ ). IR (neat)  $\nu_{\text{max}}$ : 3279, 2926, 1627, 1350, 1180  $\text{cm}^{-1}$ . HRMS (ESI) calcd for  $\text{C}_{18}\text{H}_{28}\text{N}_2\text{NaO}_4\text{S}$   $[\text{M}+\text{Na}]^+$  391.1662  $m/z$  found 391.1644  $m/z$ .



**4-[1-(4-Trifluoromethyl-benzenesulphonyl)-1,4,5,6-tetrahydro-pyridazin-3-yl]-benzene-1,3-diol (RCZ34):**

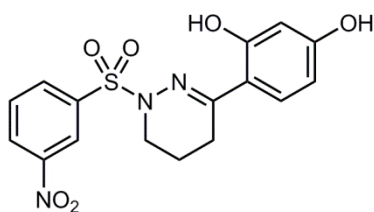
The product was purified by flash column chromatography (40% ethyl acetate in petroleum ether) to obtain a white solid (54 mg, 0.13 mmol) in 20% yield over two steps. m.p. 190 °C.  $^1\text{H}$ -NMR (Acetone 400 MHz)  $\delta$  12.03 (1H, s, COH), 8.79 (1H, s, COH), 8.12 (2H, d,  $J$  = 7.8 Hz, 2x C( $\text{CF}_3$ )CH), 8.04 (2H, d,  $J$  = 8.3 Hz, 2x C( $\text{SO}_2$ )CH), 7.28 (1H, d,  $J$  = 8.8 Hz, C(CN)CH), 6.44 - 6.33 (2H, m, C(CN)CHCH, C(OH)CHC(OH)), 3.57 - 3.43 (2H, m,  $\text{NCH}_2$ ), 2.68 (2H, t,  $J$  = 6.7 Hz,  $\text{CNCH}_2$ ), 2.18 (2H, dt,  $J$  = 12.4 Hz, 6.7 Hz,  $\text{NCH}_2\text{CH}_2$ ).  $^{13}\text{C}$ -NMR (Acetone 101 MHz)  $\delta$  160.4 (C(OH)CHC(OH)), 160.3 (C(CN)C(OH)), 156.3 (CNN), 139.1 (C( $\text{SO}_2$ )), 128.8 (2x C( $\text{CF}_3$ )CH, 2x C( $\text{SO}_2$ )CH), 128.4 (C(CN)CH), 126.5 (t,  $J$  = 3.8 Hz) ( $\text{CCF}_3$ ), 111.4 (C(CN)), 106.8 (C(CN)CHCH), 103.3 (C(OH)CHC(OH)), 43.0 ( $\text{NCH}_2$ ), 21.7 ( $\text{CNCH}_2$ ), 18.3 ( $\text{NCH}_2\text{CH}_2$ ). IR (neat)  $\nu_{\text{max}}$ : 3121, 2487, 1628, 1322, 1173  $\text{cm}^{-1}$ . HRMS (ESI) calcd for  $\text{C}_{17}\text{H}_{22}\text{F}_3\text{N}_2\text{NaO}_4\text{S}$   $[\text{M}+\text{Na}]^+$  423.0597  $m/z$  found 423.0579  $m/z$ .



**4-[1-(4-Isopropyl-benzenesulfonyl)-1,4,5,6-tetrahydro-pyridazin-3-yl]-benzene-1,3-diol (RCZ33):**

The product was purified by flash column chromatography (40% ethyl acetate in petroleum ether) to obtain a colourless oil (55 mg, 0.14 mmol) in 22% yield over two steps.  $^1\text{H}$ -NMR (Acetone 400 MHz)  $\delta$  12.19 (1H, s, COH), 8.76 (1H, s, COH), 7.82 (2H, d,  $J$  = 8.4 Hz,

2xC(SO<sub>2</sub>)CH), 7.53 (2H, d, J = 8.3 Hz, 2xC(iPr)CH), 7.27 (1H, d, J = 8.5 Hz, C(CN)CH), 6.41 - 6.29 (2H, m, C(CN)CHCH, C(OH)CHC(OH)), 3.46 - 3.38 (2H, m, NCH<sub>2</sub>), 3.02 (2H, quint., J = 6.9 Hz, CH<sub>3</sub>CH), 2.66 (2H, t, J = 6.7 Hz, CNCH<sub>2</sub>), 2.16 (2H, dt, J = 13.5 Hz, 6.7 Hz, NCH<sub>2</sub>CH<sub>2</sub>), 1.26 (6H, d, J = 6.9 Hz, 2xCHCH<sub>3</sub>). <sup>13</sup>C-NMR (Acetone 101 MHz) δ 160.4 (C(OH)CHC(OH)), 160.1 (C(CN)C(OH)), 155.3 (CNN), 155.1 (C(SO<sub>2</sub>)), 132.7 (C(CN)CH), 128.5 (C(iPr)), 128.2 (2xC(SO<sub>2</sub>)CH), 127.3 (2xC(iPr)CH), 111.5 (C(CN)), 106.7 (C(CN)CHCH), 103.3 (C(OH)CHC(OH)), 42.9 (NCH<sub>2</sub>), 33.9 (CH<sub>3</sub>CH), 22.8 (2xCHCH<sub>3</sub>), 21.6 (CNCH<sub>2</sub>), 18.4 (NCH<sub>2</sub>CH<sub>2</sub>). IR (neat) ν<sub>max</sub>: 3070, 1628, 1357, 1170, 781 cm<sup>-1</sup>. HRMS (ESI) calcd for C<sub>19</sub>H<sub>22</sub>N<sub>2</sub>NaO<sub>4</sub>S [M+Na]<sup>+</sup> 397.1192 m/z found 397.1174 m/z.



#### 4-[1-(3-Nitro-benzenesulphonyl)-1,4,5,6-tetrahydro-

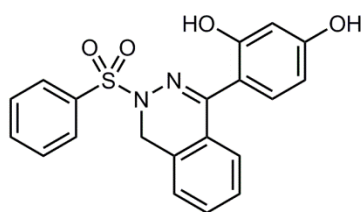
pyridazin-3-yl]-benzene-1,3-diol (RCZ36): The product was purified by flash column chromatography (40% ethyl acetate in petroleum ether) to obtain a yellow paste (87 mg, 0.23 mmol) in 32% yield over two steps. <sup>1</sup>H-NMR

(Acetone 400 MHz) δ 12.00 (1H, s, COH), 8.66 (1H, t, J = 1.9 Hz, C(SO<sub>2</sub>)CHC(NO<sub>2</sub>)), 8.61 - 8.53 (1H, m, C(NO<sub>2</sub>)CH), 8.33 - 8.24 (1H, m, C(SO<sub>2</sub>)CH), 8.01 (1H, t, J = 8.1 Hz, C(NO<sub>2</sub>)CHCH), 7.28 (1H, d, J = 8.6 Hz, C(CN)CH), 6.39 (1H, d, J = 2.4 Hz, C(OH)CHC(OH)), 6.36 (1H, dd, J = 8.6 Hz, 2.5 Hz, C(CN)CHCH), 3.63 - 3.51 (2H, m, NCH<sub>2</sub>), 2.68 (2H, t, J = 6.7 Hz, CNCH<sub>2</sub>), 2.19 (2H, dt, J = 11.4 Hz, 6.7 Hz, NCH<sub>2</sub>CH<sub>2</sub>). <sup>13</sup>C-NMR (Acetone 101 MHz) δ 160.4 (C(OH)CHC(OH)), 160.1 (C(CN)C(OH)), 156.7 (CNN), 148.5 (C(NO<sub>2</sub>)), 136.9 (C(SO<sub>2</sub>)), 133.6 (C(SO<sub>2</sub>)CHCH), 131.3 (C(SO<sub>2</sub>)CHCH), 128.4 (C(CN)CH), 128.1 (C(SO<sub>2</sub>)CHC(NO<sub>2</sub>)), 122.7 (C(NO<sub>2</sub>)CH), 111.3 (C(CN)), 106.9 (C(CN)CHCH), 103.3 (C(OH)CHC(OH)), 43.1 (NCH<sub>2</sub>), 21.7 (CNCH<sub>2</sub>), 18.3 (NCH<sub>2</sub>CH<sub>2</sub>). IR (neat) ν<sub>max</sub>: 3211, 2984, 1672, 1315, 846 cm<sup>-1</sup>. HRMS (ESI) calcd for C<sub>16</sub>H<sub>15</sub>N<sub>3</sub>NaO<sub>6</sub>S [M+Na]<sup>+</sup> 400.0574 m/z found 400.0557 m/z.

#### 12.16 General Procedure for sulphonylation/de-protection:

4-(2,4-Diisopropoxy-phenyl)-1,2-dihydro-phthalazine (0.6 mmol) was dissolved in dry DCM (10 mL) and TEA (1.22 mmol) and DMAP (0.06 mmol) were added subsequently. After 5 minutes, the desired sulphonyl chloride (0.7 mmol) was added and the reaction mixture was allowed to stir overnight. The mixture was washed with a 3 M solution of HCl (1x25 mL), a 5 M solution of NaOH (1x25 mL) and with water (2x25 mL). The organic phase was then dried over Na<sub>2</sub>SO<sub>4</sub>, filtered and concentrated. The residue was loaded into a short pad

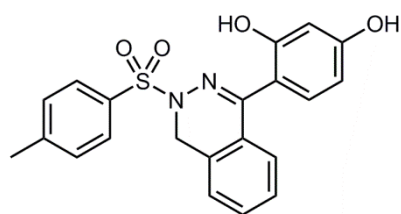
of silica and filtered with a 20% ethyl acetate in petroleum ether solution to yield a yellow oil. The crude product was dried under high vacuum and used without further purification. The crude (0.3 mmol) was dissolved in dry DCM (6 mL) and anhydrous aluminium trichloride (1.8 mmol) was added one portion. The reaction mixture was stirred at room temperature until starting material consumption, monitored by TLC (3-12 hours). Methanol (20 mL) was added to quench the excess of aluminium trichloride and the mixture was evaporated off under reduced pressure. The residue was purified by flash column chromatography to afford the desired final product.



**4-(3-Benzenesulphonyl-3,4-dihydro-phthalazin-1-yl)-benzene-1,3-diol (RCZ40):**

The product was purified by flash column chromatography (50% ethyl acetate in petroleum ether) to obtain a white solid (84 mg, 0.22 mmol) in 49%

yield over two steps. m.p. 195 °C. <sup>1</sup>H-NMR (CDCl<sub>3</sub> 400 MHz): δ 10.73 (1H, s, COH), 8.02 (2H, d, J = 8.4 Hz, 2xC(SO<sub>2</sub>)CH), 7.67 (1H, t, J = 7.4 Hz, NCH<sub>2</sub>CCHCH), 7.62 - 7.51 (4H, m, Ar-CH, 2xC(SO<sub>2</sub>)CHCH, CNCCH), 7.43 (1H, t, J = 7.8 Hz, CNCCHCH), 7.34 (1H, d, J = 7.5 Hz, NCH<sub>2</sub>CCH), 7.31 (1H, d, J = 8.6 Hz, C(CN)CH), 6.59 (1H, d, J = 2.5 Hz, C(OH)CHC(OH)), 6.42 (1H, dd, J = 8.6 Hz, 2.5 Hz, C(CN)CHCH), 5.03 (1H, s, COH), 4.35 (2H, s, NCH<sub>2</sub>). <sup>13</sup>C-NMR (CDCl<sub>3</sub> 126 MHz): δ 159.8 (C(OH)CHC(OH)), 158.4 (C(CN)C(OH)), 155.7 (CNN), 134.5 (C(SO<sub>2</sub>)), 133.8 (C(SO<sub>2</sub>)CHCHCH), 133.0 (Ar-CC), 132.0 (Ar-CC), 131.8 (Ar-CH), 129.2 (2xC(SO<sub>2</sub>)CH), 128.8 (2xC(SO<sub>2</sub>)CHCH), 128.3 (C(CN)CH), 127.8 (Ar-CH), 126.4 (Ar-CH), 124.6 (Ar-CH), 110.3 (C(CN)), 106.6 (C(CN)CHCH), 104.4 (C(OH)CHC(OH)), 46.3 (NCH<sub>2</sub>). IR (neat) ν<sub>max</sub>: 3397, 2358, 1624, 1347, 1170 cm<sup>-1</sup>. HRMS (ESI) calcd for C<sub>20</sub>H<sub>16</sub>N<sub>2</sub>O<sub>4</sub>S [M+H]<sup>+</sup> 383.0831 m/z found 383.0833 m/z.



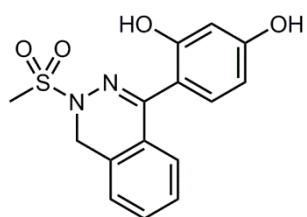
**4-[3-(Toluene-4-sulphonyl)-3,4-dihydro-phthalazin-1-yl]-benzene-1,3-diol (RCZ42):**

The product was purified by flash column chromatography (50% ethyl acetate in petroleum ether) to obtain a brownish solid (122 mg,

0.30 mmol) in 55% yield over two steps. m.p. 202 °C. <sup>1</sup>H-NMR (CDCl<sub>3</sub> 400 MHz): δ 10.78 (1H, s, COH), 7.89 (2H, d, J = 8.2 Hz, 2xC(SO<sub>2</sub>)CH), 7.56 - 7.51 (2H, m, NCH<sub>2</sub>CCHCH, NCH<sub>2</sub>CCH), 7.42 (1H, t, J = 7.3 Hz, CNCCHCH), 7.38 (2H, d, J = 7.9 Hz, 2xC(CH<sub>3</sub>)CH), 7.34 (1H, d, J = 7.6 Hz, CNCCH), 7.31 (1H, d, J = 8.5 Hz, C(CN)CH), 6.59 (1H, d, J = 2.4 Hz,



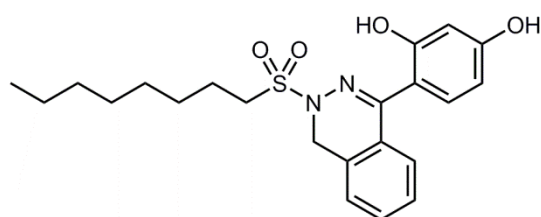
C(OH)CHC(OH)), 6.42 (1H, dd,  $J = 8.6$  Hz, 2.5 Hz, C(CN)CHCH), 4.99 (1H, s, COH), 4.33 (2H, s, NCH<sub>2</sub>), 2.45 (3H, s, CCH<sub>3</sub>). <sup>13</sup>C-NMR (CDCl<sub>3</sub> 126 MHz):  $\delta$  159.9 (C(OH)CHC(OH)), 158.1 (C(CN)C(OH)), 155.5 (CNN), 144.8 (C(SO<sub>2</sub>)), 133.1 (Ar-CC), 132.0 (Ar-CC), 131.8 (C(CN)CH), 131.5 (C(CH<sub>3</sub>)), 129.9 (2xC(SO<sub>2</sub>)CH), 128.8 (2xC(CH<sub>3</sub>)CH), 128.2 (Ar-CH), 127.7 (Ar-CH), 126.4 (Ar-CH), 124.7 (Ar-CH), 110.5 (C(CN)), 106.5 (C(CN)CHCH), 104.4 (C(OH)CHC(OH)), 46.3 (NCH<sub>2</sub>), 21.6 (CCH<sub>3</sub>). IR (neat)  $\nu_{\max}$ : 3420, 2363, 1625, 1168, 732 cm<sup>-1</sup>. HRMS (ESI) calcd for C<sub>21</sub>H<sub>18</sub>N<sub>2</sub>O<sub>4</sub>S [M+H]<sup>+</sup> 394.0987 m/z found 394.0992 m/z.



**4-(3-Methanesulphonyl-3,4-dihydro-phthalazin-1-yl)-benzene-1,3-diol (RCZ41):**

The product was purified by flash column chromatography (50% ethyl acetate in petroleum ether) to obtain a white foam (95 mg, 0.29 mmol) in 60% yield over two

steps. <sup>1</sup>H-NMR (CDCl<sub>3</sub> 400 MHz):  $\delta$  10.34 (1H, s, COH), 7.59 - 7.55 (2H, m, NCH<sub>2</sub>CCH, NCH<sub>2</sub>CCHCH), 7.46 (1H, t,  $J = 7.6$  Hz, CNCCHCH), 7.38 (1H, d,  $J = 8.6$  Hz, C(CN)CH), 7.36 (1H, d,  $J = 7.3$  Hz, CNCCH), 6.58 (1H, d,  $J = 2.3$  Hz, C(OH)CHC(OH)), 6.47 (1H, dd,  $J = 8.6$  Hz, 2.5 Hz, C(CN)CHCH), 5.10 (1H, s, COH), 4.55 (2H, s, NCH<sub>2</sub>), 3.10 (3H, s, SO<sub>2</sub>CH<sub>3</sub>). <sup>13</sup>C-NMR (CDCl<sub>3</sub> 126 MHz):  $\delta$  159.6 (C(OH)CHC(OH)), 158.5 (C(CN)C(OH)), 156.1 (CNN), 132.8 (Ar-CC), 132.3 (Ar-CC), 131.9 (C(CN)CH), 128.5 (Ar-CH), 127.9 (Ar-CH), 126.5 (Ar-CH), 124.7 (Ar-CH), 110.4 (C(CN)), 106.9 (C(CN)CHCH), 104.4 (C(OH)CHC(OH)), 46.0 (NCH<sub>2</sub>), 34.3 (SO<sub>2</sub>CH<sub>3</sub>). IR (neat)  $\nu_{\max}$ : 3345, 1624, 1343, 1219, 952 cm<sup>-1</sup>. HRMS (ESI) calcd for C<sub>15</sub>H<sub>14</sub>N<sub>2</sub>O<sub>4</sub>S [M+H]<sup>+</sup> 318.0674 m/z found 318.0675 m/z.



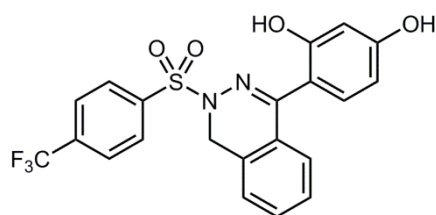
**4-[3-(Octane-1-sulphonyl)-3,4-dihydro-phthalazin-1-yl]-benzene-1,3-diol (RCZ45):**

The product was purified by flash column chromatography (50% ethyl acetate in

petroleum ether) to obtain a white foam (83 mg, 0.19 mmol) in 58% yield over two steps. <sup>1</sup>H-NMR (CDCl<sub>3</sub> 500 MHz)  $\delta$  10.38 (1H, s, COH), 7.60 - 7.52 (2H, m, NCH<sub>2</sub>CCH, NCH<sub>2</sub>CCHCH), 7.45 (1H, td,  $J = 7.8$  Hz, 1.1 Hz, CNCCHCH), 7.39 (1H, d,  $J = 8.6$  Hz, C(CN)CH), 7.35 (1H, d,  $J = 7.5$  Hz, CNCCH), 6.58 (1H, d,  $J = 2.5$  Hz, C(OH)CHC(OH)), 6.47 (1H, dd,  $J = 8.6$  Hz, 2.6 Hz, C(CN)CHCH), 5.05 (1H, s, COH), 4.61 (2H, s, NCH<sub>2</sub>), 3.28 - 3.21 (2H, m, SO<sub>2</sub>CH<sub>2</sub>), 2.02 - 1.90 (2H, m, CH<sub>2</sub>CH<sub>2</sub>CH<sub>2</sub>), 1.52 - 1.43 (2H, m, CH<sub>2</sub>CH<sub>2</sub>CH<sub>2</sub>), 1.37 - 1.26 (8H, m, 4xCH<sub>2</sub>CH<sub>2</sub>CH<sub>2</sub>), 0.89 (3H, t,  $J = 7.0$  Hz, CH<sub>2</sub>CH<sub>3</sub>). <sup>13</sup>C-NMR (CDCl<sub>3</sub> 126 MHz)  $\delta$  159.6 (C(OH)CHC(OH)), 158.3

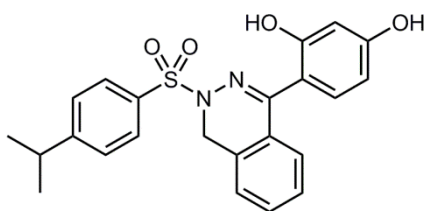


(C(CN)C(OH)), 155.6 (CNN), 132.9 (Ar-CC), 132.1 (Ar-CC), 131.9 (C(CN)CH), 128.3 (Ar-CH), 127.8 (Ar-CH), 126.3 (Ar-CH), 124.8 (Ar-CH), 110.6 (C(CN)), 106.7 (C(CN)CHCH), 104.4 (C(OH)CHC(OH)), 48.5 (SO<sub>2</sub>CH<sub>2</sub>), 46.0 (NCH<sub>2</sub>), 31.6 (SO<sub>2</sub>CH<sub>2</sub>CH<sub>2</sub>), 28.9 (CH<sub>2</sub>CH<sub>2</sub>CH<sub>2</sub>), 28.8 (CH<sub>2</sub>CH<sub>2</sub>CH<sub>2</sub>), 28.4 (CH<sub>2</sub>CH<sub>2</sub>CH<sub>2</sub>), 22.6 (CH<sub>2</sub>CH<sub>2</sub>CH<sub>2</sub>), 22.5 (CH<sub>2</sub>CH<sub>2</sub>CH<sub>2</sub>), 15.2 (CH<sub>2</sub>CH<sub>3</sub>). IR (neat)  $\nu_{\text{max}}$ : 3241, 2952, 1574, 1337, 968 cm<sup>-1</sup>. HRMS (ESI) calcd for C<sub>22</sub>H<sub>28</sub>N<sub>2</sub>NaO<sub>4</sub>S [M+Na]<sup>+</sup> 439.1662 m/z found 439.1643 m/z.



**4-[3-(4-Trifluoromethyl-benzenesulphonyl)-3,4-dihydro-phthalazin-1-yl]-benzene-1,3-diol (RCZ44):**

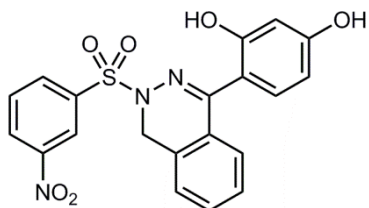
The product was purified by flash column chromatography (25% ethyl acetate in petroleum ether) to obtain a white foam (72 mg, 0.16 mmol) in 34% yield over two steps. <sup>1</sup>H-NMR (CDCl<sub>3</sub> 500 MHz)  $\delta$  10.65 (1H, s, COH), 8.05 (2H, d, J = 8.6 Hz, 2xC(CF<sub>3</sub>)CH), 7.79 (2H, d, J = 8.4 Hz, 2xC(SO<sub>2</sub>)CH), 7.55 (1H, td, J = 7.5 Hz, 1.2 Hz, NCH<sub>2</sub>CCHCH), 7.52 (1H, d, J = 7.2 Hz, NCH<sub>2</sub>CCH), 7.43 (1H, t, J = 7.6 Hz, CNCCHCH), 7.34 (1H, d, J = 7.1 Hz, CNCCH), 7.31 (1H, d, J = 8.6 Hz, C(CN)CH), 6.73 (1H, s, COH), 6.59 (1H, d, J = 2.6 Hz, C(OH)CHC(OH)), 6.42 (1H, dd, J = 8.6 Hz, 2.6 Hz, C(CN)CHCH), 4.36 (2H, s, NCH<sub>2</sub>). <sup>13</sup>C-NMR (CDCl<sub>3</sub> 126 MHz)  $\delta$  159.8 (C(OH)CHC(OH)), 159.6 (C(CN)C(OH)), 158.4 (CNN), 149.4 (C(SO<sub>2</sub>)), 145.3 (Ar-CC), 132.8 (Ar-CC), 132.2 (Ar-CH), 131.9 (Ar-CH), 129.3 (2xC(CF<sub>3</sub>)CH), 128.4 (C(CN)CH), 127.9 (Ar-CH), 127.1 (2xC(SO<sub>2</sub>)CH), 126.4 (t, J = 4.0 Hz) (CCF<sub>3</sub>), 124.6 (Ar-CH), 109.2 (C(CN)), 106.7 (C(CN)CHCH), 104.4 (C(OH)CHC(OH)), 46.4 (NCH<sub>2</sub>). IR (neat)  $\nu_{\text{max}}$ : 3087, 1606, 1404, 1284, 968 cm<sup>-1</sup>. HRMS (ESI) calcd for C<sub>21</sub>H<sub>15</sub>F<sub>3</sub>N<sub>2</sub>NaO<sub>4</sub>S [M+Na]<sup>+</sup> 471.0137 m/z found 471.0141 m/z.



**4-[3-(4-Isopropyl-benzenesulphonyl)-3,4-dihydro-phthalazin-1-yl]-benzene-1,3-diol (RCZ43):**

The product was purified by flash column chromatography (45% ethyl acetate in petroleum ether) to obtain a yellow/brownish solid (71 mg, 0.16 mmol) in 44% yield over two steps. m.p. 180 °C. <sup>1</sup>H-NMR (CDCl<sub>3</sub> 400 MHz):  $\delta$  10.72 (1H, s, COH), 7.81 (2H, d, J = 8.6 Hz, 2xC(SO<sub>2</sub>)CH), 7.45 - 7.39 (2H, m, NCH<sub>2</sub>CCH, NCH<sub>2</sub>CCHCH), 7.34 - 7.30 (3H, m, 2xC(iPr)CH, CNCCHCH), 7.25 (1H, d, J = 7.5 Hz, CNCCH), 7.22 (1H, d, J = 8.6 Hz, C(CN)CH), 6.49 (1H, d, J = 2.3 Hz, C(OH)CHC(OH)), 6.32 (1H, dd, J = 8.6 Hz, 2.4 Hz, C(CN)CHCH), 5.06 (1H, s, COH), 4.24 (2H, s,

NCH<sub>2</sub>), 2.89 (1H, quint., J = 7.0 Hz, CH<sub>3</sub>CH), 1.18 (6H, d, J = 7.0 Hz, CHCH<sub>3</sub>). <sup>13</sup>C-NMR (CDCl<sub>3</sub> 126 MHz): δ 159.9 (C(OH)CHC(OH)), 158.6 (C(CN)CH), 156.9 (CNN), 148.3 (C(SO<sub>2</sub>)), 134.4 (Ar-CC), 132.5 (Ar-CC), 132.0 (C(CN)CH), 130.8 (Ar-CH), 128.5 (2xC(SO<sub>2</sub>)CH), 128.2(C(iPr)), 128.1 (Ar-CH), 126.5 (2xC(iPr)CH), 124.5 (Ar-CH), 123.6 (Ar-CH), 110.2 (C(CN)), 106.8 (C(CN)CHCH), 104.4 (C(OH)CHC(OH)), 65.8 (CH<sub>3</sub>CH), 46.3 (NCH<sub>2</sub>), 23.5 (2xCHCH<sub>3</sub>). IR (neat) ν<sub>max</sub>: 3161, 1602, 1460, 1052, 943 cm<sup>-1</sup>. HRMS (ESI) calcd for C<sub>23</sub>H<sub>22</sub>N<sub>2</sub>NaO<sub>4</sub>S [M+Na]<sup>+</sup> 445.1192 m/z found 445.1177 m/z.

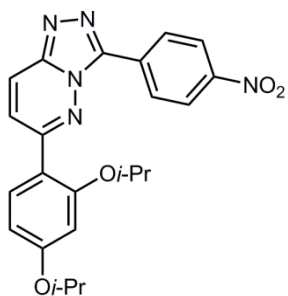


**4-[3-(3-Nitro-benzenesulphonyl)-3,4-dihydro-phthalazin-1-yl]-benzene-1,3-diol (RCZ46):** The product was purified by flash column chromatography (40% ethyl acetate in petroleum ether) to obtain a yellow paste (35 mg, 0.082

mmol) in 24% yield over two steps. <sup>1</sup>H-NMR (CDCl<sub>3</sub> 500 MHz) δ 10.42 (1H, s, COH), 8.81 (1H, t, J = 1.9 Hz, C(NO<sub>2</sub>)CHC(SO<sub>2</sub>)), 8.55 - 8.47 (1H, m, C(NO<sub>2</sub>)CH), 8.34 (1H, d, J = 7.9 Hz, C(SO<sub>2</sub>)CH), 7.83 (1H, t, J = 8.0 Hz, C(SO<sub>2</sub>)CHCH), 7.58 (1H, t, J = 7.5 Hz, NCH<sub>2</sub>CCHCH), 7.52 (1H, d, J = 7.1 Hz, NCH<sub>2</sub>CCH), 7.45 (1H, t, J = 7.6 Hz, CNCCHCH), 7.37 (1H, d, J = 7.5 Hz, CNCCH), 7.27 (1H, d, J = 8.6 Hz, C(CN)CH) (solvent peak overlap), 6.59 (1H, d, J = 2.5 Hz, C(OH)CHC(OH)), 6.42 (1H, dd, J = 8.6 Hz, 2.6 Hz, C(CN)CHCH), 4.42 (2H, s, NCH<sub>2</sub>). <sup>13</sup>C-NMR (CDCl<sub>3</sub> 126 MHz) δ 159.7 (C(OH)CHC(OH)), 158.6 (C(CN)C(OH)), 156.8 (CNN), 148.3 (C(NO<sub>2</sub>)), 136.8 (C(SO<sub>2</sub>)), 134.4 (Ar-CC), 132.5 (Ar-CC), 132.4 (Ar-CH), 132.0 (Ar-CH), 130.8 (C(SO<sub>2</sub>)CH), 128.5 (C(CN)CH), 128.1 (C(NO<sub>2</sub>)CH), 128.0 (C(SO<sub>2</sub>)CHCH), 126.5 (Ar-CH), 124.5 (Ar-CH), 123.6 (C(SO<sub>2</sub>)CHC(NO<sub>2</sub>)), 110.2 (C(CN)), 106.8 (C(CN)CHCH), 104.4 (C(OH)CHC(OH)), 46.5 (NCH<sub>2</sub>). IR (neat) ν<sub>max</sub>: 3042, 2399, 1608, 1567, 1185 cm<sup>-1</sup>. HRMS (ESI) calcd for C<sub>20</sub>H<sub>15</sub>N<sub>3</sub>NaO<sub>6</sub>S [M+Na]<sup>+</sup> 448.0574 m/z found 448.0571 m/z.

### 12.17 Procedure for triazole formation<sup>170</sup>:

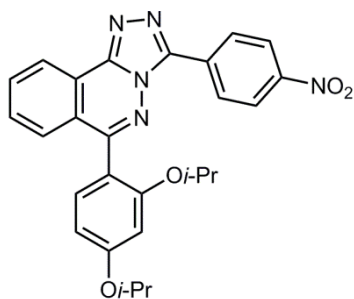
3-Chloro-6-(2,4-diisopropoxy-phenyl)-pyridazine (**26**) or 1-chloro-4-(2,4-diisopropoxy-phenyl)-phthalazine (**33**) (1.63 mmol) were dissolved in *n*-BuOH (12 mL) and then the corresponding benzhydrazide (1.79 mmol) was added. The reaction mixture was allowed to stir 140 °C overnight. The solvent was evaporated off under reduced pressure and the product was purified through flash column chromatography to afford the corresponding 1,2,4-triazole derivative.



**6-(2,4-Diisopropoxy-phenyl)-3-(4-nitro-phenyl)-**

**[1,2,4]triazolo[4,3-b]pyridazine (50) and (RCZ60):** The product was purified by flash column chromatography (2% methanol in DCM) to obtain a yellow foam (402 mg, 0.92 mmol) in 56% yield. <sup>1</sup>H-NMR (CDCl<sub>3</sub> 400 MHz) δ 8.89 (2H, d, J = 9.1 Hz, 2xC(NO<sub>2</sub>)CH), 8.42 (2H, d, J = 9.1 Hz, 2xC(NO<sub>2</sub>)CHCH), 8.14 (1H, d, J = 9.8 Hz, CNNNCH), 7.80 (1H, d, J = 9.8 Hz, CNCH), 7.71 (1H, d, J = 8.6 Hz, C(CN)CH), 6.68 (1H, dd, J = 8.7 Hz, 2.3 Hz, C(CN)CHCH), 6.60 (1H, d, J = 2.2 Hz, C(OiPr)CHC(OiPr)), 4.77 - 4.59 (2H, m, 2xCH<sub>3</sub>CH), 1.43 (6H, d, J = 6.1 Hz, 2xCHCH<sub>3</sub>), 1.39 (6H, d, J = 6.1 Hz, 2xCHCH<sub>3</sub>).

<sup>13</sup>C-NMR (CDCl<sub>3</sub> 126 MHz) δ 161.7 (C(OiPr)CHC(OiPr)), 157.3 (C(CN)C(OiPr)), 154.8 (CNN), 148.2 (C(NO<sub>2</sub>)), 146.1 (C(NNN)), 144.9 (C(CNNN)), 132.6 (C(NNNCH)), 132.0 (C(CN)CH), 128.0 (2xC(NO<sub>2</sub>)CH), 124.3 (C(NNNCH)), 123.9 (2xC(NO<sub>2</sub>)CHCH), 122.8 (CNCH), 117.0 (C(CN)), 107.2 (C(CN)CHCH), 102.4 (C(OiPr)CHC(OiPr)), 71.0 (CH<sub>3</sub>CH), 70.3 (CH<sub>3</sub>CH), 22.0 (4xCHCH<sub>3</sub>). IR (neat) ν<sub>max</sub>: 2346, 1623, 1182, 1011, 781 cm<sup>-1</sup>. HRMS (ESI) calcd for C<sub>23</sub>H<sub>23</sub>N<sub>5</sub>NaO<sub>4</sub> [M+Na]<sup>+</sup> 456.1642 m/z found 456.1627 m/z.

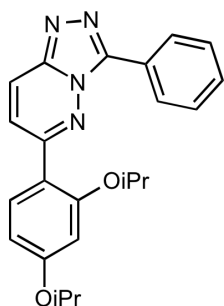


**6-(2,4-Diisopropoxy-phenyl)-3-(4-nitro-phenyl)-**

**[1,2,4]triazolo[3,4-a]phthalazine (52):** The product crystallised upon cooling of the reaction mixture. The white solid thus obtained was collected by suction filtration to afford a white powder (436 mg, 0.90 mmol) in 80% yield. m.p. 237 °C. <sup>1</sup>H-NMR (CDCl<sub>3</sub> 400 MHz) δ 8.84 (2H, d, J = 9.1 Hz, 2xC(NO<sub>2</sub>)CH), 8.80 (1H, d, J = 7.9 Hz, CNNCCH), 8.39 (2H, d, J = 9.1 Hz, 2xC(NO<sub>2</sub>)CHCH), 7.96 (1H, ddd, J = 8.1 Hz, 6.6 Hz, 1.8 Hz, CNNNCCHCH), 7.80 - 7.68 (2H, m, CNCCH, CNCCHCH), 7.42 (1H, d, J = 8.4 Hz, C(CN)CH), 6.69 (1H, dd, J = 8.5 Hz, 2.2 Hz, C(CN)CHCH), 6.64 (1H, d, J = 2.2 Hz, C(OiPr)CHC(OiPr)), 4.70 (1H, quint., J = 6.0 Hz, CH<sub>3</sub>CH), 4.56 (1H, quint., J = 6.1 Hz, CH<sub>3</sub>CH), 1.47 (6H, d, J = 6.0 Hz, 2xCHCH<sub>3</sub>), 1.13 (6H, d, J = 6.0 Hz, 2xCHCH<sub>3</sub>).

<sup>13</sup>C-NMR (CDCl<sub>3</sub> 126 MHz) δ 161.0 (C(OiPr)CHC(OiPr)), 157.1 (C(CN)C(OiPr)), 156.8 (CNN), 148.2 (C(NO<sub>2</sub>)), 147.1 (C(NNN)), 144.5 (C(CNNN)), 133.4 (C(NNNCCCH), 132.8 (Ar-CC), 132.0 (C(CN)CH), 130.3 (Ar-CC), 129.6 (Ar-CH), 128.4 (2xC(NO<sub>2</sub>)CH), 123.8 (2xC(NO<sub>2</sub>)CHCH, Ar-CH), 123.2 (Ar-CH), 123.1 (Ar-CH), 116.3 (C(CN)), 106.3 (C(CN)CHCH), 101.9 (C(OiPr)CHC(OiPr)), 70.5 (CH<sub>3</sub>CH), 70.2 (CH<sub>3</sub>CH), 22.1 (CHCH<sub>3</sub>), 22.0 (CHCH<sub>3</sub>), 21.9

(CHCH<sub>3</sub>), 21.6 (CHCH<sub>3</sub>). IR (neat)  $\nu_{\text{max}}$ : 2356, 1728, 1577, 1189, 832 cm<sup>-1</sup>. HRMS (ESI) calcd for C<sub>27</sub>H<sub>25</sub>N<sub>5</sub>NaO<sub>4</sub> [M+Na]<sup>+</sup> 506.1875 m/z found 506.1899 m/z.



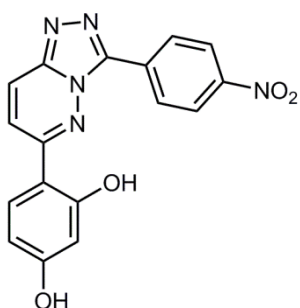
**6-(2,4-Diisopropoxy-phenyl)-3-(phenyl)-[1,2,4]triazolo[4,3-b]pyridazine**

**(51):** The product was purified by flash column chromatography (5% methanol in DCM) to obtain a white foam (172 mg, 0.44 mmol) in 68% yield. <sup>1</sup>H-NMR (CDCl<sub>3</sub> 500 MHz)  $\delta$  8.60 (2H, d, J = 6.5 Hz, 2xArCH), 8.08 (1H, d, J = 10.0 Hz, CNNNCH), 7.72 - 7.69 (2H, m, C(CN)CH, CNCH), 7.58 - 7.49 (3H, m, 3xArCH), 6.65 (1H, dd, J = 9.0 Hz, 2.5 Hz, C(CN)CHCH),

6.58 (1H, d, J = 8.9 Hz, C(OiPr)CHC(OiPr)), 4.68 - 4.62 (2H, m, 2xCH<sub>3</sub>CH), 1.39 (6H, d, J = 6.1 Hz, 2xCHCH<sub>3</sub>), 1.30 (6H, d, J = 6.1 Hz, 2xCHCH<sub>3</sub>). <sup>13</sup>C-NMR (CDCl<sub>3</sub> 126 MHz)  $\delta$  161.3 (C(OiPr)CHC(OiPr)), 157.2 (C(CN)C(OiPr)), 154.0 (CNN), 148.0 (C(CNNN)), 144.3 (C(NNN)), 132.0 (C(NNNCH)), 129.8 (C(CN)CH), 128.6 (2xArCH), 127.7 (2xArCH), 126.7 (C(NNNCH)), 123.4 (CNCH), 122.7 (ArCH), 117.6 (C(CN)), 107.2 (C(CN)CHCH), 102.4 (C(OiPr)CHC(OiPr)), 71.0 (CH<sub>3</sub>CH), 70.2 (CH<sub>3</sub>CH), 22.0 (4xCHCH<sub>3</sub>). IR (neat)  $\nu_{\text{max}}$ : 2109, 1678, 1428, 1002, 879 cm<sup>-1</sup>. HRMS (ESI) calcd for C<sub>23</sub>H<sub>24</sub>N<sub>4</sub>NaO<sub>2</sub> [M+Na]<sup>+</sup> 411.3932 m/z found 411.3921 m/z.

**12.18 Procedure for isopropyl de-protection:**

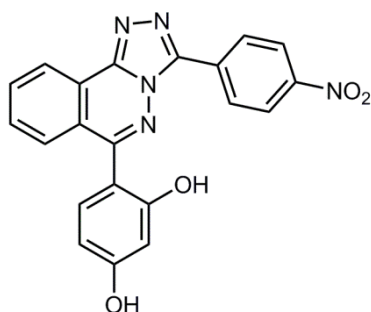
The desired bis *iso*-propoxyl derivative (0.30 mmol) was dissolved in dry DCM (10 mL) and anhydrous aluminium trichloride (1.50 mmol) was added. The reaction mixture was stirred at room temperature until starting material consumption (2-3 hours), monitored by TLC. The solvent was evaporated off under reduced pressure and the product was purified through flash column chromatography to afford the desired compound.



**4-[3-(4-Nitro-phenyl)-[1,2,4]triazolo[4,3-b]pyridazin-6-yl]-**

**benzene-1,3-diol (RCZ57):** The product was purified by flash column chromatography (2% methanol in DCM) to obtain a yellow solid (61 mg, 0.17 mmol) in 58% yield. m.p. 262 °C. <sup>1</sup>H-NMR (DMSO 400 MHz)  $\delta$  10.37 (1H, s, COH), 9.99 (1H, s, COH), 8.77 (2H, d, J = 8.6 Hz, 2xC(NO<sub>2</sub>)CH), 8.49 (2H, d, J = 8.6 Hz, 2xC(NO<sub>2</sub>)CHCH), 8.43 (1H, d, J = 9.7 Hz, CNNNCH), 7.98 (1H, d, J = 9.6 Hz, CNCH), 7.68 (1H, d, J = 8.5 Hz, C(CN)CH), 6.61 - 6.34 (2H, m, C(CN)CHCH, C(OH)CHC(OH)). <sup>13</sup>C-NMR (DMSO 126 MHz)  $\delta$  161.6 (C(OH)CHC(OH)), 158.1 (C(CN)C(OH)), 154.9 (CNN), 148.1 (C(NO<sub>2</sub>)),

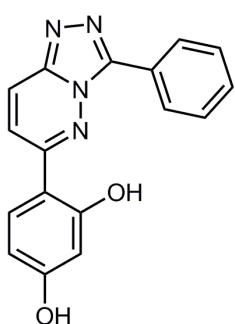
145.7 (C<sub>NNN</sub>), 145.0 (C(C<sub>NNN</sub>)), 132.8 (C<sub>NNN</sub>CH), 132.1 (C(CN)CH), 128.3 (2xC(NO<sub>2</sub>)CH), 124.6 (C<sub>NNN</sub>CH), 124.4 (2xC(NO<sub>2</sub>)CHCH), 123.9 (CNCH), 113.0 (C(CN)), 108.6 (C(CN)CHCH), 103.4 (C(OH)CHC(OH)). IR (neat)  $\nu_{\text{max}}$ : 3454, 2251, 1653, 1025, 820 cm<sup>-1</sup>. HRMS (ESI) calcd for C<sub>17</sub>H<sub>11</sub>N<sub>5</sub>NaO<sub>4</sub> [M+Na]<sup>+</sup> 372.0723 m/z found 372.0736 m/z.



**4-[3-(4-Nitro-phenyl)-[1,2,4]triazolo[3,4-a]phthalazin-6-yl]-**

**benzene-1,3-diol (RCZ59):** The product was purified by flash column chromatography (2% methanol in DCM) to obtain a yellowish solid (120 mg, 0.30 mmol) in 62% yield. m.p. 287 °C. <sup>1</sup>H-NMR (DMSO 400 MHz)  $\delta$  9.85 (1H, s, COH), 9.81 (1H, s, COH), 8.72 - 8.63 (3H, m, 2xC(NO<sub>2</sub>)CH, C<sub>NNN</sub>CCH), 8.47

(2H, d, J = 9.1 Hz, 2xC(NO<sub>2</sub>)CHCH), 8.13 - 8.04 (1H, m, C<sub>NNN</sub>CCHCH), 7.92 (1H, t, J = 7.7 Hz, C<sub>NNN</sub>CCHCH), 7.77 (1H, d, J = 7.9 Hz, C<sub>NNN</sub>CCH), 7.30 (1H, d, J = 8.3 Hz, C(CN)CH), 6.53 (1H, d, J = 2.2 Hz, C(OH)CHC(OH)), 6.48 (1H, dd, J = 8.3 Hz, 2.3 Hz, C(CN)CHCH). <sup>13</sup>C-NMR (DMSO 126 MHz)  $\delta$  160.8 (C(OH)CHC(OH)), 157.2 (C(CN)C(OH)), 157.1 (C<sub>NNN</sub>), 148.3 (C(NO<sub>2</sub>)), 146.9 (C<sub>NNN</sub>), 144.3 (C(C<sub>NNN</sub>)), 134.4 (C<sub>NNN</sub>CCH), 132.8 (Ar-CC), 132.3 (C(CN)CH), 131.6 (Ar-CC), 129.9 (Ar-CH), 128.7 (2xC(NO<sub>2</sub>)CH), 124.6 (2xC(NO<sub>2</sub>)CHCH), 124.0 (Ar-CH), 122.9 (Ar-CH), 122.9 (Ar-CH), 112.9 (C(CN)), 107.6 (C(CN)CHCH), 103.1 (C(OH)CHC(OH)). IR (neat)  $\nu_{\text{max}}$ : 3400, 2249, 1658, 1053, 821 cm<sup>-1</sup>. HRMS (ESI) calcd for C<sub>21</sub>H<sub>13</sub>N<sub>5</sub>NaO<sub>4</sub> [M+Na]<sup>+</sup> 422.0965m/z found 422.0987 m/z.



**4-[3-(Phenyl)-[1,2,4]triazolo[4,3-b]pyridazin-6-yl]-benzene-1,3-diol**

**(RCZ58):** The product was purified by flash column chromatography (2% methanol in DCM) to obtain a beige foam (58 mg, 0.19 mmol) in 78% yield. <sup>1</sup>H-NMR (DMSO 400 MHz)  $\delta$  10.35 (1H, s, COH), 9.96 (1H, s, COH), 8.44 - 8.42 (2H, m, 2xArCH), 8.35 (1H, d, J = 10.0 Hz, C<sub>NNN</sub>CH), 7.88 (1H, d, J = 9.6 Hz, CNCH), 7.63 - 7.55 (4H, m, 3xArCH, C(CN)CH),

6.49 (1H, d, J = 2.5 Hz, C(OH)CHC(OH)), 6.47 (1H, dd, J = 8.9 Hz, 2.5 Hz, C(CN)CHCH). <sup>13</sup>C-NMR (CDCl<sub>3</sub> 126 MHz)  $\delta$  161.8 (C(OH)CHC(OH)), 159.3 (C(CN)C(OH)), 156.1 (C<sub>NNN</sub>), 148.3 (C(C<sub>NNN</sub>)), 144.9 (C<sub>NNN</sub>), 132.2 (C<sub>NNN</sub>CH), 129.0 (C(CN)CH), 128.4 (2xArCH), 127.5 (2xArCH), 125.9 (C<sub>NNN</sub>CH), 124.4 (CNCH), 122.5 (ArCH), 116.2 (C(CN)), 106.3 (C(CN)CHCH), 100.5 (C(OH)CHC(OH)). IR (neat)  $\nu_{\text{max}}$ : 3376, 2125, 1652, 1005, 705 cm<sup>-1</sup>. HRMS (ESI) calcd for C<sub>17</sub>H<sub>12</sub>N<sub>4</sub>NaO<sub>2</sub> [M+Na]<sup>+</sup> 327.0956 m/z found 327.0998 m/z.

## 13 Biology experimental part

### 13.1 Strains, plasmids, growth media and storage

#### 13.1.1 Growth media

Luria-Bertani (LB) growth media was prepared in deionised water according to the recipe shown in Table 15 and then sterilised by means of autoclave. For LB solid media (LB-Agar) 1.5% agar was added before sterilisation. For 6% sucrose solid media (LB-Agar-Sucrose) for *sacBkan* cassette selection, 6% of sucrose was added to the final volume of the solution prior to autoclaving, while sodium chloride was omitted from the recipe. Minimal Essential Media with HEPES modification (MEM-HEPES) was purchased from Sigma-Aldrich® (M7278).

| Media   | Components per litre |
|---------|----------------------|
| LB      | 10 g tryptone        |
|         | 5 g yeast extract    |
|         | 10 g NaCl            |
| LB-Agar | 10 g tryptone        |
|         | 5 g yeast extract    |
|         | 10 g NaCl            |
|         | 15 g agar            |

**Table 15:** Media recipes.

### 13.1.2 Strains

Strains used and generated in this study are listed below in Table 16.

| Strain                              | Description and genotype  | Source         |
|-------------------------------------|---|----------------|
| <i>Escherichia coli</i>             |   |                |
| TUV 93-0                            | Derivative of EHEC O157:H7 strain EDL933 Shiga toxin negative (stx)   | <sup>190</sup> |
| TUV 93-0 $\Delta espD$              | Clean deletion of <i>espD</i> gene  | Tom Parker     |
| TUV 93-0 EspD-HA                    | TUV 93-0 producing a full-length EspD labelled with an HA tag on the carboxy-terminus   | This study     |
| TUV 93-0 EspD-HA $\Delta_{26-81}$   | TUV 93-0 producing EspD-HA where the region between amino acid 26 to 81 (Amph1/2) is deleted  | This study     |
| TUV 93-0 EspD-HA $\Delta_{138-171}$ | TUV 93-0 producing EspD-HA where the region between amino acid 138 to 171 (COIL1) is deleted  | This study     |
| TUV 93-0 EspD-HA $\Delta_{176-251}$ | TUV 93-0 producing EspD-HA where the region between amino acid 176 to 251 (TMD1/2) is deleted   | This study     |
| TUV 93-0 EspD-HA $\Delta_{333-351}$ | TUV 93-0 producing EspD-HA where the region between amino acid 333 to 356 (COIL2) is deleted  | This study     |
| Strataclone® Competent Cells        | DH5- $\alpha$ Competent cells Tetr $\Delta(mcrA)183 \Delta(mcrCB-hsdSMR-mrr)173 endA1 supE44 thi-1 recA1 gyrA96 relA1 lac Hte$ [F' <i>proAB lacIQ</i> $\Delta$ M15 Tn10 (Tet <sup>r</sup> ) Amy Cam <sup>r</sup> ]          | Agilent        |
| One Shot® TOP10 Competent Cells     | Chemically competent cells F <sup>-</sup> <i>mcrA</i> $\Delta(mrr-hsdRMS-mcrBC)$ F80/ <i>lacZ</i> $\Delta$ M15 $\Delta lacX74 recA1 ara\Delta 139 \Delta(ara-leu)7697 galU galK rpsL$ (Str <sup>R</sup> ) <i>endA1 nupG</i> | Invitrogen     |
| NEB Competent Cells                 | DH5- $\alpha$ Competent cells <i>fhuA2</i> $\Delta(argF-lacZ)U169 phoA glnV44 \Phi 80 \Delta(lacZ)M15 gyrA96 recA1 relA1 endA1 thi-1 hsdR17$  | NEB            |

**Table 16:** List of strains used and generated in this study.

### 13.1.3 Plasmids

Plasmids used and generated in this study are listed below in Table 17.

| Plasmid   | Description  | Antibiotic Resistance | Source      |
|---|--|-----------------------|-------------|
| <i>rpsM</i> :GFP  | Reporter for <i>rpsM</i>   | Chl                   | 191         |
| <i>tir</i> :GFP   | Reporter for <i>tir</i>  | Chl                   | 191         |
| <i>LEE1</i> :GFP  | Reporter for <i>LEE1</i>   | Chl                   | 191         |
| pAJR70  | <i>gfp</i> -containing plasmid   | Chl                   | pAJR70 ref. |
| pIB307  | Recombinant temperature sensitive plasmid  | Chl                   | 165,192     |
| pIB307- <i>sacBkan</i>                                    | Recombinant temperature sensitive plasmid bearing <i>sacBkan</i> cassette  | Chl/Kan               | 165,192     |
| pRZ001  | pAJR70 digested with <i>Bam</i> H1/ <i>Kpn</i> 1, <i>tir</i> promoter/ <i>espD</i> gene cloned in frame 5' to <i>gfp</i>   | Chl                   | This study  |
| pIB307- <i>LEE4</i> - <i>EspD</i> -HA                     | pIB307 digested with <i>Sac</i> 1/ <i>Pst</i> 1, <i>LEE4-espD</i> -HA construct cloned into <i>Sac</i> 1/ <i>Pst</i> 1   | Chl                   | This study  |
| pIB307- <i>LEE4</i> - <i>sacBkan</i>                      | pIB307- <i>LEE4</i> - <i>EspD</i> -HA digested with <i>Bam</i> H1, <i>sacBkan</i> gene cloned into the <i>Bam</i> H1 span  | Chl/Kan               | This study  |
| pIB307- <i>LEE4</i> - <i>EspD</i> -HA <sub>Δ26-81</sub>   | pIB307- <i>LEE4</i> - <i>sacBkan</i> digested with <i>Bam</i> H1/ <i>Apa</i> L1, <i>espD</i> -HAFrg1 and <i>espD</i> -HAFrg2 fragments assembled into <i>Bam</i> H1/ <i>Apa</i> L1 | Chl                   | This study  |
| pIB307- <i>LEE4</i> - <i>EspD</i> -HA <sub>Δ138-171</sub> | pIB307- <i>LEE4</i> - <i>sacBkan</i> digested with <i>Bam</i> H1/ <i>Apa</i> L1, <i>espD</i> -HAFrg3 and <i>espD</i> -HAFrg4 fragments assembled into <i>Bam</i> H1/ <i>Apa</i> L1 | Chl                   | This study  |
| pIB307- <i>LEE4</i> - <i>EspD</i> -HA <sub>Δ176-251</sub> | pIB307- <i>LEE4</i> - <i>sacBkan</i> digested with <i>Bam</i> H1/ <i>Apa</i> L1, <i>espD</i> -HAFrg5 and <i>espD</i> -HAFrg6 fragments assembled into <i>Bam</i> H1/ <i>Apa</i> L1 | Chl                   | This study  |
| pIB307- <i>LEE4</i> - <i>EspD</i> -HA <sub>Δ333-356</sub> | pIB307- <i>LEE4</i> - <i>sacBkan</i> digested with <i>Bam</i> H1/ <i>Apa</i> L1, <i>espD</i> -HAFrg7 and <i>espD</i> -HAFrg8 fragments assembled into <i>Bam</i> H1/ <i>Apa</i> L1 | Chl                   | This study  |

**Table 17:** List of plasmids used and generated in this study.



#### **13.1.4 Storage of bacteria**

Frozen bacterial stocks were made by adding glycerol to a final volume of 30% to an overnight LB culture, which was transferred to cryo tubes and stored at -80 °C in 1 mL aliquots.

#### **13.1.5 Growth of bacteria**

All strains were inoculated into the required media or agar plates with the appropriate antibiotics. When required, antibiotics were included at the following concentrations: 50 µg/mL kanamycin (Kan), 35 µg/mL chloramphenicol (Chl) and 100 µg/mL ampicillin (Amp). For general purposes, e.g. cloning, *E. coli* cultures were propagated from a single colony and grown at the desired temperature (28 °C, 37 °C or 42 °C) at 200 rpm for aeration.

### **13.2 Molecular techniques**

#### **13.2.1 Preparation of genomic DNA**

Cells were pelleted from 1 mL overnight LB cultures and genomic DNA (gDNA) was extracted using the ChargeSwitch gDNA Mini Bacteria kit (Invitrogen, UK), as per the manufacturer's instructions. DNA was re-suspended in 200 µL of nuclease free water (Ambion, UK) and stored at 4 °C.

#### **13.2.2 Oligonucleotide primers**

Oligonucleotide primers were synthesised by Invitrogen and used to amplify DNA by PCR as described in Paragraph 13.2.3. Primers were dissolved in nuclease free water to a 10 µM solution and stored at 4 °C. Primers used in this study are listed below in Table 18.

| Primer name   | Sequence 5' to 3'                             |
|---|---|
| pRZ001 F  | TTACTTGACAGCTCGTCCATGCC                       |
| pRZ001 R  | GGATCCCGCGATAAAGAACTTAAT                      |
| pIB307- <i>LEE4</i> -EspD-HA 1 F                                      | CGGACTGTTGTAACCTCAG                           |
| pIB307- <i>LEE4</i> -EspD-HA 1 R/<br>pIB307- <i>LEE4</i> -EspD-HA 2 R | TGCGACTCCTGCATTAGG                            |
| pIB307- <i>LEE4</i> -EspD-HA 2 F                                      | CCGTGACCAGTCTTGCTG                            |
| <i>Bam</i> H1 Span F  | CCATCGTTACTTGAGTATTATC                        |
| <i>Bam</i> H1 Span R  | TTCAGCAAATGTGCAATAC                           |
| <i>espD</i> -HAFrg1 F   | GTGCGACTAGATTGAGTAATACCAGAAGTACC              |
| <i>espD</i> -HAFrg1 R   | CATTAAATCTCTTAACGAGGTGCACGTTCTGATGTGC         |
| <i>espD</i> -HAFrg2 F   | AATAAAATTCTCTTTAATAAGGGATCCTTAAGCGTAATCTGGAAC |
| <i>espD</i> -HAFrg2 R   | ACTCAATCTAGTCGCACTGAGGAGGCA                   |
| <i>espD</i> -HAFrg3 F   | TGGCCAACCATATAAATCTCGTTAGAGTTTTTCAG           |
| <i>espD</i> -HAFrg3 R   | CATTAAATCTCTTAACGAGGTGCACGTTCTGATGTGC         |
| <i>espD</i> -HAFrg4 F   | AATAAAATTCTCTTTAATAAGGGATCCTTAAGCGTAATCTGG    |
| <i>espD</i> -HAFrg4 R   | GATTTATATGGTTGGCCAGGTCTTTGGT                  |
| <i>espD</i> -HAFrg5 F   | TACCAAATTTAAAGACCTGGCCAACAATTTTAC             |
| <i>espD</i> -HAFrg5 R   | CATTAAATCTCTTAACGAGGTGCACGTTCTGATGTGC         |
| <i>espD</i> -HAFrg6 F   | AATAAAATTCTCTTTAATAAGGGATCCTTAAGCGTAATCTG     |
| <i>espD</i> -HAFrg6 R   | CAGGTCTTTAAATTTGGTAATGTTGCTAACAAAATTG         |
| <i>espD</i> -HAFrg7 F   | CATCAGTTGACTCTCACCTAAGCTTTCAC                 |
| <i>espD</i> -HAFrg7 R   | CATTAAATCTCTTAACGAGGTGCACGTTCTGATGTGC         |
| <i>espD</i> -HAFrg8 F   | AATAAAATTCTCTTTAATAAGGGATCCTTAAGCGTAATCTG     |
| <i>espD</i> -HAFrg8 R   | GTGAGAGTCAACTGATGTCCGATTGAG                   |

**Table 18:** List of oligonucleotides used in this study.

### 13.2.3 Polymerase chain reaction (PCR)

A typical PCR used 10  $\mu$ L of GoTaq Master Mix Polymerase (Promega, UK), 100 pM of forward and reverse primers and 0.1  $\mu$ M of genomic DNA in a final volume of 20  $\mu$ L. The standard PCR cycle condition (30 cycles) used is shown in Table 19.

| Temperature (°C) | Step                 | Time (s) |
|------------------|----------------------|----------|
| 95               | Initial denaturation | 300      |
| 95               | Denaturation         | 45       |
| 55               | Annealing            | 45       |
| 72               | Extension            | 60 (/Kb) |
| 72               | Final extension      | 600      |
| 4                | Final hold           | -        |

**Table 19:** Standard PCR cycle conditions (30 cycles)

### 13.2.4 High-fidelity polymerase chain reaction (HF-PCR)

High-fidelity PCR (HF-PCR) was performed with Q5 High-Fidelity DNA Polymerase (NEB, UK) using a final concentration of 200  $\mu$ M of deoxynucleotides (dNTPs) mix, 0.5  $\mu$ M of forward and reverse primers, 0.1  $\mu$ M of DNA and 0.02 U/ $\mu$ L of Q5 HiFi polymerase in a final volume of 50  $\mu$ L per reaction. The standard HF-PCR protocol used is shown in Table 19.

### 13.2.5 Agarose gel electrophoresis

For a 1% w/v agarose gel, 1 g of ultrapure agarose was added to 100 mL of 1x Tris-acetate-EDTA buffer (TAE). The mixture was heated to dissolve the agarose and allowed to cool down to approximately 50 °C. SYBR Safe gel stain (Life Technologies, UK) or GelRED (Cambridge Biosciences, UK) were added at 1:10'000 as per manufacturer's instructions before the solution was poured into a gel tray and allowed to set. The appropriate volume of 10x loading buffer (Invitrogen, UK) was added to the DNA samples prior to loading and the gel was then run at 100 V for 40 minutes. 1Kb Reference DNA ladder was purchased from NEB, UK.

For a 1.2% w/v agarose gel, 1.2 g of ultrapure agarose were added to 100 mL of 1x Tris-acetate-EDTA buffer (TAE). The mixture was heated to dissolve the agarose and allowed to cool down to approximately 50 °C. SYBR Safe gel stain (Life Technologies, UK) or GelRED (Cambridge Biosciences, UK) were added at 1:10'000 as per manufacturer's instructions before the solution was poured into a gel tray and allowed to set. The appropriate volume of 10x loading buffer (Invitrogen, UK) was added to the DNA samples prior to loading and the gel was then run at 100 V for 70 minutes. 100bp Reference DNA ladder was purchased from NEB, UK. Agarose gels were visualised by means of an Alphamager trans-illuminator (Alpha Innotech, UK).

### **13.2.6 Restriction enzyme digestion**

All restriction enzyme digestions were performed according to the manufacturer's instructions (NEB, UK). A typical digestion reaction consisted of approximately 1 µg of DNA, the corresponding amount of the appropriate 10x restriction enzyme digestion buffer solution (typically 2 µL) and 10 U of the desired restriction enzyme (typically 1 µL). The reaction was made up to the desired volume (usually 20 µL) using nuclease free water (Ambion, UK). If more than one enzyme was used, the compatibility of the enzymes determined whether the reaction was carried out simultaneously or sequentially. The reaction was mixed and incubated at 37 °C for 1.5 hours. Digested products were resolved by agarose gel electrophoresis to visualise and to purify the DNA fragments of interest.

### **13.2.7 DNA gel purification**

Linearised DNA products generated from PCR or restriction enzyme digestion were resolved by agarose gel electrophoresis (Paragraph 13.2.5). DNA bands were visualised using a trans-illuminator and bands of interest were excised from the gel and purified by means of the Qiagen Gel Extraction Kit as per the manufacturer's instructions. The purified DNA was eluted with 20-30 µL of nuclease free water (Ambion, UK) depending on the concentration used in the reaction. The DNA concentration was calculated using a NanoDrop at 200 nm. DNA fragments were stored at 4 °C for short term storage and at -20 °C for long term storage.

### **13.2.8 Ligation reaction**

Ligation reactions were performed as per the manufacturer's instructions (NEB, UK). A standard ligation reaction consisted of 100 ng of digested plasmid, the appropriate amount of DNA insert molar ratio (typically 1:3 ratio plasmid:insert), 10x of DNA ligase buffer (typically 1 µL) and 5 U of T4 DNA ligase (typically 1 µL) (NEB,UK). The reaction final volume (usually 10-20 µL) was made up using nuclease free water (Ambion, UK), depending on the concentrations of the starting material. The reactions were incubated either overnight at 16 °C in a thermocycler or for 1 hour at 28 °C in a water bath, depending on the nature of the plasmid, and then directly used in transformation reactions.

### 13.2.9 Plasmid assembly reaction

Plasmid assembly reaction was carried out using the NEBuilder® HiFi DNA Assembly Cloning Kit (NEB, UK) according to the manufacturer's instructions. A typical assembly reaction consists of 50 ng of the digested plasmid, the appropriate molar ratio of purified DNA fragments (1:2 plasmid:fragments molar ratio for fragments > of 200 bp or 1:5 plasmid:fragments molar ratio for DNA fragments < of 200 bp) and 10 µL of NEBuilder HiFi DNA Assembly Master Mix (NEB, UK). The reaction final volume (20 µL) was made up using nuclease free water (Ambion, UK). The reaction was then incubated at 50 °C for 20 minutes and then directly used in an electroporation transformation reaction.

### 13.2.10 Heat shock transformation

5 µL of the desired ligation reaction were added to 50 µL of chemically competent cells (TOP10 from Invitrogen or Strataclone from Agilent) and incubated under ice for 30 minutes to allow cell thawing and DNA attachment to the cell surface. The cells were then heated at 42 °C in a water bath for 30 seconds and immediately returned under ice for another 2 minutes. 500 µL of SOC medium or LB were added to the transformed bacteria, followed by a 2 hours incubation at 37 °C or 28 °C and 200 rpm. The mixture was plated out onto LB agar plates containing the appropriate antibiotics and incubated at 37 °C or 28 °C, depending on the nature of the plasmid.

### 13.2.11 Production of electrocompetent *E. coli*

A single TUV 93-0 colony was amplified in 5 mL LB broth (with appropriate antibiotics when needed) overnight at 37 °C or 28 °C and 200 rpm. 500 µL of the overnight culture were added to 20 mL of pre-warmed LB broth (with appropriate antibiotics when needed) and incubated at 37 °C or 28 °C and 200 rpm until an OD<sub>600</sub> of 0.6 was reached (typically 2.5 hours). Bacteria were then placed under ice, centrifuged at 3'750 rpm and 4 °C for 10 minutes and pellets were re-suspended in 20 mL sterilised ice-cold 10% (v/v) glycerol. This step was repeated three times. After the final centrifugation step, the pellets were re-suspended in 1 mL sterilised ice-cold 10% (v/v) glycerol and centrifuged again at 6'000 rpm and 4 °C for 2 minutes. This step was repeated three times. After the final centrifugation step, the pellets were re-suspended in 100 µL of sterilised ice-cold 10% (v/v) glycerol. 40 µL of this final bacterial suspension were used per electroporation reaction.

### 13.2.12 Electroporation transformation

4  $\mu\text{L}$  of ligation reaction or plasmid assembly reaction were added to 40  $\mu\text{L}$  of electrocompetent *E. coli* cells which were transformed by electroporation using an electroporator (Invitrogen, UK) at 2.5 kV and a capacitance of 25  $\mu\text{F}$ . 1 mL of SOC medium or LB was immediately added to the mixture and incubated for 2 hours at 37 °C or 28 °C and 200 rpm according to the nature of the transformed plasmid. The mixture was then plated onto LB agar plates containing the appropriate antibiotics and incubated at 37 °C or 28 °C overnight. For plasmid assembly reactions incubation was prolonged for 48 hours at 28 °C.

### 13.2.13 Extraction of plasmid DNA

A single bacterial colony was cultured in 5 mL of LB broth overnight at 37 °C or 28 °C and 200 rpm (the appropriate antibiotics was added when needed). The bacteria were centrifuged at 3'750 rpm and 4 °C for 10 minutes. The plasmid was purified using the QIAprep Spin Miniprep Kit as per manufacturer's instructions. The purified plasmid was eluted in 25  $\mu\text{L}$  of nuclease free water (Ambion, UK). The plasmid concentration was calculated using a NanoDrop at 200 nm. Purified plasmids were stored at 4 °C.

### 13.2.14 Creation of TUV 93-0 EspD-HA strain by allelic exchange

The target gene *espD* was replaced with an *espD-HA* gene by means of a process called allelic exchange, which has been optimised for EHEC using the protocol by Emmerson *et al.*<sup>165</sup>. The method relies on the creation of a temperature sensitive exchange plasmid (pIB307-LEE4-*sacBkan*) encoding a chloramphenicol transferase gene (*cat*) to confer chloramphenicol resistance, the 3' and 5' homologous flanking regions of *espD* and a *sacBkan* cassette inserted between such homologous regions, which contains the levan sucrose gene (*sacB*), toxic for *E. coli* in presence of sucrose, and the kanamycin gene (*kan*) to confer kanamycin resistance (Fig. 53). The plasmid was then transformed into the TUV 93-0 at 28 °C and the transformants were subjected to periods of high temperatures (42 °C) and antibiotic selection (Chl), forcing the plasmid to integrate into the chromosome through homologous recombination in *espD*. The culture was then returned to low

temperatures (28 °C) and antibiotic selection (Kan) in order to allow the plasmid to replicate and excise from the chromosome. Overnight sub-culturing of the bacteria in LB at 28 °C promoted plasmid loss and successful recombinants were selected for the Kan<sup>R</sup>Chl<sup>S</sup> phenotype, generating a new strain (TUV 93-0  $\Delta$ *espD-sacBkan*) encoding the *sacBkan* cassette instead of the *espD* gene. Correct cloning was confirmed by PCR reaction (Paragraph 13.2.2 for primers sequence) across the new inserted gene.

A new temperature sensitive exchange plasmid (pIB307-*LEE4*-EspD-HA), that carries a chloramphenicol transferase gene (*cat*), the 3' and 5' homologous flanking regions of *espD* and an *espD-HA* gene flanked between such homologous regions, encoding for the HA-labelled version of the virulence protein EspD, was transformed into the new strain TUV 93-0  $\Delta$ *espD-sacBkan* at 28 °C (Fig. 54). Positive colonies were then subjected to periods of high temperatures (42 °C) and antibiotic selection (Kan), forcing the new plasmid to integrate into the chromosome through homologous recombination in the area of the *sacBkan* cassette. The culture was then incubated to low temperatures (28 °C) in LB medium, allowing the plasmid to replicate and excise from the chromosome. The recombinants were selected for the Sucrose<sup>R</sup> phenotype (using 6% sucrose LB-Agar plates) and then replica plated onto LB-Chl-Agar, LB-Kan-Agar and LB-Agar plates. Successful colonies grew only onto LB-Agar plates and generated the desired TUV 93-0 EspD-HA strain, which produces the HA-labelled version of the virulence protein EspD. Correct cloning was confirmed by PCR reaction (Paragraph 13.2.2 for primers sequence) across the new inserted gene. Expression and secretion of the new tagged-protein were analysed by  $\alpha$ -HA Western blot.

#### 13.2.15 Creation of plasmids for TUV 93-0 EspD-HA allelic exchange

Temperature sensitive exchange plasmids to perform allelic exchange were generated in our lab through standard molecular biology techniques (Fig. 52). The synthetic *espD-HA* gene flanked by homologous flanking regions of the *espD* gene was synthesised by Genescript, UK. The plasmid was transformed in TOP-10 competent cells (Paragraph 13.2.10) and then purified with the QIAprep Spin Miniprep Kit (Paragraph 13.2.13). The plasmid was digested with both *Sac*I and *Pst*I restriction enzymes (Paragraph 13.2.6) and the *espD-HA* flanked gene was extracted and purified from agarose gel (Paragraph 13.2.7). This construct was cloned (Paragraph 13.2.8) into the temperature sensitive exchange

vector (pIB307), generating the first allelic exchange plasmid pIB307-*LEE4*-EspD-HA. The correct cloning of the plasmid was confirmed by PCR reaction (Paragraph 13.2.2 for primers sequence) across the pIB307 backbone and the *espD*-HA flanked gene and by enzymatic digestion of the PCR product with *HindIII*.

pIB307-*LEE4*-EspD-HA was digested with *BamHI* restriction enzyme and the pIB307 backbone with the 5' and 3' homologous flanking regions was extracted and purified from agarose gel. Purified *sacBkan* cassette was cloned into this backbone between the homologous regions of the *espD* gene, creating the second allelic exchange plasmid pIB307-*LEE4*-*sacBkan*. The correct cloning of the plasmid was confirmed by PCR reaction (Paragraph 13.2.2 for primers sequence) across the pIB307 backbone and the *sacBkan* flanked gene and by enzymatic digestion of the PCR product with *NcoI*.

#### 13.2.16 Creation of truncated-EspD-HA strains by allelic exchange

Truncated-EspD-HA clones were generated following the second step (Fig. 54 and Fig. 55, Paragraph 13.2.14) of the allelic exchange protocol using the appropriate temperature sensitive exchange plasmid (pIB307-*LEE4*-EspD-HA $_{\Delta 26-81}$ , pIB307-*LEE4*-EspD-HA $_{\Delta 138-171}$ , pIB307-*LEE4*-EspD-HA $_{\Delta 176-251}$  or pIB307-*LEE4*-EspD-HA $_{\Delta 333-356}$ ) transformed into the intermediate strain TUV 93-0  $\Delta$ *espD*-*sacBkan*. Successful recombinants were selected for the Sucrose<sup>R</sup>Kan<sup>S</sup>Chl<sup>S</sup> phenotype as previously performed and confirmed by PCR reaction (Paragraph 13.2.2 for primers sequence) across the new inserted gene. Expression and secretion of the new tagged/truncated-proteins were analysed by  $\alpha$ -HA Western blot. A total of 4 new clones were created each one producing a different truncated-EspD-HA protein (refer to Table 12 for description of the strains).



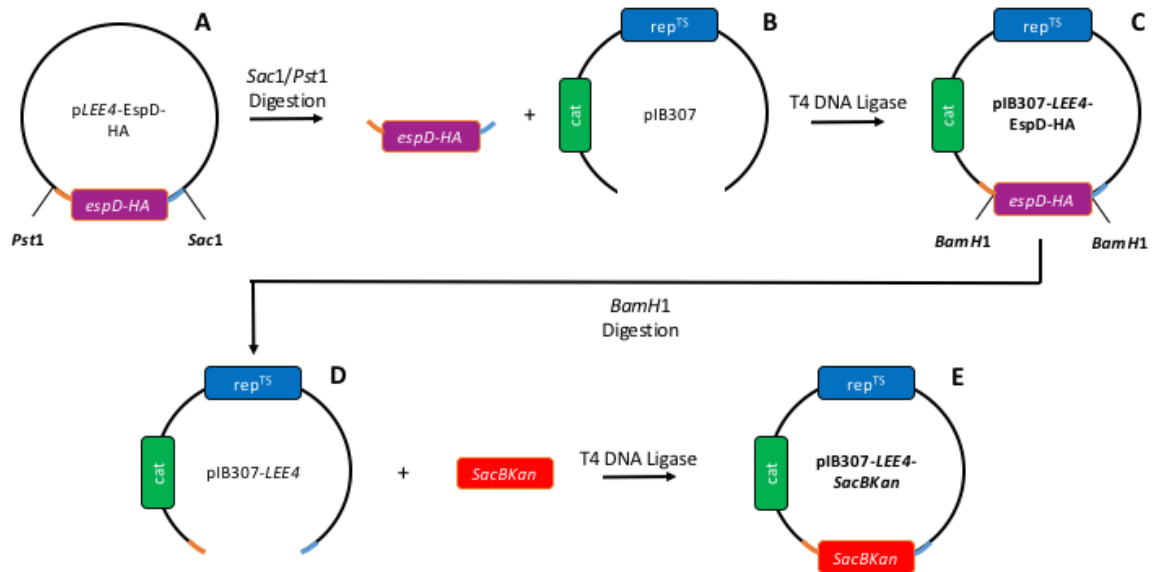


**Fig. 52: Creation of temperature sensitive plasmids for allelic exchange:** **A)** Synthetic *pLEE4-EspD-HA* from Genscript was subjected to sequential digestion with *Sac1* and *Pst1*. **B)** The purified construct from the digestion was ligated into the temperature sensitive backbone *plB307*. **C)** *pB307-LEE4-EspD-HA* is the first temperature sensitive exchange plasmid for the allelic exchange. The plasmid was subsequently digested with the restriction enzyme *BamH1* to excise the *espD-HA* gene from the backbone. **D)** *sacBkan* was cloned between the 3' and 5' homologous regions of the *BamH1* digested backbone. **E)** *pB307-LEE4-sacBkan* is the second temperature sensitive exchange plasmid for the allelic exchange.

### 13.2.17 Creation of plasmids for truncated-EspD-HA allelic exchange

The 4 temperature sensitive exchange plasmids for the formation of the truncated-EspD-HA clones were generated using the NEBuilder HiFi DNA Assembly Cloning Kit (NEB, UK) (Paragraph 13.2.9) and the Q5 High-Fidelity DNA Polymerase (NEB, UK) (Paragraph 13.2.4) (Fig. 55). The *pB307-LEE4-EspD-HA* plasmid was subjected to multiple HiFi PCR reactions with different sets of primers (Paragraph 13.2.2 for primers sequence) to amplify 8 different gene fragments (*espD-HAFrgs*). Fragments were coupled into 4 different pairs (*espD-HAFrg1+espD-HAFrg2*, *espD-HAFrg3+espD-HAFrg4*, *espD-HAFrg5+espD-HAFrg6*, *espD-HAFrg7+espD-HAFrg8*) and designed in order to have 15-30 bp overlap between each other or with either the 5' and 3' homologous flanking regions of the gene *espD*. Once these gene fragments were amplified, DNA gel extraction and purification from agarose gel was performed (Paragraph 13.2.7). The *pB307-LEE4-sacBkan* was then subjected to double enzymatic digestion with *BamH1* and *Apa1* and the vector, thus obtained, was used as main backbone for all 4 new plasmids. Generation of the 4 exchange plasmids was achieved using the digested *plB307* vector, the correct couple of *espD-HAFrgs* and the

NEBuilder HiFi DNA Assembly reaction conditions (Paragraph 13.2.9). After transformation in DH5- $\alpha$  competent cells, the plasmids were purified using the QIAprep Spin Miniprep Kit (Paragraph 13.2.13). Correct assembly of the new 4 plasmids was confirmed by PCR reaction (Paragraph 13.2.2 for primers sequence) across the pIB307 backbone and the newly assembled *espD*-HATr flanked genes (*espD*-HA $_{\Delta 26-81}$ , *espD*-HA $_{\Delta 138-171}$ , *espD*-HA $_{\Delta 176-251}$  or *espD*-HA $_{\Delta 333-356}$ ) and by enzymatic digestion of the PCR product with *HincII*. Plasmids were consequently transformed in the intermediate strain TUV 93-0  $\Delta$ *espD-sacBkan* to integrate the *espD*-HATr genes into the chromosome.

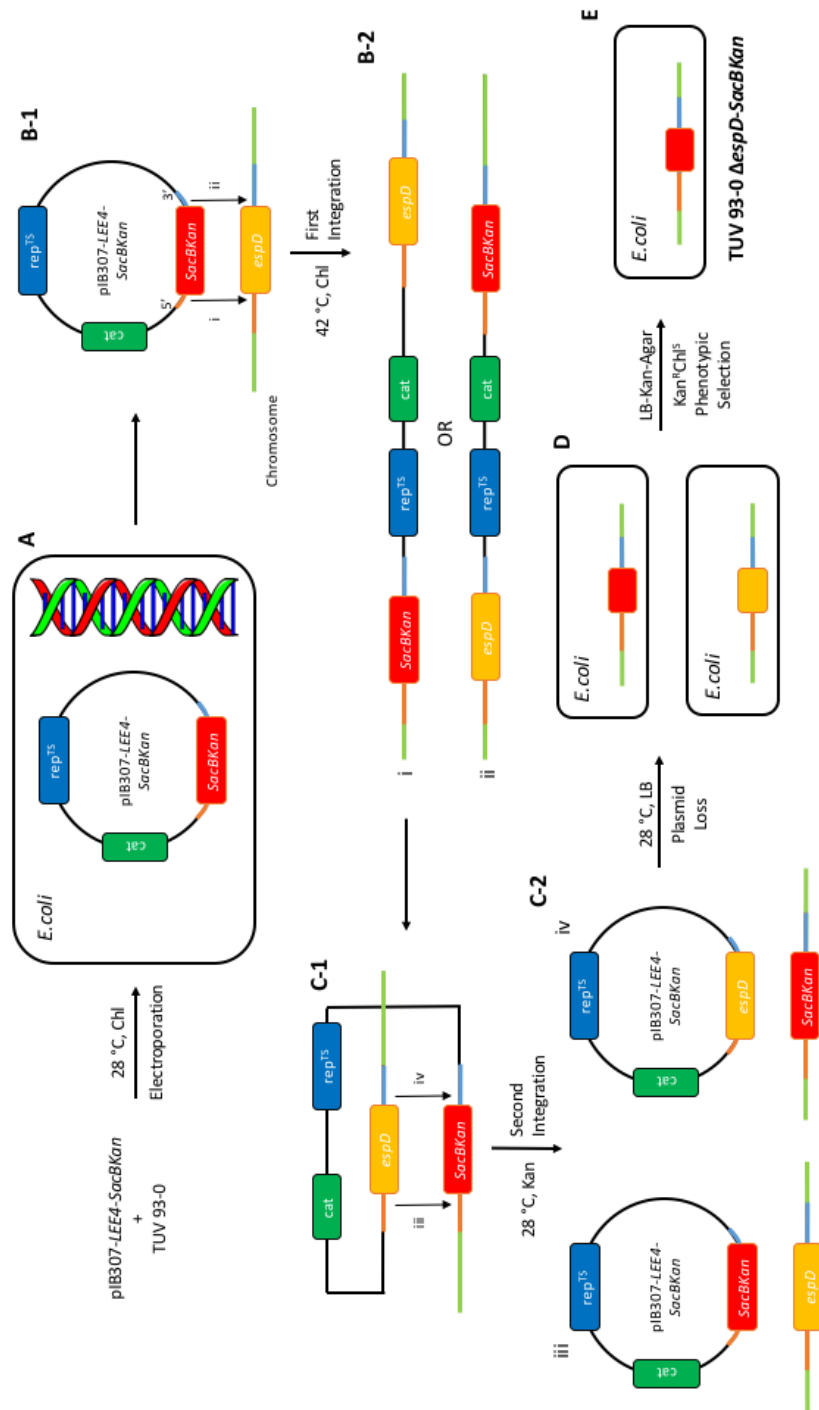


**Fig. 53: Creation of TUV 93-0  $\Delta$ espD-sacBkan intermediate strain:** **A**) pIB307-LEE4-sacBkan is transformed into TUV 93-0 at 28 °C. **B-1**) Transformants are subjected to periods of high temperatures (42 °C) in LB-Chl, allowing the plasmid to integrate the *sacBkan* cassette by homologous recombination into the chromosome. **B-2**) The first integration generates two different intermediates (i or ii). **C-1**) Bacteria are returned to low temperatures (28 °C) in LB-Kan in order to enable the second integration process into the chromosome. **C-2**) The *sacBkan* cassette can either return into the plasmid (iii) or integrate correctly into the chromosome (iv). **D**) Sub-culturing overnight in LB at 28 °C promotes plasmid loss from both possible recombinants iii and iv. **E**) The *sacBkan* recombinant is selected by the Kan<sup>R</sup>Chl<sup>S</sup> phenotype, replica plating the colonies in LB-Chl and LB-Kan plates, to yield the TUV 93-0  $\Delta$ espD-sacBkan strain.

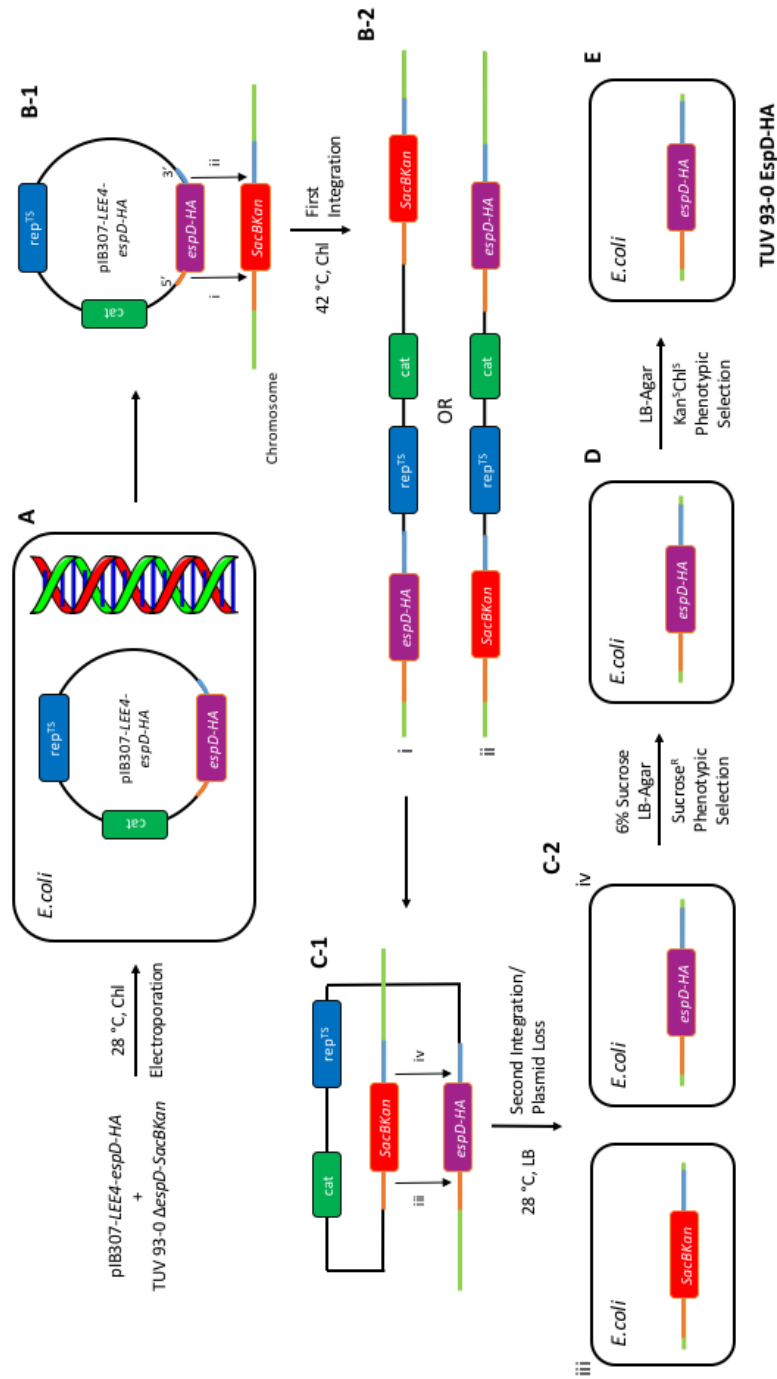


**Fig. 54: Creation of TUV 93-0 EspD-HA strain:** **A**) *piB307-LEE4-EspD-HA* is transformed into TUV 93-0  $\Delta espD-sacBkan$  strain at 28 °C. **B-1**) Transformants are subjected to periods of high temperatures (42 °C) in LB-Chl., allowing the plasmid to integrate the *espD-HA* gene by homologous recombination into the chromosome. **B-2**) The first integration generates two different intermediates (i or ii). **C-1**) Bacteria are returned to low temperatures (28 °C) in LB-Kan in order to enable the second integration process into the chromosome and to promote plasmid loss by the bacteria. **C-2**) The *espD-HA* gene can either rearrange back into the plasmid (iii) or integrate correctly into the chromosome (iv). **D**) The correct recombinant (iv) is selected by the *Sucrose<sup>R</sup>* phenotype by plating onto 6% sucrose LB-Agar plates. **E**) The recombinant is then selected by the *Kan<sup>S</sup>Chl<sup>S</sup>* phenotype, replica plating the colonies in LB-Chl, LB-Kan and LB plates, to yield the TUV 93-0 EspD-HA strain.

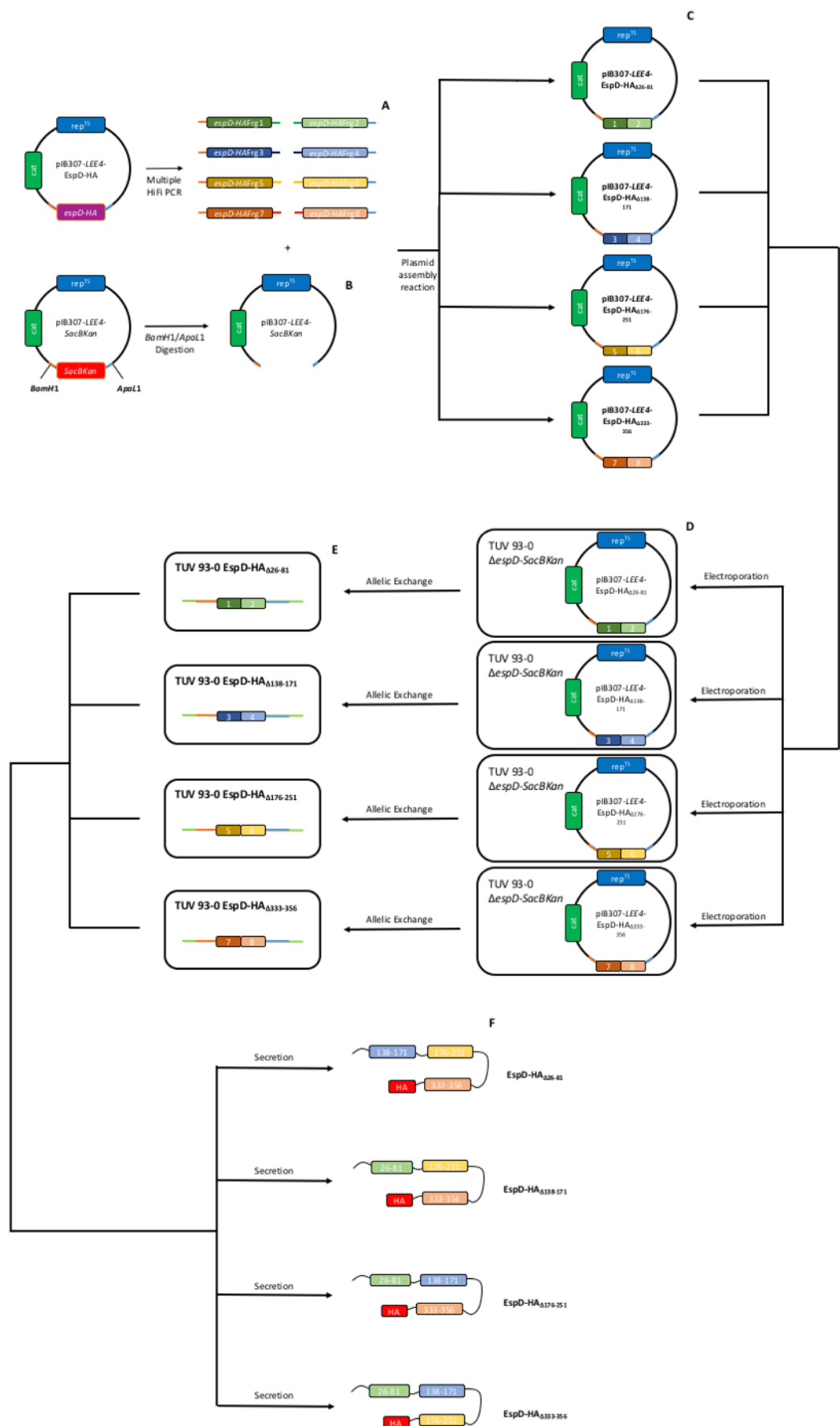


**Fig. 55: Creation of truncated EspD-HA strains:** **A)** High fidelity PCR was employed to amplify 8 different fragments of the *espD-HA* gene (*espD-HAFrg1-8*). **B)** *Bam*H1/*Apa*L1 digestion provided the desired temperature sensitive vector to use as a backbone for the new plasmids. **C)** Plasmid assembly reaction was performed to create the new allelic exchange plasmids: the *espD-HAFrgs* were coupled (1-2, 3-4, 5-6 and 7-8) and then cloned into the digested vector. 4 new plasmids were created, namely pIB307-*LEE4*-EspD-HA<sub>Δ26-81</sub>, pIB307-*LEE4*-EspD-HA<sub>Δ138-171</sub>, pIB307-*LEE4*-EspD-HA<sub>Δ176-251</sub> and pIB307-*LEE4*-EspD-HA<sub>Δ333-356</sub>. **D)** The new plasmids were transformed into the allelic exchange intermediate strain *ΔespD-sacBkan*. **E)** Allelic exchange was performed on the new strains, allowing the insertion of the desired *espD-HATr* gene into the *sacBkan* cassette area, thus generating 4 new strains producing a truncated HA-labelled version of the virulence protein EspD. **F)** Correct insertion of the gene was assessed by PCR across the determined *espD-HATr* gene and by α-HA Western blot analysis to evaluate the correct expression and secretion of the new construct.

## 13.3 Biochemical techniques

### 13.3.1 SDS-PAGE

Secreted proteins and whole cell lysate samples were analysed and prepared for western blotting by SDS-PAGE electrophoresis using the NuPage system (Invitrogen). Samples were mixed with 4x NuPage LDS loading buffer and boiled at 95 °C for 10 minutes before loading onto a NuPage 4-12% Bis-Tris pre-cast gel (Invitrogen). Samples were generally loaded in 10 µL aliquots and SeeBlue plus2 pre-stained protein marker (Invitrogen) was employed as a molecular weight marker. Concentrations of each sample were estimated using a NanoDrop 2000 to assure an equal loading of the proteins. SDS-PAGE gels were run using NuPage MES running buffer (Invitrogen) at 180 V for 45 minutes. Gels were then stained with Coomassie Brilliant Blue stain (Table 20 for recipe) for 1 hour on an orbital shaker and destained with 3 washes of destain solution (Table 21 for recipe) for 2 hours or with deionised water overnight. Protein bands to be analysed for identification using tandem mass-spectrometry (MS/MS) were excised from the gels using a clean and sterile scalpel blade and placed into individual sterile 1.5 mL microcentrifuge tubes. These bands were prepared and analysed by Dr. Richard Burchmore in the University of Glasgow Polyomics division.

| Component           | Volume/Amount per litre |
|---------------------|-------------------------|
| ddH <sub>2</sub> O  | 500 mL                  |
| Acetic Acid         | 100 mL                  |
| Methanol            | 400 mL                  |
| Coomassie blue R250 | 0.5 g                   |

**Table 20: Coomassie Brilliant Blue stain recipe.**

| Component          | Volume/Amount per litre |
|--------------------|-------------------------|
| ddH <sub>2</sub> O | 500 mL                  |
| Acetic Acid        | 100 mL                  |
| Methanol           | 400 mL                  |

**Table 21: Destain solution recipe**

### 13.3.2 Western blot

Proteins for western blot were transferred from SDS-PAGE gels to Amersham Hybond ECL nitrocellulose membrane (GE Healthcare) at 30 V for 90 minutes using the XCell SureLock

system (Invitrogen). The membrane was then blocked with 5% skimmed milk (Marvel) in PBST overnight. Primary antibody was made up at the specified concentration (Table 22) in PBST and incubated on the membrane for 1 hour at room temperature on an orbital shaker. The membrane was washed three times with PBST for 10 minutes each before incubation with the secondary horseradish-peroxidase (HRP) conjugated antibody for 1 hour at room temperature. The secondary antibody concentration employed was usually half of the primary antibody concentration. After 1 hour, the membrane was washed 3 times with PBST for 10 minutes each and then developed with SuperSignal West Pico Chemiluminescent ECL Substrate (Thermo Scientific). All Western blots were performed in triplicates coming from 3 independent experiments.

| Antibody | Source | Primary Concentration | Secondary Concentration |
|----------|--------|-----------------------|-------------------------|
| EspD     | Mouse  | 1/4'000               | 1/8'000                 |
| Tir      | Mouse  | 1/1'000               | 1/2'000                 |
| GroEL    | Rabbit | 1/10'000              | 1/25'000                |
| HA       | Mouse  | 1/2'500               | 1/10'000                |

**Table 22: Antibodies and relevant concentrations used in this study**

### 13.3.3 Pull-down assay with biotinylated RCZ12 and RCZ20

The pull-down assay was performed using Dynabeads™ M-280 Streptavidin magnetic beads (Invitrogen) and MagnaRack (Invitrogen) for beads separation from the solution. *E. coli* O157 TUV 93-0 strain was cultured overnight in LB and then diluted to an  $OD_{600} \leq 0.05$  in pre-warmed MEM-HEPES medium. Cultures were grown at 37 °C to an  $OD_{600} \geq 0.9$ . The cells were pelleted, washed several times with PBS and concentrated in PBS to a final volume of 2 mL. The suspended cells were lysed by means of a sonicator and kept under ice. The magnetic beads were aliquoted in Eppendorf tubes and washed with PBS using a MagnaRack (Invitrogen) for beads separation from the solution. A 250  $\mu$ M solution of biotin-RCZ12 or biotin-RCZ20 in PBS:DMSO (100:1) was added to the beads and incubated shaking for 1 hour at room temperature. The biotin-RCZs solution was removed and the beads were washed three times with PBS. 500  $\mu$ L of the suspended cell lysate solution was then added to the tubes and incubated shaking for another hour at room temperature. The lysate solution was removed and the beads were washed three times with PBS. Once finished, 15  $\mu$ L of SDS solution (Novex, UK) was added to the tube and the beads were



boiled at 95 °C for 10 minutes to promote specific bound proteins denaturation. Equals volumes of PBS washes and SDS samples were loaded onto a gel, the proteins were separated through SDS-PAGE electrophoresis and visualised by Coomassie Brilliant Blue staining (Table 20 and 21 for recipes). Specific bound proteins were excised for subsequent in-gel digestion and analysis by tandem mass-spectrometry <sup>193</sup>. Proteins analysed by peptide mass fingerprinting were given a MOWSE score <sup>194</sup> to indicate the probability of the identification being correct. We set a threshold MOWSE value of 100 or greater, ensuring a significance of  $P < 10^{-8}$ .

#### 13.3.4 Sample preparation for metabolomics analysis

Preparation of samples was adapted from Creek *et al.* 2011 <sup>195</sup>. Bacterial cultures were grown to an OD<sub>600</sub> of 0.9 in M9 medium (10 mL). 2.5 mL of the bacteria solution was added to 2.5 mL of fresh M9 medium and the appropriate compound concentration. The solution was incubated for 1 hour at room temperature. 10-Bromodecane oil (100 µL) was added to 1 mL of the incubated solution and the mixture was then centrifuged at 13'000 rpm and 4 °C for 2 minutes to separate the bacteria. 12.5 µL of the supernatant solution were transferred into a sterile micro-centrifuge tube and 500 µL of a 1:3:1 chloroform:methanol:water extracting solution were added to generate the supernatant sample. The remnant of the supernatant solution from the centrifuged solution was removed and 200 µL of a 1:3:1 chloroform:methanol:water extracting solution were added to create the bacteria sample. Every biological samples were performed in triplicates from different solutions and all the samples were stored at -80 °C until MS analysis. Dr. Karl Burgess and Dr. Stefan Weidt of the University of Glasgow Polyomics division carried out the metabolomics analysis. Samples were analysed through hydrophilic interaction liquid chromatography (HILIC) on a Dionex UltiMate 3000 RSLC system (Thermo Fischer Scientific, Hemel Hempstead, UK) using a ZIC-pHILIC column (Merck Sequant). The column was maintained at 30 °C and samples were eluted with a linear gradient (20 mM ammonium carbonate in water, A and acetonitrile, B) over 26 min at a flow rate of 0.3 mL/min. The injection volume was 10 µL and samples were maintained at 4 °C prior to injection. For the MS analysis, a Thermo Orbitrap Exactive (Thermo Fisher Scientific) was operated in polarity switching mode with a resolution of 50'000. Samples of cell-free

medium and appropriate compound concentration and extraction solution were used as controls for the analysis.

### 13.4 Transcriptome analysis

Transcriptome analysis was carried out by Dr. James Connolly (University of Glasgow) and a brief description of the method used is described below.

#### 13.4.1 Total RNA extraction and mRNA enrichment

Bacterial cells were cultured as described above (Paragraph XX) before being mixed with two volumes of RNeasy Protect reagent (Qiagen, Valencia, CA, USA), incubated for 5 minutes at room temperature and harvested by centrifugation. Total RNA was extracted using an RNeasy kit (Qiagen) according to the manufacturer's specifications. Genomic DNA was removed using TURBO DNase (Ambion, Carlsbad, CA, USA). Total RNA samples were enriched for mRNA using a MICROBexpress mRNA enrichment kit (Ambion). Integrity of enriched mRNA samples for sequencing were tested using an Agilent Bioanalyzer 2100 at the University of Glasgow Polyomics Facility.

#### 13.4.2 RNA-sequencing and transcriptome analysis

cDNA synthesis, library generation and sequencing was performed at the Edinburgh Genomics facility (Illumina HiSeq 2500) obtaining 100 bp single end reads. Three biological replicates were used for each condition of the transcriptome analysis. Samples of TUV 93-0 cultured in MEM-HEPES with and without 50  $\mu$ M of **RCZ20** were used to extract mRNA. Raw sequencing reads were assessed for quality using FastQC (Babraham Bioinformatics, Cambridge, UK) and trimmed where necessary using CLC Genomics Workbench (CLC Bio, Aarhus, Denmark). Sequence reads were then mapped to the EDL933 reference genome (NCBI NC\_002655.2) allowing for 3 mismatches per read and at least 5 reads per open reading frame under all conditions tested. To determine differential expression between conditions, analysis was performed using the Empirical analysis of DGE tool in CLC Genomics Workbench, which implements the EdgeR Bioconductor tool<sup>196</sup>. Differentially expressed genes were identified by positive or negative absolute fold change and considered significant if the corrected *P*-value was  $\leq 0.05$  (false-discovery rate of 5%). Differentially expressed genes (DEGs) were grouped by biological function according to

their designated gene ontology (GO) terms obtained from the EMBL-EBI QuickGO database (<https://www.ebi.ac.uk/QuickGO/>). Bar charts summarizing the data were generated in GraphPad Prism version 5.0 (San Diego, CA, USA) and heat-maps of gene expression patterns were generated in Microsoft Excel. The raw sequence reads in this study have been deposited in the European Nucleotide Archive.

### **13.5 Phenotypic characterisation techniques**

#### **13.5.1 *E. coli* O157 secreted protein profiling**

Secreted protein extraction from *E. coli* O157 TUV 93-0 was performed as previously described<sup>197</sup>. Overnight cultures were sub-cultured to a starting OD<sub>600</sub> of approximately 0.05 into 50 or 25 mL of pre-warmed MEM-HEPES and were grown at 37 °C and 200 rpm until OD<sub>600</sub> of 0.6-0.7. Culture were centrifuged at 3'750 rpm and 4 °C for 15 minutes. The cell pellet was separated by the supernatant solution, re-suspended in 500 µL of BugBuster Mix (Novagen) and incubated for 30 minutes at room temperature. The sample was centrifuged at 13'000 rpm and room temperature for 5 minutes and the clear solution was transferred to a sterilised Eppendorf tube. The whole cell pellet was stored at -20 °C. The supernatant solution was carefully separated from the centrifuged cell pellet and filtered through a 0.2 µm filter (Fischer, UK). A 6.1 N solution of trichloroacetic acid (TCA) was added to a final concentration of 10% v/v and the sample was mixed and left at 4 °C overnight. Secreted protein fractions were then harvested by centrifugation at 3'750 rpm and 4 °C for an hour. The supernatant solution was carefully removed and the protein pellet was allowed to dry at room temperature. The pellet was re-suspended in 80-100 µL of Tris-HCl (pH=8.0) and stored at -20 °C. Both whole cell and supernatant samples were subjected to SDS-PAGE electrophoresis for western blot analyses.

#### **13.5.2 GFP reporter fusion assay**

Population based gene expression analysis was carried out using *E. coli* O157 TUV 93-0 transformed with different GFP-promoter transcriptional fusion constructs (Table X) that have been described elsewhere<sup>191</sup>. Overnight cultures of the desired strain were sub-cultured to an initial OD<sub>600</sub> of approximately 0.05 into pre-warmed MEM-HEPES and then grown at 37 °C and 200 rpm. A 800 µL aliquot was taken hourly from the sample and the OD<sub>600</sub> was measured by means of a refractometer. 200 µL of the aliquot were then

transferred to a black flat-bottomed 96-well microtitre plate for GFP expression analysis by a FLUOstar Optima Fluorescence Plate Reader (BMG Labtech, UK). TUV 93-0 without any GFP-promoter plasmid was used as a negative control to measure the background fluorescence. Data are presented as the mean and standard deviation of three biological replicates. Readings for fluorescence (RFU values) were plotted against OD<sub>600</sub> values using GraphPad Prism 5 (GraphPad Software, USA). The curves were then analysed by linear regression and interpolated at the determined OD<sub>600</sub> of 0.6. Student's t test was employed for statistical comparison of the untreated samples (WT) with the treated samples.

## **13.6 Microscopy techniques**

### **13.6.1 Transmission electron microscopy (TEM)**

Margaret Mullin, head of the University of Glasgow electron microscopy service, prepared bacterial samples for imaging. Bacterial samples were fixed on ice with 1% paraformaldehyde/PBS for an hour and washed three times in PBS for 5 minutes each time. Sample suspension droplets (5 µl) were placed onto Formvar/Carbon nickel-coated support grids which had been pre-treated with a 0.1% poly-L-lysine solution. Bacterial suspensions were left to settle for 20 minutes, the grids were floated sample on 0.05 M glycine/PBS droplets for 5 minutes and then rinsed three times with 3% BSA/PBS for 5 minutes. Bacterial samples were placed onto an α-EspA (1:100 dilution) for an hour, washed six times on 3% BSA/PBS for 5 minutes each and then placed onto droplets of secondary GAR 10 nm gold for an hour. Samples were washed six times in 3% BSA/PBS for 5 minutes each, rinsed with PBS six times for 3 minutes, fixed on 1% glutaraldehyde/PBS for 5 minutes, washed six times in distilled water and then left to dry. Immuno-stained bacterial samples were viewed on a FEI Tecnai T20 TEM running at 200 kV and dm4/tiff images were captured using Gatan Digital Imaging software.

### **13.6.2 Transmission electron microscopy (TEM) for membrane morphology**

Bacterial suspensions were washed twice in PBS for 5 minutes each before an initial fixation with 2% glutaraldehyde, 2% paraformaldehyde, 0.1 M sodium cacodylate buffer for an hour. Samples were rinsed three times with 0.1 M sodium cacodylate buffer for 5 minutes each then post fixed for an hour in 1% osmium tetroxide, 0.1 M sodium cacodylate buffer. The osmium tetroxide was removed by washing three times in distilled

water for 10 minutes each before en bloc staining with 0.5% aqueous uranyl acetate for an hour (light sensitive stain, samples kept in dark). Samples were given two washes in distilled water then dehydrated through an ethanol series as follows 30, 50, 70, 90% ethanol for 15 minutes each, 100% ethanol for 5 minutes and then 100% dried ethanol (3 Å molecular sieves) for 5 minutes. Samples were given three 5 minutes rinses in propylene oxide and then left overnight in a 1:1 mixture of propylene oxide:epon araldite resin. Samples were given three changes of pure resin throughout the following day before fresh embedding and polymerising at 60 °C for 48 hours. Ultrathin 50 nm sections were cut using a Leica EM UTC Ultratome and a Diatome diamond knife, sections were collected on 200 mesh formvar copper-coated support grids then contrast stained with 2% methanolic uranyl acetate stain for 5 minutes followed by 5 minutes in Reynolds lead citrate. Bacterial samples were viewed on a FEI Tecnai T20 TEM running at 200 kV and dm4/tiff images captured using Gatan Digital Imaging software.

### **13.7 Bioinformatics and statistical analysis**

#### **13.7.1 Bioinformatic and database tools**

Nucleotide and amino acid sequences were obtained from NCBI (<http://www.ncbi.nlm.nih.gov>) and Colibase<sup>198</sup>. Alignments were performed using Clustal Omega (<http://www.ebi.ac.uk/Tools/msa/clustalo/>) and cloning strategies were designed using MacVector.

#### **13.7.2 Statistical analysis**

Statistical analysis for comparison of two samples was carried out using a Student's unpaired t-test in GraphPad Prism unless otherwise stated. Error bars were calculated using the standard error from the mean. RNA-seq analysis was performed by Dr. James Connolly using CLC Genomics Workbench (CLC Bio). Significance levels are depicted in the figures as \*, \*\* or \*\*\* denoting  $P \leq 0.05$ ,  $P \leq 0.01$  and  $P \leq 0.001$  respectively.